Spring 5-15-2016

Environmental Fullerene Chemistry: Elucidating Critical Reaction Pathways and Resulting Products in the Aqueous Phase

Jiewei Wu
Washington University in St. Louis

WASHINGTON UNIVERSITY IN ST. LOUIS

School of Engineering & Applied Science
Department of Energy, Environmental & Chemical Engineering

Dissertation Examination Committee:

John Fortner, Chair

Parag Banerjee

Daniel Giammar

Young-Shin Jun

Jaehong Kim

Brent Williams

Environmental Fullerene Chemistry: Elucidating Critical Reaction Pathways and Resulting Products in the Aqueous Phase

by

Jiewei Wu

A dissertation presented to the
Graduate School of Arts & Sciences
of Washington University in
partial fulfillment of the
requirements for the degree
of Doctor of Philosophy

May 2016
St. Louis, Missouri

Table of Contents

List of Figures

List of Tables

Acknowledgements

Above all, I would like to express my deepest gratitude to my advisor, Dr. John D. Fortner. Without his guidance, I would have had no chance to step into this fullerene 'wonderland', which I have really enjoying working in for the past 5 years. This dissertation would not have been possible without his continuing support, persistent help, and inspiring encouragement. His dedication to research, a keen sense of integrity, commitment to highest standards of work - as well as his optimism, kind-heartedness have inspired me and will continue to motivate me in every aspect of my life.

I also wish to thank Dr. Parag Banerjee, Dr. Daniel Giammar, Dr. Young-Shin Jun, Dr. Jaehong Kim, and Dr. Brent Williams for serving on my committee. I especially thank Dr. Daniel Giammar, Dr. Young-Shin Jun and Dr. Brent Williams for their help in during my time within the EECE department. A special thank you goes to Dr. Jaehong Kim, for his valuable suggestions, support, and help. I would also like to thank Dr. Parag Banerjee for his suggestions regarding my course of study and my dissertation.

I would also like to extend my gratitude to my friends and department staff for their encouragement, the great joy they brought to me, and all the help along this way. In particular, my prior and current colleagues of the Fortner's Lab: Dr. Seung Soo Lee, Dr. Wenlu Li, Dr. Lin Wang, Peter Colletti, Yining Ou, Yi Jiang, Changwoo Kim, Siyuan An, Che Tan, Yao Nie, Kelsey Haddad have been supporting me and made this journey a memorable experience. I would like to thank all the undergraduate researchers for their contribution to the fullerene project: Liza Petrie, Cara Welker, Kathy Peter, Brittany Radke, Matt Epplin, Brittany Luntz, Adan Montoya, and Loli Baquerizo.

Financial support from Washington University in St. Louis faculty start-up funding, National Science Foundation (NSF), and technique support form Nano Research Facility (NRF) and Institute of Materials Science and Engineering (IMSE) at Washington University in St. Louis are gratefully acknowledged.

I would like to thank my parents for their invaluable sources of support and love. They have made what I am today and they are the best.

Finally, the deepest thank you goes to my dearest husband, Li Du. He is always there by my side, cheering me up, erasing sorrow, tear, and fear from my life.

Jiewei Wu

Washington University in St. Louis

January, 2016

ABSTRACT OF THE DISSERTATION

Environmental Fullerene Chemistry: Elucidating Critical Reaction Pathways and Resulting Products in the Aqueous Phase

by

Jiewei Wu

Doctor of Philosophy in Energy, Environmental & Chemical Engineering

Washington University in St. Louis, 2016

Professor John Fortner, Chair

As the production of fullerenes and fullerene-based materials approaches industrial scale, there are increasing interests/concerns regarding their (potential) environmental impact(s) upon release. To date, a number of critical, aqueous-based fullerene transformation pathways under environmentally relevant conditions remain poorly understood. Comprehensive, fundamental, and quantitative understanding of the potential (major) reaction pathways and resulting products of fullerene materials, particularly in aquatic systems, is now crucial for their accurate fate, transport, life cycle, risk assessment(s), and thus ultimate material sustainability.

Herein, this dissertation is focused on identifying and elucidating aqueous transformation pathways of fullerene materials, focused on C_{60} as a model fullerene, under a variety of relevant environmental scenarios. First, we elucidate the mechanisms by which hydrophobic, solid fullerene and hydrogenated C_{60} derivatives become water available/stable through extended mixing, without transferring solvents, in the presence of light and electron acceptors (e.g. oxygen). Resulting products exist as stable nano-scale C_{60} aggregates (termed as

aqu/nC_{60}) or, depending on the reaction, as oxidized fullerenes (termed as fullerol), respectively. Additionally, water stable/soluble fullerenes (nC_{60} and fullerol) can undergo further oxidation by common oxidants such as free chlorine, which is dramatically enhanced via photo-irradiation (under sunlight mimicked conditions). Finally, under environmentally relevant reducing scenarios, oxidized fullerene derivatives (fullerol) were also observed to be susceptible to reduction reactions by effective electron donors (e.g. zero-valent zinc). For all, reactions were explored and described via kinetic analyses with resulting products completely characterized via a battery of analytical techniques (e.g.^{13}C-NMR, FTIR, Raman Spectroscopy, XPS, TEM, UV-vis, QCM-D, etc.) as well as comparative (physical) partitioning behaviors. Overall, these new findings highlight the likely potential for fullerene aqueous-based transformations within a variety of common environmental scenarios. It is demonstrated that such reactions will also generate products with significantly altered physicochemical properties, which correspondingly result in relatively different partitioning/transport behavior(s) in natural systems. This body of work also underscores the clear and present need to consider and fundamentally understand other advanced (nano)material(s) aqueous reactivities, in both natural and engineered treatment systems if a sustainable nanomaterial industry is to be eventually realized.

Chapter 1 :**Introduction**

1.1. Background

1.1.1. **Fullerene Structure and Physical Property**

Engineered, nanoscale carbon based materials (including fullerenes, and carbon nanotubes) possess inherently unique physical and chemical properties, underpinning their broad application potential in a range of materials based technologies.[1] Fullerenes are particularly novel carbon based nanomaterials, which were first hypothetically proposed by Eiji Osawa in 1970[2] and observed experimentally later by Drs. Kroto, Smalley and Curl at Rice University in 1985.[3]

Buckminsterfullerene (C_{60}), was the first fullerene empirically observed and as Osawa hypothesized, C_{60} is a carbon allotrope, existing as a symmetrical, caged molecule consisting of 60 carbon atoms (or more for larger fullerenes) with each junction as an identical carbon vertex (sp^2 hybridized), arranged as 12 pentagons isolated by 20 hexagons, which is similar to that of a soccer ball structure.[4] The structure of C_{60} is depicted in Figure 1.1, with the bonding of the two hexagons ([6,6] bonds) being shorter than that between a hexagon and a pentagon ([5,6] bonds).[4] The diameter of C_{60} has been determined by NMR measurements to be 7.10 ± 0.07Å, with the volume of a single C_{60} molecule was estimated to be 1.87×10^{-22} cm^3 (effective π-electron cloud was considered).[5]

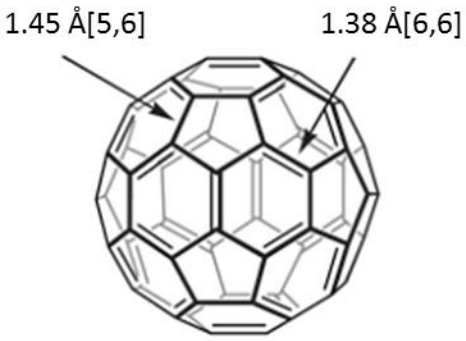

Figure 1.1: Schematic representation of a C_{60} molecule.[4]

The properties of C_{60}, in solid state as well as in solution (as dissolved molecule), have been widely investigated and selected physical properties related to this thesis are tabulated in Table 1-1. Based on its icosahedral symmetric structure, C_{60} exhibits significant non-polarity in various organic solvents, including polar and H-bonding solvents (e.g. acetone and methanol), and thus C_{60} is extremely insoluble in most monopolar or bipolar solvents. In more apolar solvents, such as benzenes and naphthalene, the solubility of C_{60} is appreciable. The solubility of C_{60} in various solvents is listed in Table 1-2. UV-vis absorption spectra of C_{60} in selected solvents are shown in Figure 1.2, existing between 190 to 400 nm, which is due to $^1T_{1u}$-^1A_g transitions, as well as between 410 to 620 nm which is contributed by orbital forbidden singlet-singlet transitions.[4, 6]

Table 1-1: Selected physical properties of C_{60} [4, 5, 7-10]

Solubility in Water	2.6-8 ng/L
Density	1.65 g/cm^3
Standard Heat of Formation	9.08 kcal/mol
Index of Refraction	2.2 at 630 nm wavelength
Sublimation Point	800 K
Resistivity	1014 ohms/m
Crystal Structure	Face centered cubic (>255K);
Cage Diameter	7.1 Å
Vapor Pressure	5×10^{-6} torr at room temperature

Table 1-2: Solubility of C_{60} in a variety of solvents.[4, 11]

Solvent	**[C_{60}] mg/mL**
n-Hexane	0.043
n-Decane	0.071
Chloroform	0.16
Benzene	1.7
Toluene	2.8
Acetone	0.001
Methanol	0.000
1-Methylnaphthalene	33
1-Chloronaphthalene	51

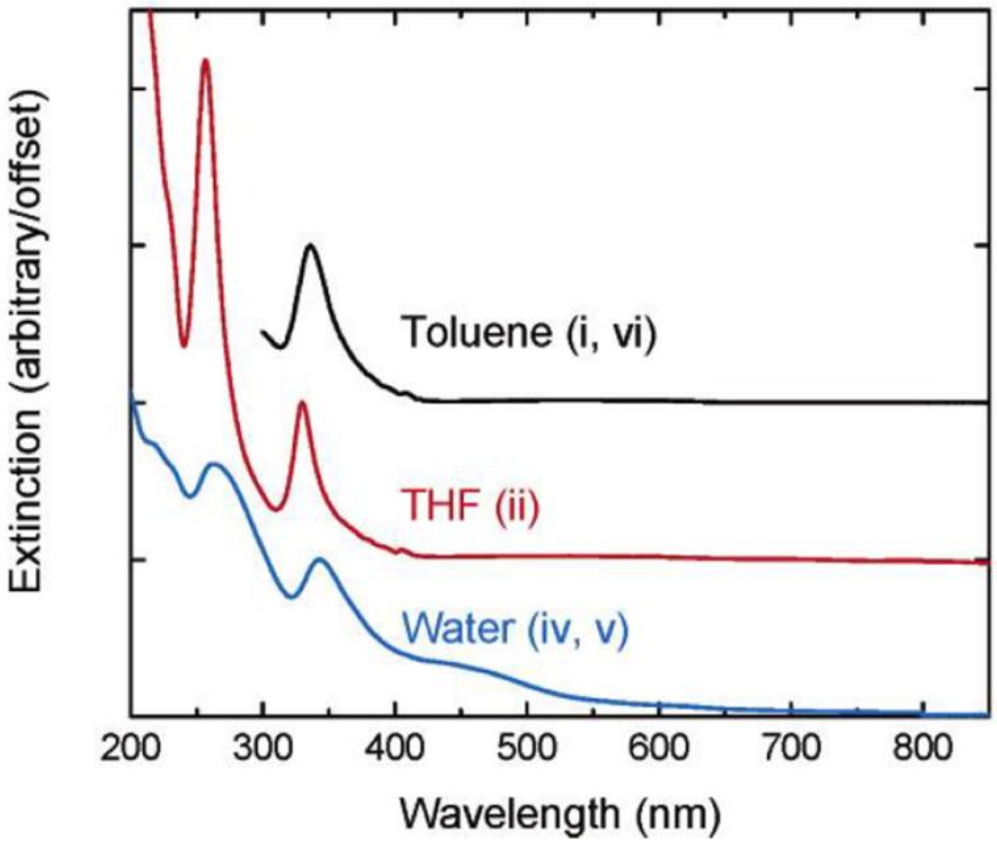

Figure 1.2: UV-vis spectra of C_{60} dissolved in different solvents.[6]

1.1.2. **Fullerene Chemical Reactivity**

Ground-state Reactivity

With 12 pentagonal rings and 20 hexagonal rings arranged as a symmetrical (icosahedral), closed-cage molecule, C_{60} is considered to be a highly stable compound with only sp^2 hybridized carbon system.[4] However, due to the arranged structure, there are no double bonds within the pentagon rings, which results in poorly delocalized (regional confined) electrons, and thus C_{60} is more reactive than initially expected, displaying both aromatic and olefinic-like properties.[10] Due to sp^2 carbons, which are typically strongly electron-withdrawing (inductive effects), fullerenes are normally electron-attracting (electrophilic).[12] The energy

difference between the lowest unoccupied molecular orbitals (LUMO, t_{1u}-symmetry) and the LUMO+1 (t_{1g}-symmetry) molecular orbitals is comparatively low, at 0.243 eV.[13] Therefore, C_{60} acts as an electron deficient compound and one molecule can accept up to 6 electrons in vacuum.[4, 14-19] In a mixed solvent with toluene and acetonitrile, the reduction of C_{60} was identified via cyclic voltammetry study with a reversible slow scan rate at 100 mV/s, and the stepwise half reduction potentials ($E_{1/2}$ of Fc/Fc^{+}) were characterized which ranging from -0.98 to -3.26 V.[15] Among all the possible reaction routes, addition reactions of C_{60} have been widely studied, leading to various fullerene derivatives which have been applied / suggested for a number of different fields, and include: cycloadditions[20, 21], bridging involved additions[22-24], and additions of separate (isolated) functional groups (e.g. hydrogen, halogens, etc.)[25-28]. Substitution reactions, which can only occur for fullerene derivatives, can be categorized, classically, as nucleophilic or electrophilic substitution.[10] For example, chlorinated C_{60} readily reacts with sodium methoxide, resulting in products such as $C_{60}(OMe)_{34}$.[29] Another important 'group' of C_{60} reactivity is polymerization, with two typical types as "pearl necklace" and "pendant chain" polymers-based arrangements.[10] For example, polymerization of C_{60} can be achieved through reaction with $Pd_2(dibenzylideneacetone)_3CHCl_3$, resulting $C_{60}Pd_n$, which was the first organometallic polymer of C_{60}.[30] Primary reaction routes of C_{60} are organized in Figure 1.3.

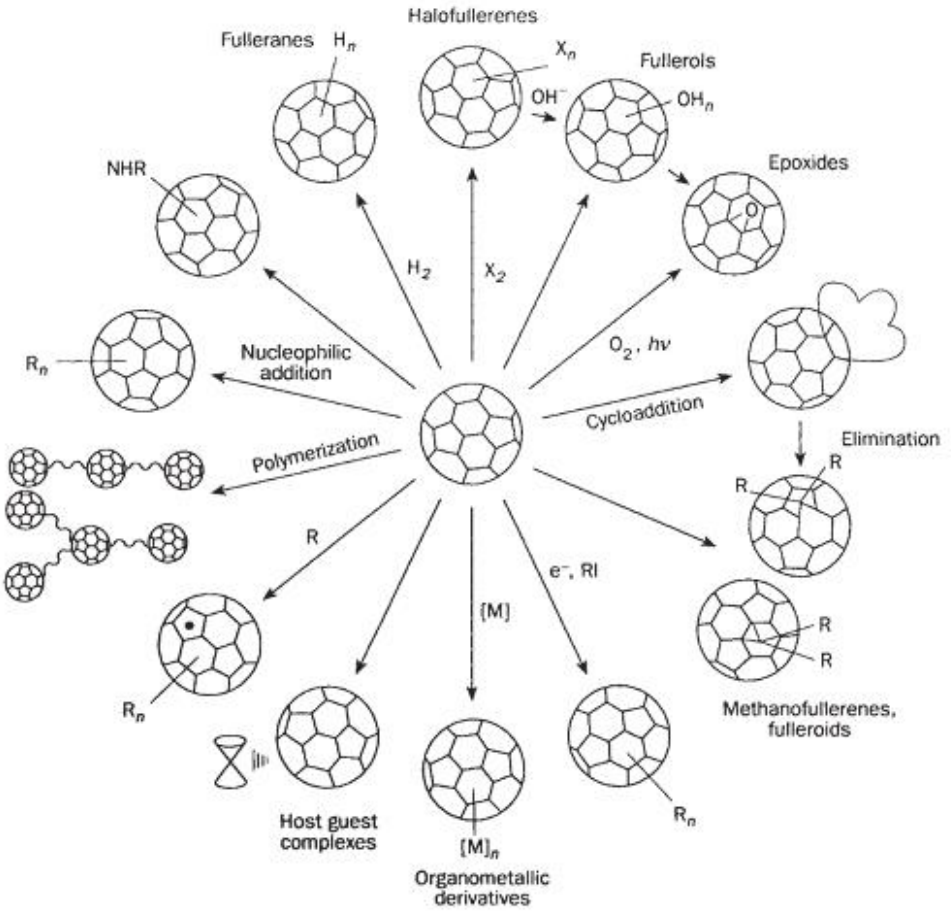

Figure 1.3: Primary C_{60} reaction routes.[10]

Photo-reactivity

C_{60} is known to be photo sensitive and easily excited to $^1C_{60}{}^*$ (state) from the ground singlet state ($^1C_{60}$), as well as being partially transformed to an excited triplet state ($^3C_{60}{}^*$) through intersystem crossing.[22, 31] The triplet excited state ($^3C_{60}{}^*$) is susceptible to various quenching processes, including ground state quenching, triplet-triplet annihilation, and self-quenching. The singlet oxygen ($^1O_2$), produced by the quenching of triplet excited state $^3C_{60}{}^*$ in presence of O_2, is also capable of accepting electrons from (other) electron donors, leading to the formation of superoxide radical ($O_2\bullet^-$). Additionally, there is an alternative pathway for electron

transfer to occur as triplet excited state $^3C_{60}^*$ can also accept an electron from other electron donor(s) and consequently transfer it to an electron acceptor. If said electron acceptor is oxygen, the superoxide radical ($O_2\bullet^-$) will be produced.[31, 32] Figure 1.4 shows possible electron transfer processes through C_{60} photo-excitation in the presence of oxygen and other appropriate electron donors.

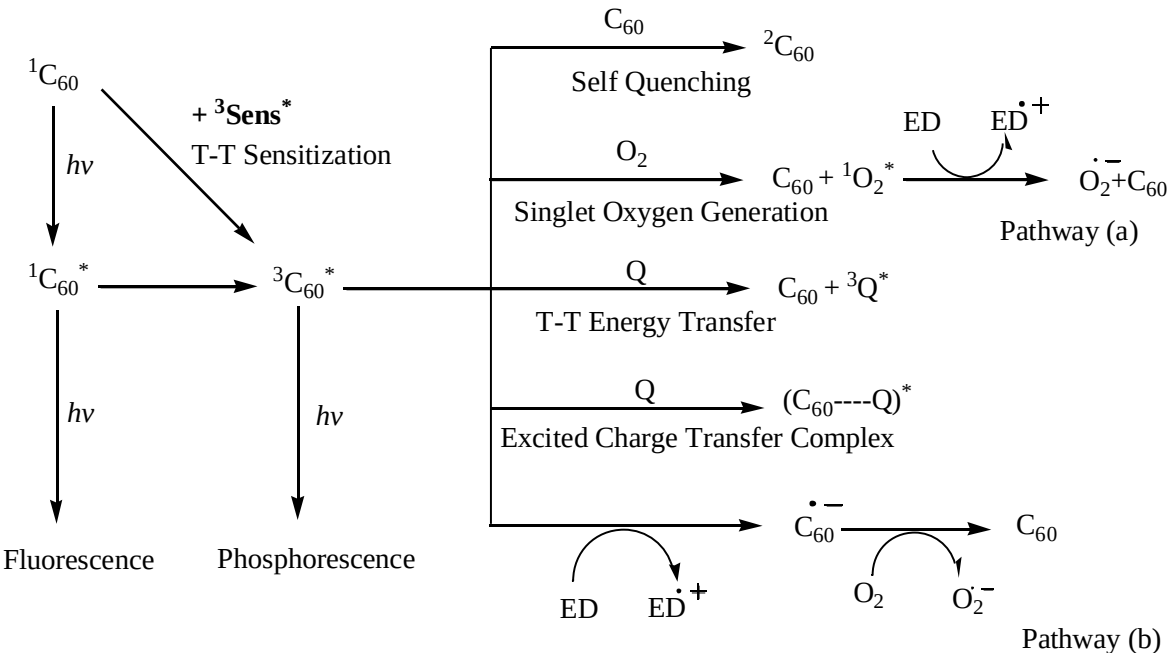

Figure 1.4: Photo-excited C_{60} electron transfer mediating scheme.[13, 32]

1.1.3. **Fullerenes in Water**

C_{60} exhibits exceedingly low solubility in polar solvents, including water, which is estimated to be 8 ng/L.[33] Despite such (seemingly) incompatibility, fullerenes are able to enter aqueous systems via the following routes[34]: (1) formation of nanoscale fullerene aggregates in the aqueous phase; (2) surface interaction/encapsulation with polymers or coatings, such as

natural organic matter (NOM) and surfactants; (3) chemical reactions resulting in covalent functional group additions that are polar in nature (e.g. oxygen-based moieties).

Water Stable C_{60} Aggregates (nC_{60})

The formation of water-stable, nano-scale, colloidal C_{60} aggregates, termed as 'nano-C_{60}' or 'nC_{60}', occurs through a number of processes including direct or indirect solvent exchanges,[6, 35-37] or even through simple, extended mixing of solid C_{60} with water (whereby no transfer solvent is used)[33, 38-40]. Stability and dispersion status of the resulting aggregates are mainly determined by the electrostatic repulsive forces created by the negative charges on the particle surface. One proposed charge transfer mechanism hypothesis, termed as "localized hydrolysis", has been proposed by Andrievsky et al. whereby hydrophobic C_{60} is stabilized by electron donor-acceptor (EDA) complexation with water, which can be expressed as $C_{60} + H_2O \leftrightarrow C_{60}(OH)^- + H^+$.[41] However, for this to occur, the energy barrier of exciting the electron for initiation of such a surface charge complex formation would require additional energy to the system.[42] Others also have suggested that hydroxyl ions sorption onto the C_{60} aggregates surfaces to provide as the net negative charge source.[43-45] The current state of theory with regard to nC_{60} surface negative charge formation is later discussed, in detail, within Chapter 2. Once formed, the physicochemical behavior of fullerene cluster is significantly different compared to the parent form, especially in aqueous environmental systems. Distinct from the solid-state fullerene, which undergoes assumingly heterogeneous reactions at the water-solid interface, water stable, nanoscale clusters/crystals of fullerenes should prove more reactive in the aqueous phase based on increasing surface area and/or dispersion status.[46, 47]

Hydroxylated fullerene (Fullerenol/Fullerol)

Hydroxylated fullerenes (termed as fullerenol or fullerol) are the most extensively studied fullerene family of derivatives and are soluble in water by orders of magnitude more than parent C_{60}, with a maximum solubility of 59 mg/mL (>10 orders of magnitude higher than C_{60}), upon extensive oxidation.[48] Used extensively as primers for the synthesis of fullerene-containing polymers in biomedical applications[36, 43], hydroxylated fullerene can be obtained through a variety of approaches. For example, polynitroadducts precursors $C_{60}(NO_2)_n$ can be hydrolyzed by NaOH to form $C_{60}(OH)_x$.[49, 50] Similarly, it can also be synthesized through the hydrolysis of polycyclosulfonated fullerene derivatives via reactions in NaOH solutions at room temperature.[51] Fullerols can also be prepared through the interaction of fullerene-borane derivatives with a mixture of H_2O_2 and NaOH.[52] Reactions of fullerene with metal potassium can produce water-soluble fullerols with ca. 27 hydroxyl groups.[53] In addition to controlled synthesis routes, fullerols were observed as the major product when water-soluble, C_{60} nanoscale aggregates (nC_{60}) are exposed to photo irradiation, including sunlight. Lee et al. studied the photochemical transformation of nC_{60} upon exposure to UVC irradiation (256 nm) and identified water-soluble hydroxylated fullerene (fullerol) as the major product.[54] Additionally, hydroxylation and surface oxygenation occurred upon exposure of nC_{60} to UVA irradiation (300-400 nm) in the presence of dissolved oxygen, with the intermediate product broadly identified as fullerol.[55] Hou et al. suggested that the products of a 947 h exposure of nC_{60} to sunlight had oxygen-containing functional groups and were similar to commercial fullerols ($C_{60}(O)_x(OH)_y$, where $x+y = 22$).[56]

Significant variations of the energy difference(s) between the highest occupied molecular orbital (HOMO) and lowest unoccupied molecular orbital (LUMO) have been observed in highly hydroxylated fullerenes.[57] Depending on the derivative, hydroxylated fullerenes can catalyze reactive oxygen species (ROS) via ultraviolet[58-61], visible light[60] and laser irradiation[22]. Further,

the reactivity of fullerol is largely dependent on the number and position(s) of hydroxyl groups.[62] For these systems, primary reactive oxygen species (ROS) include singlet oxygen and superoxide with secondary ROS (hydroxyl radicals, hydrogen peroxide and perhydroxyl radicals) produced by the subsequent (side chain) reactions.[60], In the dark, fullerols can act as an efficient ROS scavengers, including hydroxyl radicals[63], superoxide[64, 65] and hydrogen peroxide[66] - with higher scavenging activity for hydroxyl radicals (•OH), compared superoxide (O_2•$^-$).[67] As C=C bonds can be vulnerable to free radical attack, the electrophilic potential of the fullerol decreases and the free radical scavenging ability is diminished for higher levels of hydroxylation.[67]

1.2. Research Significance

Since their discovery, fullerenes have been detected in nature, occurring in materials produced by high-energy, oxygen limited events, such as lightening striking carbonaceous earth and even at meteor impact sites (e.g. K2 boundary layer).[68-70] C_{60} was also found in soot generated from the combustion of hydrocarbons (coal) [71], as well as from simple candle flame soots.[69] Besides pristine (parent) fullerene as C_{60}, fullerene derivatives (e.g. hydroxylated fullerene, hydrogenated fullerene, carboxylated fullerene, oxygenated fullerene, amino fullerene, etc.) have been produced with specific, yet different material properties, including specific (and highly varied) biological response(s). Finally, oxidized fullerene derivatives (e.g. fullerol) have also been shown to occur naturally, as discussed above.[54, 55, 72, 73]

With now realized that industrial scale use for a variety of applications, including electronics, solar cells, pharmaceuticals, optics, lubricants, and cosmetics[49, 74-76], the probability of fullerenes to inadvertently enter the environment is highly likely. In this context, the chemistry

of fullerenes as it relates to abiotic transformations, transport, and eventual fate, to date, has not been quantitatively characterized with many common environmental reactants/reaction scenarios. In (environmentally) relevant reduction-oxidation conditions, cycling reaction kinetics, and pathways of pristine fullerene and corresponding daughter species will likely guide the ultimate material risk as it relates both to exposure in nature and human beings. In other words, the environmental chemistry will, to a high degree, determine the stable daughter species in (longest) contact with biota. Therefore, a comprehensive understanding of the chemical behavior of fullerenes and their environmental derivatives, focused here on aqueous systems, is essential toward the accurate evaluation of the toxicity risk and appropriate formulation of effective waste disposal/management design and protocols.

1.3. Research Objectives

The overall research objective of this Ph.D. thesis aims to identify and detail, key oxidative and reductive pathways, reaction kinetics, and resulting derivatives of fullerenes, using C_{60} as a model material, in aqueous systems. This work, for the first time in many cases, provides quantitative data needed to understand the material's life cycle with regard to transformation processes (within the carbon cycle). Specific objectives of this thesis include:

Objective 1: Quantitatively elucidate surface reactions associated with aqueous solvation processes of hydrophobic fullerenes (fullerene aggregation formation and molecular derivatization) at the solid-liquid / aggregates interfaces.

Objective 2: Identify and elucidate additional (secondary) transformation pathways of water-stable and soluble fullerene in common oxidizing (aqueous) environments. Reaction descriptions

aim to quantify the transformation pathways, products, and inform basic kinetic modeling efforts.

Objective 3: To identify and elucidate transformation pathways, kinetics and products of oxidized C_{60} derivatives within reducing aqueous systems/reactions.

1.4. Overview of Dissertation

Based on the stated objectives, this dissertation is structured around three tasks, which are organized in Figure 1.5. Each task is addressed in one or two subsequent chapters, with additional background, motivation, experimental approach/methodology and frame of reference also provided, accordingly.

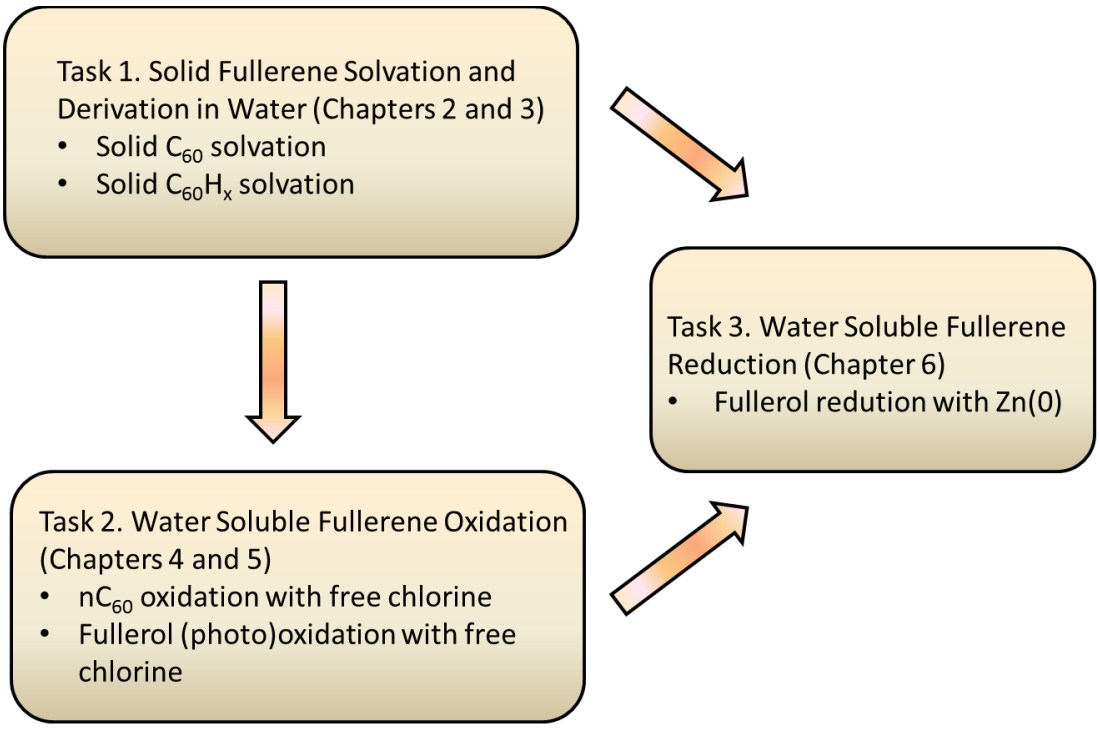

Figure 1.5: Overview of research tasks.

Task 1: Solid State Fullerene Solvation and Derivation in Water

Task 1 is addressed in Chapters 2 and 3. Solvation processes of solid hydrophobic fullerene and hydrogenated fullerenes (termed as fulleranes, $C_{60}(H)_x$) were evaluated through batch experiments under a series of environmentally relevant conditions. For these systems, solvation (reaction) kinetics were described and compared within different reacting scenarios, including those in ground-state and photo-excited (UVA) state. Reactive oxygen species (e.g. •OH, $^1O_2$, and $O_2•^-$) were observed to be key reactants during all solvation processes; and their relative contributions were quantitatively described with multiple regression models. Transformations products were characterized and described through a battery of analytical techniques and instrumentation, including FTIR, XPS, DLS, and TEM.

Task 2: Water Soluble Fullerene Oxidation Reaction Kinetics and Pathways

Task 2 is addressed in Chapters 4 and 5. In Task 2, oxidation pathways of the fullerene aggregates and fullerene derivatives (nC_{60} and fullerol, respectively) were explored in the presence of electron acceptors (free chlorine here), with corresponding reaction kinetics and mechanisms detailed. Each process was evaluated under both dark and photo-irradiation conditions as batch reactions. Parent materials, intermediates, and stable products were analyzed by a suite of analytical approaches (^{13}C-NMR, FTIR, XPS, Raman Spectroscopy, QCM-D, partitioning experiments, etc.). The reaction pathways and mechanisms were identified and illustrated through integration of kinetics modeling and resulting product characterization.

Task 3: Water Soluble Fullerene Reduction Reaction Kinetics and Pathways

Task 3 is addressed in Chapter 6. Reduction of water-soluble oxidized fullerene (fullerol) was described with zero-valent zinc (Zn(0)). Reaction kinetics was compared through

batch experiments under a series of environmentally relevant conditions (e.g. oxidation-reduction potentials, dissolved oxygen). Resulting products were characterized and described through ^{13}C-NMR, FTIR, XPS, UV-vis, DLS, and TEM analyses. In addition, (surface) physical properties were evaluated through traditional water-octanol partition experiments and QCM-D measurements. Finally, a reduction mechanism is proposed.

Conclusions are summarized in Chapter 7 along with recommendations for future research.

Chapter 2 :**Photo-enhanced Fullerene Solvation in Water: Reactive Oxygen Species Generation and Roles in nC_{60} Formation Process**

Abstract

Despite negligible water solubility, solid fullerenes (e.g. C_{60}, C_{70}) have been widely reported to become available in water through extended stirring (without transferring solvents), forming stable nano-scale C_{60} aggregates (termed as aqu/nC_{60}). However, to date, mechanistic understanding of such colloidal formation(s) remains outstanding. To address this, photo-enhanced nC_{60} formation through the extensive mixing of solid fullerene powder in water is fundamentally described in this work through a matrix of batch reaction experiments over a range of environmentally relevant scenarios (e.g. oxidation-reduction potentials, photo-irradiation, etc.). Formation kinetics indicates that electron acceptors (e.g. dissolved oxygen/ROS) and photo-irradiation simultaneously play key roles in the colloidal (nC_{60}) formation process. nC_{60} formation rates were correlated with concentrations of reactive oxygen species using simple and multiple linear regression models with relative contributions observed to be: $\bullet OH > {}^1O_2 > O_2\bullet^-$. Advanced surface characterizations using XPS and FTIR indicate nC_{60} surfaces were oxidized as a function of ROS concentration.

2.1. Introduction

Fullerene materials are now produced at the industrial scale[77, 78] and applied in a variety of fields (e.g. electronic materials, superconductor, fuel cells, cosmetics and medical therapeutics).[79-83] As a model fullerene, C_{60} is extremely hydrophobic, resulting in very low water solubility (ca. 10^{-9} mg/L).[11, 84, 85] However, the *availability* of C_{60} in water can be enhanced by ~11 orders of magnitude (up to 100 mg/L) through the formation of the water-stable, colloidal nanoscale aggregates termed here as "nano-C_{60}" (nC_{60}). nC_{60} formation has been reported mostly through solvent exchange methods, starting with dissolution of C_{60} in organic solvents, such as tetrahydrofuran (THF), toluene, acetone and ethanol, before mixing into (forming) water. Organic transfer solvents can then be subsequently removed through distillation, sonication, and/or solvent exchange.[6, 35, 36, 43, 86] Without a transfer organic solvent, Cheng et al. observed that, through extended mixing of C_{60} powder, in water, a yellow suspension of "small stable aggregates" with the size of 1-3 μm in diameter was formed after two days.[87] Different from a "bottom-up" approach through solvent exchange process, bulk solid powder C_{60} was mechanically broken up through mixing, seemingly experiencing a "top-down" process of colloid formation in water.[38-40, 88] Since, others have also observed this phenomenon with a large size range of nC_{60} reported (from ~10 to 3000 nm), which is also termed as aqu/nC_{60}.[38-40, 45, 87-92] When compared to solvent exchange methods, these materials exhibited less crystallinity and typically larger (size) dispersivitiy (smooth and round for smaller clusters, blunt and angular for large clusters).[40, 89, 90, 93] Dhawan et al. evaluated the genotoxicity of aqu/nC_{60} towards the response of human lymphocyte, demonstrating that there is stronger associated genotoxicity of aqu/nC_{60} than with EthOH/nC_{60} (ethanol to water solvent exchange).[86] Antibacterial activity of aqu/nC_{60} was also demonstrated with *Bacillus subtilis*, with minimal inhibitory concentrations

(MIC) observed to be less than 1 mg/L, which is 1 order magnitude less than that of THF/nC_{60} (THF to water solvent exchange).[40]

Compared with controlled solvent exchange synthesis approaches, simple mixing of C_{60} in water reflects a more likely pathway for environmental release/exposure. There have been a variety of mechanisms proposed for this phenomenon. Chang et al. proposed simultaneously occurring "top-down" and "bottom-up" processes (compared with solvent exchange routes) for nC_{60} formation in the presence of carboxylic acids in water.[38] After reducing the pristine size of C_{60} to 20 ~ 100 nm with hand-grinding in agate mortar, hydrophobic C_{60} powder was found being dispersible (17 wt. % total) in water even without the aid of surfactant/solvent.[94] As reported by previous studies, (negative) charge formation on aqu/nC_{60} clusters surfaces (zeta potential from -20 to -60 mV), provides repulsive electrostatic interactions endowing aqueous stability of nC_{60}.[39, 45, 86, 91, 93] For nC_{60} generated through solvent exchange processes, the negative surface charge is hypothesized to originate from organic solvent molecules (for example, as for THF as the transfer solvent, it occurred between ether oxygen to C_{60} molecule).[41, 44] For aqu/nC_{60}, with a less negative charge compared with solvent/nC_{60}, interactions with aqueous constituents can only be considered. Brant et al. hypothesized that a hydration process was the main source of aq/nC_{60}'s negative surface charges.[4] It was also proposed that adsorption of hydroxyl ions on the fullerene cluster surface, or that fullerene can being surrounded with clathrate-like icosahedral water cluster via weak hydrogen bonding, may be responsible for the negative charge formation.[41, 45] It has also been revealed that the formation of aqu/nC_{60} is affected by solution chemistry, such as solution pH, types and concentrations of electrolytes, natural organic matters (NOM), carboxylic acids, initial C_{60} concentration, and particles size, etc.[38, 45, 88, 90, 91, 95, 96] Other studies have reported that the formation of aqu/nC_{60} was significantly

enhanced in the presence of NOM, forming colloids with smaller sizes and more uniform distribution.[90, 95, 96] Steric effects (hindrance) exerted by NOM molecules adsorbed on nC_{60} surface was proposed as the major factor controlling the stability of these systems.[90, 95] It has also been shown that under sunlight irradiation, the dispersion of nC_{60} with NOM was shown to be dramatically enhanced, with a smaller size distribution. Under these conditions, it was hypothesized that a small amount of transformed (oxidized) nC_{60} adduct on the pristine nC_{60} surface in the presence of NOM, plays a significant role in suspending aqu/nC_{60}.[91, 95] In the absence of NOM, Indeglia et al. recently reported that the formation kinetics of aqu/nC_{60} was significantly enhanced under ambient light irradiation.[92] It was suggested that increased amounts of partially mono-oxygenated derivatives (early-stage as epoxide groups; late-stage as hydroxyl groups), produced through reactive oxygen species in the presence of light, were involved in the repulsion forces between particles.[92] Murdianti et al. suggested that aqu/nC_{60} formation strongly relied on the small quantity of an [6,6]-closed epoxide derivative, which was produced through exposure to ambient ozone.[97] As previously reported, partially oxidized C_{60} cluster surfaces play a crucial role in the dispersion/formation of aqu/nC_{60} through extensive mixing in water.

Fullerene photo-reactivity has been extensively studied and a variety of reactive oxygen species have been demonstrated in the presence of oxygen and light.[4] Among fullerene-based photocatalytic systems, singlet oxygen ($^1O_2$) has been identified as the primary species produced (in the presence of electron acceptors, e.g. O_2), superoxide can be produced with an effective electron-donor; and hydroxyl radicals can be generated as a secondary ROS species after primary oxygen species formation.[58, 98-101] Regarding the photo-reactivity of fullerenes in aqueous phase, it has also been demonstrated that singlet oxygen and superoxide can be generated upon irradiating a nC_{60} suspension[102], furthermore, water-soluble oxygenated fullerene derivatives (e.g.

fullerols) were proved to show higher ROS production efficiency under UV or sunlight irradiation compared with nC_{60}[60, 102, 103]. Besides ROS generation, C_{60} itself in triplet excited state ($^3C_{60}^*$) under photo-irradiation is susceptible to various deactivation processes (e.g. ground-state quenching, triplet-triplet annihilation, etc.), thus exhibiting enhanced reactivity compared to the ground-state.[4]

In this study, aqu/nC_{60} formation, through extensive mixing in water and under a variety of environmentally relevant conditions, was investigated through a matrix of batch experiments. *For the first time*, three types of possible involved ROS ($^1O_2$, $O_2\bullet^-$, and •OH) were monitored during the solvation processes, and the relationships between aqu/nC_{60} formation rates and ROS concentration were quantitatively correlated. Solvated products under different experimental conditions were characterized using Fourier transform infrared spectroscopy (FTIR), total organic carbon (TOC) analysis, and X-ray photoelectron spectroscopy (XPS).

2.2. Materials and Methods

2.2.1. **Materials**

C_{60} and fullerol ($C_{60}(OH)_x(ONa)_y$, y=8-10, x+y ~24, purity > 99%) were purchased from MER (Tucson, AZ). Fullerol stock suspensions (40 mg/L) were prepared by adding powder fullerol to ultrapure water and stirring for 24 hours in the dark. The golden colored suspensions were vacuum filtered through 0.22 μm PES membrane (Corning, NY) and stored in the dark at room temperature (21.0 ± 1.0 ℃). nC_{60}/THF suspensions were prepared through solvent exchange using C_{60} saturated tetrahydrofuran (THF) solution following the method described by Fortner et al.[6] The residual THF in suspension was removed in a stirred-cell membrane unit (Amicon, molecular weight cutoff (MWCO) of 10,000 Da) through > 99.5% (volume) water

replacement. Fullerol and nC_{60}/THF solutions remained stable in water for months based on the measurement by UV-vis, DLS, and visual inspection. Hydrogen peroxide, furfuryl alcohol, sodium benzoate, 4-hydroxybenzoic acid, trifluoroacetic acid, methanol, acetonitrile were all purchased from Sigma Aldrich (St. Louis, MO). The purities of all chemicals are at reagent level and solvents are at HPLC level.

2.2.2. **Aqu/nC_{60} Formation Batch Experiments**

The solvation experiments were conducted as batch reactions with 0.5 g/L solid C_{60} powder extensively mixed via magnetic stirring (500 rpm) in 50 mL of ultrapure water in customized quartz reactors (Technical Glass Products) under a series of environmentally relevant conditions, listed in Table 2-1. Photo-irradiated experiments were conducted in a customized bench-scale photo-reactor built with two circuitous monochromatic UV-A lamps (BHK, CA) on each wall and fans on each side for heat dissipation. For photo-irradiation conditions, the light intensity was initially calibrated to (2000 ± 50 μW/cm^2) with a radiometer (UVP, Inc.), and was monitored regularly during the reactions (corrected if needed). The solvation experiments were also conducted with different dissolved oxygen concentrations during the reactions. For anaerobic and 5% oxygen conditions , solutions (50 mL) were sparged with N_2 gas and 5% oxygen/N_2 (Airgas, Bowling Green, KY) for at least 1 hour before the reaction, to reduce the dissolved oxygen concentration to 0.3 ± 0.1 ppm and 2.1 ± 0.3 ppm, respectively. The dissolved oxygen concentrations for the above conditions were maintained by Teflon crimp-sealed caps (Wheaton Industries Inc.) and sparged with N_2 or 5% oxygen/N_2 gas for 30 minutes after every sampling, leaving the sealed reactor with a slightly positive pressure. For aerobic conditions, the reaction solutions were open to the air and the dissolved oxygen concentrations remained at 8.9 ± 0.5 ppm during the reaction. The DO concentrations of the reacting solutions were tested initially

and monitored with a microprobe DO meter (Neofox system, Oceanoptics) during the reaction. Hydrogen peroxide was also added initially into 0.5 g/L C_{60} solutions to achieve the concentrations at 0.025%, 0.05%, 0.1%, and 0.25% (w/w). Also, fullerene derivatives were created initially through mixing 0.5 g/L C_{60} solution with 5 mg/L fullerol or 2.5 mg/L THF/nC_{60}. During the reactions, sample aliquots were taken and filtered with 0.45 μm PES membranes (Millipore Corporation, MA) to separate and collect solvated products in water. UV-vis spectra (190-800 nm) of the solvated products were obtained by a Varian Cary Bio50 UV-vis spectrometer (Agilent Technology, CA). The absorptions at a wavelength of 340 nm (as one of $^1T_{1u}$-^1A_g transition peaks, molar adsorption coefficient = 4.486×10^4 $M^{-1}cm^{-1}$) were selected to identify the concentration of formed nC_{60} during the solvation experiments because the concentrations of nC_{60} was linearly correlated to that measured via HPLC after extraction to toluene.[47, 54, 55, 84] To create the conditions with different levels of ROS, t-BuOH (100 mM) was initially added into the system in the presence of H_2O_2 with selected concentrations (Table 2-1). All of the above experiments were conducted in duplicate at room temperature (21.0 ± 1.0 ℃). Dark control experiments were also conducted and listed in detail in Table 2-1. Solvated C_{60} products in water (filtered with 0.45 μm membrane) were collected at the end of the reaction (3 days) for TOC analyses with a TOC-L total carbon analyzer (Shimadzu Scientific Instrument, Inc., MD).

2.2.3. **Reactive Oxygen Species Concentration Measurement**

The concentrations of the possible involved reactive oxygen species, •OH, $^1O_2$, and O_2•$^-$, were monitored over the reactions, using specific molecular probes and assays. For detection of hydroxyl radicals' concentration, 10 mM sodium benzoate (BA), as the indicator, was added initially into the reactions under different experimental conditions listed in Table 2-1. The

concentrations of p-hydroxybenzoic acid (p-HBA) and sodium benzoate were measured using a Waters e2695 HPLC (Waters Corporation, MA) equipped with Waters 2648 UV-vis detector and a Cosmosil C18-PAQ column (4.6×250mm). The mobile phase was a mixture of acetonitrile and 1% TFA/water (65:35, v/v) at 1 mL/min. The wavelengths for p-HBA and sodium benzoate quantification were 255 and 270 nm, respectively.[104] Here, p-HBA was detected under certain conditions with comparably lower levels of hydroxyl radicals (the change of BA concentrations was below detection limit). The reactions and reaction rates between hydroxyl radical and benzoate acid can be expressed as[104, 105]

$$\bullet OH + BA \rightarrow \text{Intermediates} \quad (k_B = 4.3 * 10^9\ M^{-1}s^{-1}) \qquad (1)$$

$$-\frac{d[BA]}{dt} = 5.87\frac{d[p\text{-}HBA]}{dt} = k_B[BA][\bullet OH] \qquad (2)$$

The concentration of $^1O_2$ were determined using furfuryl alcohol (FFA, 10 mM) as an indicator and quantified by HPLC with the mobile phase as the mixture of methanol and water (1:1, v/v) at 1 mL/min at wavelength of 219 nm.[106] The reaction and reaction rates for $^1O_2$ reacting with FFA can be expressed as[102, 107]:

$$^1O_2 + FFA \rightarrow \text{Products} \qquad (k_F = 1.2 \times 10^8\ M^{-1}s^{-1}) \quad (3)$$

$$-\frac{d[FFA]}{dt} = k_F[FFA][^1O_2] \qquad (4)$$

Productions of $O_2\bullet^-$ were quantified by the spectrophotometric methods using 2,3-Bis(2-methoxy-4-nitro-5-sulfophenyl)-2H-tetrazolium-5-carboxanilide (XTT) sodium salt as an indicator. The stock solution was prepared and stocked for no longer than one week at 4^{o}C. The products of XTT-formazan were formed through XTT reduction by $O_2\bullet^-$, the concentration of which was measured using UV-vis spectroscopy with a wavelength of 470 nm.[108, 109] The

concentration of XTT formazan generated was calculated with the molar extinction coefficient 2.16×10^4 $M^{-1}cm^{-1}$. The reaction and reaction rate between superoxide and XTT can be expressed as[109]:

$$XTT + 2O_2\bullet^- + H^+ \rightarrow \text{XTT Formazan (Reduced)} + O_2 \quad (k_X = 8.59 \times 10^4\ M^{-1}s^{-1}) \quad (5)$$

$$-\frac{d[XXT]}{dt} = \frac{d[\text{XTT Formazan}]}{dt} = k_X[XTT][O_2\bullet^-] \qquad (6)$$

Here, the concentration of each reactive oxygen species (•OH, $^1O_2$, and $O_2\bullet^-$) at steady-state were employed to quantitatively evaluate the roles of those during nC_{60} formation. These concentrations can be calculated by (indicator degradation reactions followed different reaction rate laws, shown in Figure S2.1-S2.3) equation (7) and (8):

$$[ROS]_{ss} = \frac{k_{obs}}{k*[\text{Indicator}]_0} \qquad (7)$$

$$[ROS]_{ss} = \frac{k_{obs}}{k} \qquad (8)$$

Equations (7) and (8) were employed if indicator degradation followed zero-order reaction and first-order reaction, respectively. $[ROS]_{ss}$ is the calculated steady-state concentration of three types of reactive oxygen species, $[\text{Indicator}]_0$ is the initial concentration of BA, FFA, and XTT, k_{obs} is the experimentally derived zero-order or first-order rate constant (simulated in Figure S2.1-S2.3), and k (k_B, k_F, and k_X) is the rate constant for the reaction of ROS (•OH, $^1O_2$, and $O_2\bullet^-$) towards the corresponding indicator (Equation (1), (3), and (5)). Control experiments in pure water system (no solid C_{60}) were conducted in order to remove the ROS background derived from water with UV irradiation.

2.2.4. **Products Characterization**

Solvated nC_{60} products were collected at the end of the reaction for 3 days, and those formed in the presence of different levels of H_2O_2 were washed with a stirred-cell (Amicon, molecular weight cut-off (MWCO) of 1000 Da) for at least 5 times until the residual H_2O_2 background was completely removed (indicated by UV-vis spectra and pH of the out-flow solutions). Here a low MWCO membrane (1000 Da) was used in order to avoid losing partial oxidized fullerene soft clusters. The solvated products were analyzed by attenuated total reflection Fourier transform infrared spectroscopy (Nexus 470 FT-IR, Thermo Nicolet, NC) with a ZnSe trough. Liquid samples in the trough were dried in a vacuum oven (Thermo Scientific, NC) at room temperature. For XPS analyses, solvated fullerene products were dried on lithium wafers (Sigma Aldrich, MO) in the vacuum oven at room temperature by dropping samples until the total volume reached to ca. 1 mL. XPS spectra were obtained by using a Physical Electronic 5000 Versa Probe II Scanning ESCA Microprobe with an Al K-α X-ray source at 23.5 eV pass energy at a 100 μm X-ray spot size.

2.3. Results and Discussion

Figure 2.1 shows C_{60} solvation occurring (i.e. aqu/nC_{60} formation) upon mixing solid fullerene in pure water over a range of reaction scenarios. As indicated by both the products solution's golden color hue (left) and resulting UV absorption spectra (300 – 600 nm) with $^1T_{1u}$ - ^1A_g transition peaks (right), nC_{60} formation was monitored over time.[4, 6] nC_{60} formation was also confirmed with periodic DLS and TEM measurements. In general, mixing solid C_{60} in water for 3 days, nano-scale C_{60} aggregates were formed in the presence of light (351 nm, reactor described above) and oxygen (Figure 2.1 (iv)-(vii)), whereas in the absence of light (Figure 2.1 (i)

and (ii)), even under aerobic conditions (DO ~ 9 ppm), no obvious formation was observed after 3 days (clear heterogeneous system). In the presence of H_2O_2, significant formation enhancement was observed under similar photo irradiation (Figure 2.1(vi) and (vii)). In contrast, negligible formation occurred with H_2O_2 under dark conditions (Figure 2.2c). Complicating these results is the fact that not only C_{60} is photo-excited under these irradiation conditions, but that H_2O_2 degrades under UVA irradiation to form hydroxyl radicals.[110]

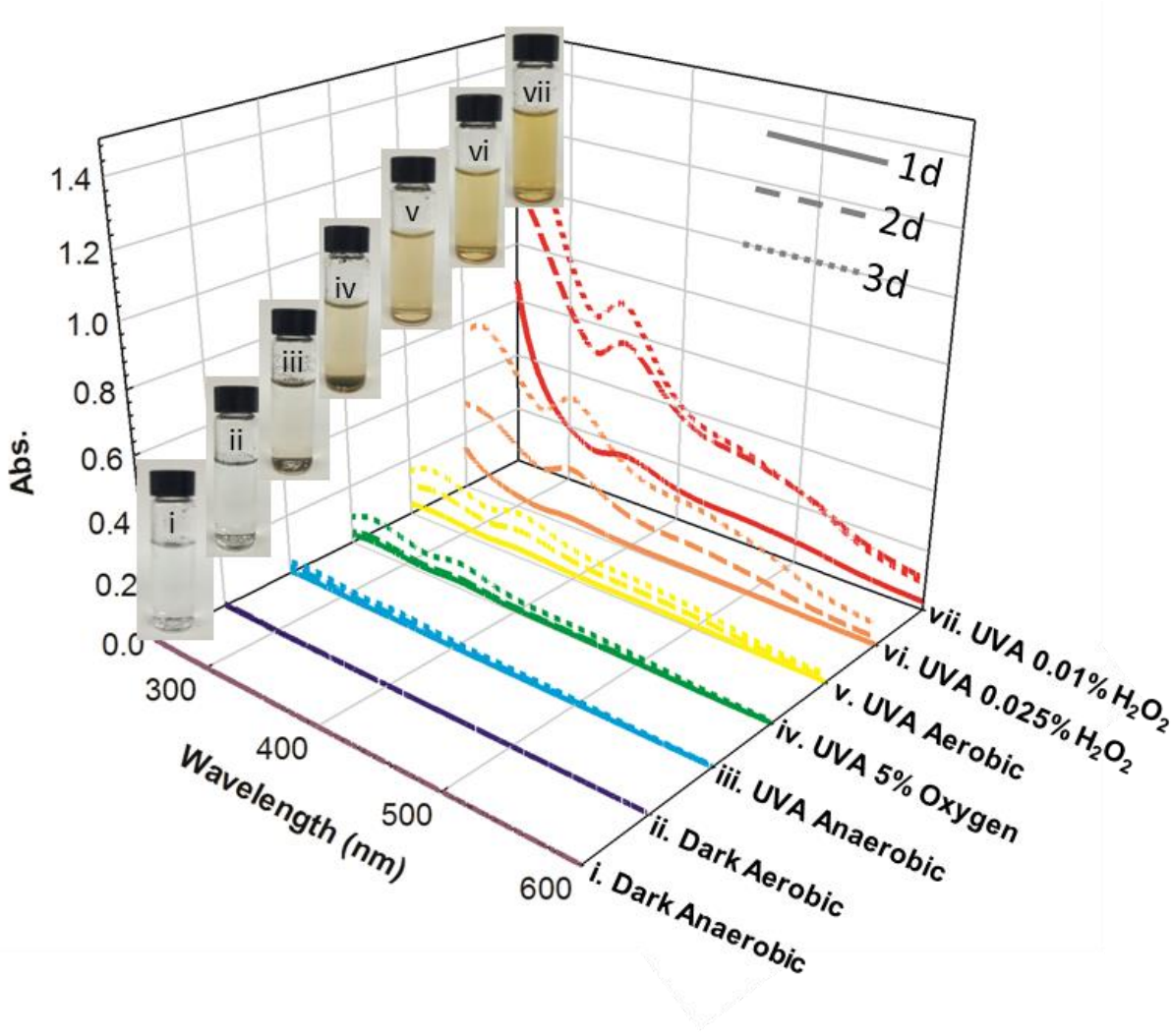

Figure 2.1: nC_{60} formation in water and corresponding UV spectra (0.5 g/L solid C_{60} stirred) under varied experimental conditions for 3 days: (i) dark anaerobic; (ii) dark aerobic; (iii) UVA

(351 nm, 2 mW/cm^2) anaerobic (DO ~ 0.3 ppm); (iv) UVA, 5% Oxygen atmosphere (DO ~ 2.5 ppm); (v) UVA aerobic (DO ~ 9 ppm); (vi) UVA aerobic condition with initial 0.025% H_2O_2; (vii) UVA aerobic condition with initial 0.1% H_2O_2.

UV adsorption at 340 nm, taken here as the characteristic absorbance C_{60} peak ($^1T_{1u}$-^1A_g transition peak), was selected to investigate the (aqu/)nC_{60} formation kinetics under different experimental conditions (listed in Table 2-1). Results are summarized in Figure 2.2. Formation rates for all reacting scenarios were observed to be zero-order which is likely due to excess reacting (solid) surface areas of bulk fullerenes system. Under photo-irradiation (UVA 351 nm, 2 mW/cm^2), with varied levels of dissolved oxygen (ca. 0.3 ppm - 9 ppm), aqu/nC_{60} formation rates increased with increasing DO concentration (Figure 2.2a). As mentioned, C_{60} is photo sensitive under UVA irradiation, and can be excited to $^1C_{60}^*$ from a ground singlet state ($^1C_{60}$), as well as partially transformed to excited triplet state ($^3C_{60}^*$) through intersystem crossing.[22, 31] The triplet excited state $^3C_{60}^*$ is susceptible to various quenching processes, among which (in the presence of O_2) singlet oxygen formation has been widely demonstrated.[4, 72] In the presence of singlet oxygen and corresponding with other ROS, it is hypothesized here that the formation rates will be enhanced due to partial oxidation on the surfaces of bulk fullerene or small fragments fullerene (after mechanical break-up). This hypothesis includes the potential for additional/other surface reactions with •OH and O_2•$^-$, which are also produced via electron transfer to $^1O_2$.[111, 112] Further, the electron rich properties of C_{60}, with delocalized, conjugated π-systems, are favorable candidates for electrophilic addition process.[4, 10] It should be noted that, under UV irradiation with oxygen, further oxidation of stable C_{60} clusters (nC_{60}) may also happen simultaneously along with the nC_{60} formation process, resulting in soluble oxidized fullerene derivatives (e.g. fullerol) production, as observed by others.[54, 72] In order to evaluate the

effect(s) of such oxidized fullerene intermediates or nC_{60} itself during the solvation process, commercial fullerol ($C_{60}(OH)_x(ONa)_y$, y=8-10, x+y ~24, purity > 99%, MER) and THF/nC_{60} (through THF/water solvent exchange approach[6]) were selected and added into the reacting systems (C_{60} powder / UVA light) with initial concentrations of 5 mg/L and 2.5 mg/L, respectively. These formation kinetics are shown in Figure 2.2b with an obvious enhancement of aqu/nC_{60} observed in the presence of 5 mg/L fullerol, which we hypothesize is due to additional ROS production by the fullerol amendment.[60, 102, 103] In the presence of THF/nC_{60}, formation rates were not observed to change. Reaction kinetics in Figure 2.2c clearly shows that nC_{60} formation rates were significantly enhanced as a function of H_2O_2 concentration. Specifically, as the concentration of H_2O_2 reach 0.25% (w/w), the nC_{60} formation rate was approximately one order of magnitude higher compared with control system (no H_2O_2 added), suggesting that there is likely hydroxyl radical (from H_2O_2 photolysis) involved in the aqu/nC_{60} formation process(es). Under dark conditions, with an even higher concentration of H_2O_2 (0.5%), no obvious formation was observed (Figure 2.2c), excluding the effect/reaction directly with H_2O_2. To further clarify the roles of ROS, individual species concentrations were also monitored during solvation processes (Figure S2.1-S2.3). In addition, the total organic carbon (TOC) of solvated products after 3 days reactions, as shown in Figure 2.1b, increased with the electron acceptor concentration (oxygen, H_2O_2), which is consistent with the kinetics results from UV-vis analyses.

Table 2-1: Experimental conditions and results summary of nC_{60} formation kinetics

No.	Experimental Conditions	nC_{60} Formation Rates and ROS Steady State Concentrations				
		TOC[a] (mg/L)	nC_{60} (Abs/s*10^{-7})	$[^{\bullet}OH]_{ss}$ (M/s*10^{-17})	$[^1O_2]_{ss}$ (M/s*10^{-14})	$[O_2^{\bullet-}]_{ss}$ (M/s*10^{-12})
#1	Anaerobic (Dark)[b]	0.21±0.02	----	----	----	----
#2	Aerobic (Dark)	0.24±0.09	0.04±0.03	----	----	----
#3	Anaerobic[c]	0.39±0.13	1.39±0.18	0.10±0.037	0.34±0.12	0.73±0.01
#4	5% Oxygen	0.92±0.37	3.06±0.55	0.46±0.037	0.69±0.10	0.92±0.05
#5	Aerobic	3.87±1.30	5.27±0.26	0.54±0.005	1.33±0.15	1.36±0.07
#6	Aerobic+5mg/L Fullerol	----	8.10±0.83	4.42±0.27	2.11±0.21	1.11±0.14
#7	Aerobic+2.5mg/L nC_{60}	----	6.43±0.86	6.35±0.94	1.18±0.20	1.24±0.07
#8	Aerobic+0.025% H_2O_2	8.31±1.79	9.72±7.63	84.61±11.84	12.76±0.29	4.49±0.96
#9	Aerobic+0.05% H_2O_2	10.25±1.29	16.1±4.89	113.84±14.64	20.73±0.73	7.03±1.08
#10	Aerobic+0.10% H_2O_2	12.32±0.95	25.6±4.91	158.69±8.67	35.96±9.65	8.94±1.32
# 11	Aerobic+0.25% H_2O_2	29.65±1.76	56.9±0.84	254.43±43.08	68.56±0.10	13.06±0.95
# 12	0.025%H_2O_2+100 mM t-BuOH[d]	----	2.05±0.55	36.90±9.27	3.65±0.15	1.77±0.39
#13	0.1% H_2O_2+100mM t-BuOH[d]	----	3.20±1.40	55.92±0.79	6.19±0.28	2.34±0.23
#14	Aerobic+0.25% H_2O_2 (Dark)	----	0.34±0.06	----	----	----

a. TOC of the solvated products were obtained after 3-day reaction; b. Dark conditions; c. All the conditions without marked as "dark" are under photoirradiation with UVA at 351 nm as intensity of 2 mW/cm^2; d. Condition within aerobic environments under photoirradiation.

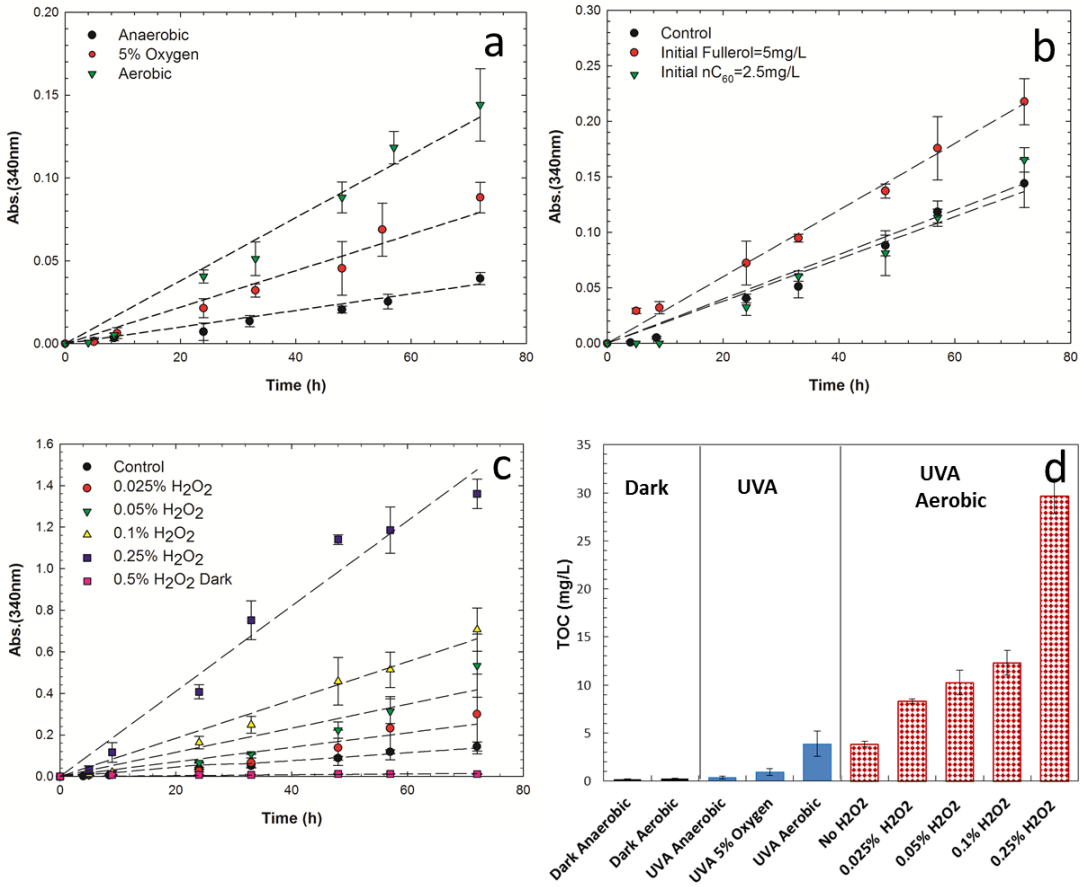

Figure 2.2: Aqu/nC_{60} formation through extensive mixing of solid C_{60} in water (C_{60} concentration: 0.5 g/L, Rotation speed: 500 rpm): UV adsorption at 340 nm as functions of time with different concentrations of (a) dissolved oxygen (UVA 351 nm, 2 mW/cm^2); (b) initial fullerene (UVA 351 nm, 2 mW/cm^2); (c) initial H_2O_2 (Aerobic, UVA 351 nm, 2 mW/cm^2); (d) Total organic carbons of solvated products in solution under varied experimental conditions (0.5 g/L solid C_{60}, 3 days). (Only selected conditions are shown, and all others are listed in Table 2-1.)

Three types of indicators, BA, FFA, and XTT, were used as the probes for •OH, $^1O_2$, and O_2•$^-$, respectively, with the concentrations of the indicators monitored over the reaction time (Figure S2.1-S2.3). The production rates of ROS species (as measured by the degradation

kinetics of the indicators) was observed to be varied depending on the ROS type(s) and reaction conditions. For example, zero-order production rates of •OH were obtained in the absence of H_2O_2 (Figure S2.1a and S2.1b) whereas first-order production rates were observed in the presence of H_2O_2 (Figure S2.1c). Steady-state concentrations of each ROS were calculated following different numerical equations (Equation (7) and (8)), which are also listed in Table 2-1 for each experimental condition.

Quantitative correlation of nC_{60} formation rates as function of the steady state concentrations of •OH, $^1O_2$, and O_2•$^-$ are shown in Figure 2.3. Here, a simple linear regression was derived to model the formation rates with ROS concentrations at steady state (Figure 2.3(a)-(c)). Two linear relationships were identified by dividing the solvation kinetics into two reaction regimes with different levels of ROS concentrations: (1) the conditions in the absence of H_2O_2 (Regime 1: conditions #3-7) which have comparably lower radicals concentrations and (2) the conditions in the presence of H_2O_2 (Regime 2: conditions #8-13). For the three types of ROS species, positive linear relationships were obtained for all conditions, demonstrating that the formation rates were enhanced by all ROS production. Equations (9) - (11) represent these simple linear models:

$$\frac{d(nC_{60})}{dt} = k[\bullet OH]_{ss}^{a};\ \ln(V_{nC_{60}}) = k' + a\ln[\bullet OH]_{ss} \qquad (9)$$

$$\frac{d(nC_{60})}{dt} = k[^1O_2]_{ss}^{b};\ \ln(V_{nC_{60}}) = k' + b\ln[^1O_2]_{ss} \qquad (10)$$

$$\frac{d(nC_{60})}{dt} = k[O_2\bullet^-]_{ss}^{c};\ \ln(V_{nC_{60}}) = k' + c\ln[O_2\bullet^-]_{ss} \qquad (11)$$

where V_{nC60} is the nC_{60} formation rates derived from the slope of the zero-order reaction (Figure 2.2); a, b and c are the orders of the reactions with respect to the concentrations of •OH, $^1O_2$, and

$O_2\bullet^-$, respectively; k is the rate constant corresponding to each ROS concentration. The fitted parameters of the reaction kinetics are compared in Table 2-2, which shows that the formation kinetics are functions of the different types and concentration ranges of ROS (Regime 1 and 2). In this case, the reaction conditions were simplified as unitary ROS systems. In order to develop the kinetics model involving all three ROS species, multiple linear regressions was derived using SPSS 21.0 software to build a formation kinetics model described by Equation (12):

$$\frac{d(nC_{60})}{dt} = k[\bullet OH]_{ss}^{a}[^1O_2]_{ss}^{b}[O_2\bullet^-]_{ss}^{c};$$

$$\ln(V_{nC_{60}}) = k' + a\ln[\bullet OH]_{ss} + b\ln[^1O_2]_{ss} + c\ln[O_2\bullet^-]_{ss} \qquad (12)$$

where a, b and c are the orders of the reactions corresponding to the concentration of •OH, $^1O_2$, and $O_2\bullet^-$, respectively, representing the relative contributions from the three radicals during the solvation processes; k is the reaction rate constant. Based on the data series (Table 2-1) collected from varied experimental conditions, the multiple linear regression models were developed as shown by Equation (13) and (14), and the regression coefficients of the equation are listed in Table 2-3 together with results of the t-test and collinearity diagnostics.

$$\ln(V_{nC_{60}}) = 41.7 + 0.92\ln[\bullet OH]_{ss} + 0.56\ln[^1O_2]_{ss} + 0.09\ln[O_2\bullet^-]_{ss} \quad \text{(Regime 1, } R^2=0.956\text{)} \quad (13)$$

$$\ln(V_{nC_{60}}) = 30.8 + 0.85\ln[\bullet OH]_{ss} + 0.46\ln[^1O_2]_{ss} + 0.03\ln[O_2\bullet^-]_{ss} \quad \text{(Regime 2, } R^2=0.806\text{)} \quad (14)$$

Good correlations ($R^2 > 0.8$ for both regimes) suggest that most of the differences in $V(nC_{60})$ can be ascribed with the above three parameters (explicative variables). The t-test results (values of Beta, t, and sig.) suggest that all the explicative variables influence the dependent variable (V_{nC60}), and for both reacting regimes, the significant degrees follow the order: $\bullet OH > {}^1O_2 > O_2\bullet^-$. Good linear relationships between the formation rates and steady state concentrations of each

radical, indicate the all of these three radicals significantly affect the aqu/nC_{60} formation process. Within the reacting scenarios with lower ROS concentrations (in the absence H_2O_2, Regime 1), the regression coefficients of •OH, $^1O_2$, and $O_2•^-$ were identified as 0.92, 0.56 and 0.09, respectively, implying that the relative contribution of each ROS as: •OH (58.0%) > $^1O_2$ (36.0%) > $O_2•^-$ (6.0%) (Table 2-3). With H_2O_2 addition, the fitting constants of •OH, $^1O_2$, and $O_2•^-$ were quantified as 0.85, 0.46 and 0.03, with relative contributions of ROS as: •OH (64.1%) > $^1O_2$ (32.6%) > $O_2•^-$ (3.3%). This contribution similarity for both regimes demonstrates that within all of the reacting scenarios, the relative contributions of •OH, $^1O_2$, and $O_2•^-$ remained at or near the same level but coupled with different reaction constants (k' = 41.7 and 30.8 for regime 1and regime 2, respectively). The relationships between the expected accumulative probabilities versus with the observed cumulative probability are shown in Figure 2.3 (d) and (e), which verify good fits of the multiple linear regression models. These results are also supported by the ROS redox potential as hydroxyl radical has a higher oxidizing capacity ($E_{1/2}$(•OH/OH^-) = 1.98 V) compared to the $^1O_2$ ($E_{1/2}$($^1O_2$/$O_2•^-$) = 0.62 V) and $O_2•^-$ ($E_{1/2}$($O_2•^-$/H_2O_2) = 0.94 V).[113, 114,111, 115]Additionally, the comparably lower involvement of $O_2•^-$ might also be due to its (relatively) extremely short lifetime (~1.25 μs) in water compared to •OH as ~ 2.7-3.92 μs and and $^1O_2$ as ~ 4.4 μs.[116-118]

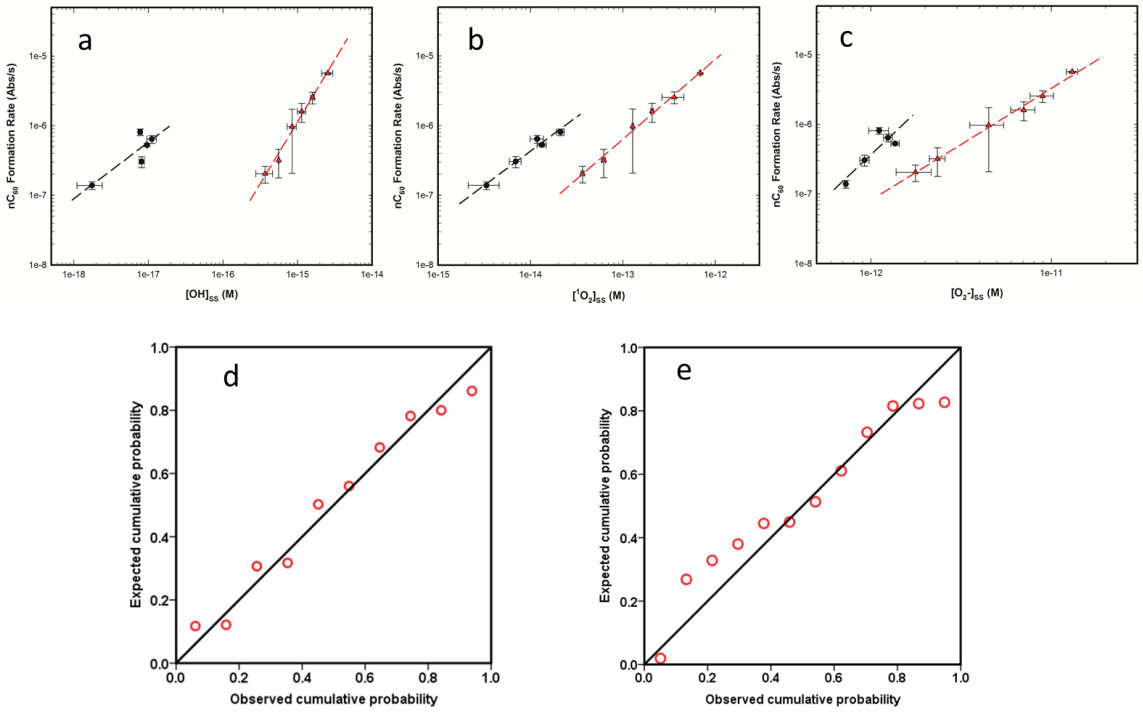

Figure 2.3: nC_{60} formation rates under varied experimental conditions as functions of steady state concentrations of (a) hydroxyl radical; (b) singlet oxygen; (c) superoxide; The SPSS v21.0 normal P-P plot of the multiple regression model of nC_{60} formation rates as functions of three ROS concentration within (d) Regime 1 (in the absence of H_2O_2) and (e) Regime 2 (in the presence of H_2O_2).

Table 2-2: Regression coefficients of simple linear curve fitting

Regime 1[a]					Regime 2[b]				
k'	a	b	c	R^2	k'	a	b	c	R^2
17.4	0.81	---	---	0.74	48.0	1.78	---	---	0.99
17.0	---	0.98	---	0.96	20.1	---	1.15	---	0.99
52.8	---	---	2.45	0.76	28.1	---	---	1.61	0.99

a. Conditions in the absence of H_2O_2; b. Conditions in the presence of H_2O_2.

Table 2-3: Regression coefficients of multiple linear curve fitting

	Explicative Variables		k'	[•OH]	[$^1O_2$]	[O_2•$^-$]
Regime 1	Unstandardized Coefficients		41.7	0.92	0.56	0.09
	Coefficients	Std.	8.7	0.41	0.34	0.05
	Standardized Coefficients	Contribution	----	58.0%	36.0%	6.0%
		T	3.0	6.6	3.6	1.0
		Sig.	0.036	0.452	0.005	0.235
	Collinearity Statistics	Tolerance	----	0.233	0.276	0.256
		VIP	----	4.3	3.6	3.9
Regime 2	Unstandardized Coefficients	Value	30.8	0.85	0.46	0.03
		Std.	4.2	0.56	0.34	0.02
	Standardized Coefficients	Contribution	----	64.1%	32.6%	3.3%
		T	2.9	5.7	2.9	0.29
		Sig.	0.023	0.000	0.001	0.262
	Collinearity Statistics	Tolerance	----	0.103	0.024	0.037
		VIP	----	9.7	41.0	27.0

a. Variance of inflation factor, VIP=1/Tolerance

XPS spectra of solvated products (aqu/nC_{60}), taken for reaction scenarios (after 3 days) are shown in Figure 2.4. The XPS spectrum of nC_{60} (THF/nC_{60}) freshly produced by solvent exchange is shown as a control (Figure 2.4g) and slight surface oxidation was observed (mono-oxidized carbon: C-O, 15.3%; di-oxidized carbon: C=O, 5.6%)[54, 119, 120] in addition to underivatized surface carbon (284.8 eV), indicating that oxidation of the nC_{60} cluster's surface occurred, even though the solvent exchange process(es) under inert atmosphere, which is similar to reports by others.[41, 93] Through extensive mixing of solid fullerene in water under UVA irradiation (351 nm, 2 mW/cm^2) under anaerobic conditions (DO ~ 0.3 ppm) for 3 days, trace amount of aqu/nC_{60} was formed (observed through UV-vis spectrometer and TOC analyses with a total organic carbon concentration as 0.39±0.13 mg/L), with mono-oxidized and di-oxidized carbons at relative amounts of 9.5% and 8.3%, respectively (Figure 2.4a). As oxygen concentrations increased, the surface oxidation of nC_{60} correspondingly increased. For example, with 5% oxygen in the atmosphere (DO ~ 2.5 ppm), the relative ratios of C-O and C=O in the products increased to 14.6% and 9.0%, respectively (Figure 2.4b). Under ambient conditions (DO ~ 9 ppm), the ratio of surface oxidized carbons increased to ca. 30% total (C-O, 22.1%; C=O, 6.0%). Further with hydrogen peroxide addition, not only were nC_{60} formation rates enhances but aggregates had higher oxygen-containing surface functionality as illustrated in Figure 2.4d-4f. With 0.25% H_2O_2 (w/w) and light, the surface oxidized carbons of aqu/nC_{60} increased to ca. 50% among the total surface carbons measured. FTIR analyses for additional identification of solvated products surface functionalization were also conducted, and the spectra are displayed in Figure 2.5. As reported by others, pure C_{60} solid powder (Figure S2.4) shows five characteristic peaks at 528, 576, 1180, 1430, and 1540 cm^{-1}, which are attributed to C-C vibration modes of C_{60}.[89, 121] Upon nC_{60} formation in water via solvent exchange, THF/nC_{60}

(Figure 2.5g) losses the adsorption peak intensity at 1180, 1430 and 1540 cm^{-1}, whereas minor surface oxygenation occurred indicated by the peaks appearing at 1830-1684 cm^{-1} (centered at 1726 cm-1, carbonyl groups) and 1000-1240 cm^{-1} (centered at 1100 cm^{-1}, C-O stretching).[54, 55, 84, 120] Via extensive mixing in water under varied reacting scenarios (Figure 2.5a-6f), generally, aqu/nC_{60} exhibits the main C-C vibration mode of C_{60} as well as having surface oxygen containing functional groups. Under UVA irradiation (351 nm, 2 mW/cm^2), at different levels of oxygen (Figure 2.5a-2.6c), surface oxidation levels were enhanced as indicated by peaks centered at 1060 cm^{-1} (C-O stretching), 1400 cm^{-1} (C-OH in-plane bending), and double peaks at 1640cm^{-1}/1720 cm^{-1} (carbonyl groups)[54, 84], which is consistent with the XPS results. In the presence of hydrogen peroxide and light, aqu/nC_{60} was produced at comparably larger amounts, which was apparent in the relative increase in C_{60} characteristic peaks at 1180 cm^{-1} and 1430 cm^{-1}; in addition, the surface oxidation of the aqu/nC_{60} clusters was also enhanced at higher level of H_2O_2 and light, which is also consistent with XPS results.

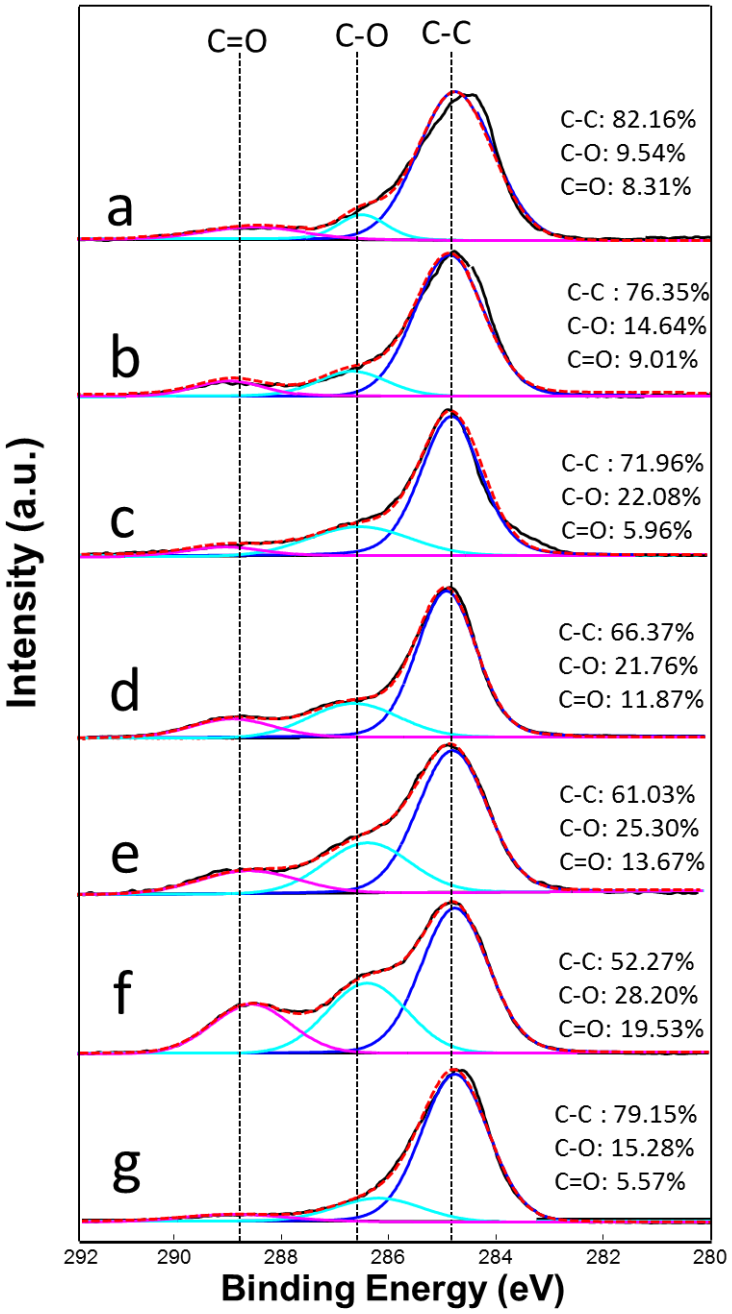

Figure 2.4: C1s XPS spectra and curve-fitting analyses of the solvated C_{60} products (nC_{60}) from (3 days): (a) UVA anaerobic condition; (b) UVA 5% oxygen condition; (c) UVA aerobic condition; (d) UVA 0.025% H_2O_2 condition; (e) UVA 0.1 % H_2O_2 condition; (f) UVA 0.25% H_2O_2 condition; (g) THF/nC_{60} produced with solvent exchange method.

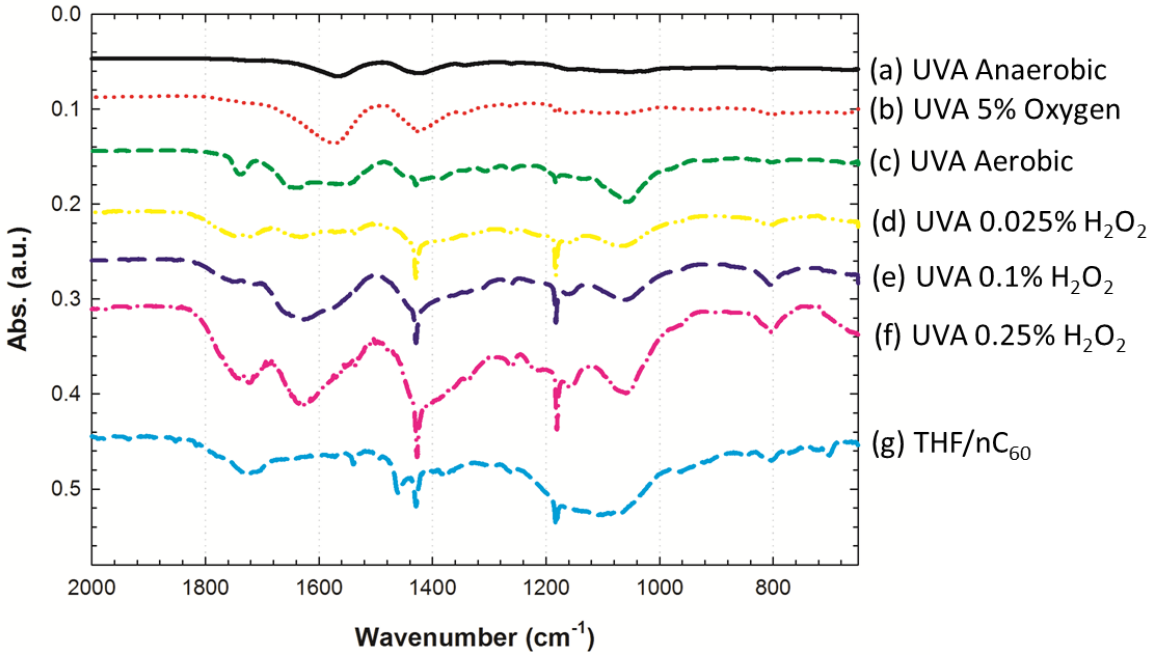

Figure 2.5: FTIR spectra of solvated products C_{60} products (nC_{60}) from (3 days): (a) UVA anaerobic condition; (b) UVA 5% oxygen condition; (c) UVA aerobic condition; (d) UVA 0.025% H_2O_2 condition; (e) UVA 0.1% H_2O_2 condition; (f) UVA 0.25% H_2O_2 condition; (g) THF/nC_{60} produced with solvent exchange method.

Extensive mixing of solid C_{60} in water under photo-irradiation results in nano-scale C_{60} aggregates formation and the following processes were hypothesized to be involved in general: (1) mechanically break-up of the solid C_{60} with micro-scale sizes to unstructured smaller fragments through stirring or shear forces (with nanoscale size) and even surface oxidation;[38] (2) re-aggregation of the smaller C_{60} fragments to micro-scale particles, driven by the surface energy reduction (energetically favorable process) through elimination of surface-water interactions via particle-particle interfaces;[93, 122, 123] (3) Further oxygen-containing functionalization of the unstable C_{60} cluster surface, leads to the stabilization of the nano-scale C_{60} through electronic (and to a less extent, steric) repulsion forces (negative charge obtained) and/or by hydration

repulsion effects (more hydrophilic surfaces created);[124] (4) further oxidization of the nano-scale C_{60} aggregate may occur to higher level, soluble oxidized derivatives (e.g. fullerol)[54, 55, 72]. The aqu/nC_{60} formation rates are controlled as a function of these individual processes simultaneously. For example, in the absence of ROS, the aggregation of the smaller fragments (Step 2) to form particles with larger size (precipitation/sedimentation) might be the most important limiting step for stable nC_{60} formation under the dark conditions due to the unstable surfaces with less negative charge and oxygen containing functional groups (less electron-repulsion forces and higher hydrophobic attraction forces).[124] In systems with oxygen and H_2O_2 as effective sources of ROS, oxidizing the surface of C_{60} fragments is significantly enhanced (kinetically), thus resulting in the retardation of the (re)aggregation process. Further, oxidizing fullerene derivatives, as intermediates, are produced in the solvation system, which could further enhance ROS production via a positive feedback loop.

2.4. Conclusions

In summary, aqueous stable nano-scale C_{60} aggregates are readily formed via extensive mixing of solid (powder) C_{60} in water under photo-irradiation (UVA) in the presence of oxygen and/or hydrogen peroxide; Self-catalyzed, reactive oxygen species (•OH, $^1O_2$, and $O_2•^-$) were demonstrated to be critical in the formation process. The quantitative analysis of the formation kinetics, described by multiple linear regression models, shows the relative contributions of the ROS follows: •OH > $^1O_2$ > $O_2•^-$ for all reaction regimes evaluated. For faster formation rates, colloid surface (partial) oxidation percentages were observed to relatively increase, as evaluated by XPS and FTIR analyses. Additionally, under UVA irradiation, photo-excited C_{60} reactivity enhancement will play a role in the overall thermodynamics of the reaction; however, this

variable was not independently evaluated and will be focused in future studies. In natural systems, releasing solid C_{60} into surface water in the presence of light could directly lead to water available aggregates formation and subsequent daughter products. Environmental parameters, such as light irradiation wavelength/intensity and effective electron acceptors are essential with regard to formation extent/rates. These findings provide the first steps toward mechanistic understanding likely pathways for fullerenes to enter aqueous matrixes and thus should prove to be crucial for accurate material fate transport and risk models in the future.

Acknowledgement

This study was supported by Washington University in St. Louis faculty startup funding for Dr. John D. Fortner and National Science Foundation (NSF). We appreciate the XPS facility supporting by Institute of Materials Science and Engineering (IMSE) at Washington University in St. Louis. We sincerely thank Dr. Marcus Foston and James Meyer for their kind help in the HPLC measurements. We would also thank Materials and Electrochemical Research (MER) Corporation (Tucson, AZ) for their help in material preparation.

Chapter 2. Supporting Information

Reactive oxygen species concentration detection (as scavengers' degradation: BA, FFA, and XTT) profiles and FTIR spectrum of pristine solid C_{60} are included in supporting information.

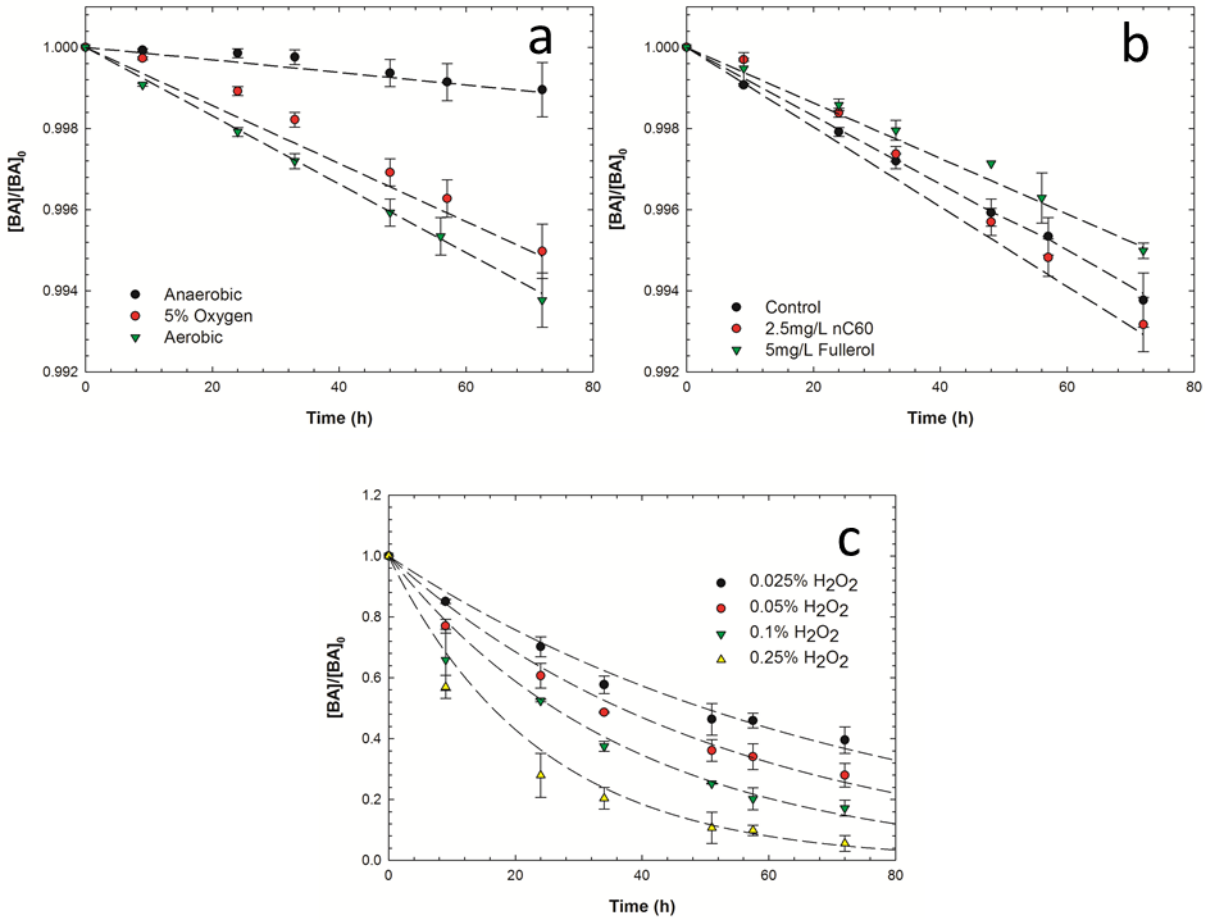

Figure S1.1: Degradation of BA (as •OH detection probe) during nC_{60} formation through extensive mixing in water under varied experimental conditions.

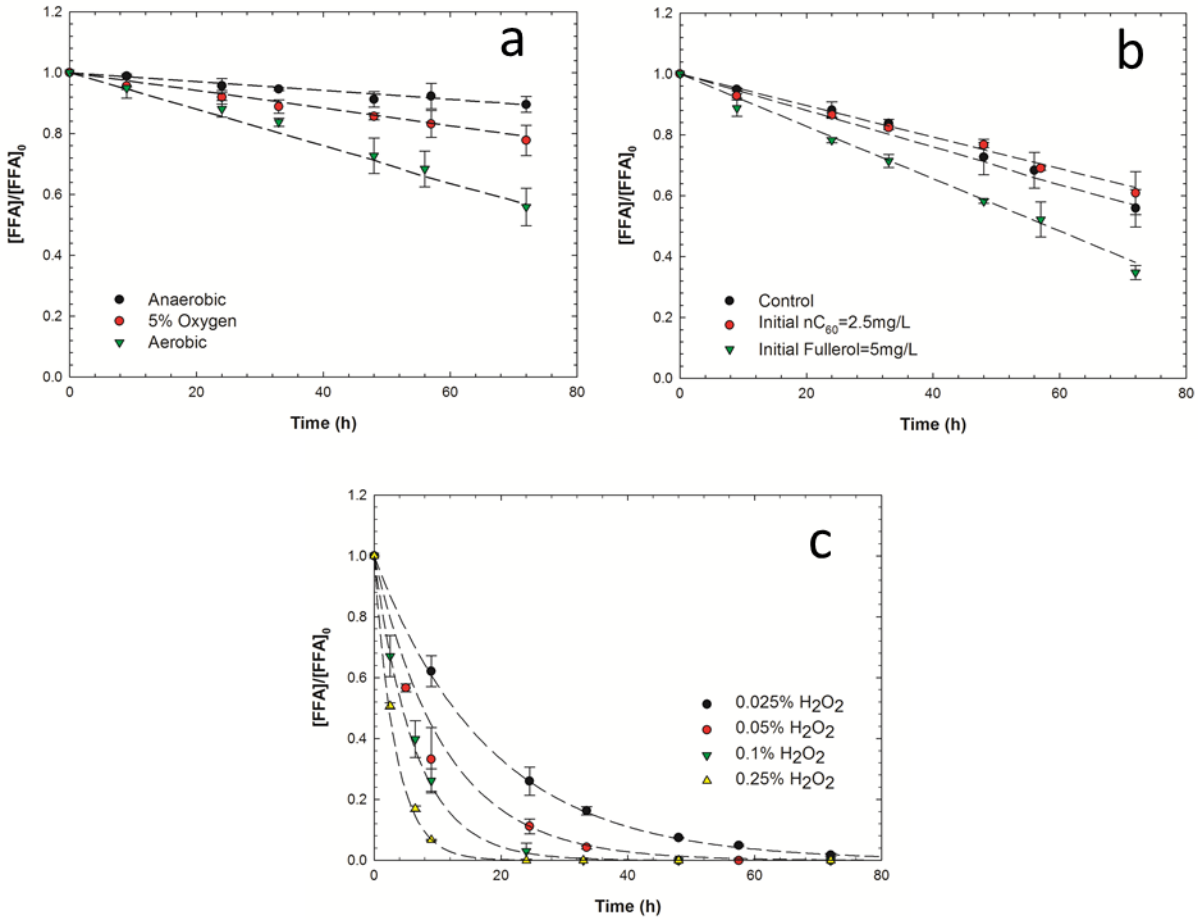

Figure S1.2: Degradation of FFA (as $^1O_2$ detection probe) during nC_{60} formation through extensive mixing in water under varied experimental conditions.

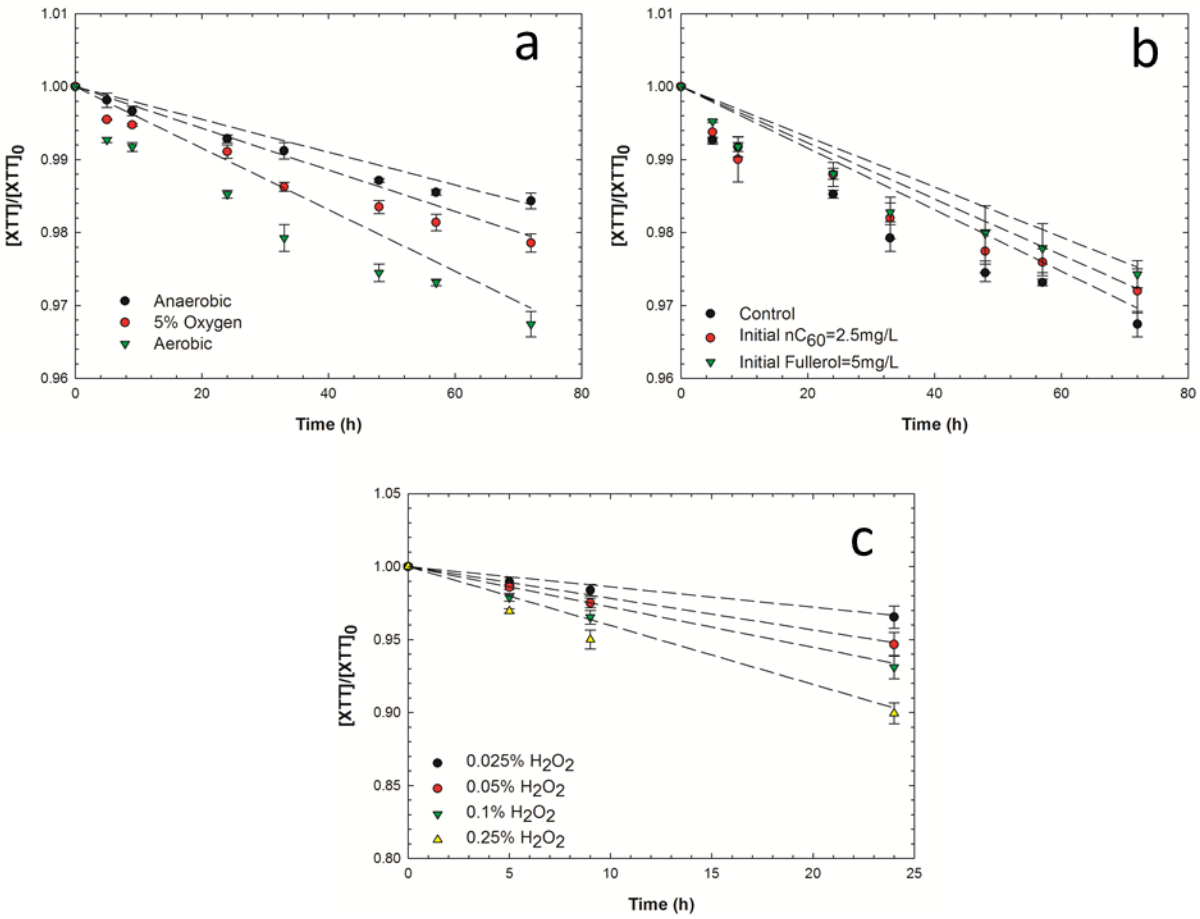

Figure S1.3: Degradation of XTT (as $O_2^{\bullet -}$ detection probe) during nC_{60} formation through extensive mixing in water under varied experimental conditions.

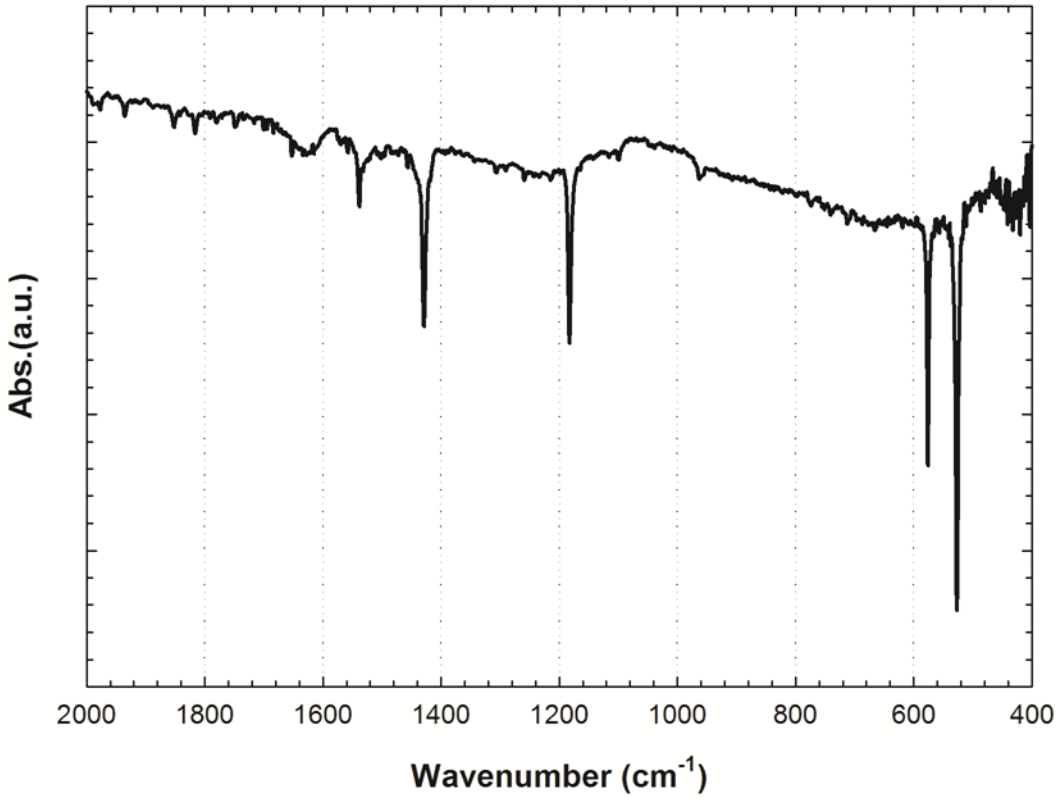

Figure S1.4: FTIR spectrum of pristine solid C_{60} powder.

Chapter 3 :**Photo-Oxidation of Hydrogenated Fullerene (Fullerane) in Water**

Results of this chapter have been published in *Environmental Science & Technology Letters,* **2014**, *1*, (12), 490-494.

Abstract

Hydrogenated fullerenes (termed as fulleranes) have been demonstrated as key material components in advanced hydrogen storage and lithium battery technologies, among other applications; however, their potential environmental reactivity has not been evaluated to date. Here, for the first time, photo-induced oxidation and corresponding dissolution of solid fulleranes ($C_{60}H_x$, x = 39.9-45.5) into water is demonstrated to rapidly occur under attenuated-sunlight, UVA irradiation and even under dark conditions, albeit more slowly as long as oxygen is present. Through a series of batch experiments, reaction kinetics demonstrate that both light and oxygen play key roles in the solvation process as reaction rates were a function of both irradiation intensity and wavelengths along with dissolved oxygen concentration. Resulting products, which were characterized by FTIR, XPS, UV-vis, TOC and DLS, showed significant loss of hydrogenation and extensive oxygen-based functional group addition(s). Hydroxyl radical was identified as one of the major reactive oxygen species involved in the reaction. The increased hydrophilicity of product materials was quantified through classic octanol-water partition experiments (K_{ow}).

3.1. Introduction

Since discovery and subsequent mass production, carbon fullerenes have been derivatized and modified for a variety of diverse applications.[4, 10, 48, 125-128] Among such, fullerene reduction via hydrogenation is recognized as a promising process for reversible hydrogen storage (through stable hydrogenation / dehydrogenation cycling).[128-130] Hydrogenated fullerenes, also termed as "fulleranes"[10], have been also applied to lithium ion batteries for enhanced efficiency and extended lifetimes.[131] The first fullerene hydrogenation protocol was developed by Haufler et al. through a Birch-Hückel reduction, resulting in $C_{60}H_{18}$ - $C_{60}H_{36}$ as major products.[132] Higher levels of C_{60} hydrogenation, with up to 50 hydrogen atoms per molecule, has been achieved via 5 % Ru/carbon catalyst under high hydrogen pressures (12 MPa).[133] Relatively fast fullerene reduction with Zn and concentrated HCl (12 M) in toluene/benzene solution has also been demonstrated, resulting in a $C_{60}H_{36}$ product.[134] Lower levels of fullerene hydrogenation (oligohydrofullerene, $C_{60}H_x$, x = 2-12) have been demonstrated via reduction by a number of metals (e.g. Cu/Zn) and even by organic reducing agents.[135, 136]

With commercial production and application, the potential for these and other fullerene materials to enter natural systems increases. Upon environmental exposure, associated reaction pathways with (ubiquitous) reactants such as oxygen are critical to elucidate, as the identification of stable daughter products, if any, is key for accurate lifecycle and risk assessments. This fact is highlighted by recent observations of facile fullerene transformation to oxidized, water soluble products (termed as fullerols) when exposed to water, oxygen and light.[54, 72] Compared with parent fullerenes, previous studies have shown the generation of reactive oxygen species (ROS) through fullerols photocatalyzed reactions was more efficient, and suggested ROS as a potential

causative agent for cells inactivation.[72, 98, 137-139] Further, published evaluations of potential fullerane environmental implications are few. Lovern et al. evaluated the toxicity of fullerane using *Daphnia magna* as a biological receptor and reported physiological changes upon exposure, including reproductive decline.[140] A major limitation of such studies is extremely low aqueous fullerane solubilities. [141-143] To date, there is no literature report regarding measured or estimated aqueous solubility of hydrogenated fullerenes.

Based on the increasing electronegativity of fullerene carbon atoms when bound to hydrogen, fulleranes should be more susceptible to electrophilic addition (i.e. oxidation), compared to parent fullerenes. Such reactions have been demonstrated and include: oxidation of fulleranes (dissolved in *n*-hexane) under UV irradiation (254 nm)[144] and oxidation of $C_{60}H_{36}$ (dissolved in toluene open to the atmosphere) while exposed (48 hrs) to ambient light.[134] To date, however, potential reactions of fulleranes directly in water have not been identified or evaluated. Herein, this work describes the oxidation and molecular solvation of solid fullerane in contact with water, which is significantly enhanced in the presence of light. Reaction kinetics of product dissolution, due to carbon cage oxidation, were examined through UV-vis spectroscopy and total organic carbon (TOC) analyses over a range of conditions including varied photo-irradiation and dissolved oxygen levels. Water soluble, oxidized products were identified and characterized through Fourier transformation infrared spectroscopy (FTIR) and X-ray photoelectron spectroscopy (XPS). Product behavior and aqueous (physical) status were further characterized with traditional octanol-water partition experiments and dynamic light scattering (DLS) analyses.

3.2. Materials and Methods

3.2.1. **Materials**

Solid fulleranes ($C_{60}H_x$, x ~ 45.5 and x ~ 39.9 as averaged) were purchased from MER Corporation (Tucson, AZ) where they were prepared through direct hydrogenation in a high isostatic pressure reactor with a hydrogen atmosphere at elevated temperature. As received, parent fullerane materials were stored in a vacuum desiccator to avoid transformation by humidity and/or oxidation. Starting materials as received ($C_{60}H_x$, x ~ 45.5 as average) were characterized through FTIR and XPS, shown in Figure 3.2a and Figure 3.3a, indicating high purity, which has also been reported elsewhere.[145, 146]

3.2.2. **Photo-induced Solvation Experiments**

Solvation experiments were conducted as batch reactions with 40 mg/L solid fullerane ($C_{60}H_x$, x ~ 45.5 as average) mixed via magnetic stirring (500 rpm) in 50 mL ultrapure water (18.2 Ω) in customized quartz reactors (Technical Glass Products, OH) under varied photo-irradiation scenarios. Experiments done with attenuated-sunlight (A-sunlight, filtered by borosilicate glass windows) were carried out next to a lab window (St. Louis, MO, 90°18'W, 38°38'N, 07/21/2012-08/06/2012). Light intensities were monitored daily with a radiometer (UVP, Inc. CA) and summarized in Figure S3.1. Reactions performed under monochromatic UVA irradiation were carried out in a customized photo-reactor, with fans on each side for heat dissipation, between two circuitous, monochromatic UVA lamps (BHK Inc. CA) at a wavelength of 351 nm. The light intensity was calibrated as 2000 ± 50 $\mu W/cm^2$ by the radiometer before the reaction and corrected regularly during the reaction as needed. To delineate the role, if any, of

hydroxyl radicals during the reaction(s), 10 mM t-BuOH was used as a hydroxyl radical scavenger.[84] Dark control experiments, wrapped in aluminum foil, were conducted in parallel. For anaerobic conditions, solutions (50 mL) were bubbled with N_2 gas (Airgas, Bowling Green, KY) for at least 1 hour to lower the dissolved oxygen concentration below 1 ppm, as tested with a microprobe DO meter (Neofox system, Oceanoptics, FL). Anaerobic conditions were maintained via Teflon crimp sealed caps (Wheaton Industries Inc., NJ) and sparged with N_2 gas for 10 minutes after every sampling event, leaving the sealed reactor under slightly positive pressure. For reaction kinetics studies, sample aliquots were taken at stated time intervals and filtered with 0.45 μm PES membrane (Millipore corporation, MA) to separate and collect solvated products, which were in water. UV-vis spectra (190-800 nm) of the products were obtained by using a Varian Cary Bio50 UV-visible spectrometer. All experiments were performed in triplicate at room temperature (21.0 ± 1.0 ^{o}C). Samples after 1 day and 12 days were also collected and filtered with 0.45 μm PES membrane for total organic carbon analysis (TOC-L total organic carbon analyzer, Shimadzu). Particle size distributions of solvated products over the course of reactions were determined with dynamic light scattering (DLS) analysis by using a ZetaSizer Nano (Malvern Instruments, UK).

3.2.3. **Products Characterization**

Solid-state FTIR analysis for parent fulleranes was conducted with diffuse reflectance infrared Fourier transform spectroscopy (Nexus 470 FT-IR, Thermo Nicolet, NC). Unreacted fullerane were mixed and homogenized with KBr powder (Spectrograde, International Crystal Lab, NJ) matrix in an agate mortar by a pestle as 1:20 ratio. KBr background was subtracted appropriately during sample spectrum collection. The solvated products were analyzed through attenuated total reflection Fourier transform infrared spectroscopy (Nexus 470 FT-IR, Thermo

Nicolet, NC) with a ZnSe trough. Liquid samples in the trough were dried in a vacuum oven (Thermo Scientific, NC) at room temperature. Samples for X-ray photoelectron spectroscopy (XPS) analysis were prepared by continuous drop-casting of product solutions (filtered with 0.45 μm PES syringe membrane) onto gold-coated silicon wafers for a total volume of 1-2 mL. The wafers were dried in a vacuum oven at room temperature. XPS sample wafers were prepared by first sputter coating gold to at least a 20 nm thickness and dried before samples were added. Powder samples that included fullerene, fullerane, and fullerol were dusted onto 0.5 cm^2 copper tape. Samples were run using a PHI 5600 XPS system ($P_{base} < 5x10^{-9}$ Torr) with Mg Kα X-rays (1253.6 eV, 15 kV, 300 W) and a high energy electron energy analyzer, operating at a constant pass-energy of 5.85 eV with a scan rate of 0.050 eV/step and a slot aperture of 800 μm^2. Commercially available software (CasaXPS) was used for data analysis. Each C(1s) region was given a Shirley background and energy adjusted to the CC/CH fitted spectral feature within the C (1s) region at 284.5 eV. The commercial fullerol sample had four clearly distinguishable components (CC/CH, C-O, C=O, and COOH features) due to its high level of carbon bonded to oxygen (28.8 %) and were propagated to the other samples; these fits were in line with those used in the literature.[147-155] A π-π* shake-up peak was fit only into the fullerene XPS spectrum (SI Figure S3.5) since it was only apparent for this sample.[147, 149-151, 154, 155] Positions for all components were set to drift no more than ± 0.2 eV of the peak position used. The full width at half maximum (FWHM), using a Gaussian-Lorenzian (GL(30)) fit, was not allowed to drift more than ± 0.2 of the FWHM used for the commercial fullerol sample. Component area analysis of each C(1s) spectrum was used to determine the percent oxygen-containing functionalities with respect to the total C(1s) area.

3.2.4. **Octanol-Water Partition Coefficients Measurements**

Octanol-water partitioning (K_{ow}) experiments were performed for products resulting from varied experimental conditions. Here, 3 mL of product solution was mixed with 3 mL of 1-octanol in glass bottles, placed on a rotary shaker (Labquake, Thermo Scientific, UT) for 3 hours in dark and then left static for 24 hours to equilibrate. The partition coefficients were determined by the ratio of the amount of products in water phase to that in the octanol phase according to equation (1):

$$K_{ow} = \frac{C_o}{C_w} = \frac{[Abs]_i - k*[Abs]_f}{[Abs]_f} \qquad (1)$$

where C_o is the concentration of products in octanol phase which was determined by subtracting the initial concentration in water phase ($[Abs]_i$) from the concentration of products left in the water phase after partition ($k*[Abs]_f$). The coefficients were also corrected with the concentrating factor (volume change factor) k determined experimentally, as the volume of water dissolved into octanol phase, changing the final volumes, during the mixing process cannot be ignored.

3.3. Results and Discussion

As solid fullerane reacted in water, the observed (aqueous) product UV-vis spectra exhibited a single significant absorbance peak centered at ca. 210 nm (7 day reaction, UVA aerobic conditions, Figure S3.2), which is consistent with the report describing the photo-oxidization (and consequent solubilization) of fullerenes to fullerols in water.[54] Under direct monochromatic UVA (351 nm wavelength) irradiation and in the presence of dissolved oxygen (under open, atmospheric headspace conditions), UV-vis absorbance (primarily in the UV region

of the product spectrum) of dissolved products increases significantly as the reaction proceeds (Figure 3.1b and Figure S3.2), consistent with the increasing (transparent) yellow hue of the solution (Figure 3.1a). Additionally, the absorption peak centers of the products under UVA irradiation shifted to longer wavelengths (from 203 nm to 212 nm) as the reaction continued from 1 day to 12 days, which is shown in Figure S3.3. Cataldo et al. also observed such shifts during the photolysis of fullerane in n-hexane (peak max shifted from 217 nm to 220 nm after 360 seconds of photo-irradiation at 254 nm). The phenomenon is hypothesized to be an artifact of sp3 hybridized carbons (hydrogenated carbon), which are predominant in the parent fulleranes, transforming back to sp2 hybridized carbon upon dehydrogenation.[156] For comparison, under UVA aerobic conditions, fullerane starting material with a slightly lower number of hydrogen numbers per molecule ($C_{60}H_x$, x ~ 45.5 vs. x ~ 39.9) was also evaluated (Figure 3.1b). While exhibiting a similar initial reaction rate, a lower final peak absorbance value was observed, which may result from an overall lower oxidation (product) status and/or due to different (lower) product extinction coefficient(s). Compared with UVA irradiation, the increase of product absorbance under attenuated-sunlight irradiation was significantly slower as the absorbance of the sunlight products after 3 days reaction is about 19 % compared to UVA irradiation conditions over the same time. Fullerane solvation was also observed under dark experiments in the presence of dissolved oxygen, as indicated by a low level appearance of product peaks over the described reaction time, which were the slowest rates observed. In contrast, under anaerobic conditions (dissolved oxygen below 1 ppm), for both light and dark conditions, no apparent product peaks occured over the same reaction times. The maximum UV absorption values at specific wavelength (peak center) under different experimental conditions are compared in Figure 3.1b. Further, in the presence of 10 mM t-BuOH, which is as a hydroxyl

radical scavenger[84], a significantly slower reaction rate was observed (Figure 3.1b) under UVA / aerobic conditions, suggesting hydroxyl radical involvement in the reaction. It is hypothesized that hydroxyl radicals could be formed as secondary ROS after initial reactive oxygen species (e.g. singlet oxygen and superoxide) are produced (via fullerene intermediates) as observed by others[60, 157, 158]. Singlet oxygen and superoxide, as the initial ROS, could also play roles in the oxidation of hydrogenated fullerene through electrophilic substitution/addition. However, the exact oxidation mechanism(s) remains unclear and is currently being investigated further. TOC analysis of 1-day and 12-day samples in Figure 3.1c was consistent with the UV-vis analysis, correlating dissolved carbon with solvation observations. Total organic carbon of soluble products under open, UVA irradiation reached 36 mg/L after 12 days of reaction which is 95.7 % of the initial solid fullerane carbon added to the reactor. Under the same conditions, pH correspondingly decreased as the reaction proceeded to a final value of near pH 4 due to hydrogen elimination and oxygen-based functional group additions.

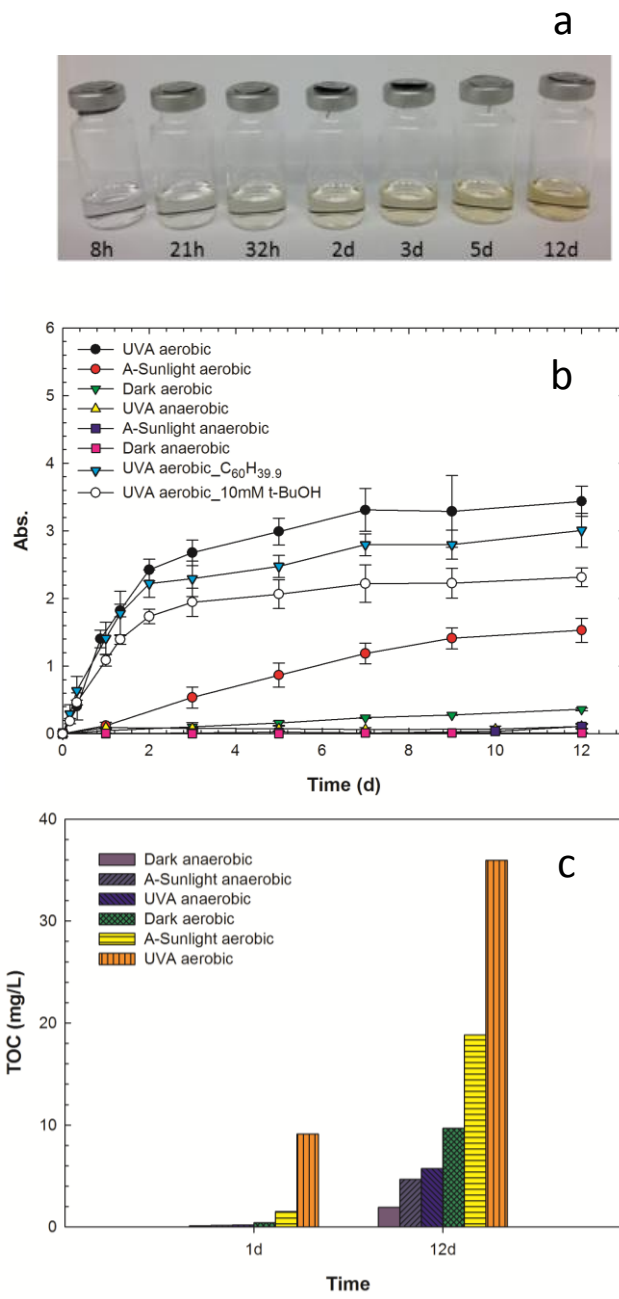

Figure 3.1: Fullerane solvation experiments: (a) Fullerane product solutions filtered with 0.45 µm membrane over the reaction (UVA irradiation under ambient conditions); (b) UV maximum adsorption of products as a function of time; (c) Total organic carbon of product solutions after 1 day and 12 days reaction.

Parent fullerane and solvated water-soluble products were characterized by FTIR and compared in Figure 3.2. Parent fullerane exhibited strong absorption at ca. 2860 and 2780 cm^{-1}, which are assigned to C-H stretching bonds, as reported by Cataldo et al. for $C_{60}H_{36}$.[145] For all aerobic reaction conditions, a concurrent loss of C-H bonds and appearance of oxygen functionalities were observed at ca. 3400 cm^{-1} (OH stretching), 1700 cm^{-1} coupled with shifts at 1600 cm^{-1} (C=O), 1400 cm^{-1} (C-OH in plane bending) and 1050 cm^{-1} (C-O stretching).[54, 84, 159, 160] Absorbance peaks typical of carbonyl groups (1700 cm^{-1} and 1600 cm^{-1}) and C-OH (1400 cm^{-1}) increased significantly as the light intensity increased (monochromatic UVA reactions). An IR spectrum of one type of commercial fullerol ($C_{60}(OH)_x(ONa)_y$, y ~ 6-8, x+y ~ 24, MER Corp., AZ) is also provided (as the bottom line) in Figure 3.2 for comparison with a well characterized, water soluble oxidized fullerene (fullerol), as reported elsewhere.[54, 84, 159, 161] TEM observations, show amorphous, aggregated products cluster, similar to soft aggregated fullerols, as shown by others.[162]

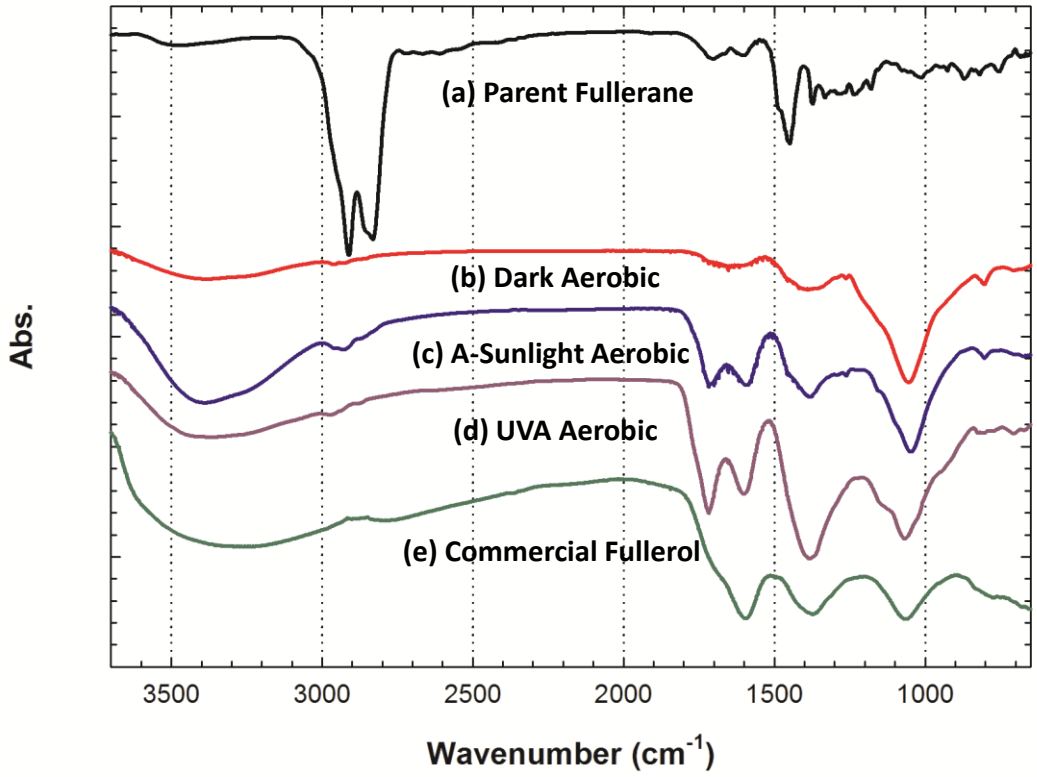

Figure 3.2: FTIR spectra of unreacted fullerane and products: (a) Parent fullerane; (b) Products under dark aerobic condition; (c) Products under attenuated-sunlight aerobic condition; (d) Products under UVA (351 nm) aerobic condition; (e) Commercial fullerol ($C_{60}(OH)_x(ONa)_y$, where x+y ~ 24, MER Corp.).

Product XPS spectra under different reaction conditions are compared in Figure 3. The dominant carbon peak (98.8 % peak area) for parent fullerane at a binding energy of 284.5 eV (Figure 3.3a) is assigned to C-C/C-H carbon[56, 154, 163], which was also observed in parent C_{60} at a lower ratio (Figure S3.5). Low levels (1.2 %) of (initially) oxidized carbon also appeared in the parent fullerane materials, which has also been observed by others.[164] The XPS spectrum of the products collected from the aerobic reaction in the dark (Figure 3.3b), showed decreased C-C/C-H signal at 284.5 eV (69.2 % peak area) coupled with increased mono-oxidized carbon signal

(286.4 eV, 29.7 %).[154, 163] It should be noted that 12-day soluble products, measured as TOC, for aerobic dark conditions were only ca. 25 % (10 mg/L TOC, solubilized) of the original 40 mg/L carbon added as solid fullerane reactant (Figure 3.1c). Carbonyl (288.0 eV, 6.2 %) and carboxyl groups (289.9 eV, 1.3 %) were observed in oxidized products with attenuated-sunlight irradiation (Figure 3.3c).[54, 84, 163] Upon UVA irradiation (Figure 3.3d), the C-C/C-H ratio of the oxidized products decreased to 68.5 %, indicating one third of the carbon atoms had been oxidized. Additionally, compared to all other conditions, higher levels of carbonyl (C=O, 11.3 %) and carboxyl (-O=C-O, 5.1 %) were observed for these products. XPS analysis of previously described commercial fullerol showed a very similar oxidized carbon distribution when compared to the UVA/aerobic (oxidized) fullerane products (Figure 3.3e).

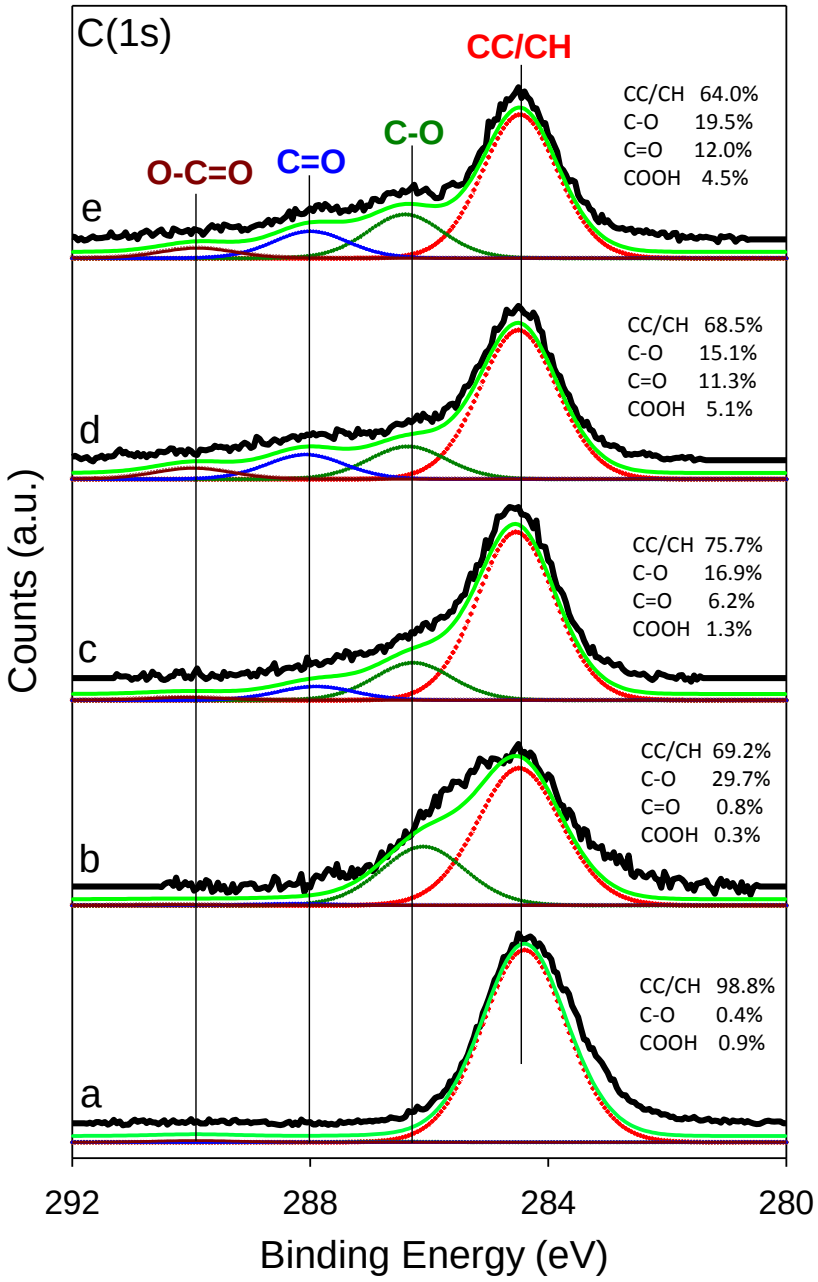

Figure 3.3: C(1s) XPS spectra and curve-fitting analysis of the solvated fullerane products: (a) Unreacted fullerane; Products from (b) dark aerobic condition; (c) attenuated-sunlight aerobic condition; (d) UVA aerobic condition; (e) Commercial fullerol ($C_{60}(OH)_x(ONa)_y$, where x+y ~ 24, MER Corp.).

Upon reaction, the hydrodynamic size of water stable product clusters was evaluated by DLS (Figure S3.6a). The cluster size (number averaged) decreased over the reaction time for all aerobic conditions. Smaller size distributions suggest looser aggregation/disaggregation of clustered products as the solvation proceeds, due to a molecular enhancement in water solubility (i.e. increasing oxygen functionality as noted by others).[165, 166] After 5 days of reaction, the average cluster size of the products under UVA/aerobic irradiation was reduced to 39 nm compared to dark aerobic conditions, which was measured to be 95 nm. Stable clusters formed under attenuated-sunlight irradiation, exhibited broader size distributions, compared with that under UVA/aerobic and dark/aerobic conditions. Such polydispersity may be due to the diversity (and varied reaction kinetics) of the soluble products generated when exposed to a broader spectrum of wavelengths associated with sunlight irradiation. In a study by Hou et al. on the aqueous C_{60} cluster photo-transformation, it was demonstrated that the quantum yields and ROS production depend on the wavelength of the irradiating lights[56], which could further effect the oxygen moiety distribution in the products thus also effecting the relative driving force for the cluster formation in the aqueous phase.[162] Product partitioning behavior was evaluated via octanol-water partition (expressed as K_{ow}) experiments Figure S3.6b. As expected, significantly decreased K_{ow} was observed for reacted products, which is consistent with the presence of oxygen-based functional groups and thus enhanced aqueous solubility. Partition coefficients for products formed under UVA/aerobic conditions approach a K_{ow} of zero.

3.4. Conclusions

In summary, this study, for the first time, demonstrates insoluble solid hydrogenated fullerene readily undergoes extensive oxidation and corresponding solvation (solubility) into

water in the presence of oxygen. For all reactions, enhancement was observed in the presence of light. Product characterization indicates significant loss of hydrogen groups along with extensive addition(s) of oxygen-based functionalities. Further, oxidation extent was correlated with photo-irradiation conditions – higher light intensity resulted in near complete reactant solvation (after 12 days) with higher product oxidation levels and the lowest K_{ow} values. In addition to the role of hydroxyl radical, experiments towards specific (molecular) mechanistic understanding of these reactions are currently ongoing and will be detailed in future reports. Based on these key initial observations, significant fullerane reactivity and transformation under aqueous conditions, which include oxygen and light, should be expected to occur. For these and other advanced materials, understanding such reactivity is critical for material fate, transport and exposure models used for accurate lifecycle and risk analyses.

Acknowledgements

This study was supported by Washington University in St. Louis faculty startup funding. We sincerely thank Matt Epplin for his involvement in this research as part of his EECE independent study course work. We also thank the TEM and DLS facility supported by the Nano Research Facility (NRF) at Washington University in St. Louis. We would also like to thank Materials and Electrochemical Research (MER) Corporation, (Tucson, AZ) for their key role in material synthesis and preparation.

Chapter 3. Supporting Information

Profiles of sunlight intensity monitoring and system pH, products UV spectra, XPS spectra of solid pristine fullerene, size distribution and water-octanol coefficients of products are included.

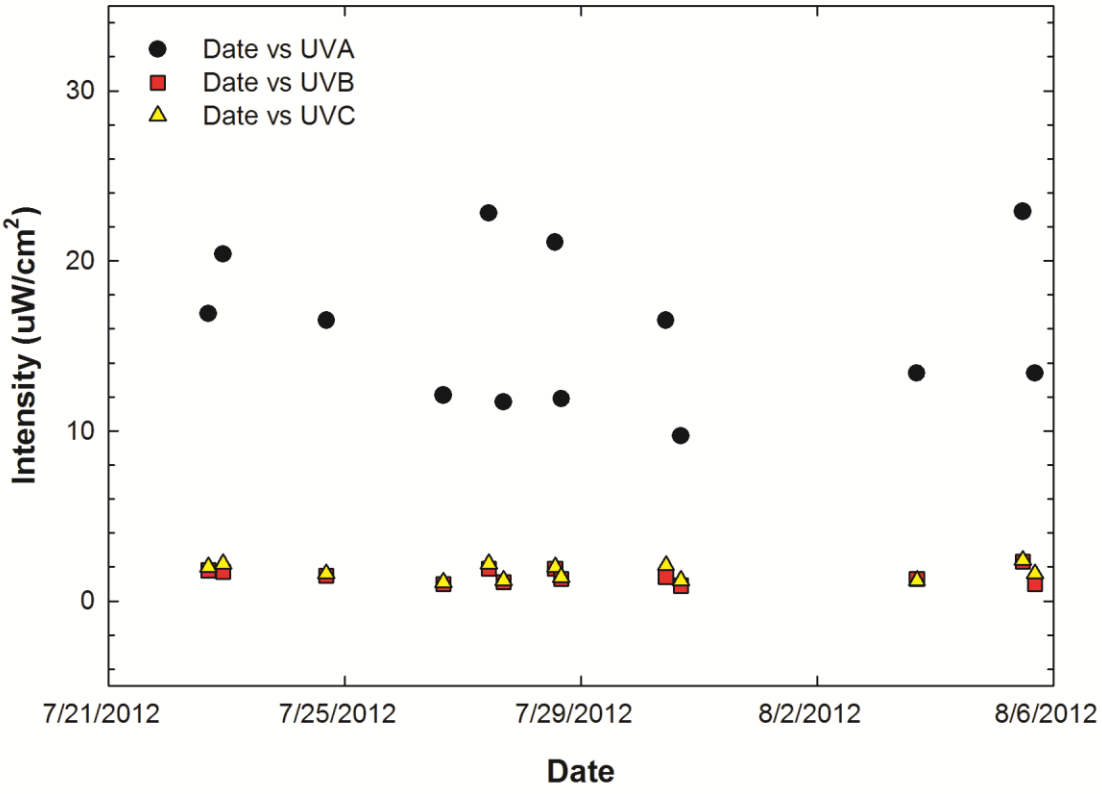

Figure S3.1: Attenuated-sunlight intensities (UVA range) besides window during reaction from July 22th to August 6th, 2012

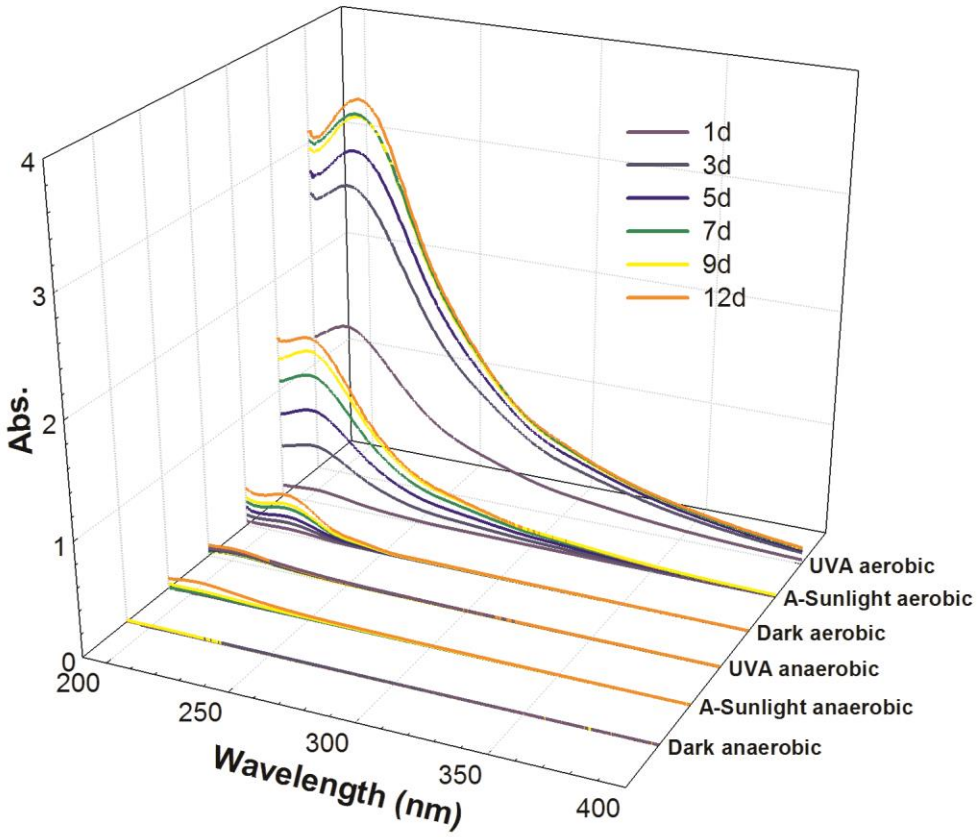

Figure S3.2: UV-vis spectra of fullerane (40 mg/L) solvation products under varied reaction conditions

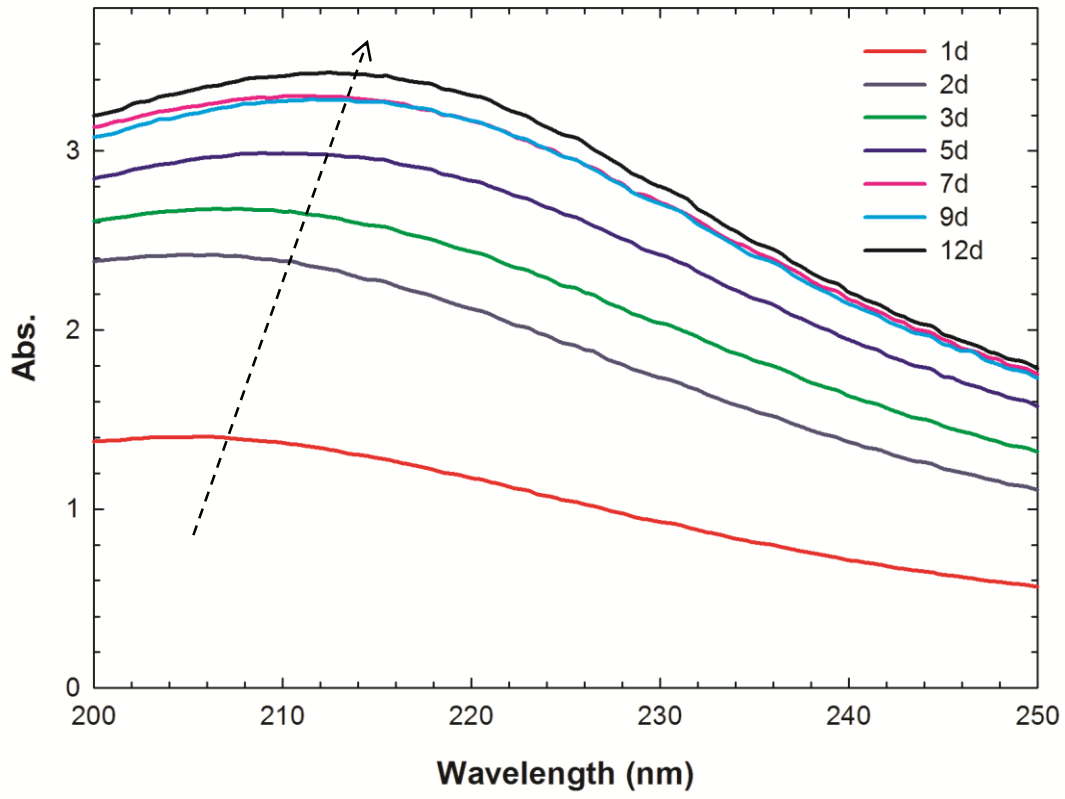

Figure S3.3: UV spectra of 40 mg/L fullerane ($C_{60}H_x$, x ~ 45.5) under 2 mW/cm^2 UVA (351 nm) irradiation, ambient conditions over 12 days

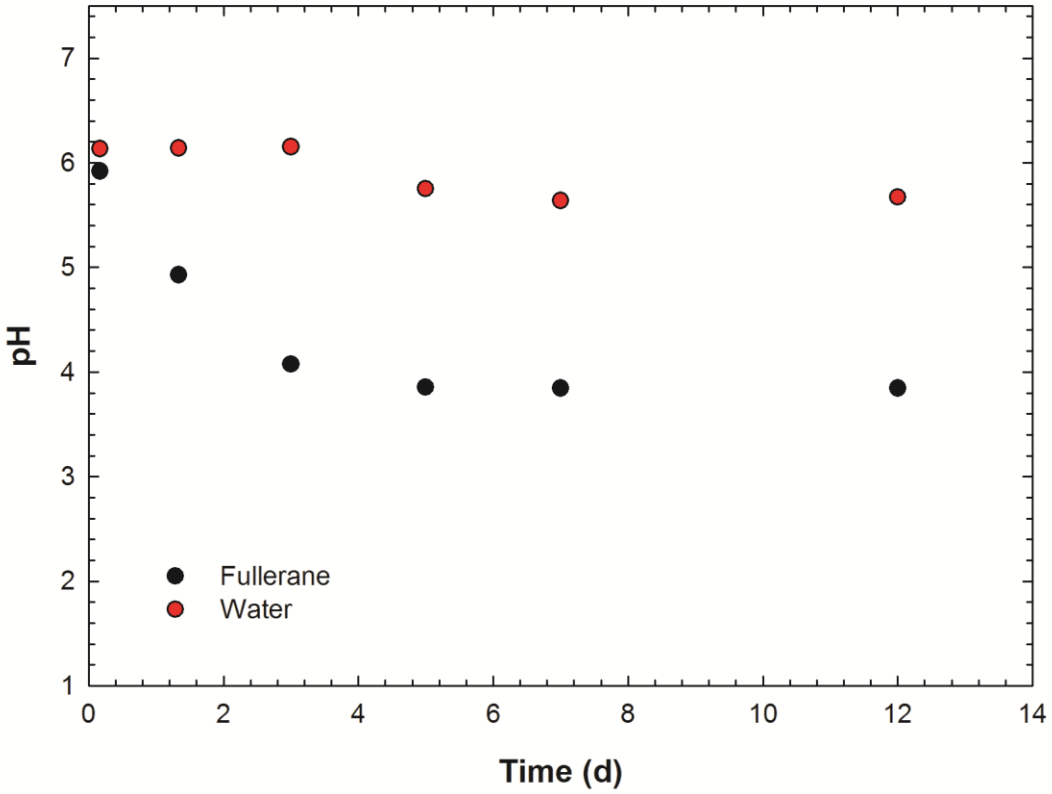

Figure S3.4: Solution pH change during reaction (● 40 mg/L fullerane ($C_{60}H_x$, x ~ 39.9) under 2 mW/cm^2 UVA (351 nm) irradiation, open; ● Ultrapure water)

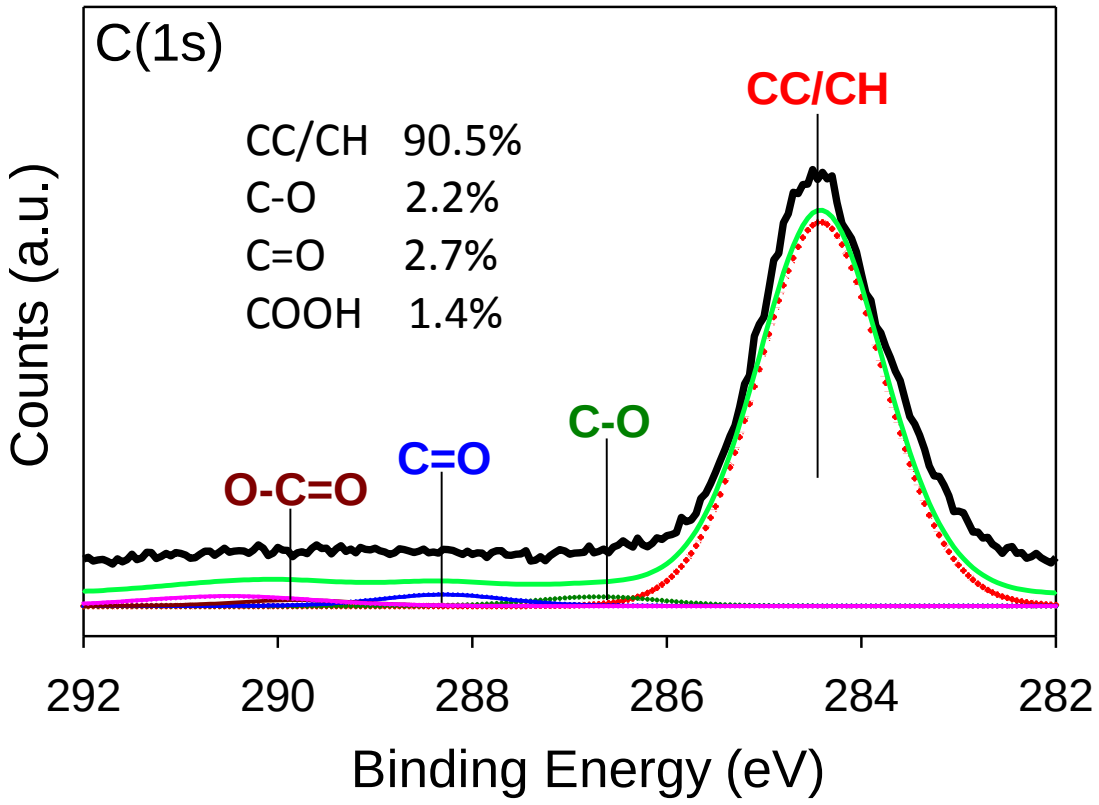

Figure S3.5: C(1s) XPS spectra and curve-fitting analysis of fullerene (C_{60}, MER Corp).

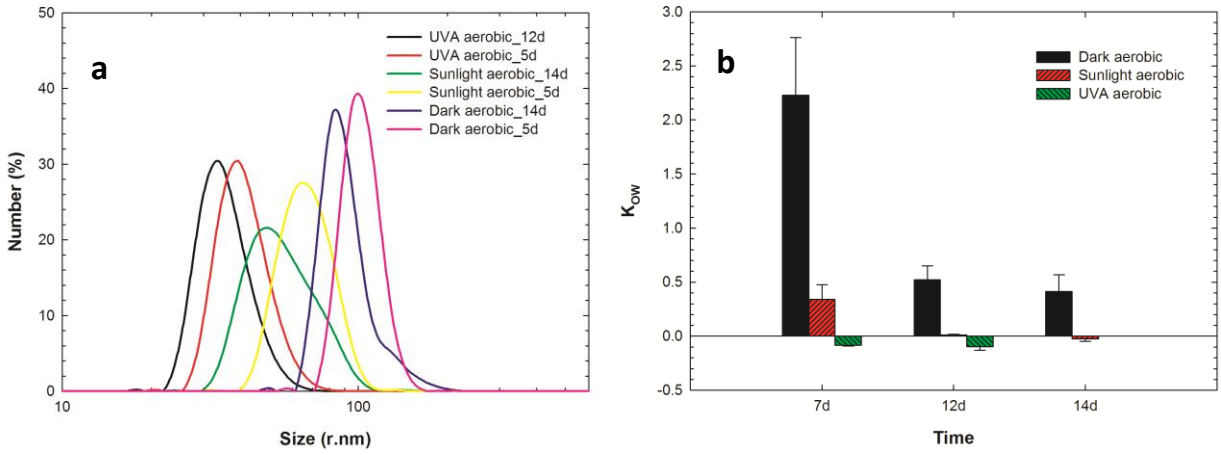

Figure S3.6: DLS size distribution and partition coefficients analyses for fullerane solvated products: (a) number averaged size distribution of products; (b) octanol-water partition coefficients of products.

Chapter 4 :**Ground State Reactions of nC_{60} with Free Chlorine in Water**

Results of this chapter have been published in *Environmental Science & Technology*, **2015**.

Abstract

Facile, photo-enhanced transformations of water-stable C_{60} aggregates (nC_{60}) to oxidized, soluble fullerene derivatives, have been described as key processes in understanding the ultimate environmental fate of fullerene based materials. In contrast, fewer studies have evaluated the aqueous reactivity of nC_{60} during ground-state conditions (i.e. dark conditions). Herein, this study identifies and characterizes the physicochemical transformations of C_{60} (as nC_{60} suspensions) in the presence of free chlorine, a globally used chemical oxidant, in the absence of light under environmentally relevant conditions. Results show that nC_{60} undergoes significant oxidation in the presence of free chlorine and the oxidation reaction rates increase with free chlorine concentration while being inversely related to solution pH. Product characterization by FTIR, XPS, Raman Spectroscopy, TEM, XRD, TOC, collectively demonstrate that oxidized C_{60} derivatives are readily formed in the presence of free chlorine with extensive covalent oxygen and even chlorine additions, and behave as soft (or loose) clusters in solution. Aggregation kinetics, as a function of pH and ionic strength/type, show a significant increase in product stabilities for all cases evaluated, even at pH values approaching 1. As expected with increased (surface) oxidation, classic K_{ow} partitioning studies indicate that product clusters are relatively more hydrophilic than parent (reactant) nC_{60}. Taken together, this work

highlights the importance of understanding nanomaterial reactivity and the identification of corresponding stable daughter products, which are likely to differ significantly from parent material properties and behaviors.

4.1. Introduction

Based on unique applications in a number of technologies[49, 74-76], multi-ton quantities of fullerenes are now being produced globally.[167] At this scale, material release into the environment over time becomes probable. This reality has motivated numerous reports investigating the physical behavior of fullerenes in water, primarily focused on C_{60} as a model fullerene.[36, 44, 85, 168-170] In particular, C_{60} clusters (nC_{60}), which are stable in the aqueous phase, thus enhancing the availability by orders of magnitude, have been well characterized, including a number of transport and biological response studies.[36, 37, 44, 168, 171-184] While the precise mechanism(s) of colloidal stabilization is not completely clear, it is agreed in general that the net negative surface charge, which arises from the formation of (surface-based) oxygen moieties, is a primary factor involved.[37, 93, 168, 185] Interestingly, far fewer investigations have focused on potential environmental (chemical) transformation pathways, which could significantly alter the ultimate fate and transport of the material.[153, 186-189] Further, as C_{60} is quite (photo)reactive, the majority of these aqueous transformation studies have been performed under photo-irradiated conditions.[149, 187, 188, 190, 191] Fewer studies have demonstrated that ground state nC_{60} can also readily react in the absence of light, with ozone or hydroxyl radicals, leading to significant physicochemical transformation(s) in water.[153, 189]

Due to electron availability (with half reduction potential ranging from -0.98 to -3.26 V through cyclic voltammetry measurement[192]) via an extensively conjugated-pi system, and a

strained, olefin-like structure, C_{60} is vulnerable to electrophilic attacks by oxygen, ozone, a series of halogens, and osmium tetroxide, among others.[4, 126, 193-198] Fullerene halogenation in particular has been widely studied in organic solvents and solid state reactions.[126, 199, 200] C_{60} chlorination can be achieved in solid state by simple exposure to chlorine gas at 200-400 ^{o}C, which leads to products with an average of 24 chlorine additions while maintaining a C_{60} (truncated icosahedral) carbon cage based structure.[201] At lower temperatures (-35 ^{o}C), liquid chlorine can be used to achieve a less oxidized product ($C_{60}Cl_x$, x~6).[202] Reactions between C_{60} and ICl, ICl_3, $KICl_4$ and VCl_4 have also been observed, resulting in polychlorofullerenes as $C_{60}Cl_x$ (x=6-30).[203-205] Under UV irradiation, Cataldo et al. developed a synthesis protocol with chlorine gas in CCl_4 or CS_2 under UV irradiation, leading to the formation of polychlorofullerenes (average of 40 and 43 chlorine additions per C_{60}, respectively).[126, 206]

Used globally as a chemical oxidant, typically, target concentrations of free chlorine for water system can range from 1-3 mg/L in drinking water systems, and from 2-70 mg/L in wastewater systems[207-210]. As a possible unwanted side reaction, disinfection by-products (DBPs) can also be formed via chlorine oxidation of dissolved organic species and, at elevated concentrations, can pose potential human health risks.[211-214] The redox potentials of both C_{60} ($E^{o}(C_{60}/C_{60}^{-/6-})$ = -0.98/-3.26V)[192] and free chlorine (as $E^{o}(OCl^{-}/Cl^{-})$= 0.89 V)[215], indicate that fullerene chlorine oxidation reactions may also occur in water. Similar in concept, we have reported the reaction between nC_{60} and ozone in the aqueous solution, which led to the formation of highly oxidized, water soluble, fullerene-based hemiketal derivatives with ca. 29 oxygen additions per C_{60} molecule.[189] Others have also observed aqueous oxidation reactions in the ground state of nC_{60}, including Lee et al. who investigated nC_{60} oxidation via high concentrations of hydroxyl radicals and found that ca. 30% of carbon was (mono)oxidized, under

the described conditions.[153] Recently, surface oxychlorination of nC_{60} in the presence of free chlorine under florescent light irradiation (245 $\mu W/cm^2$) was reported by Wang et al. and a change in particle size was observed, even in the absence of light, in a high salinity solution (15 g NaCl/L).[216] Additionally, the chlorination of nC_{60} (i.e. chlorination of oxidized/ozonated fullerenes) was reported, with chlorine covalently bonded to carbon (C-Cl) identified, both before (for a single reaction condition designed as a control) and after pretreatment (C_{60} oxidation) by ozone.[217] However, to date, the reaction between nC_{60} and free chlorine in dark (ground state) conditions have not been comprehensively investigated with regard to reaction and product characterization.

In this work, we quantitatively describe the ground state C_{60} (as nC_{60} in water) reaction with free chlorine over a range of relevant aqueous conditions (e.g. pH, chlorine level) resulting in significantly oxidized fullerene products with enhanced aqueous stabilities. Along with reaction kinetics, detailed product characterization using X-ray photoelectron spectroscopy (XPS), Fourier transformation infrared spectroscopy (FTIR), Raman spectroscopy, X-ray diffraction (XRD) and transmission electron microscopy (TEM) are described. Lastly, reactant and product physical properties, including organic partitioning and aggregation behaviors (with varied ionic strengths/types and pH) are compared and discussed.

4.2. Materials and Methods

4.2.1. **Materials**

nC_{60} suspensions were prepared through solvent exchange using C_{60} saturated tetrahydrofuran (THF) solution according to our previous report.[189] In order to eliminate the possible interference from the residual THF, nC_{60} suspensions were purified with > 99.5%

(volume) water replacement through a stirred-cell membrane unit (Amicon, molecular weight cutoff (MWCO) of 10,000 Da). Dibasic potassium phosphate (K_2HPO_4), sodium chloride (NaCl), calcium chloride dihydrate ($CaCl_2 \cdot 2H_2O$) and 1-octanol were purchased from Sigma Aldrich (St. Louis, MO). Sodium hypochlorite solution (Laboratory Grade, 5.65-6.00 %), phosphate buffer solution (for chlorine determination DPD method), and di-sodium ethylenediaminetetraacetic acid (Di-sodium EDTA) were purchased from Fisher Scientific (Pittsburgh, PA). Sodium hypochlorite (NaOCl) solution here used as the chlorine source was quantified as 60.32 g/L as Cl_2 through the iodometric method.[218] All the reaction solutions used in the experiment were prepared in ultrapure water (>18.2 MΩ-cm resistivity, Milli-Q, Millipore Corp., MA).

4.2.2. **Chlorination Batch Experiments**

nC_{60} chlorination batch experiments were all conducted in 100 mL borosilicate glass vials covered with aluminum foil to avoid the light irradiation during the reaction. The total carbon concentration of starting nC_{60} solution was identified with TOC-L total carbon analyzer (Shimadzu Scientific Instrument, Inc., MD) as 7 mg/L. The free chlorine in the reaction system was created by adding NaOCl to nC_{60} solutions achieving Cl_2 concentrations as 10, 50 and 100 mg/L. The pH of the system was adjusted initially to 4.5, 6.5 and 8.5 by nitric acid (HNO_3) or sodium hydroxide (NaOH) and stabilized with 10 mM phosphate buffered saline throughout the reactions. HNO_3 was employed here to adjust pH, rather than hydrochloric acid (HCl) to avoid the effect derived from the additional chloride ions from HCl during the chlorination process. System pH was monitored periodically over the course of the reactions. As the reaction proceeded, 2 mL sample aliquots were taken at specific time intervals and immediately analyzed via UV-vis spectroscopy (Varian Cary Bio50, Agilent Technology, CA) to monitor nC_{60}

absorbance changes. 340 nm (molar adsorption coefficient = 4.486×10^4 $M^{-1}cm^{-1}$), a fundamental absorbance C_{60} peak (as an $^1T_{1u} - {}^1Ag$ transition peak), was selected to evaluate reaction kinetics. Within the concentration range studied, nC_{60} absorption at 340 nm is linearly proportional to molecular C_{60} concentrations measured by HPLC upon solvent extraction (toluene).[153, 187-189] Upon sampling, residual free chlorine was immediately quenched immediately with excess sodium thiosulfate (molar ratio: 1/4 of $Na_2S_2O_3/Cl_2$).[219] As the UV-vis scanning time is less than 10 seconds (with all free chlorine quenched), additional oxidation/chlorination reactions occurring during UV-vis measurements are considered negligible. The free chlorine concentration was monitored during the reaction by the standard DPD colorimetric method (Figure S4.1).[218] All of the experimental conditions were conducted in triplicate at room temperature (21.0 ± 1.0 ℃). Control experiments of nC_{60} with no free chlorine in dark conditions at the same levels of pH were also conducted for comparison. Reacted products were collected at the end of the reaction for FTIR, XPS, Raman, XRD, TOC, TEM, DLS, aggregation kinetics studies and water-octanol partition experiments for product characterizations.

4.2.3. **Product Characterization**

Solid products for FTIR analysis were prepared by mixing 200 mL nC_{60} solution as 7 mg/L with 10 mg/L (or 100 mg/L) of Cl_2 in the aqueous solution. Diffuse reflectance infrared spectroscopy (DRIFTS) of the solid sample was conducted using a DRIFTS optical accessory (Praying Mantis, Harrick Scientific) coupled to a Nexus 470 FTIR instrument (Thermo Nicolet, NC). The residual NaOCl background in the reacted nC_{60} solution was removed through being washed in the stirred-cell (Amicon, MWCO of 1000, in order to prevent oxidized products losing) for more than 5 times until the NaOCl background was completely removed, indicated by UV-vis spectra and pH of the out-flow solutions. The chlorinated products were collected from

the purified solution in the vacuum oven (Thermo Scientific, NC) at room temperature overnight. nC_{60} or chlorinated products were mixed with KBr at 1:200 w/w, for a signal optimized ratio. The mixture was grounded in an agate mortar with pestle to be homogenized. The KBr spectrum was collected for background subtraction before sample spectra collection. Samples for X-ray photoelectron spectroscopy (XPS) analysis were prepared in a vacuum oven at room temperature by continuously dropping sample to achieve ca. 1 mL total volume on a gold coated silica wafers. Wafers were prepared by sputter coated silica with gold to at least 20 nm thickness before sample addition. XPS analyses of parent and reacted nC_{60} at different Cl_2 levels were conducted using a PHI Quantera SXM scanning X-ray microprobe with an Al mono source. The analyses were all conducted at 26 eV pass energy at a 200 μm X-ray spot size. The TEM micrographs were taken using FEI Spirit transmission electron microscopy at 120 kV voltage. TEM specimens were prepared by evaporating ca.30 μL of parent or reacted nC_{60} suspension on the 400 mesh carbon-coated copper grids (Electron Microscopy Sciences, PA). TOC concentrations of the nC_{60} solution before and after the reaction were determined through TOC-L total carbon analyzer (Shimadzu Scientific Instrument, Inc., MD). nC_{60} solution as ca. 7 mg/L reacted with 10 mg/L and 100 mg/L Cl_2 respectively, and the resulting samples after 3 days and 54 days were collected to test the carbon conservation during the chlorination (oxidation) process (if there is mineralization after long-term free chlorine exposure). Raman spectra were obtained by using a Laser Raman spectrometer (Kaiser HoloLab5000) with a 532 nm wavelength laser (Nd:YAG CW) focused through a ×20 objective lens. A silica reference calibration was conducted before the measurement with solid samples. X-ray powder diffraction (XRD) patterns were obtained using a Bruker D8 Advance with a LynxEye XE detector. 2θ range was from 10 to 75 degree with a Cu Kα X-ray source (1.54 Å), generated at 40 kV and 40 mA.

4.2.4. **Octanol-Water Partition Coefficients Measurements**

1-octanol was selected as the reference organic phase to determine the octanol-water partitioning coefficients (K_{ow}) of nC_{60} before and after chlorination. K_{ow} was selected because it is one of most common empirical parameters to evaluate the fate and distribution of organic contaminants in the natural environment, including fullerene and its derivatives.[220-222] 8 mL parent or reacted nC_{60} product solutions were mixed with 1-octanol solvent of the same volume at three different pH values (pH = 4.5, 7.5 and 10.5) in amber glass vials and shook by a rotary shaker (Labquake, Thermo Scientific, UT) for 3 hours. The mixtures were then stood for 24 hours to allow layer separation and samples in the water phase was collected for UV-vis analysis (at 340 nm) to determine the concentration of nC_{60} left in the water phase. The octanol-water partition coefficient (K_{ow}) of the parent and reacted nC_{60} was calculated as the ratio of the fullerol concentration in the octanol phase to that in the water phase, according to equation (1):

$$K_{ow} = \frac{C_0}{C_w} = \frac{[Abs]_{340nm,i} - k \times [Abs]_{340nm,f}}{[Abs]_{340nm,f}} \qquad (1)$$

The concentrations of nC_{60} in octanol phase were calculated by subtracting the nC_{60} absorbance in the water phase after partitioning ($[Abs]_{340nm,f}$) from the initial absorbance at 340 nm ($[Abs]_{340nm,i}$) according to mass balance. This partitioning coefficient was corrected by the concentrating factor k determined experimentally, in order to correct for the volume of water dissolved into octanol phase. The pH effect (at 4.5, 7.5 and 10.5) was also covered, and adjusted before partition by NaOH and HNO_3. All the above experimental conditions were conducted in triplicate at room temperature (21.0 ± 1.0 ℃).

4.2.5. **Aggregation Kinetics**

The initial aggregation rates were determined by the linear regression of the initial slope (k_i) of the increasing of the hydrodynamic size of fullerene clusters in the presence of NaCl or $CaCl_2$ at different concentrations. As the ionic strength increased to the diffusion-limited regime, the aggregation rate (k_{fast}) was independent of the electrolyte concentration, which was chose to normalize the attachment efficiency[223-228]:

$$\alpha = \frac{1}{W} = \frac{k_i}{k_{fast}} \qquad (2)$$

The solutions of parent nC_{60} or reacted nC_{60} (with 100 mg/L Cl_2 for 5 days and 20 days) at the same concentration (ca. 7 mg/L) were injected with certain amount of electrolyte stock solution to achieve a total volume of 1 mL. Besides, 1.4 mM NaCl was presented initially in the parent nC_{60} solutions in order to create the same ionic strength background as that of 100 mg/L Cl_2 within the reacted nC_{60} samples. The pH of the reacted nC_{60} solution was adjusted to the same level as the parent nC_{60} solution (pH = 6.3) before partition. The hydrodynamic diameters of nanoparticles changing over time in the presence of NaCl, $CaCl_2$, and $MgCl_2$ were monitored via time-resolved dynamic light scattering measurement (Zetasizer, Malvern Instruments, UK) for 20 minutes, which has been used for critical coagulation concentration (CCC) determination for a wide range of nanoparticles.[44, 229-238] The hydrodynamic diameters of particles as a function of time are shown in Supporting Information as Figure S4.6. The initial slope of the size changing over time was calculated over a time range 0-150 seconds. The critical coagulation concentration is determined at the electrolyte concentration whereby the aggregation kinetics transit from unfavorable (reaction-limited) to favorable regime (diffusion-limited).[229] Experimentally, CCC

was determined by the intersection of the reaction-limited stability curve with the diffusion-limited stability curve.[224]

4.3. Results and Discussion

In the dark, nC_{60} readily reacts with free chlorine in water. Characteristic nC_{60} spectra (over 280 nm - 600 nm, with $^1T_{1u} - {}^1Ag$ transition peaks of 260 nm, 340 nm and 450 nm[4]) in the presence of Cl_2 (100 mg/L) are lost over an exposure time of 23 days, as shown in Figure 4.1a. We have observed similar phenomena of characteristic peaks for semi-batch reactions of ground state nC_{60} oxidation with dissolved ozone.[189] Carbon mass balance determinations, before and after the chlorination reactions, indicate no mass loss due to precipitation and/or mineralization (Table S4-1). Effective reaction rates (shown in Figure 4.1b) were derived from the initial slopes of the absorbance changes (0 - 60 minutes, linear) of nC_{60} at 340 nm during the reaction (SI, Figure S4.2).[239-241] Reaction rates increased as the Cl_2 concentration increased due to the raised oxidation potential (via concentration). Further, reaction rates were observed to increase by decreasing pH due to the resulting chlorine species distribution ($HOCl$ /OCl^-). For reference, the acid-base behaviors of hypochlorite in the water are presented in equations (3) and (4):

$$Cl_2 + H_2O = HOCl + Cl^- + H^+ \quad , \qquad K_{Cl_2} \qquad (3)$$

$$HOCl = ClO^- + H^+, \qquad K_{HOCl} \qquad (4)$$

The acidity constants for equation (3) and (4) are 5.1×10^{-4} M ($pK_{Cl_2, 25^oC} = 3.29$) and 2.9×10^{-8} M ($pK_{HOCl,\ 25^oC} = 7.54$), respectively.[242, 243] As OH^- is typically better leaving group than O^{2-} (from hypochlorite species), hypochlorous acid, at lower pH, is more reactive towards the reduced organic compounds.[208, 244] It should be noted that Cl_2(aq) may also exist in the reaction

system with higher chloride concentrations (Cl_2(aq) typically undergoes complete hydrolysis at pH > 4).[208] Additionally, other chlorine intermediates (e.g. Cl^{3-} and Cl_2O) may also play a role(s) in observed reactions, however these typically exist very low concentrations as reported for similar systems.[208, 244-246] Previous studies have reported a number of chlorination reactions with polyaromatic hydrocarbons (PAHs) which follow second-order reactions (or pseudo-first order reaction when chlorine is excessive).[247-249] However, the chlorination reaction rates (SI, Figure S4.2) for these systems did not follow a simple second-order reaction behavior(s), suggesting that a heterogeneous reaction is taking place. Similarly, aqueous nC_{60} reaction kinetics with dissolved ozone was also observed to be a complex, heterogeneous reaction.[189] nC_{60} particle morphology alteration over a reaction is shown in Figure 4.1c. After 4 hours, nC_{60} faceted crystal edges are observed pit and soften, and after 5 days, finally lose the organized structure (in the presence of 200 mg/L Cl_2). Similar nC_{60} morphological changes (i.e. crystalline to amorphous) were also observed during the referenced nC_{60} ozonation reaction.[189] The observed product (amorphous) disorder was also clearly observed via XRD analysis as shown in Figure S4.3; the reacted nC_{60} products (Figure S4.3c) diffraction patterns showed significant decrease in (short range) order (extensive peak merging and broadening) compared with the parent nC_{60} and pure C_{60} (reference) powders. Additionally, parallel diffraction patterns of the reacted nC_{60} products (Figure S4.3d) suggest a greater distance between C_{60} molecules after oxidation(s) as noted by others.[250] Soft cluster aggregation of hydroxylated fullerenes has been observed by Brant et al. for (fullerols) in water, with hydrodynamic particle (cluster) size reported to be ca. 100 nm.[251]

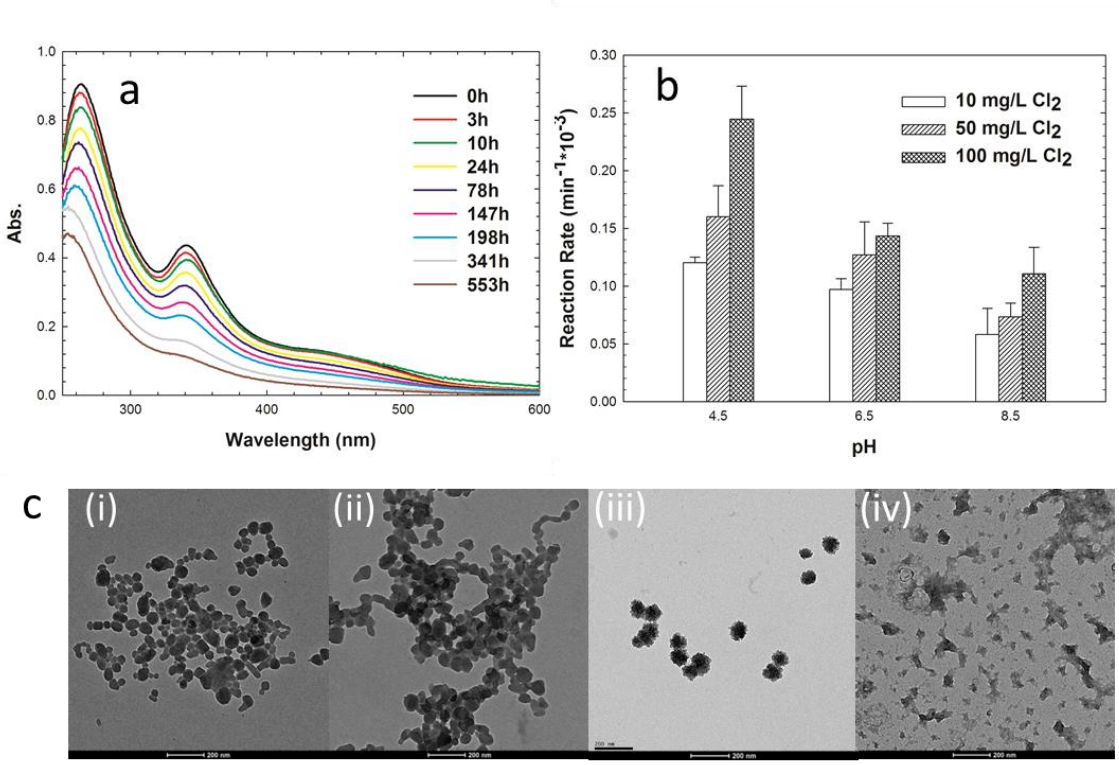

Figure 4.1: Reaction of C_{60} aggregates and free chlorine in water: (a) nC_{60} (ca. 7 mg/L) UV spectra as a function of reaction time for batch reaction studies (100 mg/L Cl_2; no buffer added); (b) Reaction rate of nC_{60} with 10, 50 and 100 mg/L free chlorine at pH 4.5, 6.5 and 8.5 (Error bars represent standard deviation calculated from triplication experiments); (c) TEM images of nC_{60} morphology during chlorination: (i) parent nC_{60} at pH 4.5; (ii) nC_{60} with 100 mg/L Cl_2 for 4 hours; (iii) nC_{60} with 100 mg/L Cl_2 for 48 hours; (iv) nC_{60} with 200 mg/L Cl_2 (5 days, additional 100 mg/L Cl_2 added at 48 hours). All scale bars are 200 nm.

FTIR spectra for nC_{60} and reacted products are presented as a function of free chlorine concentration and reaction time in Figure 4.2. Parent C_{60} powder exhibits five characteristic peaks at 528, 576, 1180, 1430 and 1540 cm^{-1} attributed to C-C vibration modes of C_{60}, as reported by our group and elsewhere.[89, 121] In water (Figure 4.2b), nC_{60} losses peak intensity at

1180, 1430 and 1540 cm^{-1}. This has been hypothesized to result from minor (surface) carbon oxidation upon nC_{60} formation[89, 184], which is supported by new peaks appearing within 1830-1684cm^{-1} (centered at 1726 cm-1, carbonyl group), 1000-1250 cm^{-1} (centered at 1100 cm^{-1}, C-O stretching).[187-189] After nC_{60} reacted with 10 mg/L free chlorine for 5 days (Figure 4.2c), C_{60} characteristic peaks decrease although absorbance peaks around 1000 cm^{-1} remain when compared with unreacted nC_{60}. As Cl_2 concentration is increased (Cl_2 = 100 mg/L, reacted for 5 days, Figure 4.2e), a group of new peaks from 500 – 900 cm^{-1} is observed, which are typical of C-Cl stretching.[126] Mechanistically, chlorination reactions likely involve the electrophilic additions of chlorine atom(s) at unsaturated ethyletic sites of C_{60} hexagonal rings, similar to other reports.[252] As nC_{60} surface molecules are partially oxidized upon formation (Figure 4.2b and as observed by Labille et al.[89]), there is also possibility that chlorination occurs via electrophilic substitution through OCl^-/HOCl attack on the oxygen moieties in ortho- or para-positions of sp3 derivatized carbon of parent C_{60}.[208, 217] In addition, the peak centered at 1100 cm^{-1} (1280 cm^{-1} to 1020 cm^{-1}) significantly increases , which can be attributed to both C-O stretching and/or aryl C-Cl stretching.[159, 253] Further, absorbance peaks centered at 1730 cm^{-1} and 1621 cm^{-1} also increase, indicating that C=O is being formed with increased amounts of free chlorine.[187, 189] Carbonyl groups may also evolve via Cl elimination (dehydrohalogenation) mechanisms, as demonstrated by others.[248, 254] Product spectrum for the case for higher levels of Cl_2 (as 100 mg/L) for 1 day exposure, is shown for comparison (Figure 4.2d), and also demonstrates increasing levels of oxidation, as indicated by the relative decrease in parent associated absorbance peaks in addition to increase in carbon - oxygen and carbon - chlorine absorbance peaks at ca. 1700 cm^{-1}, 1100 cm^{-1} and also 500 – 900 cm^{-1}, respectively. With longer exposure time (20 days), the characteristic parent peaks of 1180, 1430 and 1540 cm^{-1} disappear

completely (Figure 4.2f), along with a relative increase oxygen related peaks, supporting possible dehydohalogenation / hydrolysis processes. The relative intensity of characteristic peaks at 528 and 576 cm^{-1} remained nearly same compared to the 5 day sample, with chlorinated carbon occurrence actually decreasing over a longer reaction time, indicating intermediate C-Cl occurrence. Under (photo)irradiation for 32 hours with a free chlorine concentration 400 mg/L (as Cl_2), C_{60} oxychlorination was reported by Wang et al. with oxygen moiety functional groups, and aryl-Cl and C-Cl stretching identified by FTIR analysis.[216] FTIR spectrum of a commercial fullerol ($C_{60}(OH)_x(ONa)_y$, (y ~ 6-8, x+y ~ 24, MER. Corp) is also provided for comparison (Figure 4.2g) and while similar to oxychlorinated nC_{60}, it is not identical.

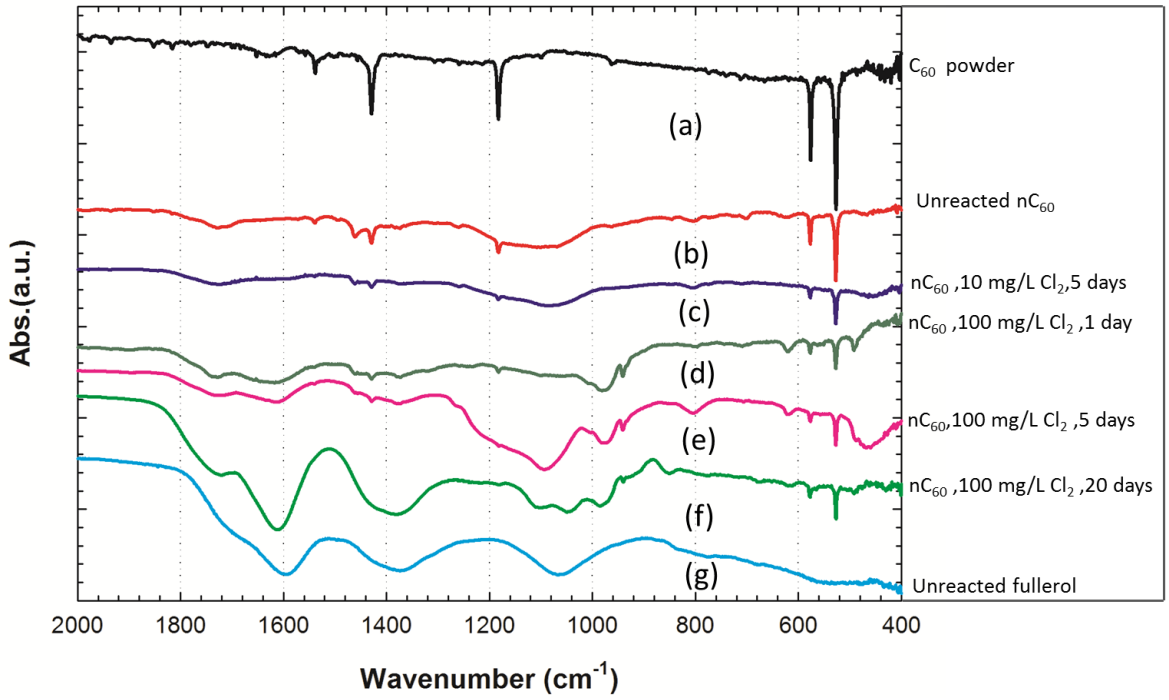

Figure 4.2: FTIR-DRIFTS unreacted nC_{60} and chlorinated products spectra: (a) C_{60} powder; (b) Unreacted nC_{60} control; nC_{60} products after reaction with (c) 10 mg/L Cl_2 for 5 days; (d) 100 mg/L Cl_2 for 1 day; (e) 100 mg/L Cl_2 for 5 days; (f) 100 mg/L Cl_2 for 20 days; (g) Parent fullerol ($C_{60}(OH)_x(ONa)_y$, y ~ 6-8, x+y ~ 24).

XPS absorption spectra of nC_{60} and chlorinated products are compared in Figure 4.3. Similarly to FTIR results, parent nC_{60} is slightly (surface) oxidized (Figure 4.3a). While the majority of parent material carbon remains underivatized (elemental) (ca. 284.4 eV, 86.1%), a low degree of mono-oxidized carbon and di-oxidized carbon are observed at ca. 286.3 eV (7.7%) and 288.4 eV (6.2%).[187, 255] For C1s analysis of the products (Figure 4.3b and 4.3c), both mono-oxidized carbon (ca. 286 eV) and di-oxidized carbon and/or chlorinated carbon (ca. 288 eV) significant increased upon free chlorine exposure (Figure 4.3b, c). It should be noted that

oxidized carbon observed at 288 eV can be assigned to either di-oxidized carbon (-C=O or –O-C-O-) and/or chlorinated carbon (C-Cl).[187, 216, 256] Qualitatively, these results are similar to XPS characterization of photoirradiated nC_{60} (fluorescent light = 245 μW/cm^2, 400 mg/L free chlorine, pH 7, 32 hour reaction time) by Wang et al., which also identified mono-oxidized, di-oxidized carbon products; however, Cl oxidation states were not reported. Further, Wang et al. conclude that oxidation reactions with free chlorine under irradiated conditions occurred/remained on the outer surface of nC_{60} aggregates.[216] Recognizing the limitation of XPS to differentiate such types of carbons via C (1s) analysis, Cl (2p) analysis was also performed and provided in Figure 4.3d-f. Upon 10 mg/L Cl_2 exposure (Figure 4.3e), nC_{60} products show chlorine peaks ($Cl2p_{3/2}$/$Cl2p_{1/2}$), which occurs as a split response (to a single oxidation state), located at 200.2/201.9eV (62.1/18.2%) and 201.5/203.1eV (12.9/6.8%). While Cl signal at lower binding energies (200.2/201.9eV) may be complicated here any NaOCl residual background signal (NaOCl control XPS, Cl spectrum is shown in Figure S4.4)[257], the second group of Cl split peaks, appearing at 201.5/203.1eV, are indicative of Cl covalently bonded to carbon.[256] Alpatova et al. also observed Cl covalently bonded to nC_{60} carbon when treated with sequential ozonation/chlorination, and the extent of chlorination decreased (C-Cl amounts) with increasing (pre)ozonation dosage.[217] Further, when exposed to 100 mg/L Cl_2 (Figure 4.3f), an increased C-Cl signal at 201.4/203.1eV (30.9/9.1%) is observed indicating a relative higher degree of chlorination. Taken together, XPS results are consistent with FTIR observations, indicating relative increase of product oxychlorination as free chlorine concentration was increased.

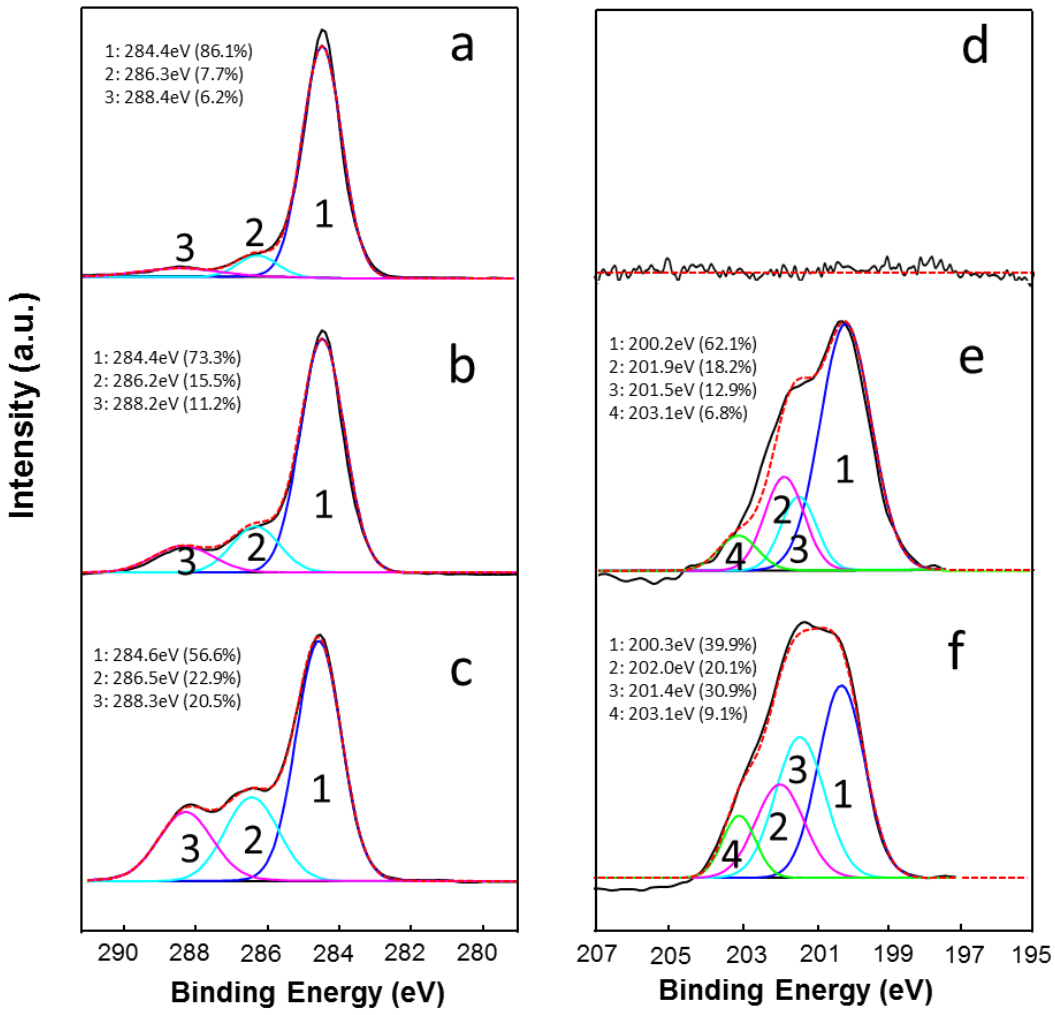

Figure 4.3: XPS spectra and curve-fitting analyses of nC_{60} and reacted products: (a) unreacted nC_{60} (C1s); (b) nC_{60} products with 10 mg/L Cl_2 for 5 days (C1s); (c) nC_{60} products with 100 mg/L Cl_2 for 5 days (C1s); (d) unreacted nC_{60} (Cl2p); (e) nC_{60} products with 10 mg/L Cl_2 for 5 days (Cl2p); (f) nC_{60} products with 100 mg/L Cl_2 for 5 days (Cl2p).

Raman spectra of parent C_{60}, nC_{60} and the reacted nC_{60} products obtained by the chlorination reaction with 100 mg/L of Cl_2 are shown in Figure 4.4. Characteristic Raman peaks appeared for the parent C_{60} solid sample, with shifts as 1355 cm^{-1} (D-band), 1417 cm^{-1} ($7H_g$), 1458 cm^{-1} ($2A_g$), 1571 cm^{-1} ($8H_g$), and 1604 cm^{-1} (G-band).[258, 259] The G-band at ca. 1600 cm^{-1}

and D-band at ca. 1355 cm^{-1} represent sp2 and sp3 carbon atoms in an underivatized fullerene structure, respectively.[260] Here, the intensity ratio of D-band (I_D) to G-band (I_G), is used for relative comparison of the extent of derivatization, as done for graphenes and fullerenes.[260, 261] The spectrum of nC_{60} solid sample collected from a highly purified aqueous solution is relative similar to pure C_{60}, with the same I_D to I_G ratio as 0.718. After exposure to 100 mg/L Cl_2 for 5 days, the I_D to I_G ratio increased to 0.915, indicating a relative increase in sp2 carbon being covalently modified to sp3 carbon.[260] The bottom spectrum is a commercial fullerol ($C_{60}(OH)_x(ONa)_y$, y ~ 6-8, x+y ~ 24, MER.Corp) which is similar in I_D to I_G ratio to the observed chlorinated product(s), which would be expected with increased sp3 carbon occurrence.

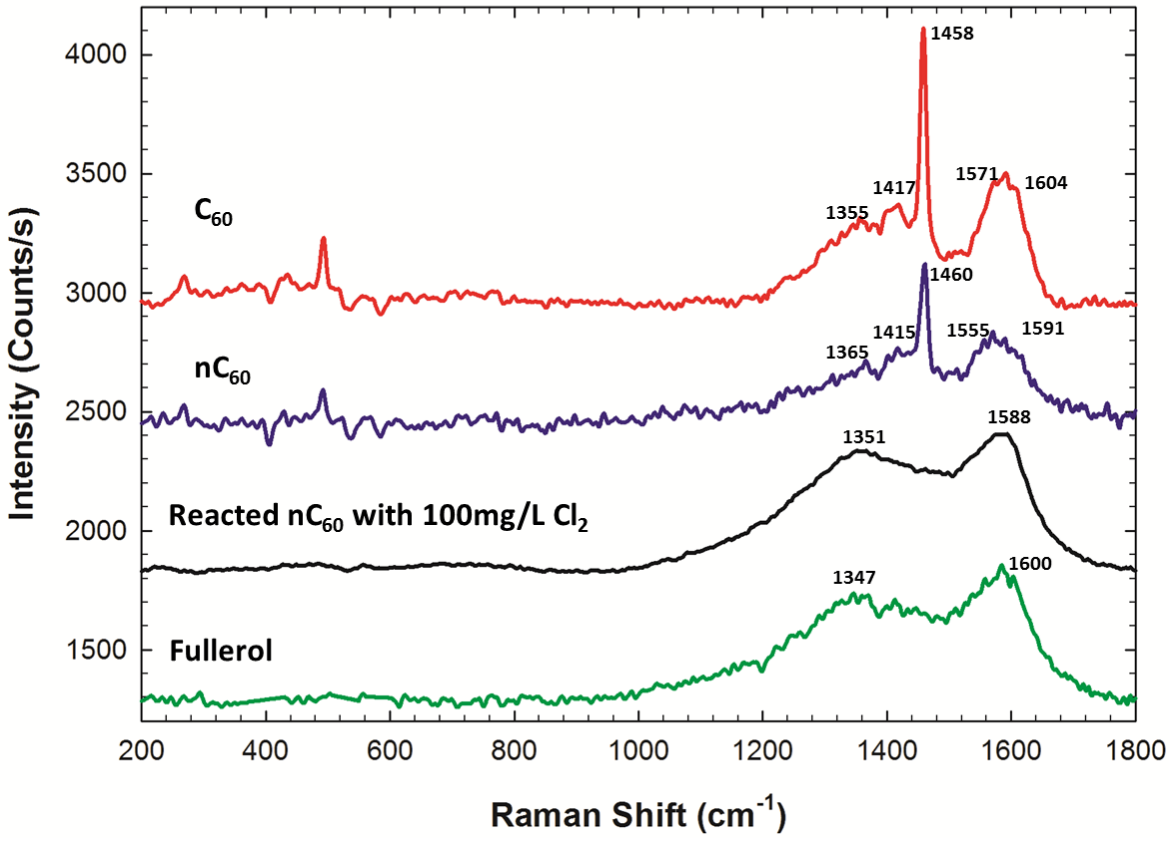

Sample	C_{60}	nC_{60}	Reacted nC_{60}	Fullerol
I_D/I_G	0.718	0.718	0.915	0.909

Figure 4.4: Raman spectra of C_{60} and reacted products (from top to bottom lines): (1) C_{60} powder; (2) Unreacted nC_{60}; (3) nC_{60} reacted products with 100 mg/L Cl_2 for 5 days; (4) Parent fullerol ($C_{60}(OH)_x(ONa)_y$, y ~ 6-8, x+y ~24). Table: I_D/I_G ratios for samples.

Material physical properties/behavior, before and after reactions, were compared through octanol-water partition behavior at pH 7.5 (SI, Figure S4.5). The K_{ow} of nC_{60} after a 20 day reaction with 100 mg/L Cl_2 was evaluated at 3 different pH levels (at pH 4.5, 7.5 and 10.5), and were all observed to be significantly lower than that after a 5 day reaction, indicative of a

relatively more hydrophilic interface (upon longer reaction time). The aggregation status of nC_{60} and the reacted products were also evaluated (Figure 4.5a) as a function of pH. While parent nC_{60} is stable (monodispersed) from pH 5 to 10 as observed previously[41, 168], upon reaction (100 mg/L Cl_2 for 5 days), products, as soft clusters, were observed to remain stable over an extended pH range from 2 to 10.[41, 168, 226, 262] Further, 20 day reactions resulted in product clusters that were colloidally stable at pH values near 1.

Parent and product aggregation kinetics were evaluated through attachment efficiencies (α) calculations as shown in Figure 4.5b-4.5d. In the presence of NaCl, parent nC_{60} remains monodispersed (ca. 90 nm as measured by average intensity response)[96, 168, 263] at or below 20 mM NaCl with a CCC value of 104 mM. Previous studies identified the CCC of water stable C_{60} aggregates from 84 mM to 260 mM, with differences attributed to synthesis routes and surface charge sources.[223, 224, 226, 230, 231] The stability of chlorinated nC_{60} after 5 days was significantly enhanced, with an observed CCC of 648 mM for NaCl. The NaCl CCC value increased even further to 817 mM after a 20 day reaction time. A similar increase in nC_{60} CCC (NaCl) was also observed by Qu et al. after 7 days' oxidation via UV irradiation in water.[224] Significantly enhanced colloidal stability of the reacted nC_{60} products is likely due to both increased electron repulsion forces (a more net negative surface charge) in addition to increased steric repulsion forces (Figure S4.7). As observed by XPS and FTIR analyses, product cluster surfaces have additional / new oxygen and chlorine functionality which changes the molecular-scale charge landscape (placement/order) and thus the net hydration-based repulsion forces (likely decreasing hydrophobic interactions between particles).[124] According to the Schulze-Hardy rule[264], divalent cations are typically more effective screening negative surface negative charge and accordingly, the CCC values for both parent and reacted nC_{60} in $MgCl_2$ solution (5 days reaction) were

observed to be lower, 8.0 mM and 14.8 mM, respectively (Figure 4.5c). CCC values for parent and reacted nC_{60} in $CaCl_2$ solutions were even lower than $MgCl_2$, with values of 4.56 mM and 4.83 mM, respectively (Figure 4.5d). Such a decrease, and deviation from the Schulze-Hardy rule, is hypothesized to be due to relatively strong physicochemical complexation of Ca^{2+} with carboxyl groups.[224, 225, 265-267,268] Relative to Ca^{2+} ions, Mg^{2+} ions typically have significantly lower stability constants than that of monodentate calcium carboxyl complexes.[227, 228, 265, 269] In-line with previous reports, upon 20 days of reaction, we observe the CCC for Ca^{2+} to further decrease (3.77 mM), whereas the CCC of Mg^{2+} ($MgCl_2$) actually increased to 25.7 mM.

4.4. Conclusions

Taken together, this work describes aqueous available C_{60} (as nC_{60}) reacting with free chlorine, which is broadly used for range of disinfection and oxidation processes, in the absence of light irradiation (i.e. without fullerene photo-excitation). Kinetic and product analyses collectively indicate that C_{60} is covalently derivatized, with oxygen and chlorine additions, and the extent of oxychlorination increases with both reaction time and chlorine concentration. Further, the physical properties of the resulting (and stable) product clusters are significantly altered, resulting in enhanced product stabilities over expanded pH and ionic strength ranges. Specific product form, product behavior, and resulting implications will depend on the resulting level of C_{60} oxycholorination (i.e. the available chlorine concentration × exposure time, CT). This work highlights the need to fundamentally understand potential nanomaterial reaction pathways and stable products, in both the environment and common engineered systems, for accurate fate, transport, life cycle, and risk assessments.

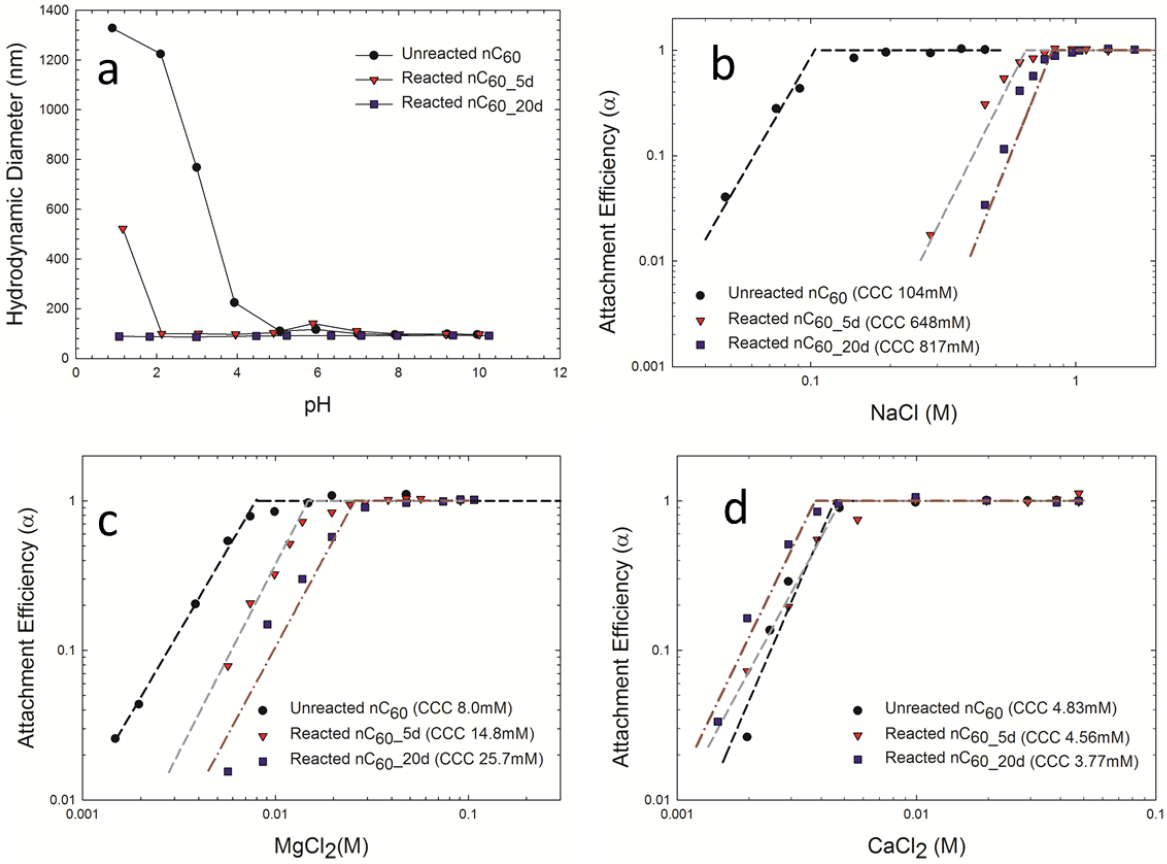

Figure 4.5: Aggregation stability curves of pristine nC_{60} and reacted nC_{60} for 5 and 20 days with 100 mg/L Cl_2: (a) Hydrodynamic diameter at different pH; (b) Attachment efficiencies in NaCl solutions; (c) Attachment efficiencies in $MgCl_2$ solutions; (d) Attachment efficiencies in $CaCl_2$ solutions.

Acknowledgements

This study was supported by Washington University in St. Louis faculty startup funding for Dr. John D. Fortner. We thank for the TEM and DLS facility supporting by Nano Research Facility (NRF) at Washington University in St. Louis, a member of the National Nanotechnology Infrastructure Network (NNIN), which is funded by the National Science Foundation under

Grant No. ECS-0335765. We would also thank Materials and Electrochemical Research (MER) Corporation (Tucson, AZ) for their help in material preparation.

Chapter 4. Supporting Information

Profiles of free chlorine concentrations, nC_{60} UV absorbance at 340 nm, XRD diffractograms of nC_{60} and reacted products, XPS spectra of NaOCl, water-octanol coefficients of products, aggregation and zeta potential profiles, and table of TOC analyses are included.

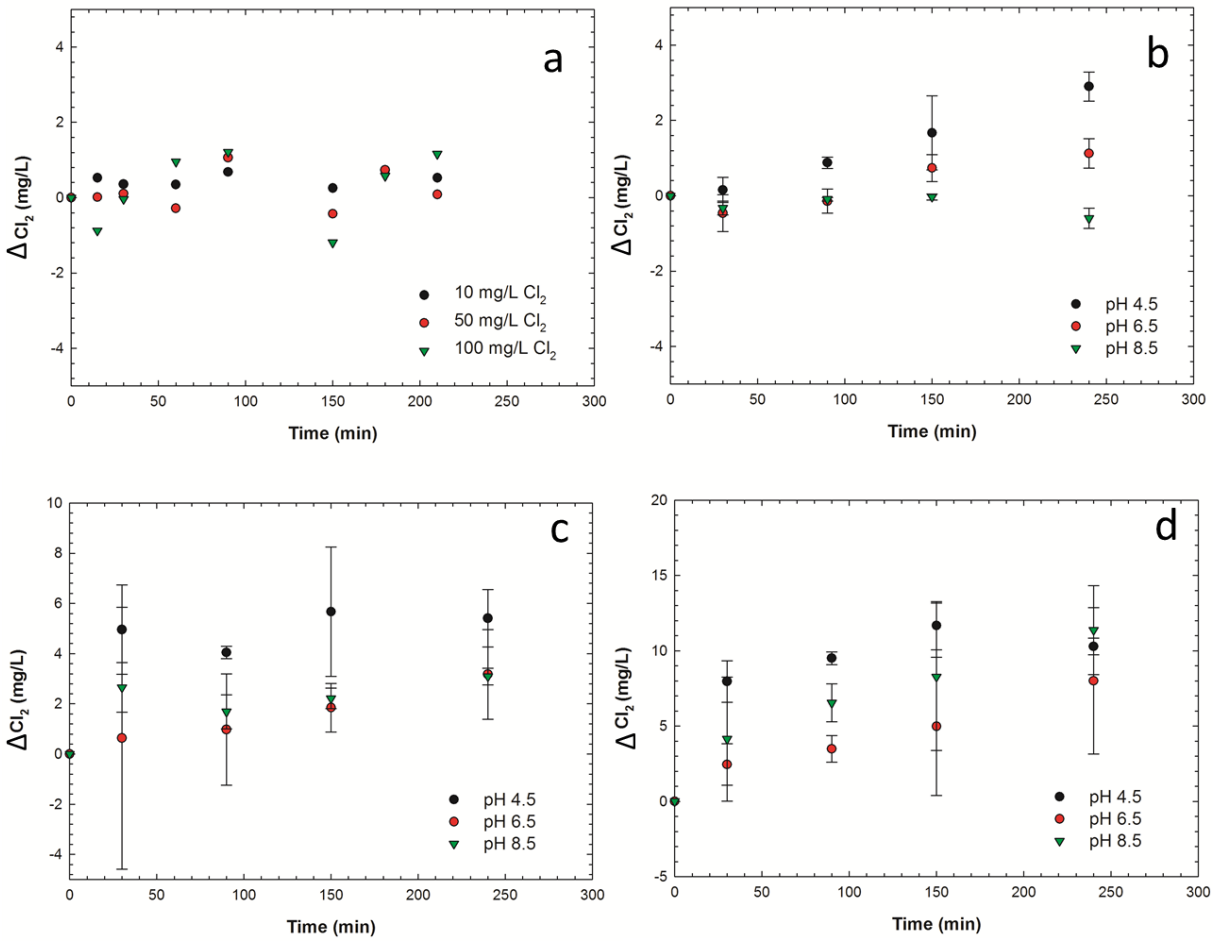

Figure S4.1: Free chlorine concentration measured as the difference between initial and current concentrations ($[Cl_2]_0$-$[Cl_2]$) during the reaction: (a). no nC_{60} at pH 6.5; nC_{60} solution (ca. 7 mg/L) with initial Cl_2 concentration as (b) 10 mg/L; (c) 50 mg/L; (d) 100 mg/L. (Error bars represent standard deviation calculated from triplication experiments)

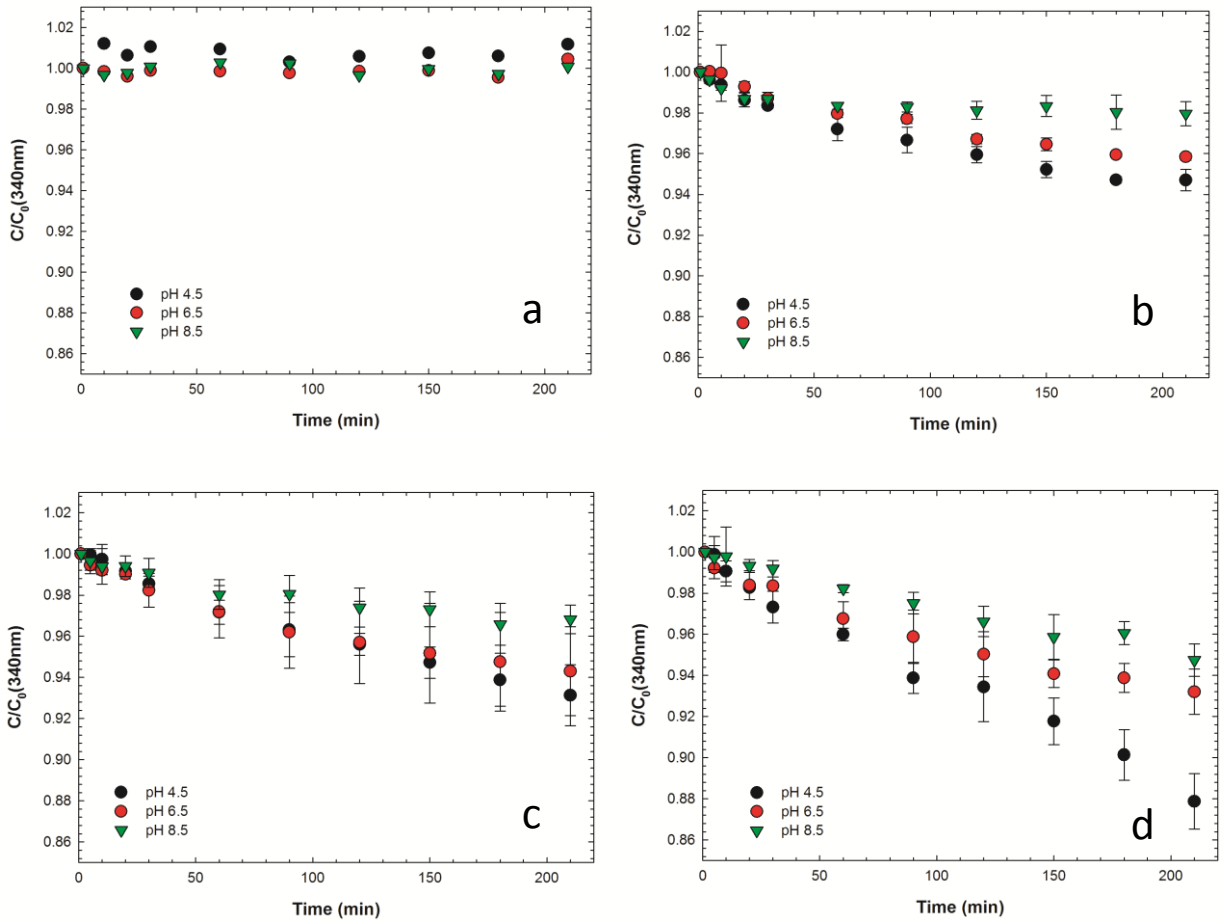

Figure S4.2: nC_{60} UV absorbance ratios at 340 nm (C/C_0) over reactions. ((a). Cl_2 = 0 mg/L; (b). Cl_2 = 10 mg/L; (c). Cl_2 = 50 mg/L; (d). Cl_2 = 100 mg/L.) (Error bars represent standard deviation calculated from triplication experiments)

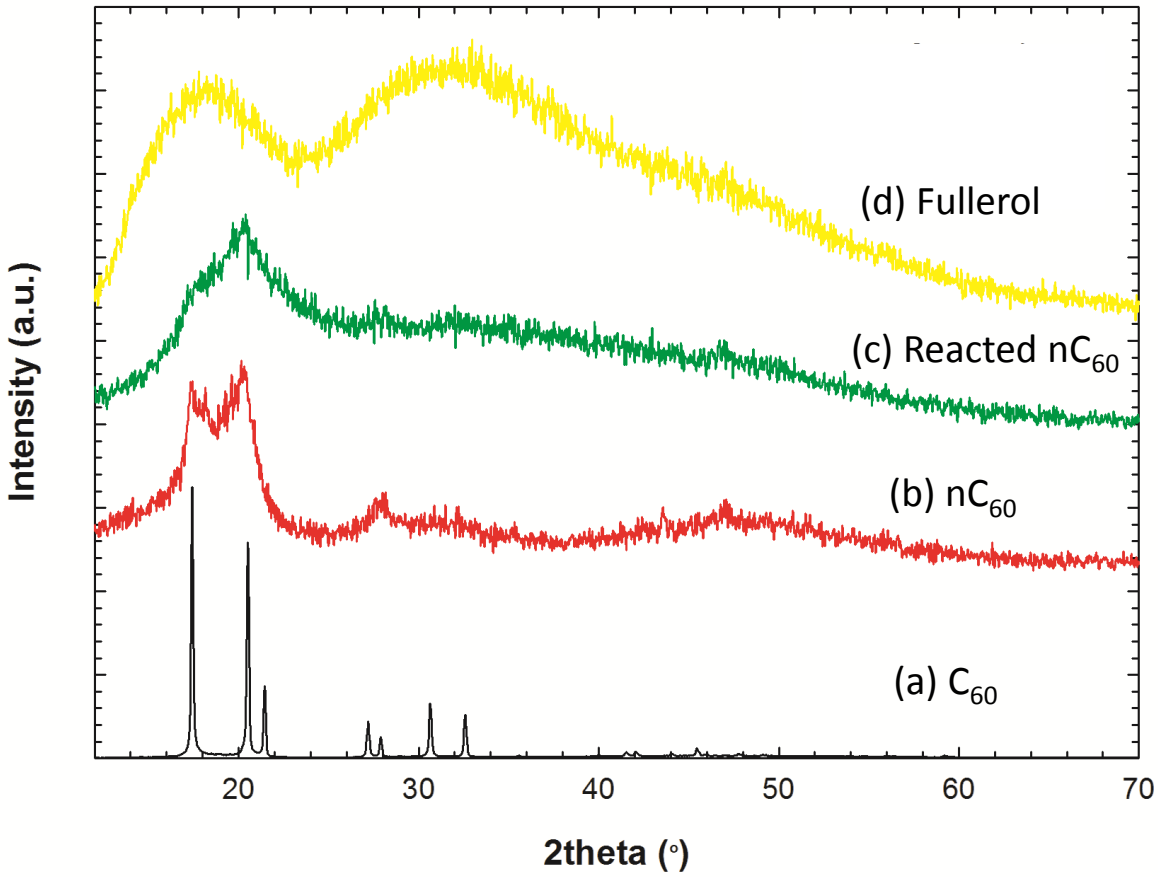

Figure S4.3: XRD diffractograms of parent nC_{60} and the reacted products: (a) C_{60} powder (JCPDS #44-0558); (b) Unreacted nC_{60}; (c) Reacted nC_{60} (treated with 100 mg/L Cl_2 for 5 days); (d) Parent fullerol ($C_{60}(OH)_x(ONa)_y$, y ~ 6-8, x+y ~24).

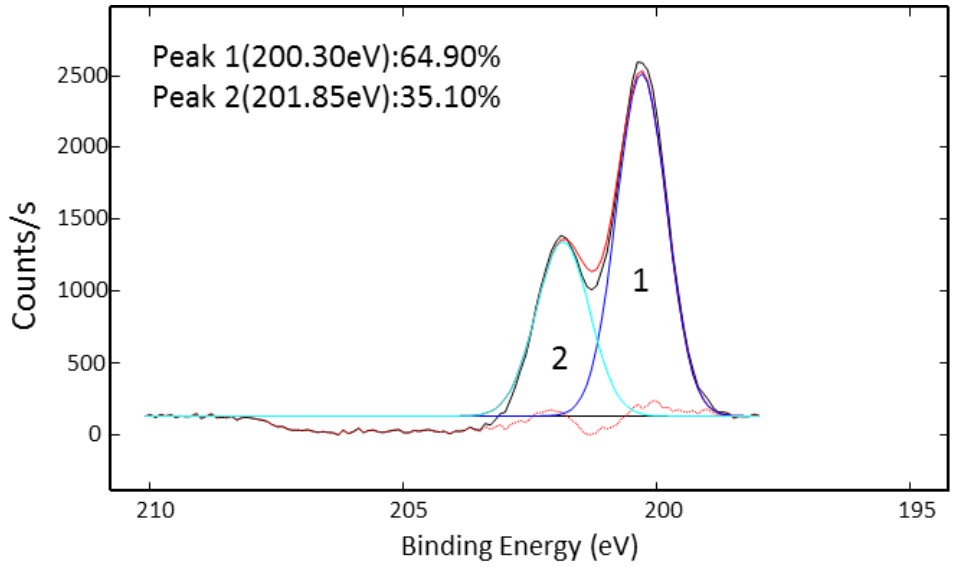

Figure S4.4: Cl(2p) XPS spectrum of NaOCl and curve-fitting analysis.

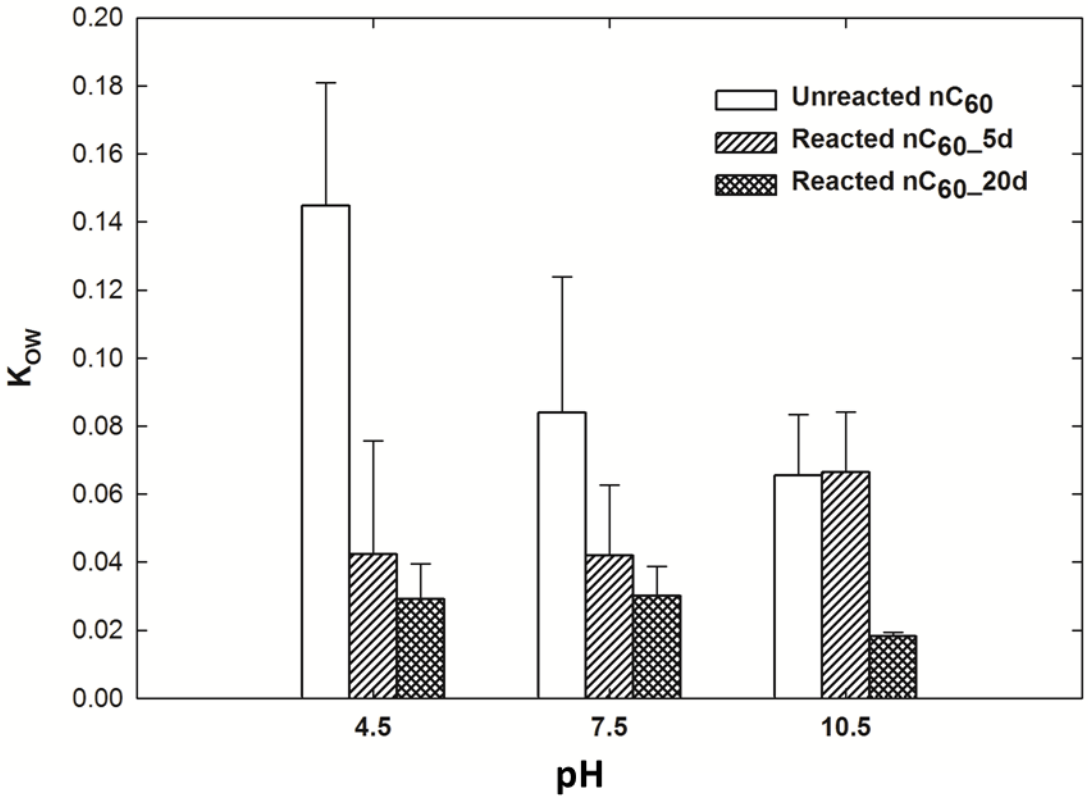

Figure S4.5: Water-octanol coefficients (K_{ow}) of pristine nC_{60} and reacted nC_{60} with 100 mg/L Cl_2 for 5 days and 20 days. (Error bars represent standard deviation calculated from triplication experiments)

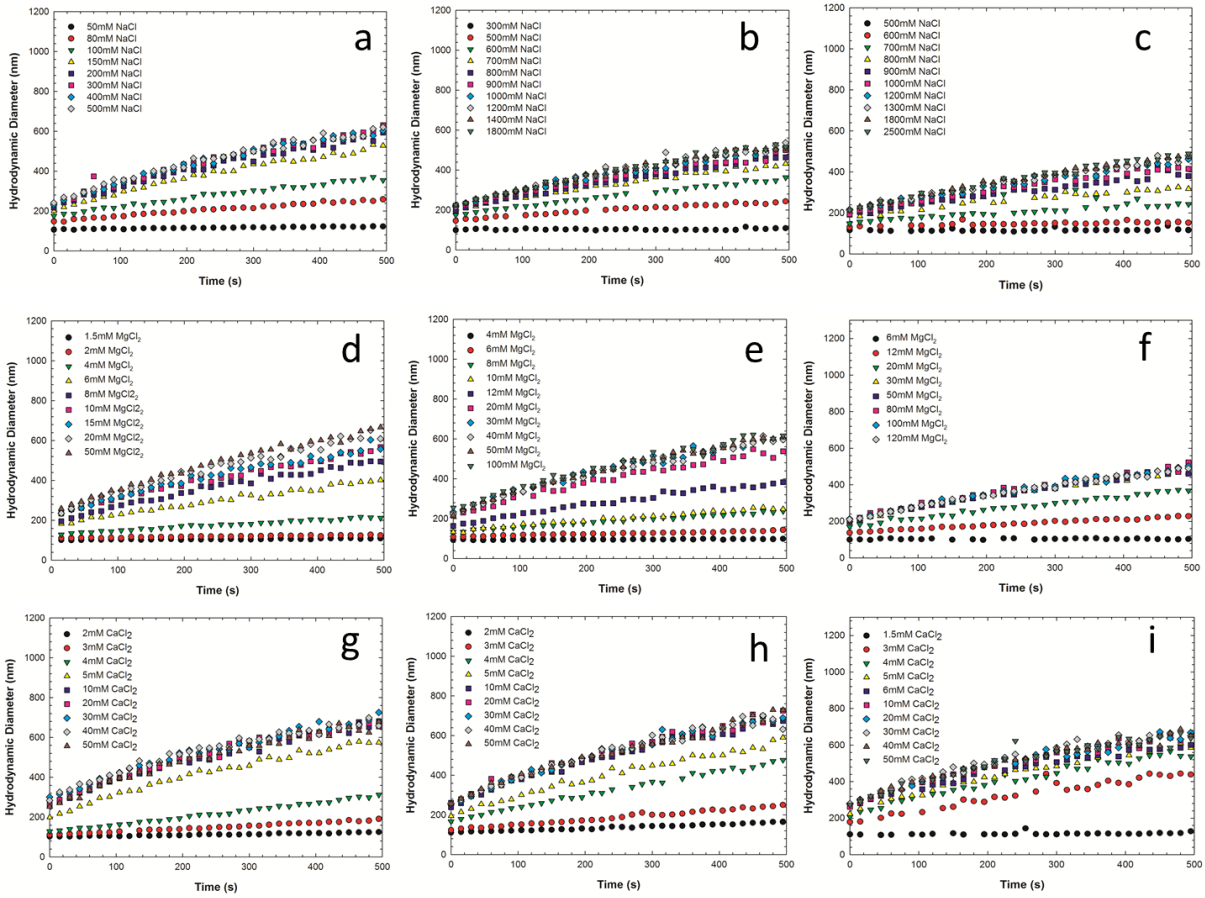

Figure S4.6: Aggregation profiles of nC_{60} and reacted products in the presence of NaCl, $CaCl_2$ and $MgCl_2$: (a) Unreacted nC_{60} in NaCl; (b) Reacted nC_{60} (100 mg/L Cl_2) for 5 days in NaCl; (c) Reacted nC_{60} (100 mg/L Cl_2) for 20 days in NaCl; (d) Unreacted nC_{60} in $MgCl_2$; (e) Reacted nC_{60} (100 mg/L Cl_2) for 5 days in $MgCl_2$; (f) Reacted nC_{60} (100 mg/L Cl_2) for 20 days in $MgCl_2$; (g) Unreacted nC_{60} in $CaCl_2$; (h) Reacted nC_{60} (100 mg/L Cl_2) for 5 days in $CaCl_2$; (i) Reacted nC_{60} (100 mg/L Cl_2) for 20 days in $CaCl_2$.

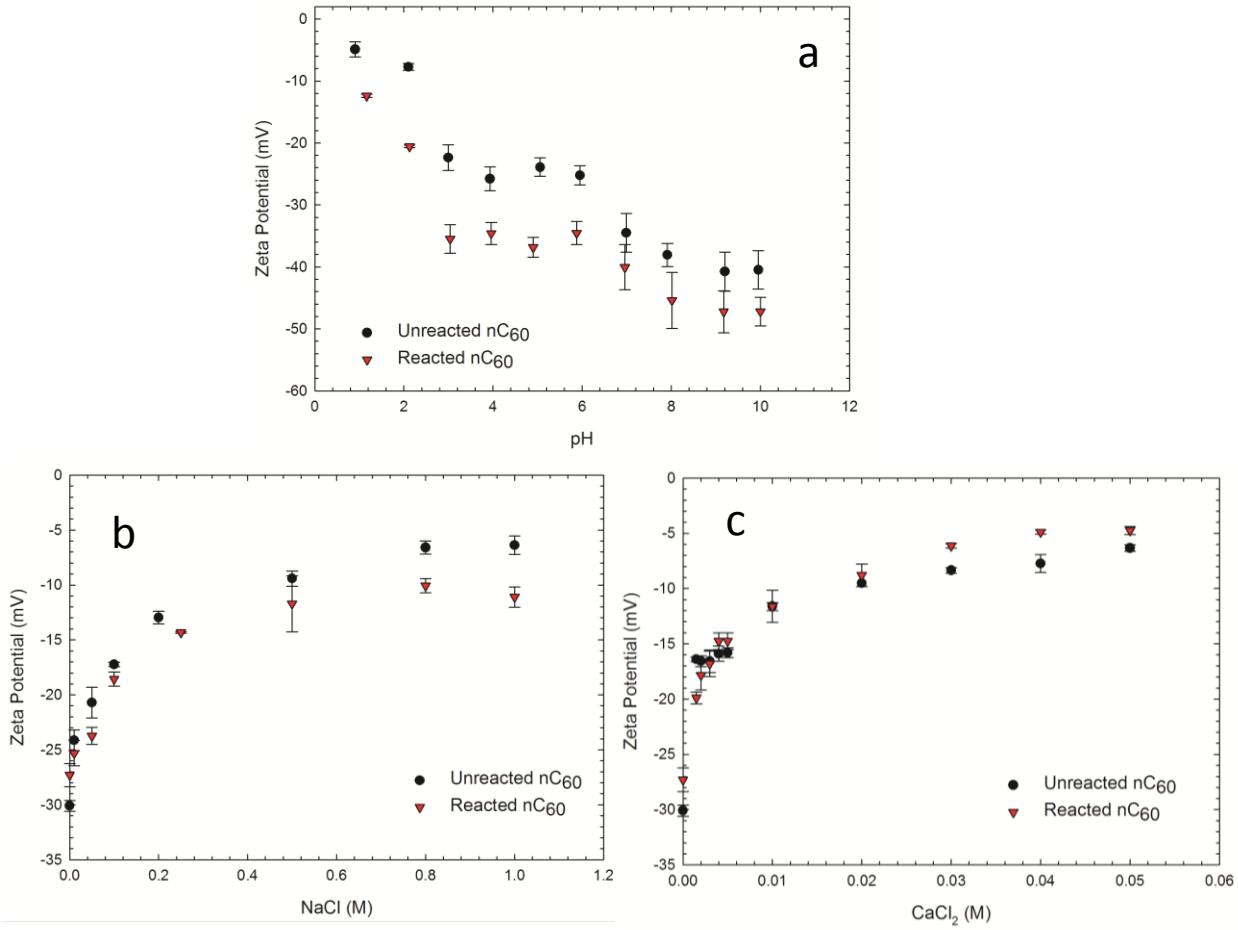

Figure S4.7: Zeta potential of unreacted nC_{60} and nC_{60} products (reaction with 100 mg/L Cl_2 for 5 days): (a) pH effect; (b) NaCl as electrolyte; (3) $CaCl_2$ as electrolyte. (Error bars represent standard deviation calculated from triplication experiments)

Table S4-1: Total organic carbon analysis for parent nC_{60} and reacted products.

Cl_2 (mg/L)	0 day (mg/L)	3 day (mg/L)	54 day (mg/L)
10	6.98 ±0.13	6.68 ±0.10	7.06 ±0.08
100	6.98 ±0.13	6.80 ±0.53	7.35 ±0.48

Chapter 5 :**Photo-enhanced Transformation of Hydroxylated Fullerene (Fullerol) by Free Chlorine in Water**

Abstract

Water-soluble, hydroxylated fullerenes (termed fullerols or fullerenols) have gained increasing attention as they have been identified as the primary oxidized product(s) during exposure of C_{60} (aggregated nC_{60}) to UV light (including sunlight UVA) or ozone in water. However, subsequent and resulting environmental reactivity of such daughter products is still not clearly defined. Here, we examine the chemical and physical transformation of a model fullerol in the presence of free chlorine, a globally applied oxidant in water treatment systems. Under both light (photo-excited state) and dark (ground state) conditions with free chlorine, fullerol reactivity and kinetics are described for batch systems over a range of environmentally relevant conditions. The resulting fullerene-based (C_{60} carbon cage), oxy-chlorinated products were characterized and described with a suite of analytical techniques, including ^{13}C-NMR, FTIR, XPS, and UV-vis spectroscopy. Product physical (behavior) properties were characterized via quartz crystal microbalance (QCM-D) and classic water-octanol partition experiments. For all conditions evaluated in the presence of free chlorine, fullerol readily reacts, resulting in significant surface (functional) alteration with differing physical (partitioning) behaviors when compared to parent materials. Further, the presence of light (UVA, 351 nm) was observed to

significantly enhance reaction rates and product oxidation stoichiometry (i.e. relative oxidation extent).

5.1. Introduction

Despite negligible water solubility, C_{60} forms water-stable nano-scale aggregates (also termed as "nC_{60}") in aquatic environments, through various environmentally relevant routes.[6, 36, 97, 270] Upon exposure to light, resulting in a photoexcited state, and in the presence of oxygen, nC_{60} readily forms water-soluble fullerene derivatives (with oxygen functionalities, also termed as fullerenols and/or fullerols).[55, 72, 271] Similar fullerols have also been identified as primary oxidized products for hydrogenated fullerenes (fulleranes) in the presence of ambient oxygen and UVA or sunlight irradiation.[119] In addition to being identified as environmentally relevant products, fullerols have also been specifically synthesized and applied for industrial applications (e.g. fullerene-containing polymers).[272, 273]

As a general class of fullerene derivatives, the chemical formulas of fullerols are often expressed as $C_{60}(OH)_x$, whereby the number of hydroxyl groups is typically distributed from 8 to 40.[48, 57, 159, 274-277] Typically, fullerols exhibit considerably different physicochemical behaviors compared to parent fullerene.[55, 166, 220, 278] In particular, fullerols are significantly more water-soluble in comparison to the parent fullerenes, which is a critical difference when considering environmental lifecycle, fate, and transport models. For example, it has been demonstrated that, through heating Na^+-free fullerol ($C_{60}(OH)_{12}$) in 30% aqueous hydrogen peroxide at 60 ^oC under air for 2 weeks, the solubility of fullerol can reach 58.9 mg/mL, which is ca. 10 orders of magnitude higher than molecular C_{60}.[48] Fullerol-catalyzed ROS (reactive oxygen species) production systems (in aqueous media) have also been evaluated under varied conditions (e.g.

controlled UV or sunlight) with relatively high quantum yields observed for ROS production.[58, 60, 61] Singlet oxygen ($^1O_2$) has been demonstrated as one of the primary ROS species, in addition to superoxide ($O_2^{\bullet -}$) in the presence of available electron donors. [58, 98] Additionally, while the hydroxyl radical is not observed as a primary product in these systems, it can exist in these systems as secondary ROS species.[60] Such ROS (e.g. $^1O_2$, $O_2^{\bullet -}$, •OH) production, which is more efficient than nC_{60}, has also been implicated in cell membrane damage mechanisms.[72, 98, 137-139, 279] Interestingly, fullerols can also act to quench ROS (in dark) in the aqueous phase (e.g. •OH, $O_2^{\bullet -}$, H•, e_{aq}^-), forming fullerol radical adducts and radical anions.[64, 100, 280, 281] Fullerol has also been shown to be reactive with superoxide radicals ($O_2^{\bullet -}$) and nitric oxide, even under dark conditions.[64, 67, 282] In addition, fullerol reduction via cyclic voltammetry and in the presence of zero-valence metals (e.g. Zn) has also been reported.[161, 283] With both aromatic-like and olefin-like regions, fullerene can be oxidized through a variety of oxidative pathways, among which, chlorination has been extensively investigated.[126, 203, 206, 284, 285] In water and under fluorescent light, nC_{60} has been reported to readily react with free chlorine, resulting in surface oxidation and particle disaggregation.[286] However, to date, specific fullerol reactions with free chlorine have not been reported.

In this study, the reactivity of fullerol with free chlorine, a globally applied disinfectant, is described under dark (i.e. ground state) and UVA irradiation (351 nm, 2 mW/cm^2, mimicking sunlight UVA irradiation). Reaction kinetics are described and modeled for a series of batch reactions over a range of conditions, with resulting products characterized by UV-vis spectroscopy, ^{13}C–nuclear magnetic resonance spectroscopy (^{13}C–NMR), X-ray photoelectron spectroscopy (XPS), Fourier transform infrared spectroscopy (FTIR), and total organic carbon (TOC) analyses. Finally, phase partitioning and surface deposition behaviors for both parent

fullerol and products were evaluated and compared using classic water-octanol partition coefficients (K_{ow}) and deposition rates (via quartz crystal microbalance).

5.2. Materials and Methods

5.2.1. **Materials**

Fullerol ($C_{60}(OH)_x(ONa)_y$, y=8-10, x+y ~24, purity > 99%) and ^{13}C-labeled (~25% enriched) fullerol ($C_{60}(OH)_x(ONa)_y$, y=8-10, x+y ~24, purity > 99%) were purchased from MER (Tucson, AZ). Fullerol stock suspensions (40 mg/L) were prepared by adding powder fullerol to ultrapure water and stirring it for 24 hours in the dark. The golden-colored suspensions were vacuum filtered through 0.22 μm PES membrane (Corning, NY) and stored in the dark at room temperature (21.0 ± 1.0 ℃). Stock suspensions remained stable in water for months according to UV-vis, DLS, and visual inspection. Total carbon concentration of the stock solution was 10 mg/L. Dibasic potassium phosphate (K_2HPO_4), sodium thiosulfate ($Na_2S_2O_3$), sodium chloride (NaCl) and 1-octanol were purchased from Sigma Aldrich (St. Louis, MO). Free chlorine in the reaction was provided via sodium hypochlorite (Laboratory Grade, Fisher Scientific), which was quantified as 39.95 g/L as Cl_2 through iodometric method.[218] Phosphate buffer solution, di-sodium ethylenediaminetetraacetic acid (Di-sodium EDTA), potassium iodide, starch indicator solution and acetic acid, used for standard DPD colorimetric method to quantify free chlorine concentration, were purchased from Fisher Scientific (Pittsburgh, PA). All the reaction solutions were prepared in ultrapure water (>18.2 MΩ-cm resistivity, Milli-Q, Millipore Corp., MA). Unless indicated, all chemicals were reagent grade or higher.

5.2.2. **Fullerol (Photo)Chlorination Experiments**

Fullerol photochlorination experiments were conducted as batch experiments by mixing 20 mg/L fullerol with free chlorine (0, 10, 50 and 100 mg/L) in 100 mL customized quartz reactors (Technical Glass Products) in a bench-scale photo-reactor. The initial pH of the reaction solution was adjusted with HNO_3 or NaOH to 6.5, in the presence of 10 mM phosphate buffer. The custom photo-reactor was built with two circuitous monochromatic (wavelength at 351 nm) UVA lamps (BHK, CA) on opposing reactor walls (fans were installed on each side for heat dissipation). The light intensity was calibrated to 2000 $\pm$ 50 $\mu W/cm^2$ initially with a radiometer (UVP, Inc.), which was also monitored regularly during the reactions and corrected if needed. Chlorination reactions in dark conditions were conducted in 100 mL borosilicate glass vials coated with aluminum foil to exclude light irradiation. For anaerobic conditions, 50 mL fullerol (20 mg/L) solutions were bubbled with N_2 gas (Airgas, Bowling Green, KY) for at least 1 hour to reduce the oxygen concentration to below 0.5 ppm, tested with a microprobe dissolved oxygen meter (Neofox system, Oceanoptics, FL). For such anaerobic conditions, free chlorine was injected after the deoxygenation process, in order to avoid the reaction initiation with free chlorine during the deoxygenation process. Over the reaction, sample aliquots were taken and measured immediately through scanning from 190-800 nm using a UV-vis spectrophotometer (Varian Cary Bio50), and the absorbance at 285 nm was represented with a high molar adsorption coefficient (ranging from 2.896 to 2.971 $\times 10^4$ $M^{-1}cm^{-1}$) to quantify the unreacted fullerol ($C_{60}(OH)_x(ONa)_y$, y=8-10, x+y~24) over the reaction. The absorbance interference from free chlorine was eliminated with excess sodium thiosulfate (1/4 of $Na_2S_2O_3/Cl_2$ as molar ratio). The free chlorine concentration during the reaction was determined by the standard DPD colorimetric method, which is shown as Figure S5.1.[218] All the above experiments for reaction

kinetics study were conducted in triplicate at room temperature (21.0 ± 1.0 ^{o}C). Control experiments of fullerol, without free chlorine at the same levels of pH, were also conducted for comparison. The products after the reaction were collected at the end for ^{13}C-NMR, FTIR, XPS, TOC, QCM-D, and water-octanol partition experiments for product characterizations.

5.2.3. **Product Characterization**

To prepare the reacted fullerol products after chlorination in dark conditions, a concentrated fullerol solution (5 g/L) was mixed with free chlorine (2.5 or 25 g/L) in a 10 mL solution for 1 or 5 days. Photo-chlorinated fullerol products were prepared in the same way but conducted in the UV reactor for 1 day, because the free chlorine in the solution will be consumed in less than 24 hours via photolysis reactions. The reacted products were collected after washed with stirred-cell (Amicon, molecular weight cut-off (MWCO) of 1000) for at least 5 times until the residual NaOCl background was completely removed, indicated with UV-vis spectra and pH of the out-flow solutions. FTIR analyses of the parent fullerol and reacted products were conducted in solid-state through diffuse reflectance infrared Fourier transform spectroscopy (DRIFTS, Nexus 470 FTIR, Thermo Nicolet, NC). Parent fullerol and reacted products were dried in a vacuum oven (Thermo Scientific, NC) for several days at room temperature. Solid powders of fullerol or reacted products were mixed with KBr powder (Spectrograde, International Crystal Lab, NJ) at the optimum ratio of 1:10, in an agate mortar with pestle. A KBr background spectrum was collected for subtraction before sample spectrum collection. For XPS analyses, wafers for analyses were prepared with sputter coated silica wafers with gold to at least 20 nm thickness before the sample was added. Parent fullerol or reacted products solutions (residual free chlorine was completely removed) were dried on wafers in the vacuum oven at room temperature by dropping samples until the total volume reached to ca. 1 mL. XPS spectra

were obtained by using a Physical Electronic 5000 VersaProbe II Scanning ESCA Microprobe with an Al K-α X-ray source with 23.5 eV pass energy at a 100 μm X-ray spot size. Solid-state ^{13}C–NMR spectra were obtained on a Bruker Avance III, 4.7 T spectrometer (50.3 MHz ^{13}C, 200.1 MHz ^{1}H) with a broadband probe for spinning rotors with a 4 mm outer diameter. For reacted products, ^{13}C-enriched fullerol ($C_{60}(OH)_x(ONa)_y$, ca. 25%) was reacted with free chlorine at a fullerol to Cl_2 mass ratio of 1:5 in 10 mL D_2O (deuterium enrichment 99.9%, Cambridge Isotope Laboratories, Inc. MA) for 1 day (UVA irradiation) and 5 days (in the dark). Mineralization during the (photo)chlorination/oxidation was tested through total organic carbon concentrations of fullerol solutions before and after reactions, which were determined through a TOC-L total carbon analyzer (Shimadzu Scientific Instrument, Inc, MD).

5.2.4. **Octanol-water Partition Coefficients Measurement**

Octanol-water partition coefficients here were selected as one of the most common empirical parameters to describe the hydrophobicity of particle surface, and to some extent, could evaluate the transport behaviors of organic contaminants in the environmentally relevant scenarios.[161, 220, 222] The solution of parent fullerol/reacted products was mixed with 1-octanol solvent in the same volume (8 mL) with an initial pH of 7.5 in amber glass vials. The mixtures were shaken by a rotary shaker (Labquake, Thermo Scientific, UT) for 3 hours and then were left for 24 hours until the water and octanol completely separated. Samples in the water phase were collected for UV-vis to determine the residual fullerol concentration (absorbance at 285 nm). The octanol-water partition coefficient (K_{ow}) could be calculated as Equation (1):

$$K_{ow} = \frac{C_0}{C_w} = \frac{[Abs]_{285nm,i} - k \times [Abs]_{285nm,f}}{[Abs]_{285nm,f}} \qquad (1)$$

Here the concentration of fullerol or reacted products in the octanol phase was calculated according to mass balance by subtracting the initial amount with the concentration in the water phase measured with UV-vis. The actual K_{ow} was corrected by the concentrating factor k, which was determined through experiments, since the volume of water dissolved into octanol phase cannot be ignored. All these coefficients were obtained through triplicate experiments at each condition.

5.2.5. **Quartz Crystal Microbalance Analysis**

Quartz crystal microbalance was employed to investigate the different interaction behavior of parent fullerol or reacted products with polystyrene (PS)-coated surface, which is one of the typical hydrophobic surfaces in natural environments.[287, 288] Measurements were conducted with a Q-Sense E4 unit (Q-sense AB, Sweden) through monitoring the frequency changes (Δf) over time, while the fullerol solution flowed onto PS-coated QCM-D crystal (QSX-305, Q-sense). The sensors were prepared and cleaned by following the standard protocol developed by Penfold and Naderi.[289, 290] After introducing 1.42 mM NaCl buffer solution to the system for 10 minutes to initiate the measurement at 22 ^{o}C, in order to minimize the interference adsorption from background NaOCl (1.42 mM, which is equivalent with 100 mg/L Cl_2 as the ionic strength background), fullerol solutions were allowed to flow on PS surface for about 1 hour. The mass of fullerol adsorbed can be linearly related to the frequency change (Δf) expressed as Sauerbrey Model[291]:

$$\Delta m = -C \frac{1}{n} \Delta f \qquad (2)$$

where Δm is the total mass of fullerol nanoparticles deposited on the aiming surface, Δf is the shift in resonance frequency, n is the overtone number of the system (1, 3, 5, 7, 9 and 13) and C

is the crystal constant (17.7 ng/(Hz-cm^2)). The third overtone (n = 3) was selected in this study for calculation.[223, 292]

5.3. Results and Discussion

Typically, parent fullerol solutions (20 mg/L) were reacted with 100 mg/L free chlorine under both dark and UVA irradiation conditions as shown in Figure 5.1. As the reaction proceeded, the initial golden hue of the fullerol solution was lost, with no precipitation, under both conditions (Figure 5.1a and 5.1b), indicating a reaction had occurred. For all cases, reaction kinetics under UV irradiation (351nm, 2mW/cm^2) were observed to be significantly faster compared to dark reactions. Under dark conditions and at varied free chlorine concentrations, time resolved fullerol absorbance (taken at 285nm) is presented in Figures 5.1c and 5.1e. Pseudo-first-order kinetics, with regard to fullerol absorbance change (Equation (3)), is observed for all dark reactions ([total of all chlorine species] » [total of all reacting fullerene species]), which is similar to other observations of polycyclic aromatic hydrocarbons (PAH) chlorination reactions[293]:

$$R = -\frac{d[F]}{dt} = k[F] = k_{obs,dark}[Cl_2]_0[F] \qquad (3)$$

where [F] and [Cl_2] are the concentrations of fullerol and free chlorine (during reaction), respectively. Here, $k_{obs,dark}$ is designated as the observed rate constant of a second order reaction with regard to fullerol and free chlorine ([Cl_2] ~ [Cl_2]$_0$). The overall reaction rates were enhanced at higher free chlorine concentrations due to net increase of redox potential. Observed rate constants ($k_{obs,dark}$), shown in Table 5-1, decreased as free chlorine level increased, indicating that the reaction between fullerol clusters and free chlorine molecules was diffusion limited, rather than reaction controlled, at higher levels of chlorine concentrations. Reactions were also

conducted for anaerobic (DO ≤ 0.5 ppm) conditions, and the rate constants (Table 5-1) were nearly identical to those under aerobic conditions, implying that oxygen was not involved in the initial oxidation reaction (steps) under dark conditions. Under UVA irradiation, the overall reaction rates are expressed in Equation (4) and (5) (Supporting Information, Equation S1-S7):

$$R = -\frac{d[F]}{dt} = R_1 + R_2 = k_1[F] + k_{obs,UV}[F]([Cl_2]_0 - k_3 t) \quad \text{(Aerobic)} \quad (4)$$

$$R = -\frac{d[F]}{dt} = R_2 = k_{obs,UV}[F]([Cl_2]_0 - k_3 t) \quad \text{(Anaerobic)} \quad (5)$$

under photo-irradiation, in contrast to the dark reaction, free chlorine undergoes photolysis in addition to photoexcitation of the fullerol molecule itself.[208] Observed rate constants for reactions between free chlorine and fullerol ($k_{obs,UV}$) are presented in Table 5-1, and are at least one order of magnitude higher than parallel reactions under dark conditions. Such enhancement is due, in part, to the involvement of a variety of highly reactive radicals within the oxidation reactions, from the photolysis of free chlorine and fullerol self-catalyzing ROS production in the presence of oxygen (e.g. $^1O_2$, $O_2^{\bullet -}$, •OH, $Cl^{\bullet}$, $ClO^{\bullet}$, $Cl_2^{\bullet -}$, $O(^3P)$, etc.).[58, 60, 294] In solutions with trace amounts of dissolved oxygen (anaerobic condition, DO ≤ 0.5 mg/L, UVA irradiated), the rate constants of the reaction between fullerol and free chlorine ($k_{obs,UV}$) were comparable to aerobic conditions. Thus overall reaction processes include fullerol with oxygen and fullerol with free chlorine (R_1 and R_2 in Equation (4)), respectively.[58, 60, 61, 294, 295] Similar to ground-state reactions, the observed rate constants for photo-chlorination decreased as the free chlorine concentration increased, indicating diffusion limitations. Reaction pathways for fullerol oxy-chlorination most likely involves electrophilic addition/substitution with $HOCl/OCl^-$ (dark) or highly reactive chlorine/oxygen radicals (under light) attack of the conjugated π structure(s), with the reactive sites located at the electron-rich carbon atoms of an ortho or even para position

to an electron donating group (hydroxyl, oxide ion).[208, 252, 256, 260] The electron donating ability of substituents associated with aromatic rings may also affect relative reaction rates and extents. For example, reaction rates between HOCl with phenoxide ion was ca. 10^5 times faster compared to the neutral form of the phenol.[296] Other mechanisms have also been proposed including strong adsorption due to the formation of charge transfer complexes associated with the electron acceptor character of Cl_2; simple physical adsorption; and physical entrapment for narrow pore-like structures.[256, 297, 298] For larger (carbon) networked materials such fullerenes, multiple oxygenation/chlorination routes leading to various fullerene derivatives complicate site specific reaction kinetics analyses and modeling. Here, we do realize that there are likely different mechanisms and pathways involved in the reactions in the ground state vs. photo-excited state, and such observed secondary order reactions were provided for qualitative comparisons.

Table 5-1: Chlorination reaction rate constants (k_{obs}, $L \cdot min^{-1} \cdot mg^{-1}$) under varied experimental conditions

Initial Cl_2 (mg/L)	**10**		**50**		**100**	
Photo-irradiation Condition	Dark	UVA	Dark	UVA	Dark	UVA
Aerobic	7.00E-05	2.95E-03	3.20E-05	4.40E-04	2.70E-05	2.10E-04
Anaerobic	8.00E-05	2.37E-03	2.60E-05	4.47E-04	2.00E-05	1.96E-04

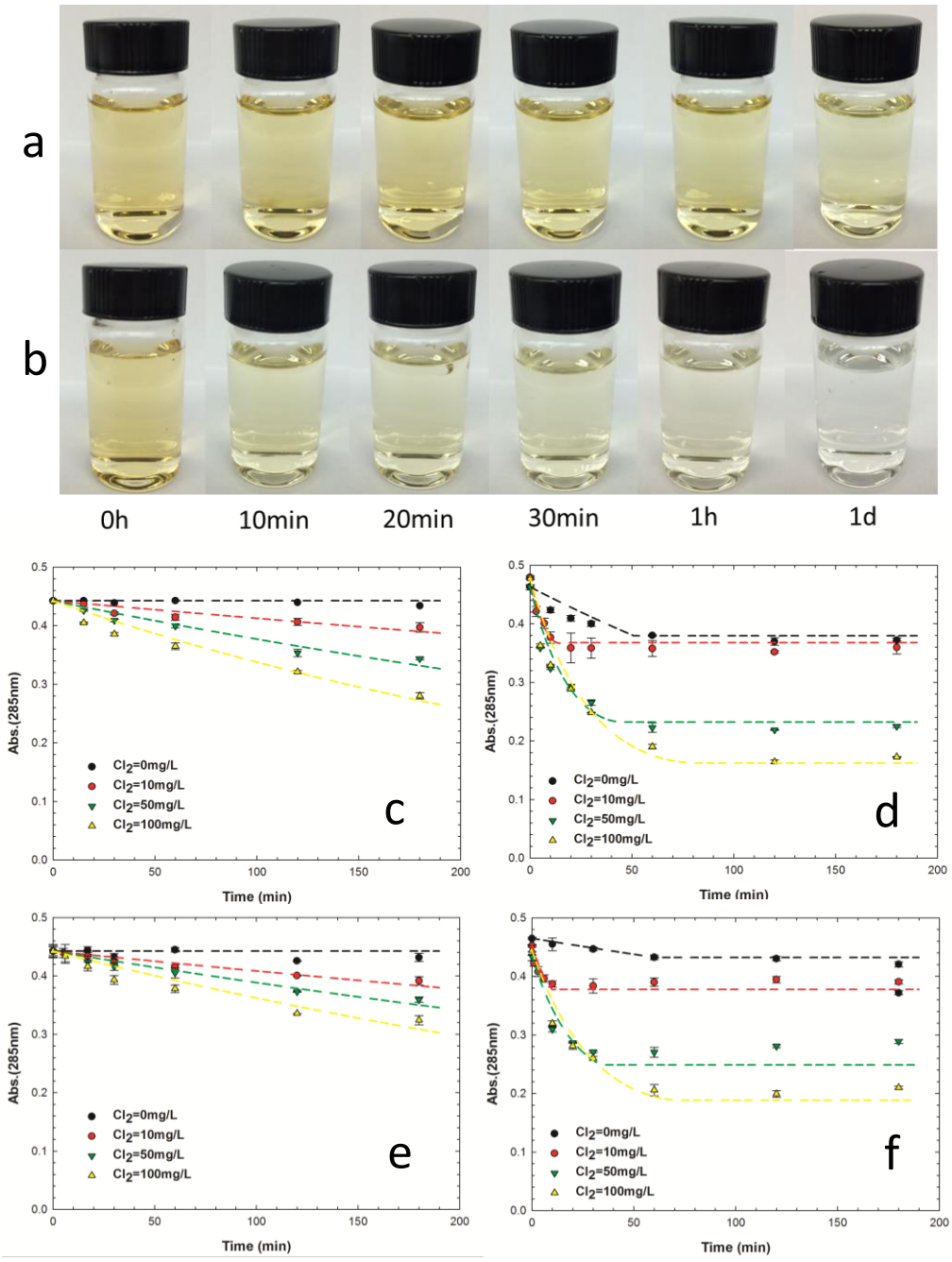

Figure 5.1: Fullerol (photo)chlorination reactions under: (a) dark condition (20 mg/L fullerol with 100 mg/L Cl_2 at pH 6.5); (b) UVA irradiating condition (20 mg/L fullerol with 100 mg/L Cl_2 at pH 6.5); Fullerol UV adsorption at 285 nm as a function of time under (pH = 6.5, phosphate buffer =10 mM) (c) dark aerobic condition; (d) UVA aerobic condition; (e) dark anaerobic condition; (f) UVA anaerobic condition.

^{13}C-NMR spectra of parent fullerol and (photo)chlorinated products with ca. 25% ^{13}C-labeled are shown in Figure 5.2. For parent fullerol (Figure 5.2a), besides the C=C peak at 146.3 ppm, there are additional signals appearing at 75.8 ppm (hydroxylated sp^3 carbons) with a shoulder at 94 ppm (ketals and hemiketals); 175.5 ppm (carbonyl carbons, as carboxyl groups); 195.2 ppm (carbonyl carbons, as ketones); and a weak signal at 166.0 ppm (as vinyl ether carbon), indicating oxygen-based derivatization of the parent fullerol before chlorination as described by others.[42,56, 148, 299] For reacted products under dark conditions (Figure 5.2b), C=C response is is shifted downfield by ca. 10 ppm to 135.8 ppm, because of numerous different substituent effects that are both electronic and steric in nature of fullerol molecule after reaction. A similar upfield shift was also observed by Hou et al.[73] after prolonged exposure of nC_{60} to sunlight and also by Fortner et al.[74] after nC_{60} oxidation by ozone. In this, and other[72,73,74] work, new peaks appearing from about 160 ppm to 180 ppm, are indicative that a variety of oxygen-containing functionalized carbons were produced (e.g., carboxyl and vinyl ether).[84, 161, 299] Signals resulting from these functional groups, especially carboxyl, are evident after oxidation by free chlorine (Figure 5.2b). A weak, sharp peak is also observed at 96.1 ppm, which has been reported to be indicative of CCl_4[300] but may also indicate single -O-C-O- species (as in a ketal or hemiketal) in these complex structures. Support for this assignment also comes from the absence of this signal in ^{1}H-^{13}C CPMAS experiments with contact times ranging from 0.3-7.5 ms (data not shown). The enhanced signal breadth upfield of ca. 115 ppm for samples chlorinated in the dark suggests the presence of numerous ketal or hemiketal species in addition to aliphatic carbons bearing just one oxygen functional group. The ^{13}C-NMR spectrum of the reacted fullerol under UVA irradiation is shown in Figure 5.2c, which is even more significantly altered from the parent fullerol. The signals for alcohols, ketals, and hemiketals are much weaker, while

the signal at 96.3 ppm attributed to CCl_4 is stronger than after chlorination in the dark. Fewer olefinic carbons are present; and the narrower signal (135.7 ppm) indicates that they are also more similar bonding environments. Carboxyl and vinyl ether environments dominate, indicating high levels of oxidation. The elimination of H-Cl may happen with hydroxyl groups and ortho-chlorinated carbons, leading to ketone or carboxyl group formation.[293] In addition, as shown in Table S5-1, total organic carbon (dissolved) remained the same under all experimental conditions, indicating there is no mineralization during these oxychlorination processes. The approximate relative abundance of oxygen containing functional groups before and after chlorination is shown in Table 5-2.

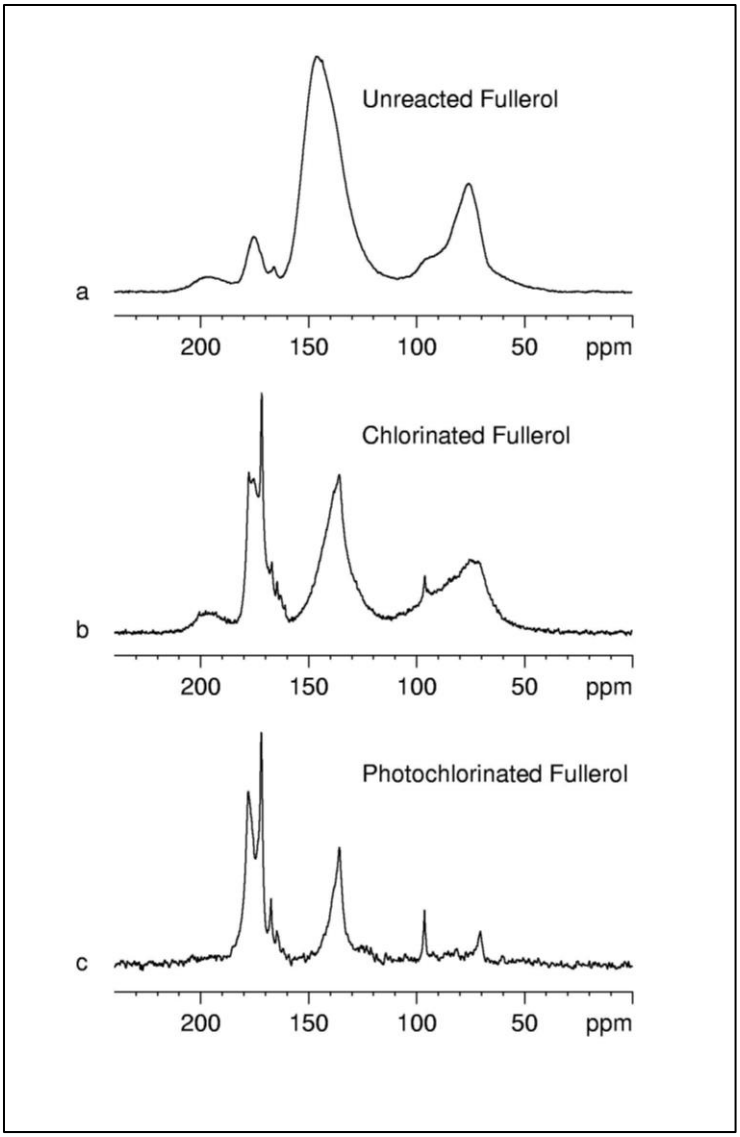

Figure 5.2: ^{13}C-NMR spectra of (a) parent fullerol (25 % ^{13}C enriched, $C_{60}(OH)_x(ONa)_y$), (b) reacted fullerol products in dark (100 mg/L Cl_2 for 5 days) and (c) reacted fullerol products under UVA irradiation (100 mg/L Cl_2 for 1 day) obtained with 12 kHz MAS, 90^o ^{13}C pulse, 41.0-ms FID, and 60-s relaxation delay for each sample. ((a) 1616 scans, 10 Hz (0.2 ppm) of line broadening applied to the FID; (b) 1888 scans, 10 Hz (0.2 ppm) of line broadening applied to the FID; (c) 2048 scans, 25 Hz (0.5 ppm) of line broadening applied to the FID.)

Table 5-2: Approximate relative abundance (%) of functional groups before and after reaction of the ^{13}C-enriched fullerol[a,b]

	Ketone	Carboxyl and Vinyl Ether	C=C	Ketal, Hemiketal, and Alcohol
Unreacted Fullerol	3	7	63	27
Dark Chlorination	5	28	36	31
Photochlorination	5	50	30	15

[a]Determined with a 12 kHz MAS, 90 ° ^{13}C pulse, 41.0-ms FID, and 60-s relaxation delay. Areas include any (weak) spinning sidebands (not shown in Figure 5.2). For each sample, only relatively small changes in the relative intensities of most of the signals were observed upon lengthening the relaxation delay from 30 s to 60 s. For each of the chlorinated samples, the signal at 171.7 ppm clearly results from the most slowly relaxing carbons, which may not be fully relaxed even with a 60-s relaxation delay. ^{1}H-^{13}C CPMAS experiments with various contact times on the dark chlorinated sample showed that quantitatively meaningful CPMAS spectra could not be obtained, which is not surprising for samples with relatively few protons. Indeed, combining CPMAS with dipolar dephasing or combining direct ^{13}C pulse with dipolar dephasing showed that each band is dominated by quaternary carbons.

[b]Only a limited amount of each sample was available. The unreacted fullerol (30 mg) was studied in a thick-bottom zirconia rotor in order to maximize the amount of material in the rf coil region. The dark chlorinated material filled about 60% of a thick-bottom zirconia rotor. The photochlorinated material filled about 60% of a standard zirconia rotor. Not enough room remained to insert an upper silicon nitride plug in any of the rotors.

FTIR spectra of the parent fullerol and reacted products under varied reaction scenarios are compared in Figure 5.3. For unreacted fullerol (Figure 5.3a), absorbance peaks centered at ca. 1597, 1367, and 1065 cm^{-1} which have been identified as C=O, C-OH in plane bending and C-O stretching, respectively.[54, 55, 148, 159] After reaction with 10 mg/L Cl_2 for 5 days (Figure 5.3b), most of the peaks (oxygen moiety functional groups) remained in similar positions but with slightly higher (relative) intensities, demonstrating that the extent of oxygenation of fullerol increased over the reaction. With 100 mg/L free chlorine reaction for 1 day (Figure 5.3c), a similar spectrum of the products was observed; for the same reaction after 5 days, a band of new peaks appeared from 500 to 900 cm^{-1}, which is likely to be due to C-Cl stretching, coupled with epoxide structure emerging at ca. 1200 cm^{-1}.[54, 126] Under UVA irradiation, even for a 1 day reaction, C-Cl stretching bonds were observed from 500 to 900 cm^{-1}, with an obvious enhanced C=O peak centered at 1600 cm^{-1} and a small shoulder at 1700 cm^{-1}. This enhancement is consistent with the increasing reaction rates observed and the oxychlorinated products characterized by ^{13}C-NMR above.

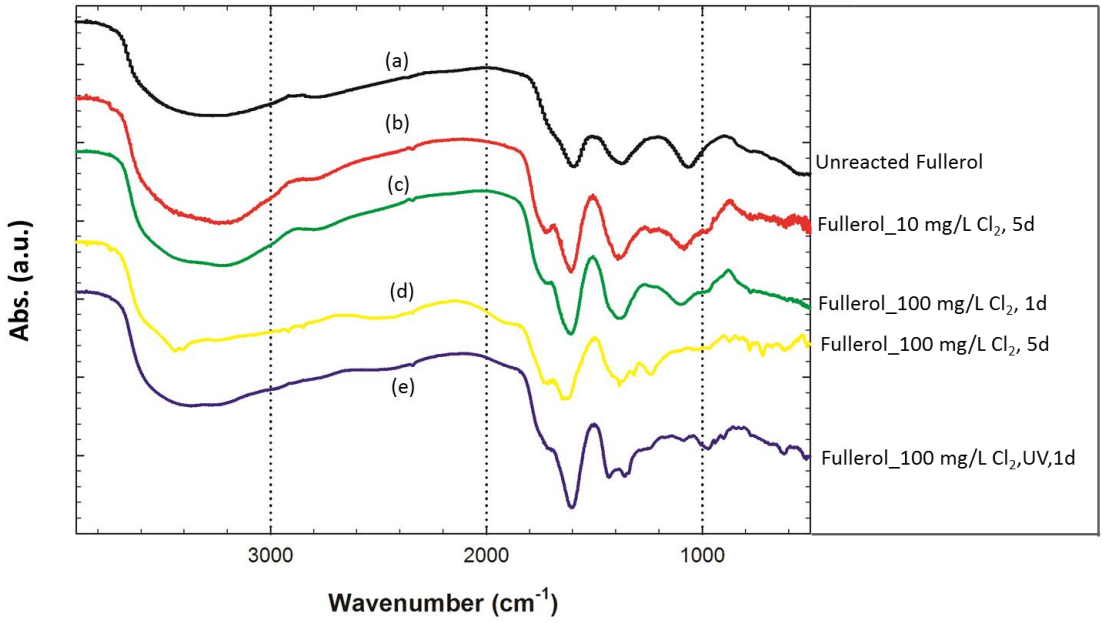

Figure 5.3: FTIR-DRIFTS fullerol and reacted products spectra: (a) Parent fullerol; Reacted fullerol with (b) 10 mg/L Cl_2 for 5 days in dark; (c) 100 mg/L Cl_2 for 1 day in dark; (d) 100 mg/L Cl_2 for 5 days in dark; (e) 100 mg/L Cl_2 for 1 day under UVA irradiation (2 mW/cm^2, 351 nm).

XPS analyses of pristine fullerol and reacted products, including both C (1s) and Cl (2p) analyses (Figure 5.4), provide insight into relative C and Cl oxidation states. For unreacted fullerol C (1s) (Figure 5.4a), (unoxidized, C=C/C-C) carbon at 284.8 eV (73.7%), but also mono-oxidized and di-oxidized carbons at 286.7 eV (19.1%) and 288.3 eV (7.2%) respectively, similar to XPS characterization of other fullerols.[54, 299, 301] After reacting with 10 mg/L free chlorine in dark (Figure 5.4b), a decreased relative amount of C=C/C-C was observed as 68.7%, coupled with the fraction of dioxidized and/or chlorinated carbons (C=O/C-Cl, 288.1 eV) increased to 11.0%.[54, 256, 286] With a higher concentration of free chlorine (100 mg/L, Figure 5.4c), underivatized carbon was further oxidized with a (decreasing) relative fraction observed at 59.1%, while those of C-O and C=O/C-Cl increased to 27.3% and 13.6%, respectively. Under

UVA, oxidation of fullerol was enhanced (Figure 5.4d), as indicated by increased C-O (26.4%) and C=O/C-Cl (16.9%) simultaneously (after 1 day reaction, 100 mg/L Cl_2). Here recognizing the limitation of XPS technique to differentiate C=O and C-Cl bonds, Cl (2p) analysis was also conducted (Figure 5.4e-4h). For unreacted fullerol, a negligible Cl (2p) signal was observed (Figure 5.4e), whereas chlorine 2p peaks (spin-orbit split peaks) at 197.3/199.0 eV (61.3%/38.7%) (Figure 5.4f) were observed for 10 mg/L Cl_2 in the dark due to the presence of the chlorine ion existing in the reaction system (Figure S5.2)[256], which is also consistent with FTIR results, suggesting no obvious chlorine covalently bonded to carbon at comparably lower chlorine concentrations. For higher Cl_2 levels (100 mg/L, Figure 5.4g), besides the chlorine ions, new split peaks with a higher binding energy appeared at 199.6/201.2 eV (13.2%/3.2%), assigned as C-Cl formation, are present.[256, 302-304] Fullerol exposure to 100 mg/L free chlorine under photo-irradiation (Figure 5.4h), even for 1-day reaction, C-Cl groups increased at 200.0/201.5 eV (19.8%/9.2%); however, quantification of the C-Cl formation could not be accurately made with confidence due to interfering background from chlorine ions.[256, 305]

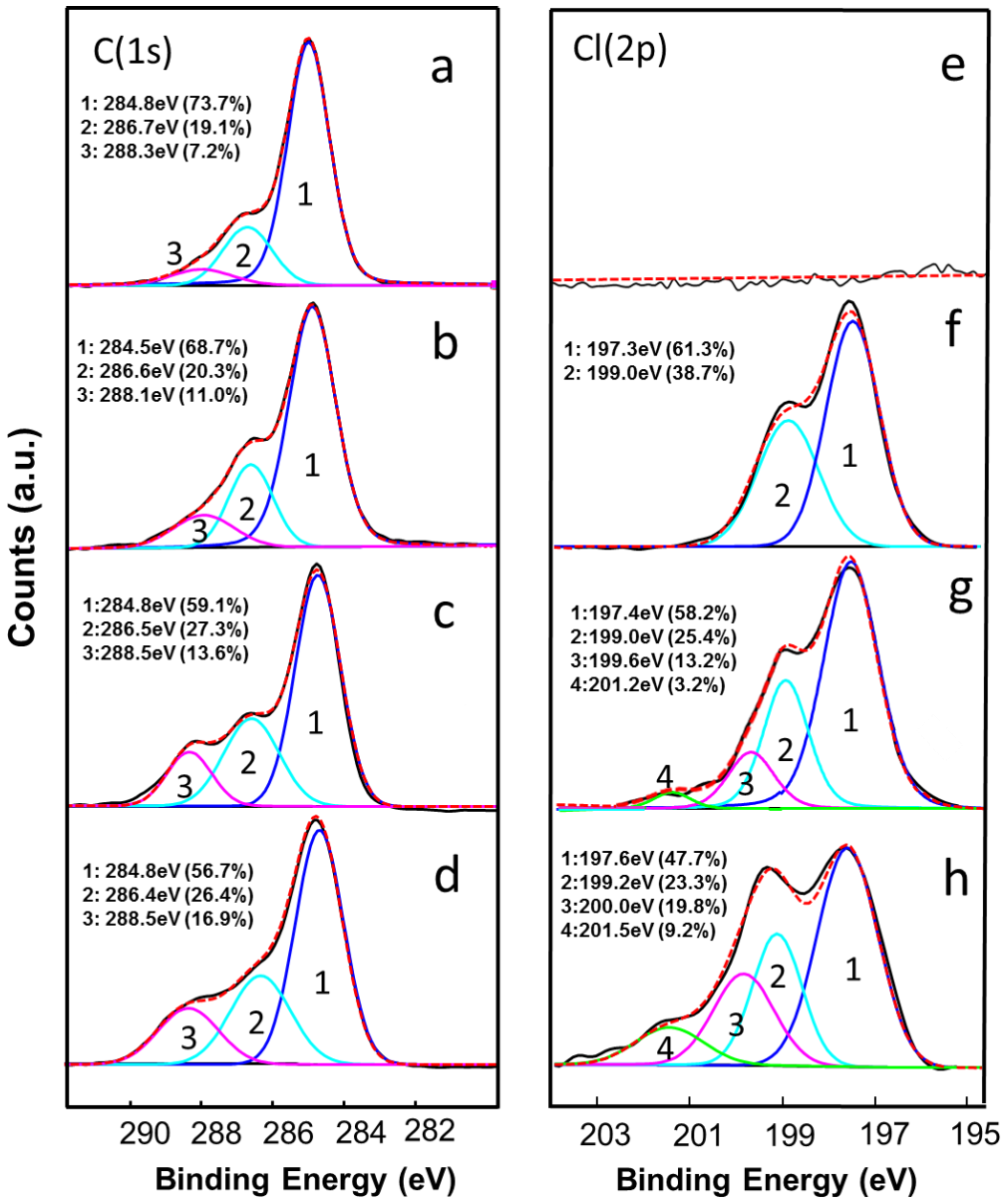

Figure 5.4: XPS spectra and curve-fitting analyses of unreacted fullerol and reacted products: (a) Unreacted fullerol (C1s); Fullerol products reacted with (b) 10 mg/L Cl_2 in dark for 5 days (C1s); (c) 100 mg/L Cl_2 in dark for 5 days (C1s); (d) 100 mg/L Cl_2 with UVA for 1 day (C1s); (e) Unreacted fullerol (Cl2p); Fullerol products reacted with (f) 10 mg/L Cl_2 in dark for 5 days (Cl2p); (g) 100 mg/L Cl_2 in dark for 5 days (Cl2p); (h) 100 mg/L Cl_2 with UVA for 1 day (Cl2p). (UVA irradiation: 2 mW/cm^2, 351 nm)

Partitioning behavior of fullerol before and after (photo)chlorination was examined with QCM-D (surface) and traditional water-octanol (phase) partition experiments (Figure 5.5). Here polystyrene was selected as a model hydrophobic surface, similar to other reports.[306, 307] After system equilibrium with 1.42 mM NaCl background electrolyte solution, parent or reacted fullerol solutions (20 mg/L, pH ~ 7.5) were flowed over the polystyrene surfaces and monitored. Compared with parent fullerol, higher frequency shifts (mass adsorbed) were observed for both reacted products in the dark and UVA irradiation conditions. The total mass of the reacted fullerol products (in the dark for 5 days) adsorbed on PS surfaces after 2500 seconds calculated with the Sauerbrey model (Equation (2) doubled after the reaction, indicating that there is a more favorable interaction with reacted products (for PS surfaces). Products reacted under UVA irradiation, even after 4 hours of reaction time, were observed prefer PS as mass loading was increased by ca. 60%, implying hydrophobic and van der Waals forces (dispersion forces) are likely involved in intermolecular - surface forces.[307-309] Initial deposition rates were calculated based on the frequency shifting rates over the first 2 minutes after introducing the fullerol solutions (Figure 5.5), which are not linearly proportional to the total mass adsorption, indicating there are different surface interaction mechanisms due to different reaction pathways for ground-state and photo-excited reactions with free chlorine. Water-octanol partition experiments (Figure 5.5 inset, pH 7.5), showing similar surface interaction behaviors compared with QCM-D results, further support the observation that reacted products are more hydrophobic. K_{ow} increased ca. 10% after a 1-day reaction, and kept increasing to ca. 55% after 5 days reaction when compared with the parent fullerol.

5.4. Conclusions

To summarize, upon exposure to free chlorine, significant, covalent transformations of hydroxylated fullerene were observed under both dark and light conditions resulting in relatively more hydrophobic products. For all cases, UVA enhanced the transformation process(es). Resulting products were involved with chlorinated and oxygenated carbons, but remaining C_{60} cage structure preserved. Chemically functional groups alteration of fullerol after reaction lead to further physical property changes of the nanoparticle's surfaces, creating more hydrophobic surfaces through a simultaneously de-hydroxylation process. As key daughter product(s) upon fullerene exposure to sunlight and oxygen, resulting fullerol chemistry in water is critical to understand for accurate material life cycle assessments, as highlighted in this work.

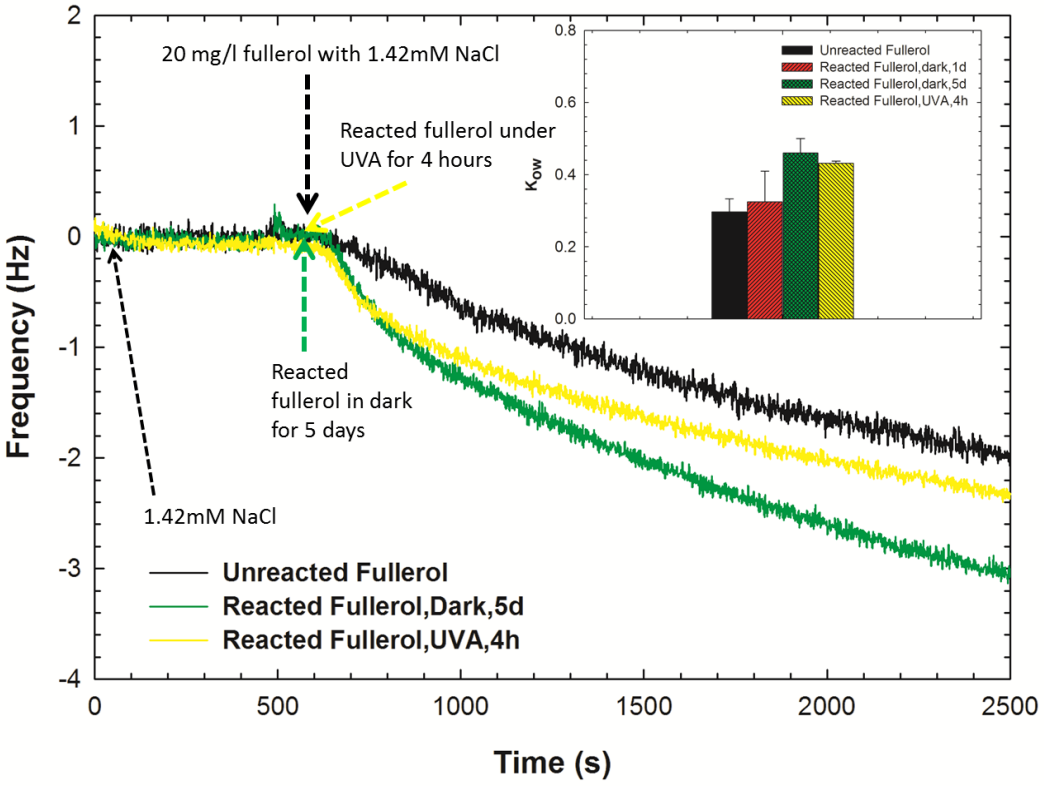

Sample	Unreacted Fullerol	Reacted Fullerol (UVA, 4h)	Reacted Fullerol (Dark, 5d)
Total Mass Deposition (ng/cm2)	27.47±12.98	44.33±3.94	56.97±4.61
Deposition Rate (ng/(cm²•s))	0.027±0.001	0.067±0.021	0.084±0.016
K_{ow}	0.297±0.001	0.432±0.006	0.460±0.0406

Figure 5.5: Surface properties characterization of fullerol and reacted products: QCM-D measurement comparison of parent fullerol and reacted products (20 mg/L fullerol, 100 mg/L Cl_2 under UVA/dark conditions) interaction with the polystyrene surface (pH = 7.5); Inset: Water-octanol coefficients of fullerol and (photo)chlorinated products at pH 7.5.

Acknowledgements

This study was supported by Washington University in St. Louis faculty startup funding for Fortner. We sincerely thank Katherine Peter and Brittany Radke for their hard working and contribution for this project during the independent study and Research Experience for Undergraduates Summer Program (REU, NNIN) at Department of Energy, Environmental, Chemical Engineering, Washington University in St. Louis. We also thank for the XPS facility supporting by Institute of Materials Sciences and Engineering (IMSE) at Washington University in St. Louis.

Chapter 5. Supporting Information

Description of reaction kinetics modeling for fullerol photochlorination, graphs for free chlorine concentrations, XPS spectrum of NaCl, and table of TOC analyses are included.

Reaction Kinetics of Fullerol Photochlorination

The reaction kinetics of fullerol and free chlorine under UV irradiation was observed differently compared with that under dark conditions. The concentration of free chlorine did not remain as constant but kept decreasing due to photo-decomposition, as shown in Figure S5.1. Here, we have simplified fullerol oxidation reactions under UVA irradiation in the presence of free chlorine to three dominant reactions, as shown in Equation S1-S3:

$$\text{Fullerol} + O_2 \xrightarrow{UV} \text{Fullerol}_{\text{products,1}} \qquad R_1 = k_1[F] \qquad \text{(S1)}$$

$$\text{Fullerol} + Cl_2 \xrightarrow{UV} \text{Fullerol}_{\text{products,2}} \qquad R_2 = k_2[F][Cl_2] = k_{obs,UV}[F][Cl_2] \qquad \text{(S2)}$$

$$Cl_2 \xrightarrow{UV} \text{Radicals species} \qquad R_3 = -\frac{d[Cl_2]}{dt} = k_3 \qquad \text{(S3)}$$

here, k_1, $k_{obs,UV}$ (k_2) and k_3 are rate constants for reaction (S1) - (S3), respectively. Free chlorine concentration during reaction can be expressed as Equation S4, since the decaying of chlorine under UV irradiation was observed as zero-order reactions with observed reaction rate constant (k_3) (Figure S5.1):

$$[Cl_2] = [Cl_2]_0 - k_3 t \qquad \text{(S4)}$$

The reaction of fullerol photo-oxidation with oxygen was observed as first-order reaction regards to fullerol concentration (Equation S1), which was also proved with Kong et al.[61], and the rate constant (k_1) can be derived from the control experiments that fullerol concentrations changes under aerobic conditions but in the absence of free chlorine (Figure 5.2b, Cl_2 = 0 mg/L). Thus, the overall reaction for fullerol chlorination/oxidation under aerobic conditions could be expressed as:

$$R=-\frac{d[F]}{dt}= R_1+ R_2 = k_1[F] +k_{obs,UV}[F]([Cl_2]_0-k_3t) \qquad \text{(Aerobic)} \qquad \text{(S5)}$$

however, as for anaerobic conditions, the reaction of fullerol photo-oxidation by oxygen (R_1) could be neglected and the overall reaction could be presented as:

$$R=-\frac{d[F]}{dt}= R_2 = k_{obs,UV}[F]([Cl_2]_0-k_3t) \qquad \text{(Anaerobic)} \qquad \text{(S6)}$$

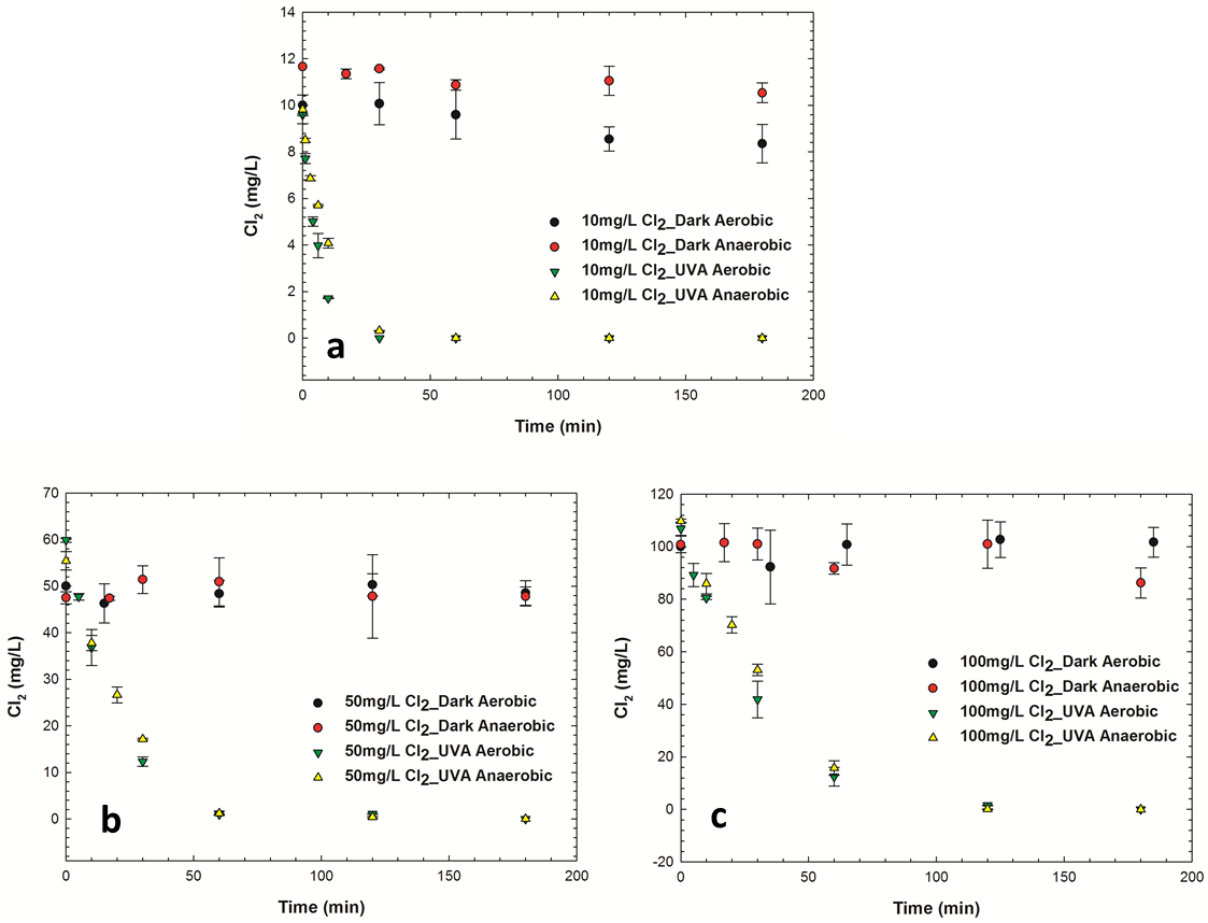

Figure S5.1: Free chlorine concentrations during the reactions with different conditions: (a) 10 mg/L Cl_2; (b) 50 mg/L Cl_2; (c) 100 mg/L Cl_2.

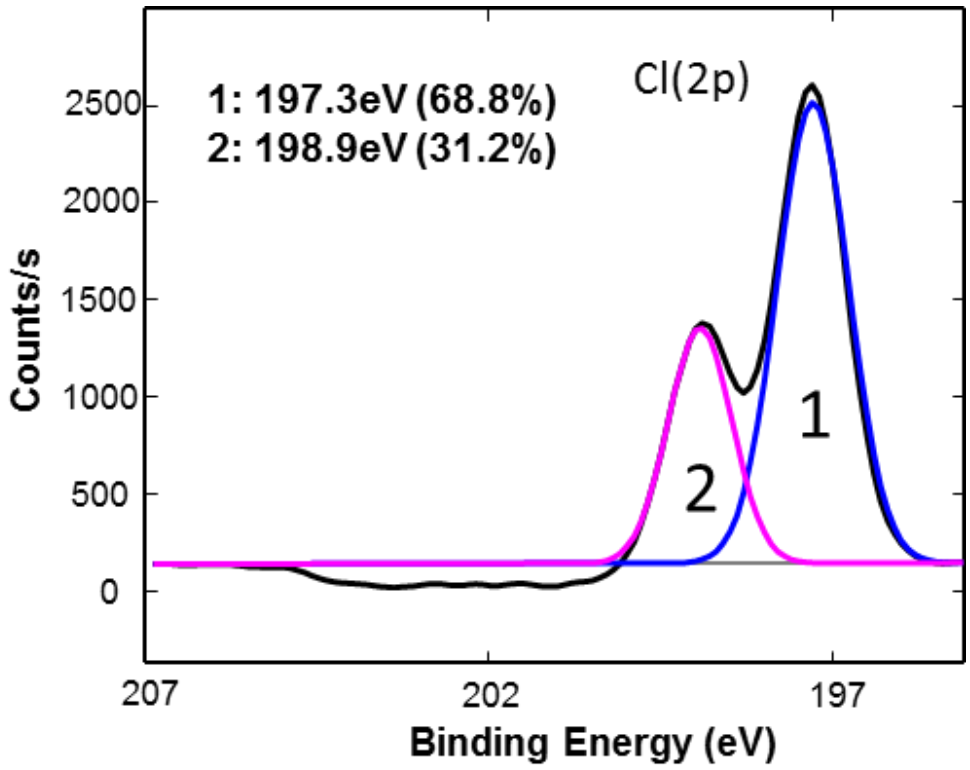

Figure S5.2: Cl2p XPS spectrum of NaCl and curve fitting analysis**.**

Table S5-1: Total organic carbon (mg/L) of fullerol solutions after reactions under different experimental conditions **(**$TOC_{unreacted\ fullerol}$ = 10.95 ± 0.19 mg/L**)**

Light Condition	**Dark (30d)**		**UVA (3h)**	
Initial Cl_2 (mg/L)	**10**	**100**	**10**	**100**
TOC (mg/L)	10.6 ± 0.55	10.9 ± 0.03	10.38 ± 0.55	10.67 ± 0.12

Chapter 6 :**Reduction of Hydroxylated Fullerene (Fullerol) in Water by Zinc: Reaction and Hemiketal Product Characterization**

Results of this chapter have been published in *Environmental Science & Technology* **2014**, 48, (13), 7384-7392.

Abstract

Water soluble, hydroxylated fullerene (fullerol) materials have recently gained increasing attention as they have been identified as the primary product(s) during the exposure of fullerenes (as water stable, nanoscale aggregated C_{60}) to UV light in water. The physical properties and chemical reactivity of resulting fullerols, however, have not been thoroughly studied. In this paper, we identified and characterized the reductive transformation of fullerol ($C_{60}(OH)_x(ONa)_y$) by solid zinc metal (Zn(0)) through a series of batch reaction experiments and product characterization, including ^{13}C NMR, FTIR, XPS, UV-vis, DLS and TEM. Results indicated the facile formation of water stable, pH sensitive hemiketal functionality as part of a relatively reduced fullerol product. Further, aqueous physical behavior of the product fullerol, as measured by octanol partitioning and surface deposition rates, was observed to significantly differ from the parent material and is consistent with a relative increase in molecular (product) hydrophobicity.

6.1. Introduction

Recently, there have been a number of reports regarding the photophysical (or photoenhanced) transformation of water stable fullerene aggregates (as C_{60}) in water under ambient sunlight or controlled UV irradiation (UVA-UVC). Such transformation(s) in the presence of sunlight, leading to oxidized, molecular soluble fullerenes, clearly demonstrate the potential of fullerene environmental reactivity under ubiquitous conditions.[54, 72] Upon UVA irradiation (315-400 nm), aggregated C_{60} (also termed as nC_{60}) in water was observed to be covalently modified to include oxygen based functionalities resulting in soluble product(s), which were identified as fullerols (also termed as fullerenols).[55] Hou et al. described the products of nC_{60} sunlight exposure over the course of 947 hours in water (open system) to be a mixture of oxygen-containing functional groups, including vinyl ether, carbonyl or carboxyl groups, resembling commercially available fullerols ($C_{60}(O)_x(OH)_y$, where x+y = 22).[56] Lee et al. observed similar, photochemical transformation(s) of nC_{60} upon UVC irradiation (254 nm) for 110 hours and also identified water-soluble, fullerols as stable products with an average of ca. 22 oxygen additions per C_{60} cage molecule.[54] Besides being a key daughter product of light-induced fullerene transformations in water, fullerols are used as starting materials for the synthesis of fullerene-containing polymers, underscoring industrial relevance.[272, 273]

Fullerols are a general class of oxidized fullerene derivatives, which are often poorly defined and normally synthesized and applied with a distribution of oxygen functionalities. Generic C_{60}-based fullerols are often expressed as $C_{60}(OH)_n$ and with hydroxyl numbers varying from 8 to 40 reported as the n average.[48, 57, 159, 274-277] The number and pattern distribution of oxygen moieties can differ widely depending on the synthesis route, significantly affect fullerol's

properties including solvent solubility, toxicity, reactivity and aggregation behavior in aqueous systems.[60, 62, 139, 162, 310-312] For example, hydroxylation of C_{60} to a fullerol can enhance its aqueous solubility by up to 10 orders of magnitude, reaching a maximum value reported as 58.9 mg/mL.[48] Further, the aqueous properties and behaviors, including simulated environmental transport of hydroxylated C_{60}, differ significantly from those of parent C_{60}.[55, 166, 220, 278] Xiao and Wiesner compared the transport behavior of aqueous stable C_{60} aggregates (termed in their work as aqu-nC_{60}) and hydroxylated C_{60} in a biofilm-laden, porous media column experiment and demonstrated that the retention of fullerols was significantly higher than water stable C_{60} aggregates.[278] Additionally, the reactivity of fullerols can differ considerably from the parent (underivatized) fullerene materials. A number of previous studies have demonstrated efficient, fullerol-catalyzed production of reactive oxygen species (ROS) under UV or sunlight irradiation.[58, 60, 61] Under similar conditions, C_{60} in water, as water stable nC_{60}, does not efficiently catalyze such ROS production.[34, 72, 137] ROS generation through fullerol photosensitization was suggested as a potential causal agent involved in inactivating exposed cells.[98, 138, 139] While clear differences have been observed in the biological response of fullerols when compared to underivatized fullerenes (as nC_{60}), to date, there is no clear structure function relationship regarding specific fullerol response despite a number of studies evaluating fullerol toxicity when exposed to human cell lines, bacteria and viruses.[98, 138, 139, 279, 313]

The chemistry of fullerenes and fullerene derivatives, including fullerols, in organic solvents has been studied extensively in contrast to aqueous systems, which have been less studied due to inherent solubility limitations.[4, 125-127, 196, 314-318] A wide variety of C_{60} oxidation reactions in organic solvents has been demonstrated including the reactions with ozone, fluorine and chlorine gas, osmium tetroxide, among others.[4, 125-127, 196, 316] Further, a number of C_{60}

reduction reactions have also been described and include reduction by metals, electrochemical approaches and even organic donor molecule reactions.[314, 319, 320] Bergosh et al. demonstrated the reduction of fullerene in toluene with a series of metals leading to $C_{60}H_x$ (x = 4-6) formation with reduction potentials ranging from -0.14 V (tin) to -2.36 V (magnesium).[314] Under strict anaerobic conditions, cyclic voltammetric characterization of C_{60} reduction reaction potentials (in CH_3CN/toluene), observed a maximum addition of up to six electrons (C_{60}^{6-}), with stepwise half reduction potential ($E_{1/2}$ of Fc/Fc^+), ranging from -0.98 to -3.26 V.[15] While not as widely studied, electrochemical reduction of a pure fullerol ($C_{60}(OH)_6$ in dimethylformamide) demonstrated two quasi-reversible reduction potentials of -1.24 V and -1.72 V ($E_{1/2}$ of Fc/Fc^+), followed with two re-oxidation reactions occurring at -1.26 V and -1.62 V.[283] To date, few other studies have systematically investigated further oxidation and/or reduction reactions of hydroxylated fullerenes (fullerols), especially in aqueous systems.

The fact that fullerols represent the major product(s) of aqueous fullerene exposure to sunlight (in the presence of oxygen)[56, 72] underpins the need for the corresponding aqueous chemistry to be well understood as it is critical for accurate environmental lifecycle and risk assessments. Building upon what is currently understood regarding fullerol reactivity in water, herein we demonstrate an aqueous fullerol *reduction* reaction for the first time. Specifically, we describe the reductive transformation of fullerol (as $C_{60}(OH)_x(ONa)_y$) by solid zinc metal (Zn(0)), which has been demonstrated to reduce a wide range of dissolved contaminants[321-325], through a series of batch reaction experiments and detailed product characterization using UV-vis spectroscopy, Fourier transform infrared spectroscopy (FTIR), total organic carbon (TOC) analysis, dynamic light scattering (DLS), X-ray photoelectron spectroscopy (XPS), transmission electron microscopy (TEM) and ^{13}C-nuclear magnetic resonance spectroscopy (^{13}C NMR). Last,

we demonstrate the aqueous physical behavior of the product fullerol differs significantly from parent material, consistent with an increase in molecular (product) hydrophobicity as measured by octanol partitioning (K_{ow}) and surface deposition rates (using a quartz crystal microbalance).

6.2. Materials and Methods

6.2.1. **Materials**

Fullerol ($C_{60}(OH)_x(ONa)_y$, y = 8-10, x+y ~ 24, purity >99%) and ^{13}C-labeled (ca. 25% enriched) fullerol ($C_{60}(OH)_x(ONa)_y$, y = 8-10, x+y ~ 24, purity >99%) were purchased from MER (Tucson, AZ). The solid zinc powder (diameter <425 μm) was purchased from Sigma Aldrich (St. Louis, MO). Solid zinc powder was washed three times with ultrapure water (>18.2 MΩ-cm resistivity, Milli-Q, Millipore Corp., MA) and separated at 1000 rpm (5810 Centrifuge, Eppendorf, NY) to remove any dissolved Zn or impurities. The specific surface area of the washed Zn powder was quantified as 0.49 m^2/g by BET-N_2 adsorption isotherm (Quantichrome Inc., FL). $ZnCl_2$ (99.99% purity, trace metal basis) was purchased from Fisher Scientific (Pittsburgh, PA). 1-Octanol was purchased from Sigma Aldrich. Fullerol stock suspensions (40 mg/L) were prepared by adding powder fullerol to ultrapure water and stirring for 24 hours in the dark. The golden-colored suspensions were vacuum filtered through 0.22 μm PES membrane and stored in the dark at room temperature (21.0 ± 1.0 °C). Stock suspensions remained stable in water for months according to UV-vis, DLS, and visual inspection.

6.2.2. **Batch Fullerol Reduction Experiments**

Batch fullerol reduction experiments were conducted, under both ambient atmospheric and anaerobic conditions. Reaction solutions of 20 mg/L fullerol were prepared in borosilicate

glass vials (coated with aluminum foil to prevent light irradiation) via 40 mg/L fullerol stock solution dilution. 0.05g/L or 0.5 g/L solid Zn was then added to each reactor which initiated the reaction. All experiments were run in triplicate on a multi-position stir plate (Variomag Poly, Thermo Scientific, NC) at room temperature. For each, pH was recorded initially, and monitored periodically throughout the reaction (SevenMulti, Mettler Toledo, OH). pHs of the system slightly increased at the beginning and remained in the range from 6.8 to 7.5 (Figure S6.1). To avoid any complications from possible buffer-metal interactions, additional buffer was not used besides the bicarbonate present from atmospheric CO_2 exposure. Sample aliquots of 1-5 mL were taken at appropriate time intervals and filtered with 0.22 μm PES syringe membrane (Millipore Corporation, MA) to remove solid zinc particulates. UV-vis absorption spectra were taken immediately after sampling, scanning from 190 nm to 800 nm with 0.5 nm interval using a UV-visible spectrophotometer (Varian Cary Bio50) with background correction of pure water. The wavelength of 285 nm was referred to quantify parent fullerol as it was determined to be a wavelength of high (sensitive) molar adsorption coefficient (ranging from 2.896 - 2.971×10^4 $M^{-1}cm^{-1}$) for the parent fullerol for this reaction (see Figure 6.1). The oxidized Zn ion and complexes (as Zn(II)) concentrations and total organic carbon present in the system during the reaction were measured by ICP-MS (7500 Series, Agilent, CA) and TOC-L total organic carbon analyzer (Shimadzu Scientific Instrument, Inc., MD), respectively. For TOC analysis samples with and without centrifugation were compared to determine if dissolved carbon (as fullerol) is lost from the supernatant (due to fullerol aggregation or sorption to solid Zn) during centrifugation. For experiments under anaerobic conditions, the solutions were bubbled with N_2 gas (Airgas, MO) for more than 1 hour to remove dissolved oxygen and were then stored in glass vials sealed with Teflon coated stoppers. During the reaction, the reactor headspace was

continuously purged with a custom N_2 / 400 ppm CO_2 gas blend (CeeKay gas, MO) to remove oxygen from the system while maintaining atmospheric level of CO_2, thus keeping pH buffering capacity consistent with those of the ambient experiments. Control experiments of 0.05g/L solid Zn loaded in ultrapure water adjusted to the same initial pH as fullerol solution were conducted concurrently to compare the Zn(II) concentrations produced as a result of any reactions with water and/or oxygen. Upon reaction cessation, products were collected for FTIR, ^{13}C NMR, XPS, TEM, DLS, QCM-D and water-octanol partition characterization described below.

6.2.3. **Product Characterization**

The particle size distributions of the fullerols before and after reaction were compared through dynamic light scattering (DLS) analysis using a ZetaSizer Nano (Malvern Instruments, UK). TEM specimens were prepared by a flash drop preparation and ca. 30 μL of parent fullerol or reduced products (filtered with 0.22 μm PES to remove any solid Zn and precipitates) suspension on the 400 mesh carbon-coated copper grid (Electron Microscopy Sciences, PA) and immediate evaporation of the remaining water at room temperature. TEM images were taken using a FEI Spirit transmission electron microscope at 120 kV voltage. Solid-state FTIR analysis was performed by diffuse reflectance infrared Fourier transform spectroscopy (Nexus 470 FT-IR, Thermo Nicolet, NC). To produce solid samples for FTIR analysis, concentrated fullerol or product fullerol suspensions were prepared by adding 5 mg fullerol and 125 mg solid Zn(0) (for the case of products) to 10 mL ultrapure water and stirring for 4 days in the dark. After centrifugation at 1000 rpm, the fullerol suspension was collected and this process was repeated for 3 times to remove all the Zn solid and precipitates from fullerol system. Parent fullerol or reduced products at varied pH (pH 1 and 12) were adjusted with HCl or NaOH before stirring for 24 hours. The fullerol or products were subsequently dried in a vacuum oven (Thermo Scientific,

NC) for 2 days at room temperature. To prepare the pristine and reacted fullerol powders for IR analysis, each was mixed, in an agate mortar and pestle, with KBr powder (Spectrograde, International Crystal Lab, NJ) at a 1:10 ratio, which was determined to be optimum. A KBr background spectrum was collected for subtraction prior to sample spectrum collection. Solid-state NMR analysis was conducted to compare the ^{13}C-enriched (ca. 25%) fullerol ($C_{60}(OH)_x(ONa)_y$) before and after Zn(0) reduction. To prepare the reduced fullerol powders, 13 mg ^{13}C-enriched fullerol powder and 100 mg Zn were placed in 10 mL D_2O (deuterium enrichment 99.99%, Sigma Aldrich, MO) and allowed to react for 4 days. The solid reduced fullerol sample was collected for NMR analysis by the procedure detailed above for FTIR solid sample preparation. Direct ^{13}C pulse NMR spectra were acquired on a Bruker Avance spectrometer (50.3 MHz ^{13}C, 200.1 MHz ^{1}H) with a probe for spinning rotors with a 4 mm outer diameter. Chemical shifts are relative to the glycine carbonyl carbon defined as 176.46 ppm.[326] (Additional details are in Figure 6.2 caption.) Samples for X-ray photoelectron spectroscopy (XPS) analysis were first centrifuged at 1000 rpm to remove solid Zn and then carefully dried (a number of sequential 100 μL sample aliquots were added/dried to preserve spot size) onto a gold coated (20 nm) silicon wafer in a vacuum oven at room temperature. XPS analyses of reduced fullerol with different Zn(0) concentrations (20 mg/L fullerol with 0, 1, 2 and 4 g/L Zn(0)) were performed with a PHI Quantera SXM scanning X-ray microprobe with monochromatic Al source and conducted at 26 eV pass energy with a 200 μm X-ray spot size.

6.2.4. **Quartz Crystal Microbalance Analysis**

Surface interactions of fullerols, both before and after reduction reactions, were evaluated using a quartz crystal microbalance-with dissipation (QCM-D E4, Q-Sense AB, Sweden) with polystyrene-coated (hydrophobic)[287] sensor (QSX-305, Q-sense). Sensors surfaces were prepared

following protocols described by Penfold and Naderi.[289, 290] Polystyrene-coated quartz crystals were presoaked in 1% Deconex 11 for 30 minutes at 30°C. Surfaces were rinsed and kept in ultrapure water for at least 2 hours, then rinsed with 99% ethanol and dried with N_2 gas.

QCM-D measurements were initiated at 22°C with flowing air for 10 minutes. Next, ultrapure water was then flowed over the sensor with a rate of 100 μL/min. A $ZnCl_2$ buffer solution was then added into the system for appropriate background correction (mimicking final reaction solution conditions with 0.5 g/L Zn). Fullerol suspensions (parent and product both at 20 mg/L) were then allowed to flow through the measurement chambers for ca. 1 hour. All of the solutions were flowed at the same rate as 100 μL/min. When switching inflowing solutions, the flow was reversed for 5 seconds to avoid air bubbles before returning the flow to the forward direction and allowing the buffer solutions to flow into the modules. All QCM-D experiments were conducted in triplicate for each experimental condition described. As the fullerol solutions were flowed over the sensor, surface deposition alters the oscillation frequency of the crystal which can be linearly correlated to mass (fullerol) adsorbed on the sensor surface using the Sauerbrey model[291]:

$$\Delta m = -C\frac{1}{n}\Delta f \qquad (1)$$

where Δm is the mass of fullerol nanoparticles deposited, Δf is the shift in resonance frequency, n is the overtone number of the system (1, 3, 5, 7, 9, 13), and C is the crystal constant(17.7 ng/(Hz-cm^2)). In this study, the third overtone was selected to calculate the mass change of the quartz surface.[223, 292]

6.2.5. **Octanol-Water Partition Coefficient Measurements**

Water-octanol partition coefficients were widely used to evaluate the potential fate and distribution of molecules, including fullerols, in the environment.[220, 222, 327] Here, 8 mL of a 20 mg/L fullerol or reduced product solution was mixed with 1-octanol of the same volume in glass bottles by the rotary shaker (Labquake, Thermo Scientific, UT) for 3 hours in the dark. The mixtures were then equilibrated for 24 hours and analyzed for the ratio of the fullerol concentrations in octanol and water phase to determine octanol-water partition coefficients according to equation (2):

$$K_{ow} = \frac{C_0}{C_w} = \frac{[Abs]_{285nm,i} - k*[Abs]_{285nm,f}}{[Abs]_{285nm,f}} \qquad (2)$$

The concentrations of fullerol or the reduced products left in the water phase were determined by the UV absorbance of fullerol in water after partitioning at 285 nm wavelength through UV-vis detection ($[Abs.]_{285nm,f}$). The concentrations in the octanol phase were calculated through subtracting the absorbance in water phase from the initial absorbance at 285 nm wavelength ($[Abs.]_{285nm,i}$). The partition coefficients were corrected by the concentrating (volume change) factor k determined experimentally, as the volume of water dissolved into octanol phase cannot be neglected for these systems. The K_{ow} of parent fullerol and reduced products were evaluated at pH as 4, 7 and 10 through treatment with NaOH or HCl before partitioning experiments. All the above experiments were conducted in triplicate to calculate K_{ow} in each condition.

6.3. Results and Discussion

Batch reaction results in Figure 6.1 show a decreasing 285 nm absorbance response for fullerol in the presence of solid zinc, with a corresponding increasing level of oxidized zinc as

Zn(II) increasing over time, indicating a reduction-oxidation (redox) reaction had occurred. The UV-vis absorption spectrum of parent fullerol starting at 20 mg/L, decreased with the reaction time (Figure 6.1b), was also visually confirmed by the gradual but distinct change of solution color from yellow to near clear after 10 days of reaction (Figure 6.1a) with no fullerol precipitation observed. Further, Figure 1c shows the final reaction rates and extent to increase with the solid Zn concentration (0, 0.05, 0.5 g/L). Such an increase in reaction rate is hypothesized to be due, in part, to increased available reactive surface area of solid zinc powder; however, rates were not linearly related to the Zn(0) concentrations in the system, implying that more complicated heterogeneous, solid-aqueous reaction mechanisms are likely involved. It should be noted that monitoring the absorption at 285 nm to quantify (decreasing) parent fullerol concentration as the reaction proceeds is limited by the fact that the heterogeneously changing products will have varied absorption coefficients, and thus, this method can only provide a relative, qualitative analysis for the reaction rate observations. Differential released zinc (as Zn(II)) during the reaction is also demonstrated in Figure 6.1d, which was significantly higher compared to a pure water (fullerol free) control. Total Zn(II) production in the system resulting from the oxidation of Zn(0) by water, oxygen and fullerol is qualitatively illustrated in Equations (3) – (5):

$$Zn + 2H_2O \rightarrow Zn^{2+} + 2OH^- + H_2 \qquad (3)$$

$$2Zn + O_2\,(aq) + 2H_2O \rightarrow 2Zn^{2+} + 4OH^- \qquad (4)$$

$$Zn + \text{Fullerol} \rightarrow Zn^{2+} + \text{Fullerol (reduced)} + 2OH^- \qquad (5)$$

Wang et al. demonstrated the minimum reduction potential of $C_{60}(OH)_6$ was -1.24 V (vs. Fc/Fc^+).[283] However, here we observe that with a higher number of oxygen atoms (more

oxidized) ($C_{60}(OH)_x(ONa)_y$, x+y ~ 24), fullerol reduction reaction can be initiated at or below -0.76 V, zinc's reduction potential.[328] Under anaerobic conditions, Zn^{2+} release rates remained at the same level compared to those observed for open atmospheric conditions (20.95% O_2 by volume), indicating that, for this system, dissolved oxygen had little observable effect on the rate of Zn(0) oxidation. Further, it also suggests that reduced fullerol products did not cycle back to their previous form (or more oxidized form) when there was available dissolved oxygen. The pH of the batch reactions increased slightly, as expected according to equations 3 and 5, but remained circumneutral from 6.8 to 7.5, during all reactions (SI, Figure S6.1). Total fullerol (carbon) concentration, measured by total dissolved organic carbon (TOC), was consistent with the initial carbon concentration and the carbon mass was conserved for all reactions indicating minimal, if any, losses to precipitation, sorption or volatilization (SI, Figure S6.2).

The number-weighted size distribution obtained from DLS analysis (SI, Figure S6.3a) indicated a bimodal distribution upon reduction. In addition to the the ca. 50 nm average radius of the parent (soft) cluster size, which has been documented for similar fullerols[162], an additional population was consistently observed with an average radius around 12 nm after reduction, indicating an altered cluster dynamic. Consistent with the changing hydrodynamic size distribution, the physical morphology of the reacted fullerol clusters, as imaged in Figure S6.3b, also differs. In agreement with DLS analysis, soft fullerol parent clusters were observed in Figure S6.3b i and ii. Also in line with DLS results, product clusters appeared to be much loser with a larger percentage of smaller and more diffuse clustering as shown in Figure S6.3b iii and iv. Altered aggregation tendencies of the product may result from the changing functional group(s) van der Waals forces and hydrogen bonding environments, which in turn effect soft cluster formation and/or stabilization. Previous studies have demonstrated that the type and

number of oxygen-based functional groups can affect the morphology of the fullerol clusters.[162, 329]

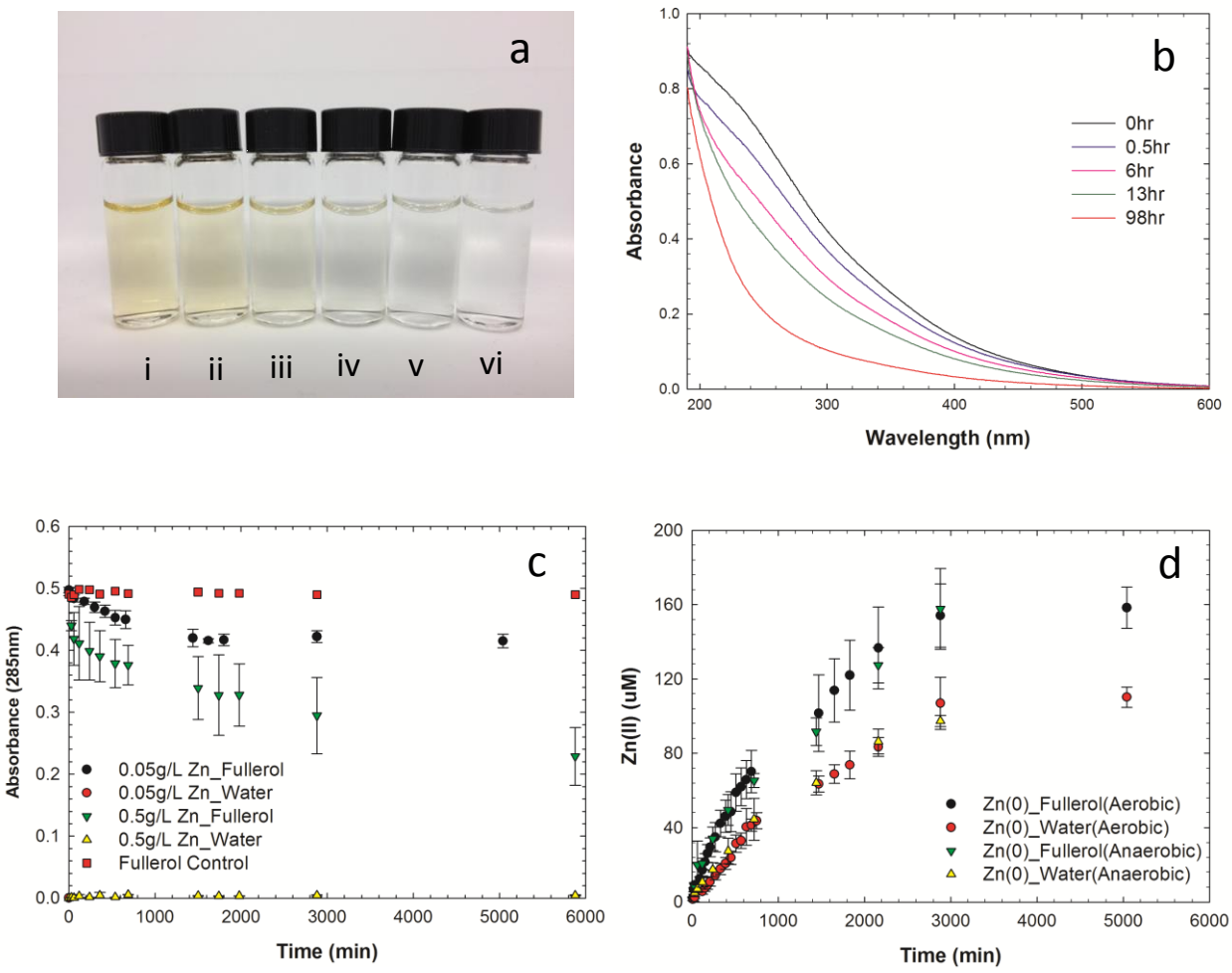

Figure 6.1: Reduction of fullerol by Zn(0): (a) Fullerol solution filtered with 0.22 μm membrane (Unreacted Fullerol (i); Zn reduced fullerol for 1day (ii), 3 days (iii), 5 days (iv), 7 days (v) and 10 days (vi)); (b) Fullerol (20 mg/L) UV spectra as a function of reaction time at pH 6-7 during the batch reaction ([Zn] = 0.5 g/L); (c) Fullerol UV adsorption at 285 nm as a function of time (Fullerol control included: [Zn] = 0 g/L); (d) Dissolved Zn(II) concentrations in the system as a function of reaction time ([Zn] = 0.05 g/L).

^{13}C NMR solid state analysis of ^{13}C-labeled (ca. 25% enrichment) parent fullerol (Figure 6.2a) showed a typical fullerene strained C=C peak at 144 ppm shift, similar to bulk C_{60} at 143 ppm (but slightly upfield from that of nC_{60} in D_2O which has an observed C=C peak centered at 146 ppm).[6, 330] Additionally, three other significant signals appear, at 75.41 ppm (hydroxylated sp^3 carbons)[277], 174.66 ppm (carbonyl carbons, as carboxyl groups)[56, 84] and 193.39 ppm (carbonyl carbons, as ketones). Compared with the parent fullerol, the ^{13}C spectrum of the reduced product (Figure 6.2b) differs significantly, particularly in the greater intensity in the region near 170-175 ppm and the more pronounced downfield shoulder on the aliphatic carbon signal. This comparable increased intensity near 100 ppm and the distinct new signal at 168.66 ppm are consistent with the formation of hemiketal functionality and vinyl ether carbon.[84, 277] The strong signal that remains at 175 ppm is consistent with the presence of carbonyl groups which are most likely carboxyl groups. Further, the C=C shift to 138.96 ppm from the original 143.97 ppm may indicate a possible change in bond angle associated with lowered molecular strain. A similar shift was reported by Fortner et al. upon the oxidation of pure C_{60} with ozone in water that also resulted in less strained products.[84]

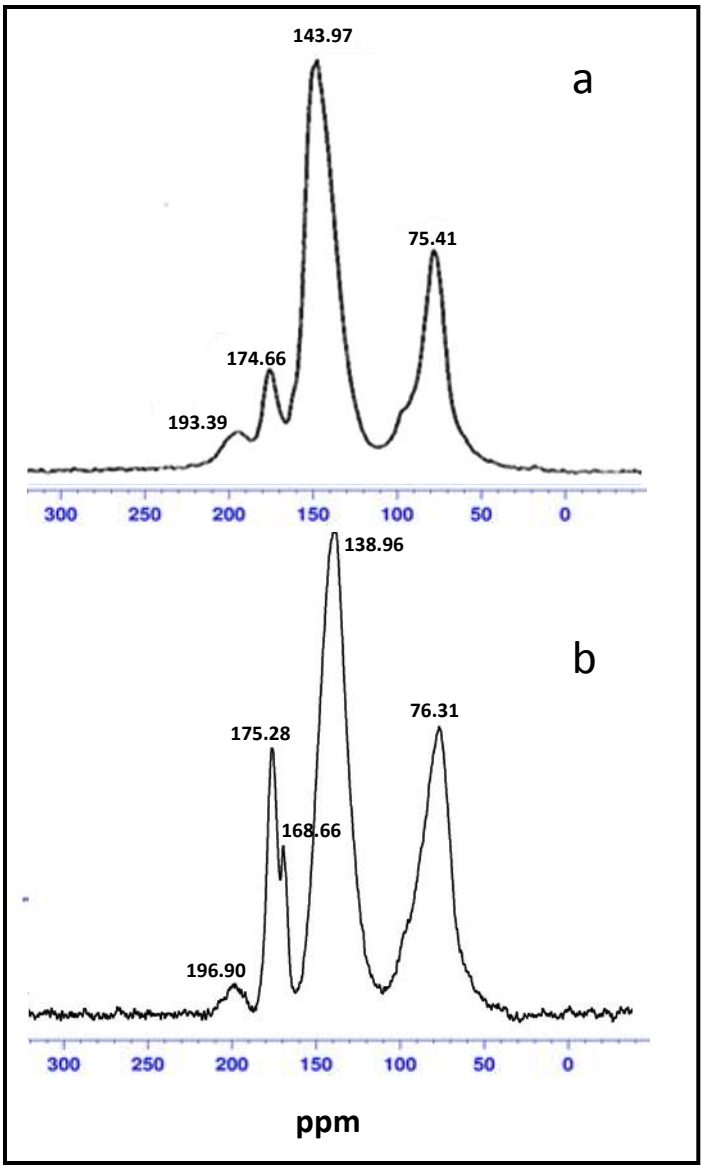

Figure 6.2: ^{13}C NMR spectrum of (a) parent fullerol (25% ^{13}C enriched) obtained with 14.2 kHz MAS, 90 ° ^{13}C pulse, 20.5-ms FID, 10-s relaxation delay, 360 scans, 50 Hz (1 ppm) of line broadening and (b) reduction product (25% ^{13}C enriched, approx. 13 mg) obtained with 13 kHz MAS, 90 ° ^{13}C pulse, 41.0-ms FID, 20-s relaxation delay, 12,200 scans, 25 Hz (0.5 ppm) of line broadening.

The FTIR solid-state spectra of the parent fullerol and the reduced products are shown for comparison in Figure 6.3a. The peaks centered at 1346 cm^{-1} and 1076 cm^{-1} are indicative of C-OH in plane bending and C-O stretching, respectively, characteristic of hydroxyl functionalization.[159] The peak centered at 1620 cm^{-1} with a small shoulder at 1700 cm^{-1} is attributed to the carbonyl carbon or ketone in the parent fullerol[54, 160, 331], which is formed through a pinacol rearrangement in the aqueous phase as described by Chiang et al.[277] FTIR spectra of the products at pH 7.5 also exhibit split peak absorbance centered 1076 cm^{-1}, indicative of C-O stretching, albeit at lower response than the parent, which is not split. Additionally, the resulting peak at 1200 cm^{-1} indicates potential presence of a strained carbon-oxygen bond scenario (e.g. C-O-C along the carbon cage) in the reduced product.[54] The changing IR response of the reduced products at varied pH (pH 1, 7.5 and 12) supports a pH sensitive hemiketal product structure which is in line with NMR results discussed above (hemiketal carbon suggested by the comparable increasing of intensity near 100 ppm and appearance of vinyl ether carbon at about 170 ppm).[84, 277] At pH 12, the reduced fullerol products lose ketone functionality (disappearance of -C=O at 1600-1700 cm^{-1}) with a complete shift to hemiketal structures as expected. To further demonstrate that hemiketal formation was a result of reduction, FTIR spectra of the parent fullerol at the same pH values are also compared in Figure 6.3b. In contrast with the reduced products, the carbonyl groups remained relatively stable at all pH values, indicating little to no ketone structure conversion and thus little to no original hemiketal functionality.

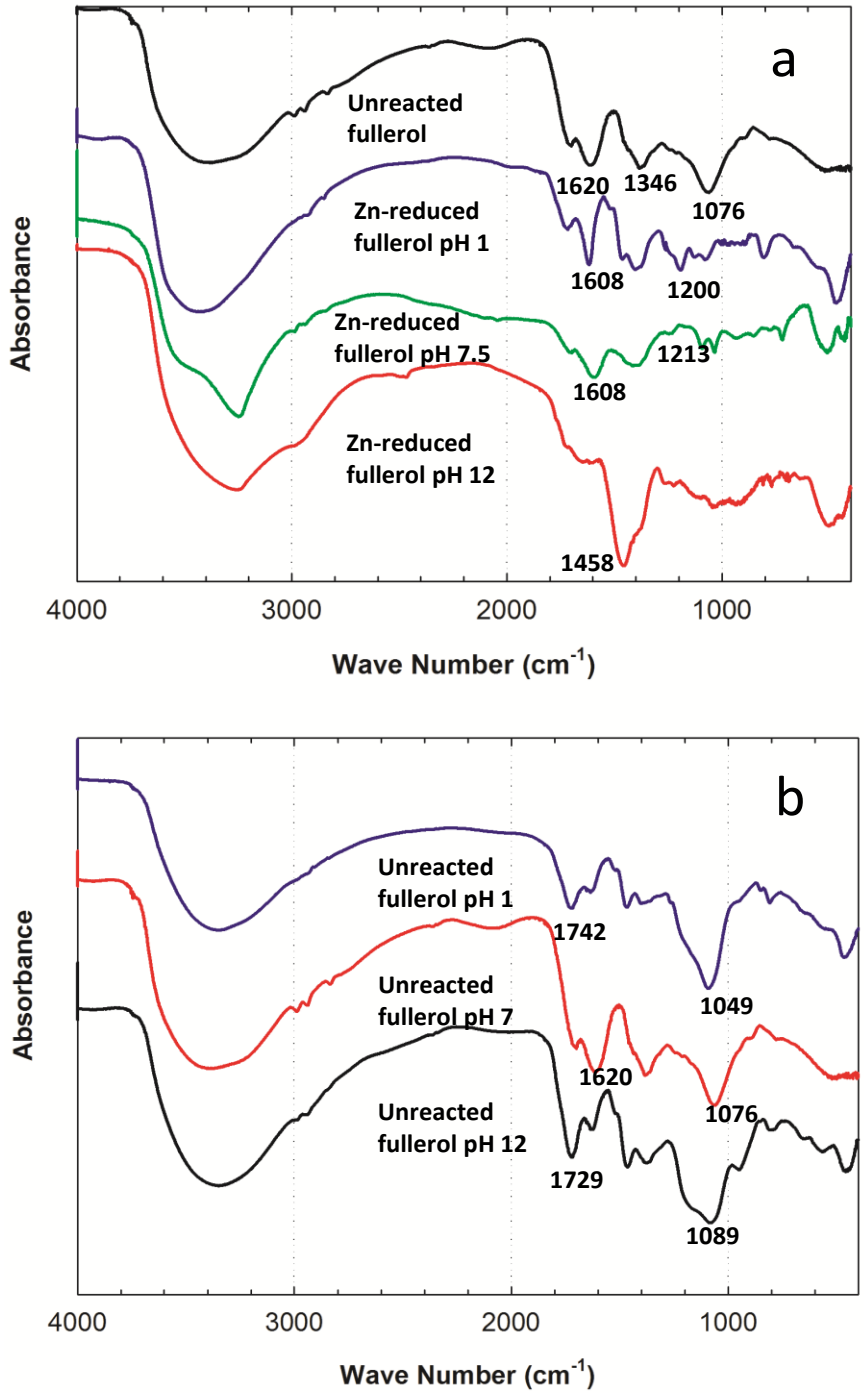

Figure 6.3: FTIR-DRIFTS fullerol spectra: (a) Before and after reduction (Reduced fullerol product at pH 1, pH 7.5 and pH 12); (b) Parent fullerol at pH 1, pH 7 and pH 12.

Based on characterization results presented and previous literature reports, product functionality is shown in Figure 6.4. In water, it has been established that similar fullerols can undergo a pinacol-like rearrangement, leading to a corresponding carbonyl group in the fullerol structure (Figure 6.4iii).[277] This is shown as the red portion of Figure 6.4 and is directly supported by parent ^{13}C NMR and FTIR analyses in this work and elsewhere.[277] Upon reduction, pH sensitive hemiketal functionality (Figure 6.4iv), which has been identified here (Figures 2 and 3), can undergo facile acid conversion (*i.e.*, pH adjustment) to corresponding ketone structures as shown in Figure 6.4iv to Figure 6.4vi, as detailed by Chiang et al.[11] As transient reaction intermediates identification was beyond the scope of this work, the authors recognize that alternative reduction pathways resulting in hemiketal functionality are possible. XPS analysis of the parent and reduced fullerol product, presented in Table S6-1, was used to compare the carbon(1s) oxidation state ratios of the reactants and products. The peaks with the lowest binding energy (ca. 284 eV) represent underivatized, elemental carbon in the fullerol structure, while other peaks with binding energy at ca. 286 eV and ca. 288 eV are assigned to mono-oxidized carbon (C-O) and di-oxidized carbon (C=O, O-C-O), respectively[47, 54, 84]. The ratios of underivatized, mono-oxidized and di-oxidized carbon in the reduced fullerol products remained at nearly the same levels compared to the parent fullerol (0 g/L Zn solid). Correspondingly, a resulting hemiketal structure should possess the same, relative amount of mono-oxidized and di-oxidized carbons, which is consistent with these XPS results. A noted limitation of XPS here is based on the difficulty in differentiating the C=O and -O-C-O- accurately.

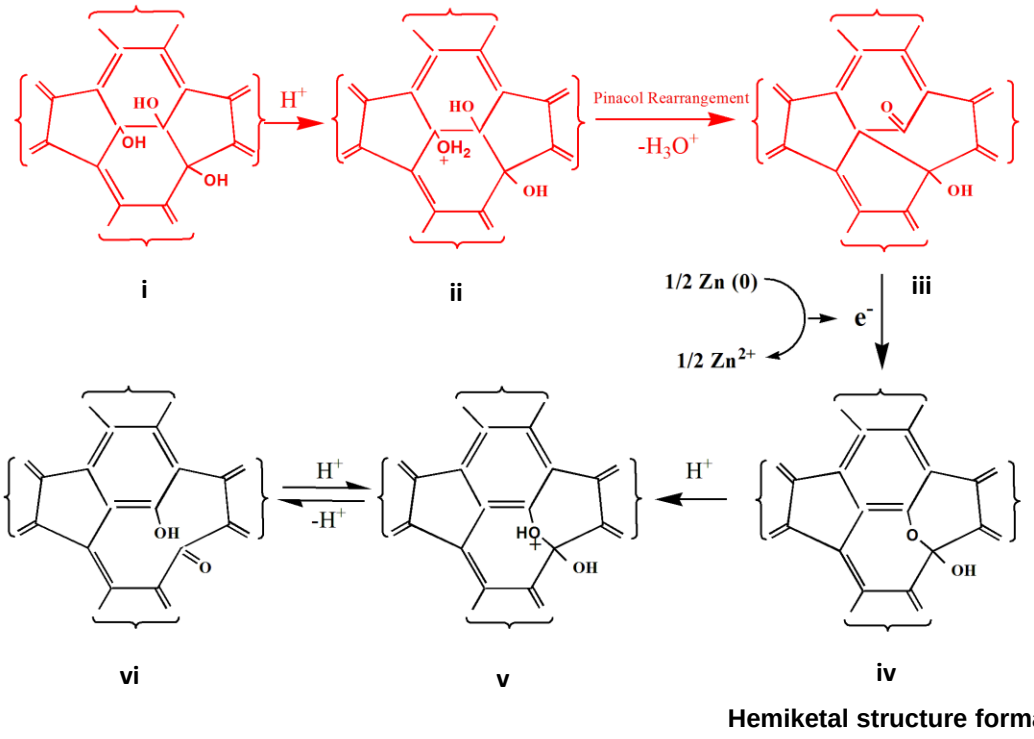

Figure 6.4: Proposed reduction pathways of fullerol by Zn(0). (Red line: Pinacol rearrangement of fullerol in the aqueous solution;[277] Black line: Hemiketal structure formation and equilibrium)

Finally, quartz crystal microbalance sorption analysis and traditional liquid-liquid partitioning measurements were employed to compare the interaction(s), of parent fullerol and reduced products with a hydrophobic surface and non-aqueous phase liquid (here as octanol, K_{ow}). Figure 6.5 shows the frequency shift (thus mass addition) over time when flowing (at a flow rate of 100 µL/min) solution of 20 mg/L fullerol (or reduced fullerol) over a polystyrene coated sensor surface at pH 7 with a normalized background concentration of Zn^{2+} and Cl^-. A faster rate of frequency change, thus higher rate of surface associated fullerol mass, was observed for the reduced products, indicating a more favorable interaction with the hydrophobic PS surface.[306, 307] Using the Sauerbrey model[291], the mass of the fullerols associated onto polystyrene surfaces was calculated at times of 3000 s, 4000 s and 5000 s, as illustrated in Figure 6.5. The adsorbed mass of reduced fullerol reached 97.7 ± 6.5 ng/cm^2 at 5000 s, which is

ca. 27% higher than the adsorbed mass of the unreacted fullerol (76.7 ± 5.7 ng/cm^2). Comparative octanol-water partition coefficients (K_{ow}) are shown in Figure S6.4. The K_{ow} of unreacted fullerol at pH 7 was 0.23 ± 0.02, which was slightly higher than that reported by a previous study of similar materials by Xiao and Wiesner as 0.12 ± 0.03.[220] The measured K_{ow} of fullerol product was 0.429 ± 0.024, which is ca. 85% higher than the parent fullerol at pH 7, supporting QCM-D observations. These results imply that the product fullerol is relatively more hydrophobic as a reduced hemiketal structure, which is possibly due to a more evenly distributed dipole moment at circumneutral pH (Figure 6.4iii vs. 6.4iv).

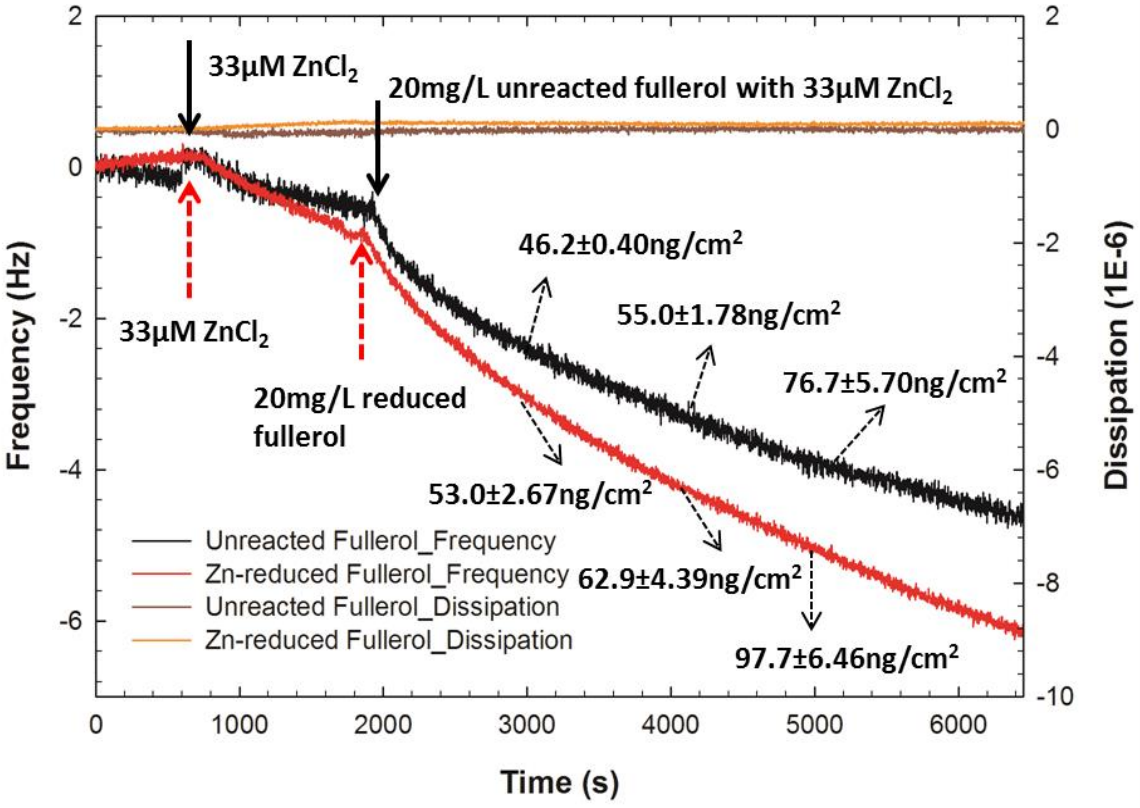

Figure 6.5: QCM-D measurement comparison of parent fullerol and reduced product interaction with the polystyrene surface.

6.4. Conclusions

To summarize, an aqueous fullerol reduction reaction with Zn(0) has been identified and characterized. The reaction rate and extent were observed to increase with Zn(0) concentration while the presence of dissolved oxygen had no observable effect. Characterization analyses indicate significant chemical transformation of parent fullerol occurred, with the 60-carbon based cage structure conserved, resulting in new pH sensitive hemiketal functionality. Reduced fullerol products, while still effectively soluble, are relatively more hydrophobic than parent material. Taken together, this work highlights the importance of the environmental aqueous chemistry of fullerenes, and other curved-carbon engineered nanostructures, as it relates to material cycling - specifically in reducing scenarios. As water-soluble fullerol generation can be reasonably expected through fullerene photo-oxidation (via sunlight) or ozone exposure, additional environmental reactions, including reductions and even further oxidizing scenarios, should be evaluated to understand the ultimate fate of these and similar materials in the environment.

Acknowledgements

This study was supported by Washington University in St. Louis faculty startup funding for Fortner. We sincerely thank Denise Benoit at Department of Chemistry, Rice University for X-ray photoelectron spectroscopy analysis and discussion and Lu Yang for his hard working and contribution for this project during his independent study at Department of Energy, Environmental, Chemical Engineering, Washington University in St. Louis. We also thank for the TEM and DLS facility supporting by Nano Research Facility (NRF) at Washington University in St. Louis, a member of the National Nanotechnology Infrastructure Network (NNIN), which is funded by the National Science Foundation under Grant No. ECS-0335765.

Chapter 6. Supporting Information

Profiles of system pH, TOC concentrations, products size distributions, TEM images, octanol-water coefficients, and table of XPS C1s analyses are included.

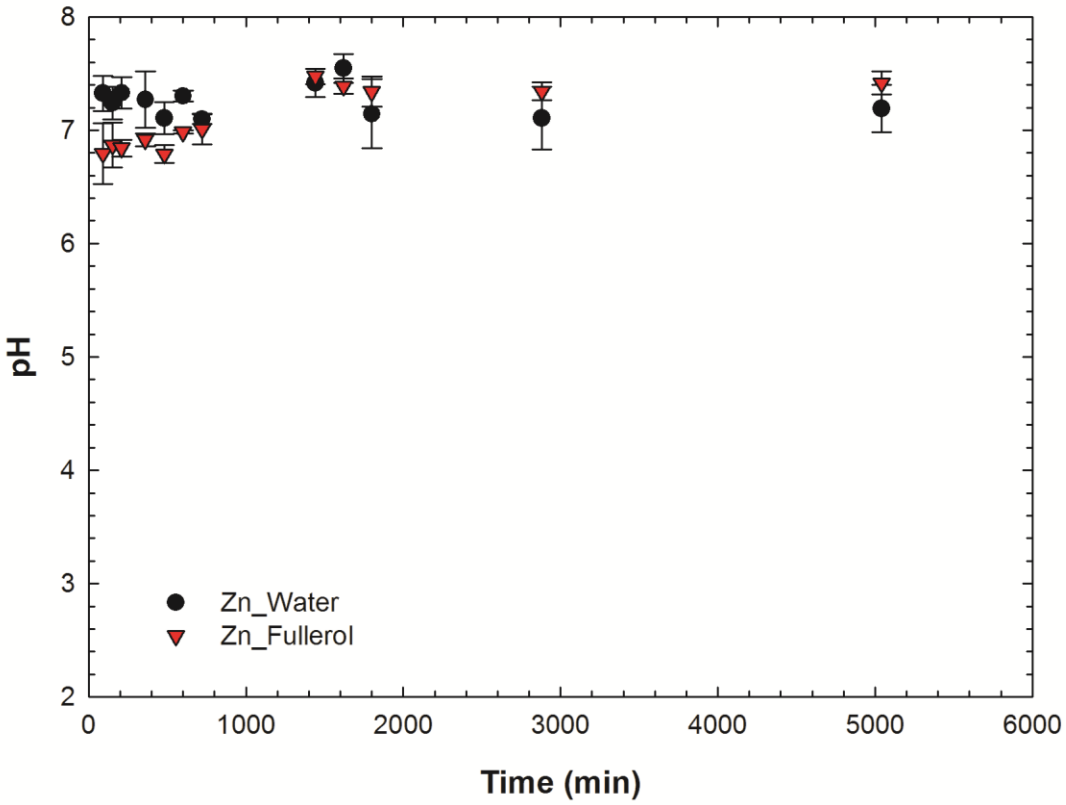

Figure S6.1: System pH of 20 mg/L fullerol reacted with 0.05 g/L Zn as a function of time.

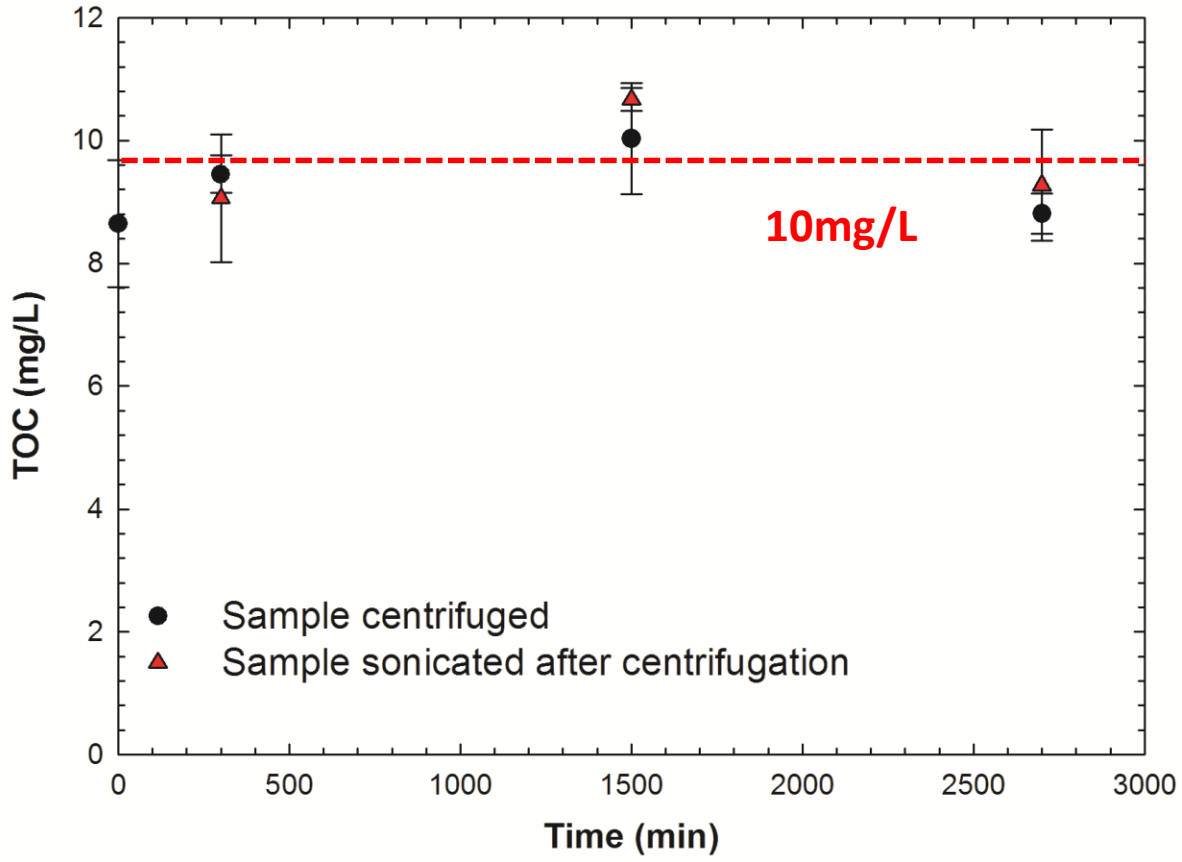

Figure S6.2: TOC concentration of 20 mg/L fullerol solution with 0.5 g/L Zn as a function of reaction time (**Sample centrifuged**: The TOC concentration of the supernatant of fullerol sample after centrifuge at 1000 rpm to remove Zn solid and other precipitates; **Sample sonicated after centrifugation**: The TOC concentration of the fullerol solution sonicated after supernatant were sampled.)

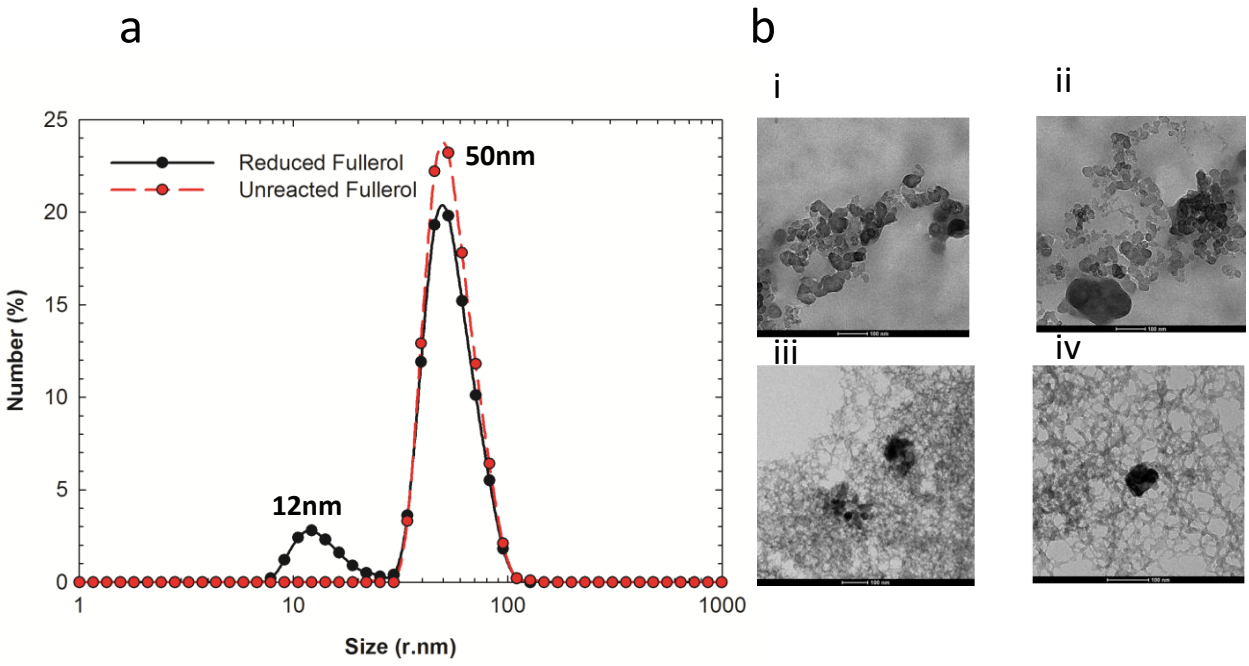

Figure S6.3: Change in fullerol particle size and shape during the reduction reaction: (a) Number-weighted size distribution of the unreacted fullerol (20 mg/L fullerol) and reduced fullerol (20 mg/L fullerol reacted 0.5 g/L Zn for 5 days); (b) The TEM images of the fullerols: (i-ii) Unreacted fullerol (20 mg/L fullerol); (iii-iv) Zn-reduced product (20 mg/L fullerol reacted with 0.5 g/L Zn for 5 days). (Scale bar:100 nm)

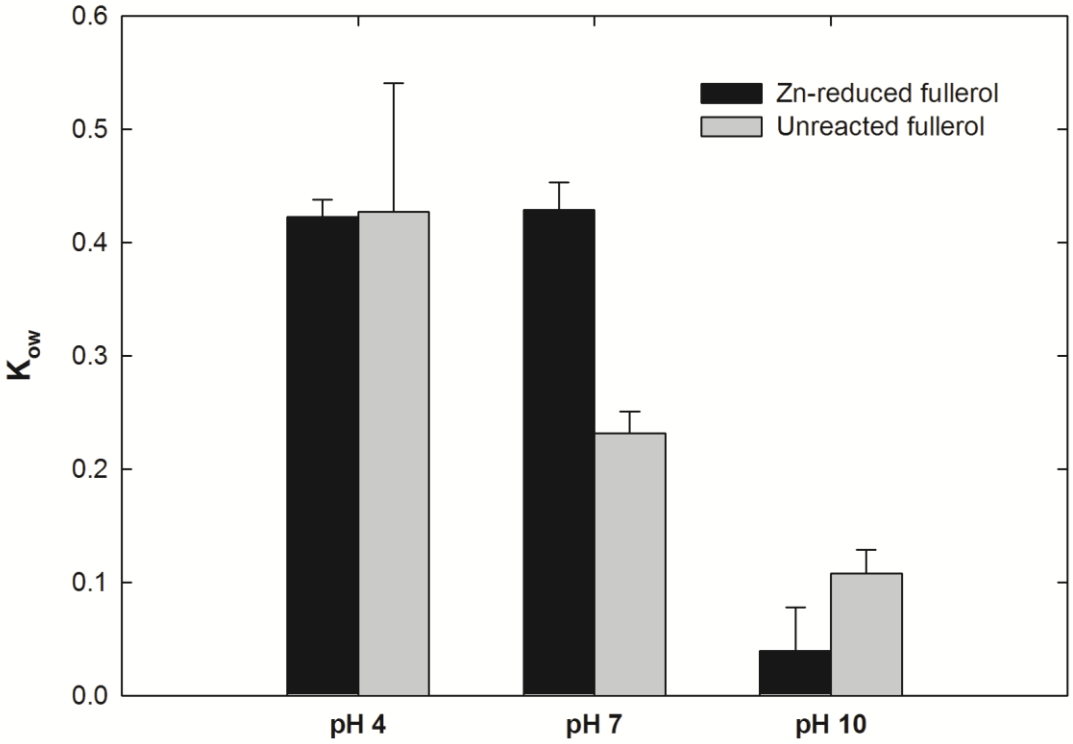

Figure S6.4: Octanol-water partitioning coefficients of fullerol and reduced product at pH 4, pH 7 and pH 10. (**Unreacted fullerol**: 20 mg/L fullerol solution; **Zn-reduced fullerol**: 20 mg/L fullerol reacted with 0.5 g/L Zn for 5 days.)

Table S6-1: C(1s) XPS analysis of fullerol and reduced fullerol products at different Zn concentrations.

Zn (g/L)	Peak 1	Underivatized Carbon_% C(1s)	Peak 2	Mono-Oxidized Carbon_% C(1s)	Peak 3	Di-Oxidized C_% C(1s)
0	284.05	74.3±5.9	285.97	18.0±3.6	287.81	7.7±2.4
1	283.99	67.7±2.2	285.68	22.3±1.0	287.74	10±3.0
2	284.04	69.7±1.7	285.86	22.7±1.5	287.75	7.6±1.6
4	284.15	67.2±1.4	286.05	22.3±2.0	287.85	10.5±2.2

Chapter 7 :**Conclusions and Recommendations**

7.1. Conclusions

In summary, this work advanced fundamental understanding of fullerene reaction pathways/mechanisms in aquatic systems. Data directly expand the current state of the art with regard to fullerene environmental chemistry and will improve understanding of the ultimate fate of these, and other similar, carbon-based materials in the natural systems. As supported by this thesis, the chemical reaction cycle of fullerenes in aqueous phase is further supported, as summarized in Figure 7.1.

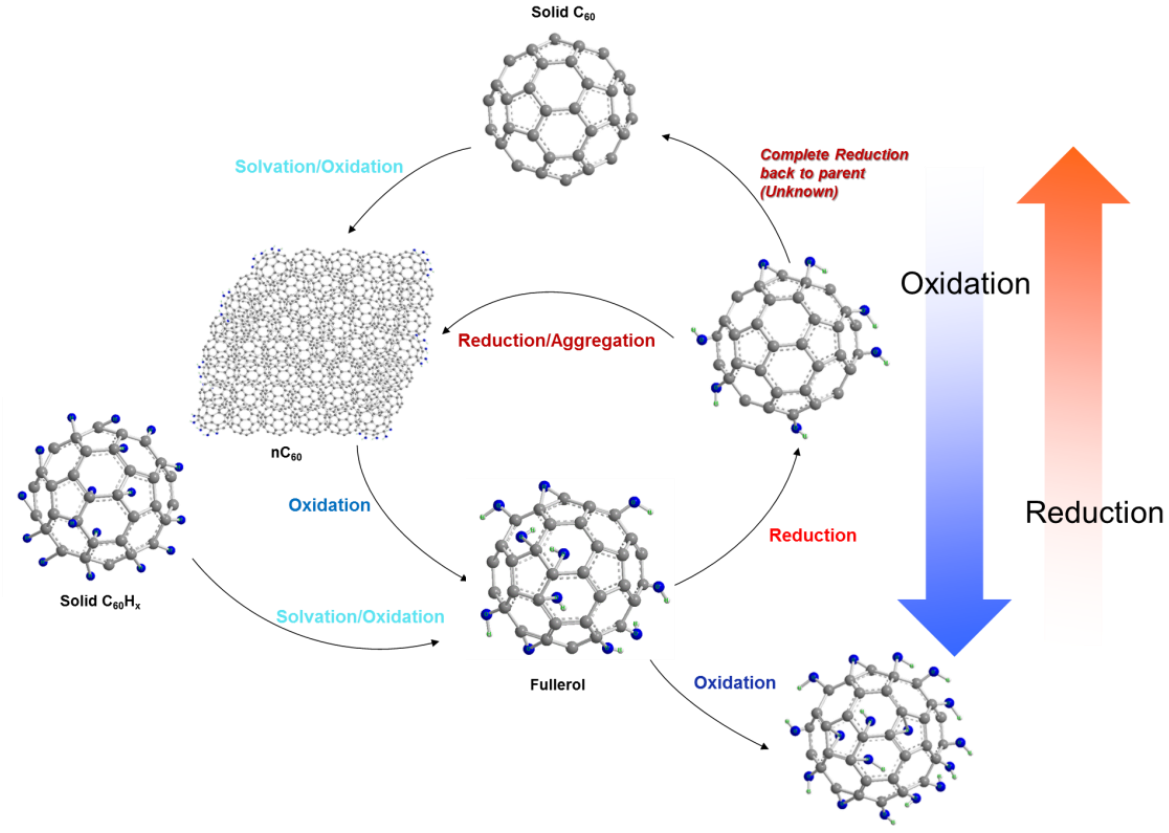

Figure 7.1: Oxidation-reduction reaction cycle of fullerenes in water.

Task 1: Solid State Fullerene Solvation and Derivation in Water

Based on the results of task 1, despite exceeding hydrophobicity, solid C_{60} and its hydrogenated derivatives ($C_{60}H_x$) can readily become water available via simple mixing into water in the presence of light and oxygen. Nano-scale C_{60} aggregates (nC_{60}) and oxidized fullerene derivatives (fullerol) were identified and characterized as the key components of solvated products in water from solid C_{60} and $C_{60}H_x$, respectively. For both of the solvation processes, the formation rates are functions of light irradiation intensity/wavelength, electron acceptors (including ROS), and oxidized fullerene intermediates. Light and effective electron acceptors were quantitatively demonstrated to play critical roles during the solvation processes.

Task 2: Water Soluble Fullerene Oxidation Reaction Kinetics and Pathways

Water stable/soluble fullerene (e.g. nC_{60} and fullerol (from Task 1)) can be further chemically transformed under environmentally oxidizing scenarios, as illustrated in Task 2. In the ground state (dark), nC_{60} was observed to undergo oxychlorination in the presence of free chlorine, a commonly used oxidant for water treatment. Oxidation reaction rates increase with free chlorine concentration, are reversely related to the system pH. Resulting products, with oxygen and chlorine covalently bonds, stabilities were significantly enhanced compared to parent materials, especially for low pH and ionic strength solutions. Further, oxidized fullerene derivatives (fullerol) can also be further oxidized with free chlorine, under both light (photo-excited state) and dark (ground state) conditions. Under photo-irradiation, both the reaction kinetics and extent of products oxidation were significantly enhanced, with reactive radical species demonstrated to be involved. Significant surfaces property alteration was also observed, and (further) oxidized products exhibit significantly different aggregation behaviors compared to parent fullerols.

Task 3: Water Soluble Fullerene Reduction Reaction Kinetics and Pathways

As demonstrated in Tasks 1 and 2, water soluble oxidized fullerene (fullerol) can form through either solvation processes or through other oxidation pathways in water. In Task 3, fullerol reduction was detailed under environmentally relevant reducing scenarios with Zn(0). Reaction rates and extents were enhanced as the reduction-oxidation potential increased (Zn(0) concentration raised). Significant chemical transformation of parent fullerol was identified, resulting in newly formed hemiketal functionality. Reduced products are relatively more hydrophobic as measured with traditional partition experiments and QCM-D analysis. Based on product characterization, a new reaction pathway was proposed.

7.2. Future Work Recommendations

Based on the results, significance, and implications of this dissertation, I offer the following future work recommendations:

(1) In order to comprehensively understand the behavior of solid fullerenes at natural occurring air-water interfaces, additional investigation of solvation and derivatization processes under a wider range of environmentally relevant scenarios is needed. The following processes are suggested: (a) in the absence of light (dark) with various electron acceptors/donors and/or radicals sources (e.g. Fenton reaction as •OH source) in order to compare/de-convolute the solvation/derivatization reactivities of C_{60} in ground state and photo-excited state; (b) additional evaluation of reductive scenarios in the presence of light (Zero-valent metals, NADH, NOM, etc.).

(2) In the aqueous phase, water stable or soluble C_{60} can be exposed to a set of oxidizing reacting scenarios or reducing reacting scenarios, over a series of effective electron

acceptors/donors (e.g. NADH (-0.32V, NADH/NAD^-), SO_3^{2-} (-0.17V, SO_3^{2-}/$HSO4^-$), Zn (-0.76V, $Zn^{2+/}$Zn), H_2 (0.41V, H^+/H_2), ClO_4^- (+1.23V, ClO_4^-/ ClO_3^-), $Cr_2O_7^{2-}$ (+1.33V, $Cr_2O_7^{2-}$ /Cr^{3+}), MnO_4^- (+1.51V, MnO_4^-/Mn^{2+}) ClO^- (+0.89V, ClO^-/Cl^-), H_2O_2 (+1.763V, H_2O_2/H_2O) etc.). Based on the developed investigation protocol/tools in this dissertation, the reaction library (kinetics and resulting products identification) of the fullerene water chemistry can be and should be integrated and explored further.

(3) Besides derivative physicochemical properties, as collected in this dissertation, resulting products from different reacting systems are suggested to be further characterized, including the evaluation of the interaction of those products with different environment media, such bacteria (toxicity assessment), nanoparticles (heterogeneous aggregation behaviors investigation), different environmental surfaces (transport behaviors through column study or QCM-D). The distribution of parent and reacted products in environmental phases (air, water, soil, and biosystems) can also be quantified with ^{13}C-labeled carbon tracking.

(4) Based on the extensive characterization of a variety of aqueous (green) reaction conditions, fullerene materials could be further developed, in water, for expanded applications. For example, with delocalized conjugated pi system and electron-accepting ability, fullerenes can effectively promote rapid photo-induced charge separation and slow charge recombination, further improving the photo-catalyzing properties of various light-sensitive materials. The composition of fullerenes with a variety of common used photo-catalysts (e.g. TiO_2, ZrO_2, $KTaO_3$, $SrTiO_3$, CdS, etc.), which can be achieved through hydro-thermal synthesis processes, may be applied in a variety of waste stream technologies, among others.

Reference

1. Mauter, M. S.; Elimelech, M., Environmental Applications of Carbon-Based Nanomaterials. *Environ. Sci. Technol.* **2008,** *42*, (16), 5843-5859.
2. Osawa, E., Superaromaticity. *Kagaku (Kyoto, Japan)* **1970,** *25*, (9), 10.
3. Kroto, H. W.; Heath, J. R.; O'Brien, S. C.; Curl, R. F.; Smalley, R. E., C60: Buckminsterfullerene. *Nature* **1985,** *318*, (6042), 162-163.
4. Hirsch, A.; Brettreich, M.; Wudl, F., *Fullerenes: Chemistry and Reactions*. Wiley: 2006.
5. Dresselhaus, M. S.; Dresselhaus, G.; Eklund, P. C., *Science of Fullerenes and Carbon Nanotubes: Their Properties and Applications*. Elsevier Science: 1996.
6. Fortner, J. D.; Lyon, D. Y.; Sayes, C. M.; Boyd, A. M.; Falkner, J. C.; Hotze, E. M.; Alemany, L. B.; Tao, Y. J.; Guo, W.; Ausman, K. D.; Colvin, V. L.; Hughes, J. B., C_{60} in Water: Nanocrystal Formation and Microbial Response. *Environ. Sci. Technol.* **2005,** *39*, (11), 4307-4316.
7. Koruga, D., *Fullerene C60: history, physics, nanobiology, nanotechnology*. North-Holland: 1993.
8. Kamat, P. V.; Haria, M.; Hotchandani, S., C60 cluster as an electron shuttle in a Ru(II)-polypyridyl sensitizer-based photochemical solar cell. *J. Phys. Chem. B* **2004,** *108*, 5166-5170.
9. Bühl, M.; Hirsch, A., Spherical Aromaticity of Fullerenes. *Chem. Rev.* **2001,** *101*, (5), 1153-1184.
10. Taylor, R.; Walton, D. R. M., The chemistry of fullerenes. *Nature* **1993,** *363*, (6431), 685-693.
11. Ruoff, R. S.; Tse, D. S.; Malhotra, R.; Lorents, D. C., Solubility of C-60 in a Variety of Solvents. *J. Phys. Chem.* **1993,** *97*, (13), 3379-3383.
12. Bent, H. A., An Appraisal of Valence-bond Structures and Hybridization in Compounds of the First-row elements. *Chem. Rev.* **1961,** *61*, (3), 275-311.
13. Hirsch, A.; Brettreich, M.; Wudl, F., *Fullerenes*. John Wiley & Sons: 2006.
14. Yildirim, T.; Zhou, O.; Fischer, J. E., Intercalation Compounds of Fullerenes I: Synthesis, Characterization, and Solid State Properties. In *The Physics of Fullerene-Based and Fullerene-Related Materials*, Andreoni, W., Ed. Springer Netherlands: 2000; Vol. 23, pp 23-66.
15. Xie, Q.; Perez-Cordero, E.; Echegoyen, L., Electrochemical detection of C606- and C706-: Enhanced stability of fullerides in solution. *J. Am. Chem. Soc.* **1992,** *114*, (10), 3978-3980.
16. Yildirim, T.; Zhou, O.; Fischer, J. E., Intercalation Compounds of Fullerenes II: Structure and Superconductivity of Alkali Metal Fullerides. In *The Physics of Fullerene-Based and Fullerene-Related Materials*, Andreoni, W., Ed. Springer Netherlands: 2000; Vol. 23, pp 67-133.
17. Yildirim, T.; Zhou, O.; Fischer, J. E., Intercalation Compounds of Fullerenes III: Other Fullenrides and Intercalated Nanotubes. In *The Physics of Fullerene-Based and Fullerene-Related Materials*, Andreoni, W., Ed. Springer Netherlands: 2000; Vol. 23, pp 249-289.
18. Subramanian, R.; Boulas, P.; Vijayashree, M. N.; D'Souza, F.; Jones, M. T.; Kadish, K. M., A facile and selective method for the solution-phase generation of C60- and C602. *Journal of the Chemical Society, Chemical Communications* **1994**, (16), 1847-1848.
19. Stephens, P. W.; Cox, D.; Lauher, J. W.; Mihaly, L.; Wiley, J. B.; Allemand, P.-M.; Hirsch, A.; Holczer, K.; Li, Q.; Thompson, J. D., Lattice structure of the fullerene ferromagnet TDAE–C60. **1992**.

20. Hare, J. P.; Kroto, H. W., A postbuckminsterfullerene view of carbon in the galaxy. *Accounts of Chemical Research* **1992,** *25*, (3), 106-112.
21. Rubin, Y.; Khan, S.; Freedberg, D. I.; Yeretzian, C., Synthesis and x-ray structure of a Diels-Alder adduct of fullerene C60. *J. Am. Chem. Soc.* **1993,** *115*, (1), 344-345.
22. Hoke, S. H.; Molstad, J.; Dilettato, D.; Jay, M. J.; Carlson, D.; Kahr, B.; Cooks, R. G., Reaction of fullerenes and benzyne. *The Journal of Organic Chemistry* **1992,** *57*, (19), 5069-5071.
23. Wood, J. M.; Kahr, B.; Hoke, S. H.; Dejarme, L.; Cooks, R. G.; Ben-Amotz, D., Oxygen and methylene adducts of C60 and C70. *J. Am. Chem. Soc.* **1991,** *113*, (15), 5907-5908.
24. Kalsbeck, W. A.; Thorp, H. H., Electrochemical reduction of fullerenes in the presence of O2 and H2O: Polyoxygen adducts and fragmentation of the C60 framework. *Journal of Electroanalytical Chemistry and Interfacial Electrochemistry* **1991,** *314*, (1), 363-370.
25. Tebbe, F. N.; Becker, J. Y.; Chase, D. B.; Firment, L. E.; Holler, E. R.; Malone, B. S.; Krusic, P. J.; Wasserman, E., Multiple, reversible chlorination of C60. *J. Am. Chem. Soc.* **1991,** *113*, (26), 9900-9901.
26. Birkett, P. R.; Hitchcock, P. B.; Kroto, H. W.; Taylor, R.; Walton, D. R. M., Preparation and characterization of C60Br6 and C60Br8. *Nature* **1992,** *357*, (6378), 479-481.
27. Haufler, R. E.; Conceicao, J.; Chibante, L. P. F.; Chai, Y.; Byrne, N. E.; Flanagan, S.; Haley, M. M.; O'Brien, S. C.; Pan, C.; et al., Efficient production of C60 (buckminsterfullerene), C60H36, and the solvated buckide ion. *The Journal of Physical Chemistry* **1990,** *94*, (24), 8634-8636.
28. Henderson, C. C.; Cahill, P. A., C60H2: Synthesis of the Simplest C60 Hydrocarbon Derivative. *Science* **1993,** *259*, (5103), 1885-1887.
29. Olah, G. A.; Bucsi, I.; Lambert, C.; Aniszfeld, R.; Trivedi, N. J.; Sensharma, D. K.; Prakash, G. K. S., Chlorination and bromination of fullerenes. Nucleophilic methoxylation of polychlorofullerenes and their aluminum trichloride catalyzed Friedel-Crafts reaction with aromatics to polyarylfullerenes. *J. Am. Chem. Soc.* **1991,** *113*, (24), 9385-9387.
30. Nagashima, H.; Nakaoka, A.; Saito, Y.; Kato, M.; Kawanishi, T.; Itoh, K., C60Pd: the first organometallic polymer of buckminsterfullerene. *Journal of the Chemical Society, Chemical Communications* **1992**, (4), 377-379.
31. Kadish, K. M.; Ruoff, R. S., *Fullerenes: Chemistry, Physics, and Technology*. Wiley: 2000.
32. Yamakoshi, Y.; Umezawa, N.; Ryu, A.; Arakane, K.; Miyata, N.; Goda, Y.; Masumizu, T.; Nagano, T., Active oxygen species generated from photoexcited fullerene (C-60) as potential medicines: O-2(-center dot) versus O-1(2). *J. Am. Chem. Soc.* **2003,** *125*, (42), 12803-12809.
33. Cheng, X.; Kan, A. T.; Tomson, M. B., Naphthalene Adsorption and Desorption from Aqueous C60 Fullerene. *Journal of Chemical & Engineering Data* **2004,** *49*, (3), 675-683.
34. Lee, J.; Kim, J.-H., Effect of Encapsulating Agents on Dispersion Status and Photochemical Reactivity of C60 in the Aqueous Phase. *Environ. Sci. Technol.* **2008,** *42*, (5), 1552-1557.
35. Scrivens, W. A.; Tour, J. M.; Creek, K. E.; Pirisi, L., Synthesis of 14C-Labeled C60, Its Suspension in Water, and Its Uptake by Human Keratinocytes. *J. Am. Chem. Soc.* **1994,** *116*, (10), 4517-4518.
36. Andrievsky, G. V.; Kosevich, M. V.; Vovk, O. M.; Shelkovsky, V. S.; Vashchenko, L. A., On the production of an aqueous colloidal solution of fullerenes. *J. Chem. Soc., Chem. Commun.* **1995**, (12), 1281-1282.

37. McHedlov-Petrossyan, N. O.; Klochkov, V. K.; Andrievsky, G. V., Colloidal dispersions of fullerene C_{60} in water: some properties and regularities of coagulation by electrolytes. *J. Chem. Soc., Faraday Trans.* **1997,** *93*, (24), 4343-4346.
38. Chang, X.; Duncan, L. K.; Jinschek, J.; Vikesland, P. J., Alteration of nC60 in the Presence of Environmentally Relevant Carboxylates. *Langmuir* **2012,** *28*, (20), 7622-7630.
39. Brant, J.; Lecoanet, H.; Hotze, M.; Wiesner, M., Comparison of Electrokinetic Properties of Colloidal Fullerenes (n-C60) Formed Using Two Procedures†. *Environ. Sci. Technol.* **2005,** *39*, (17), 6343-6351.
40. Lyon, D. Y.; Adams, L. K.; Falkner, J. C.; Alvarez, P. J. J., Antibacterial activity of fullerene water suspensions: Effects of preparation method and particle size. *Environ. Sci. Technol.* **2006,** *40*, (14), 4360-4366.
41. Andrievsky, G. V.; Klochkov, V. K.; Bordyuh, A. B.; Dovbeshko, G. I., Comparative analysis of two aqueous-colloidal solutions of C_{60} fullerene with help of FTIR reflectance and UV-Vis spectroscopy. *Chem. Phys. Lett.* **2002,** *364*, (1-2), 8-17.
42. Israelachvili, J. N., *Intermolecular and Surface Forces*. Academic Press: 2011.
43. Alargova, R. G.; Deguchi, S.; Tsujii, K., Stable Colloidal Dispersions of Fullerenes in Polar Organic Solvents. *J. Am. Chem. Soc.* **2001,** *123*, (43), 10460-10467.
44. Deguchi, S.; Alargova, R. G.; Tsujii, K., Stable Dispersions of Fullerenes, C_{60} and C_{70}, in Water. Preparation and Characterization. *Langmuir* **2001,** *17*, (19), 6013-6017.
45. Ma, X.; Bouchard, D., Formation of Aqueous Suspensions of Fullerenes. *Environ. Sci. Technol.* **2009,** *43*, (2), 330-336.
46. Lee, J.; Kim, J. H., Effect of encapsulating agents on dispersion status and photochemical reactivity of C_{60} in the aqueous phase. *Environ. Sci. Technol.* **2008,** *42*, (5), 1552-1557.
47. Lee, J.; Song, W.; Jang, S. S.; Fortner, J. D.; Alvarez, P. J. J.; Cooper, W. J.; Kim, J.-H., Stability of Water-Stable C_{60} Clusters to OH Radical Oxidation and Hydrated Electron Reduction. *Environ. Sci. Technol.* **2010,** *44*, (10), 3786-3792.
48. Kokubo, K.; Matsubayashi, K.; Tategaki, H.; Takada, H.; Oshima, T., Facile Synthesis of Highly Water-Soluble Fullerenes More Than Half-Covered by Hydroxyl Groups. *ACS Nano* **2008,** *2*, (2), 327-333.
49. Ōsawa, E., *Perspectives of fullerene nanotechnology*. Kluwer Academic Publishers: 2002.
50. Chiang, L. Y.; Upasani, R. B.; Swirczewski, J. W., Versatile nitronium chemistry for C60 fullerene functionalization. *J. Am. Chem. Soc.* **1992,** *114*, (26), 10154-10157.
51. Chiang, L. Y.; Wang, L.-Y.; Swirczewski, J. W.; Soled, S.; Cameron, S., Efficient Synthesis of Polyhydroxylated Fullerene Derivatives via Hydrolysis of Polycyclosulfated Precursors. *The Journal of Organic Chemistry* **1994,** *59*, (14), 3960-3968.
52. Schneider, N. S.; Darwish, A. D.; Kroto, H. W.; Taylor, R.; Walton, D. R. M., Formation of fullerols via hydroboration of fullerene-C60. *Journal of the Chemical Society, Chemical Communications* **1994**, (4), 463-464.
53. Zhang, J.-M.; Yang, W.; He, P.; Zhu, S.-Z., Efficient and convenient preparation of water-soluble fullerenol. *Chinese Journal of Chemistry* **2004,** *22*, (9), 1008-1011.
54. Lee, J.; Cho, M.; Fortner, J. D.; Hughes, J. B.; Kim, J. H., Transformation of Aggregate C_{60} in the Aqueous Phase by UV Irradiation. *Environ. Sci. Technol.* **2009,** *43*, (13), 4878-4883.
55. Hwang, Y. S.; Li, Q. L., Characterizing Photochemical Transformation of Aqueous nC_{60} under Environmentally Relevant Conditions. *Environ. Sci. Technol.* **2010,** *44*, (8), 3008-3013.

56. Hou, W.-C.; Kong, L.; Wepasnick, K. A.; Zepp, R. G.; Fairbrother, D. H.; Jafvert, C. T., Photochemistry of Aqueous C_{60} Clusters: Wavelength Dependency and Product Characterization. *Environ. Sci. Technol.* **2010,** *44*, (21), 8121-8127.
57. Guirado-Lopez, R. A.; Rincon, M. E., Structural and optical properties of highly hydroxylated fullerenes: Stability of molecular domains on the C_{60} surface. *J. Chem. Phys.* **2006,** *125*, (15).
58. Chae, S.-R.; Hotze, E. M.; Wiesner, M. R., Evaluation of the Oxidation of Organic Compounds by Aqueous Suspensions of Photosensitized Hydroxylated-C_{60} Fullerene Aggregates. *Environ. Sci. Technol.* **2009,** *43*, (16), 6208-6213.
59. Hotze, E. M.; Labille, J.; Alvarez, P.; Wiesner, M. R., Mechanisms of photochemistry and reactive oxygen production by fullerene suspensions in water. *Environ. Sci. Technol.* **2008,** *42*, (11), 4175-4180.
60. Pickering, K. D.; Wiesner, M. R., Fullerol-sensitized production of reactive oxygen species in aqueous solution. *Environ. Sci. Technol.* **2005,** *39*, (5), 1359-1365.
61. Kong, L. J.; Tedrow, O.; Chan, Y. F.; Zepp, R. G., Light-Initiated Transformations of Fullerenol in Aqueous Media. *Environ. Sci. Technol.* **2009,** *43*, (24), 9155-9160.
62. Fileti, E. E.; Rivelino, R.; Mota, F. d. B.; Malaspina, T., Effects of hydroxyl group distribution on the reactivity, stability and optical properties of fullerenols. *Nanotechnology* **2008,** *19*, (36).
63. Xiao, L.; Takada, H.; Maeda, K.; Haramoto, M.; Miwa, N., Antioxidant effects of water-soluble fullerene derivatives against ultraviolet ray or peroxylipid through their action of scavenging the reactive oxygen species in human skin keratinocytes. *Biomedicine & Pharmacotherapy* **2005,** *59*, (7), 351-358.
64. Chiang, L. Y.; Lu, F. J.; Lin, J. T., Free-Radical Scavenging Activity of Water-Soluble Fullerenols *J. Chem. Soc.-Chem. Commun.* **1995**, (12), 1283-1284.
65. Bogdanovic, G.; Kojic, V.; Dordevic, A.; Canadanovic-Brunet, J.; Vojinovic-Miloradov, M.; Baltic, V. V., Modulating activity of fullerol C-60(OH)(22) on doxorubicin-induced cytotoxicity. *Toxicology in Vitro* **2004,** *18*, (5), 629-637.
66. Tsai, M. C.; Chen, Y. H.; Chiang, L. Y., Polyhydroxylated C60, Fullerenol, a Novel Free-radical Trapper, Prevented Hydrogen Peroxide- and Cumene Hydroperoxide-elicited Changes in Rat Hippocampus In-vitro. *Journal of Pharmacy and Pharmacology* **1997,** *49*, (4), 438-445.
67. Sun, D.; Zhu, Y.; Liu, Z.; Liu, G.; Guo, X.; Zhan, R.; Liu, S., Active oxygen radical scavenging ability of water-soluble fullerenols. *Chinese Science Bulletin* **1997,** *42*, (9), 748-752.
68. Pizzarello, S.; Huang, Y.; Becker, L.; Poreda, R. J.; Nieman, R. A.; Cooper, G.; Williams, M., The Organic Content of the Tagish Lake Meteorite. *Science* **2001,** *293*, (5538), 2236-2239.
69. Heymann, D.; Chibante, L. P.; Brooks, R. R.; Wolbach, W. S.; Smalley, R. E., Fullerenes in the Cretaceous-Tertiary Boundary-Layer. *Science* **1994,** *265*, (5172), 645-647.
70. Jehlička, J.; Ozawa, M.; Slanina, Z.; sawa, E., Fullerenes in Solid Bitumens from Pillow Lavas of Precambrian Age (M ĺŤOV, Bohemian Massif). *Fullerene Science and Technology* **2000,** *8*, (4-5), 449-452.
71. Richter, H.; Labrocca, A. J.; Grieco, W. J.; Taghizadeh, K.; Lafleur, A. L.; Howard, J. B., Generation of Higher Fullerenes in Flames. *The Journal of Physical Chemistry B* **1997,** *101*, (9), 1556-1560.
72. Hou, W.-C.; Jafvert, C. T., Photochemical Transformation of Aqueous C_{60} Clusters in Sunlight. *Environ. Sci. Technol.* **2008,** *43*, (2), 362-367.

73. Hou, W. C.; Kong, L. J.; Wepasnick, K. A.; Zepp, R. G.; Fairbrother, D. H.; Jafvert, C. T., Photochemistry of Aqueous C(60) Clusters: Wavelength Dependency and Product Characterization. *Environ. Sci. Technol.* **2010,** *44*, (21), 8121-8127.
74. Guldi, D. M.; Martin, N., *Fullerenes: from synthesis to optoelectronic properties*. Kluwer Academic Publishers: 2002.
75. Tagmatarchis, N.; Shinohara, H., Fullerenes in Medicinal Chemistry and their Biological Applications. *Mini Rev Med Chem* **2001,** *1*, (4), 339-348.
76. Ungurenasu, C.; Airinei, A., Highly Stable C_{60}/Poly(vinylpyrrolidone) Charge-Transfer Complexes Afford New Predictions for Biological Applications of Underivatized Fullerenes. *J. Med. Chem.* **2000,** *43*, (16), 3186-3188.
77. Hendren, C. O.; Mesnard, X.; Dröge, J.; Wiesner, M. R., Estimating Production Data for Five Engineered Nanomaterials As a Basis for Exposure Assessment. *Environ. Sci. Technol.* **2011,** *45*, (7), 2562-2569.
78. Research, B., *The Global Market for Fullerenes*. BCC Research: 2006.
79. Sherigara, B. S.; Kutner, W.; D'Souza, F., Electrocatalytic Properties and Sensor Applications of Fullerenes and Carbon Nanotubes. *Electroanalysis* **2003,** *15*, (9), 753-772.
80. Da Ros, T.; Prato, M., Medicinal chemistry with fullerenes and fullerene derivatives. *Chem. Commun.* **1999**, (8), 663-669.
81. Sariciftci, N. S.; Smilowitz, L.; Heeger, A. J.; Wudl, F., Photoinduced Electron Transfer from a Conducting Polymer to Buckminsterfullerene. *Science* **1992,** *258*, (5087), 1474-1476.
82. Tsao, N.; Kanakamma, P. P.; Luh, T.-Y.; Chou, C.-K.; Lei, H.-Y., Inhibition of Escherichia coli-Induced Meningitis by Carboxyfullerence. *Antimicrobial Agents and Chemotherapy* **1999,** *43*, (9), 2273-2277.
83. Bakry, R.; Vallant, R. M.; Najam-ul-Haq, M.; Rainer, M.; Szabo, Z.; Huck, C. W.; Bonn, G. K., Medicinal applications of fullerenes. *Int J Nanomed* **2007,** *2*, (4), 639-649.
84. Fortner, J. D.; Kim, D. I.; Boyd, A. M.; Falkner, J. C.; Moran, S.; Colvin, V. L.; Hughes, J. B.; Kim, J. H., Reaction of Water-Stable C_{60} Aggregates with Ozone. *Environ. Sci. Technol.* **2007,** *41*, (21), 7497-7502.
85. Heymann, D., Solubility of C_{60} and C_{70} in seven normal alcohols and their deduced solubility in water. *Fullerene Sci. Tech.* **1996,** *4*, 509-515.
86. Dhawan, A.; Taurozzi, J. S.; Pandey, A. K.; Shan, W.; Miller, S. M.; Hashsham, S. A.; Tarabara, V. V., Stable Colloidal Dispersions of C_{60} Fullerenes in Water: Evidence for Genotoxicity. *Environ. Sci. Technol.* **2006,** *40*, (23), 7394-7401.
87. Cheng, X. K.; Kan, A. T.; Tomson, M. B., Naphthalene adsorption and desorption from Aqueous C_{60} fullerene. *J. Chem. Eng. Data* **2004,** *49*, (3), 675-683.
88. Chang, X.; Vikesland, P. J., Effects of carboxylic acids on nC60 aggregate formation. *Environmental Pollution* **2009,** *157*, (4), 1072-1080.
89. Labille, J.; Masion, A.; Ziarelli, F.; Rose, J.; Brant, J.; Villiéras, F.; Pelletier, M.; Borschneck, D.; Wiesner, M. R.; Bottero, J.-Y., Hydration and Dispersion of C_{60} in Aqueous Systems: The Nature of Water−Fullerene Interactions. *Langmuir* **2009,** *25*, (19), 11232-11235.
90. Duncan, L. K.; Jinschek, J. R.; Vikesland, P. J., C_{60} Colloid Formation in Aqueous Systems: Effects of Preparation Method on Size, Structure, and Surface Charge. *Environ. Sci. Technol.* **2007,** *42*, (1), 173-178.
91. Isaacson, C. W.; Bouchard, D. C., Effects of Humic Acid and Sunlight on the Generation and Aggregation State of Aqu/C60 Nanoparticles. *Environ. Sci. Technol.* **2010,** *44*, (23), 8971-8976.

92. Indeglia, P.; Krishna, V.; Georgieva, A.; Bonzongo, J.-C., Mechanical transformation of fullerene (C60) to aqueous nano-C60 (aqu-nC60) in the presence and absence of light. *J Nanopart Res* **2013,** *15*, (11), 1-16.
93. Brant, J. A.; Labille, J.; Bottero, J.-Y.; Wiesner, M. R., Characterizing the Impact of Preparation Method on Fullerene Cluster Structure and Chemistry. *Langmuir* **2006,** *22*, (8), 3878-3885.
94. Deguchi, S.; Mukai, S.; Tsudome, M.; Horikoshi, K., Facile Generation of Fullerene Nanoparticles by Hand-Grinding. *Advanced Materials* **2006,** *18*, (6), 729-732.
95. Li, Q.; Xie, B.; Hwang, Y. S.; Xu, Y., Kinetics of C60 Fullerene Dispersion in Water Enhanced by Natural Organic Matter and Sunlight. *Environ. Sci. Technol.* **2009,** *43*, (10), 3574-3579.
96. Zhang, W.; Rattanaudompol, U. s.; Li, H.; Bouchard, D., Effects of humic and fulvic acids on aggregation of aqu/nC60 nanoparticles. *Water Research* **2013,** *47*, (5), 1793-1802.
97. Murdianti, B. S.; Damron, J. T.; Hilburn, M. E.; Maples, R. D.; Hikkaduwa Koralege, R. S.; Kuriyavar, S. I.; Ausman, K. D., C_{60} Oxide as a Key Component of Aqueous C_{60} Colloidal Suspensions. *Environ. Sci. Technol.* **2012,** *46*, (14), 7446-7453.
98. Badireddy, A. R.; Hotze, E. M.; Chellam, S.; Alvarez, P.; Wiesner, M. R., Inactivation of Bacteriophages via Photosensitization of Fullerol Nanoparticles. *Environ. Sci. Technol.* **2007,** *41*, (18), 6627-6632.
99. Arbogast, J. W.; Darmanyan, A. P.; Foote, C. S.; Diederich, F. N.; Whetten, R. L.; Rubin, Y.; Alvarez, M. M.; Anz, S. J., Photophysical properties of sixty atom carbon molecule (C_{60}). *The Journal of Physical Chemistry* **1991,** *95*, (1), 11-12.
100. Guldi, D. M.; Asmus, K.-D., Activity of water-soluble fullerenes towards OH-radicals and molecular oxygen. *Radiat. Phys. Chem.* **1999,** *56*, (4), 449-456.
101. Yamakoshi, Y.; Sueyoshi, S.; Fukuhara, K.; Miyata, N., OH and $O_2^{\cdot}$ generation in aqueous C_{60} and C_{70} solutions by photoirradiation: An EPR study. *J. Am. Chem. Soc.* **1998**, (120), 12363-12364.
102. Hou, W.-C.; Jafvert, C. T., Photochemistry of Aqueous C60 Clusters: Evidence of 1O2 Formation and its Role in Mediating C60 Phototransformation. *Environ. Sci. Technol.* **2009,** *43*, (14), 5257-5262.
103. Hotze, E. M.; Badireddy, A. R.; Chellam, S.; Wiesner, M. R., Mechanisms of Bacteriophage Inactivation via Singlet Oxygen Generation in UV Illuminated Fullerol Suspensions. *Environ. Sci. Technol.* **2009,** *43*, (17), 6639-6645.
104. Joo, S. H.; Feitz, A. J.; Sedlak, D. L.; Waite, T. D., Quantification of the Oxidizing Capacity of Nanoparticulate Zero-Valent Iron. *Environ. Sci. Technol.* **2005,** *39*, (5), 1263-1268.
105. Keenan, C. R.; Goth-Goldstein, R.; Lucas, D.; Sedlak, D. L., Oxidative Stress Induced by Zero-Valent Iron Nanoparticles and Fe(II) in Human Bronchial Epithelial Cells. *Environ. Sci. Technol.* **2009,** *43*, (12), 4555-4560.
106. Haag, W. R.; Hoigné, J. r.; Gassman, E.; Braun, A. M., Singlet oxygen in surface waters — Part I: Furfuryl alcohol as a trapping agent. *Chemosphere* **1984,** *13*, (5–6), 631-640.
107. Haag, W. R.; Hoigne, J., Singlet oxygen in surface waters. 3. Photochemical formation and steady-state concentrations in various types of waters. *Environ. Sci. Technol.* **1986,** *20*, (4), 341-348.
108. Li, Y.; Zhang, W.; Li, K.; Yao, Y.; Niu, J.; Chen, Y., Oxidative dissolution of polymer-coated CdSe/ZnS quantum dots under UV irradiation: Mechanisms and kinetics. *Environmental Pollution* **2012,** *164*, 259-266.

109. Sutherland, M. W.; Learmonth, B. A., The tetrazolium dyes MTS and XTT provide new quantitative assays for superoxide and superoxide dismutase. *Free Radical Research* **1997,** *27*, (3), 283-289.
110. Goldstein, S.; Aschengrau, D.; Diamant, Y.; Rabani, J., Photolysis of Aqueous H2O2: Quantum Yield and Applications for Polychromatic UV Actinometry in Photoreactors. *Environ. Sci. Technol.* **2007,** *41*, (21), 7486-7490.
111. Silva, E. C. d.; Albuquerque, M. B. d.; Neto, A. D. d. A.; Junior, C. D. d. S., *Drought and Its Consequences to Plants – From Individual to Ecosystem*. 2013.
112. Krinsky, N. I., Singlet oxygen in biological systems. *Trends in Biochemical Sciences 2*, (2), 35-38.
113. Schwarz, H. A.; Dodson, R. W., Equilibrium between hydroxyl radicals and thallium(II) and the oxidation potential of hydroxyl(aq). *The Journal of Physical Chemistry* **1984,** *88*, (16), 3643-3647.
114. Koppenol, W. H.; Liebman, J. F., The oxidizing nature of the hydroxyl radical. A comparison with the ferryl ion (FeO2+). *The Journal of Physical Chemistry* **1984,** *88*, (1), 99-101.
115. Klaning, U. K.; Sehested, K.; Holcman, J., Standard Gibbs energy of formation of the hydroxyl radical in aqueous solution. Rate constants for the reaction chlorite (ClO2-) + ozone .dblarw. ozone(1-) + chlorine dioxide. *The Journal of Physical Chemistry* **1985,** *89*, (5), 760-763.
116. Attri, P.; Kim, Y. H.; Park, D. H.; Park, J. H.; Hong, Y. J.; Uhm, H. S.; Kim, K.-N.; Fridman, A.; Choi, E. H., Generation mechanism of hydroxyl radical species and its lifetime prediction during the plasma-initiated ultraviolet (UV) photolysis. *Scientific Reports* **2015,** *5*, 9332.
117. Rodgers, M. A. J.; Snowden, P. T., Lifetime of oxygen (O2(1.DELTA.g)) in liquid water as determined by time-resolved infrared luminescence measurements. *J. Am. Chem. Soc.* **1982,** *104*, (20), 5541-5543.
118. Zang, L. Y.; Misra, H. P., EPR kinetic studies of superoxide radicals generated during the autoxidation of 1-methyl-4-phenyl-2,3-dihydropyridinium, a bioactivated intermediate of parkinsonian-inducing neurotoxin 1-methyl-4-phenyl-1,2,3,6-tetrahydropyridine. *Journal of Biological Chemistry* **1992,** *267*, (33), 23601-8.
119. Wu, J.; Goodwin, D. G.; Peter, K.; Benoit, D.; Li, W.; Fairbrother, D. H.; Fortner, J. D., Photo-Oxidation of Hydrogenated Fullerene (Fullerane) in Water. *Environmental Science & Technology Letters* **2014,** *1*, (12), 490-494.
120. Wu, J.; Benoit, D.; Lee, S. S.; Li, W.; Fortner, J. D., Ground State Reactions of nC60 with Free Chlorine in Water. *Environ. Sci. Technol.* **2015**.
121. Krätschmer, W.; Lowell, D. L.; Fostiropoulos, K.; Donald, R. H., Solid C_{60}:a new form of carbon. *Nature* **1990,** *347*, (6291), 354-358.
122. Blank, M., Protein Aggregation Reactions: Surface Free Energy Model. *Journal of Theoretical Biology* **1994,** *169*, (4), 323-326.
123. Spagnoli, D.; Banfield, J. F.; Parker, S. C., Free Energy Change of Aggregation of Nanoparticles. *The Journal of Physical Chemistry C* **2008,** *112*, (38), 14731-14736.
124. Elimelech, M.; Gregory, J.; Jia, X.; Williams, R. A. F., *Particle Deposition and Aggregation: Measurement, Modelling and Simulation*. Elsevier Science: 2013.
125. Anachkov, M. P.; Cataldo, F.; Rakovsky, S. K., Ozone Reaction with C_{70} and C_{60} Fullerenes: The effect of temperature on the reaction kinetics. *Fuller. Nanotub. Carbon Nanostruct.* **2004,** *12*, (4), 745-752.

126. Cataldo, F., Photochlorination of C_{60} and C_{70} fullerenes. *Carbon* **1994,** *32*, (3), 437-443.
127. Kniaz, K.; Fischer, J. E.; Selig, H.; Vaughan, G. B. M.; Romanow, W. J.; Cox, D. M.; Chowdhury, S. K.; McCauley, J. P.; Strongin, R. M.; Smith, A. B., Fluorinated fullerenes: synthesis, structure, and properties. *J. Am. Chem. Soc.* **1993,** *115*, (14), 6060-6064.
128. Peera, A. A.; Alemany, L. B.; Billups, W. E., Hydrogen storage in hydrofullerides. *Appl. Phys. A-Mater. Sci. Process.* **2004,** *78*, (7), 995-1000.
129. Schur, D. V.; Tarasov, B. P.; Shul'ga, Y. M.; Zaginaichenko, S. Y.; Matysina, Z. A.; Pomytkin, A. P., Hydrogen in fullerites. *Carbon* **2003,** *41*, (7), 1331-1342.
130. Osawa, E., *Perspectives of Fullerene Nanotechnology*. Springer Netherlands: 2002.
131. Loutfy, R.; Katagiri, S., Fullerene Materials for Lithium-ion Battery Applications. In *Perspectives of Fullerene Nanotechnology*, Ōsawa, E., Ed. Springer Netherlands: 2002; pp 357-367.
132. Haufler, R. E.; Conceicao, J.; Chibante, L. P. F.; Chai, Y.; Byrne, N. E.; Flanagan, S.; Haley, M. M.; O'Brien, S. C.; Pan, C.; et al., Efficient production of C_{60} (buckminsterfullerene), $C_{60}H_{36}$, and the solvated buckide ion. *J. Phys. Chem.* **1990,** *94*, (24), 8634-8636.
133. Shigematsu, K.; Abe, K.; Mitani, M.; Tanaka, K., Catalytic Hydrogenation of Fullerenes in the Presence of Metal Catalysts in Toluene Solution. *Fullerene Sci. and Technol.* **1993,** *1*, (3), 309-318.
134. Darwish, A. D.; Abdul-Sada, A. a. K.; Langley, G. J.; Kroto, H. W.; Taylor, R.; Walton, D. R. M., Polyhydrogenation of [60]- and [70]-fullerenes. *J. Chem. Soc., Perkin Trans. 2* **1995**, (12), 2359-2365.
135. Meier, M. S.; Spielmann, H. P.; Haddon, R. C.; Bergosh, R. G.; Gallagher, M. E.; Hamon, M. A.; Weedon, B. R., Reactivity, spectroscopy, and structure of reduced fullerenes. *Carbon* **2000,** *38*, (11–12), 1535-1538.
136. Meier, M. S.; Weedon, B. R.; Spielmann, H. P., Synthesis and isolation of one isomer of $C_{60}H_6$. *J. Am. Chem. Soc.* **1996,** *118*, (46), 11682-11683.
137. Lee, J.; Yamakoshi, Y.; Hughes, J. B.; Kim, J.-H., Mechanism of C_{60} Photoreactivity in Water: Fate of Triplet State and Radical Anion and Production of Reactive Oxygen Species. *Environ. Sci. Technol.* **2008,** *42*, (9), 3459-3464.
138. Cho, M.; Fortner, J. D.; Hughes, J. B.; Kim, J.-H., Escherichia coli Inactivation by Water-Soluble, Ozonated C_{60} Derivative: Kinetics and Mechanisms. *Environ. Sci. Technol.* **2009,** *43*, (19), 7410-7415.
139. Sayes, C. M.; Fortner, J. D.; Guo, W.; Lyon, D.; Boyd, A. M.; Ausman, K. D.; Tao, Y. J.; Sitharaman, B.; Wilson, L. J.; Hughes, J. B.; West, J. L.; Colvin, V. L., The Differential Cytotoxicity of Water-Soluble Fullerenes. *Nano Letters* **2004,** *4*, (10), 1881-1887.
140. Lovern, S. B.; Strickler, J. R.; Klaper, R., Behavioral and Physiological Changes in Daphnia magna when Exposed to Nanoparticle Suspensions (Titanium Dioxide, Nano-C_{60}, and $C_{60}H_x$ $C_{70}H_x$). *Environ. Sci. Technol.* **2007,** *41*, (12), 4465-4470.
141. Avent, A. G.; Darwish, A. D.; Heimbach, D. K.; Kroto, H. W.; Meidine, M. F.; Parsons, J. P.; Remars, C.; Roers, R.; Ohashi, O.; Taylor, R.; Walton, D. R. M., Formation of hydrides of fullerene-C_{60} and fullerene-C_{70}. *J. Chem. Soc., Perkin Trans. 2* **1994**, (1), 15-22.
142. Talyzin, A. V.; Tsybin, Y. O.; Purcell, J. M.; Schaub, T. M.; Shulga, Y. M.; Noréus, D.; Sato, T.; Dzwilewski, A.; Sundqvist, B.; Marshall, A. G., Reaction of hydrogen gas with C_{60} at elevated pressure and temperature: hydrogenation and cage fragmentation. *J. Phys. Chem. A* **2006,** *110*, (27), 8528-8534.

143. Cataldo, F.; Iglesias-Groth, S., *Fulleranes: The Hydrogenated Fullerenes*. Springer Netherlands: 2010.
144. Cataldo, F.; Iglesias-Groth, S.; Manchado, A., Isotope Effect in the UV Photolysis of Hydrogenated and Perdeuterated Fulleranes. In *Fulleranes*, Cataldo, F.; Iglesias-Groth, S., Eds. Springer Netherlands: 2010; Vol. 2, pp 149-170.
145. Cataldo, F.; Iglesias‐Groth, S.; Manchado, A., Synthesis and FT-IR spectroscopy of perdeuterofullerane: $C_{60}D_{36}$ evidences of isotope effect in the stability of $C_{60}D_{36}$. *Fuller. Nanotub. Carbon Nanostruct.* **2009,** *17*, (4), 378-389.
146. Cataldo, F.; Iglesias-Groth, S., Characterization of Hydrogenated Fullerene Mixture of C60Hx and C70Hx. *Fuller. Nanotub. Carbon Nanostruct.* **2010,** *18*, (2), 97-106.
147. Enkvist, C.; Lunell, S.; Sjoegren, B.; Svensson, S.; Bruhwiler, P. A.; Nilsson, A.; Maxwell, A. J.; Maartensson, N., C1s shakeup spectrum of fullerene C_{60}: global charge-transfer satellites and their relation to the x-ray threshold singularities in macroscopic systems. *Phys. Rev. B: Condens. Matter* **1993,** *48*, (19), 14629-37.
148. Fortner, J. D.; Kim, D.-I.; Boyd, A. M.; Falkner, J. C.; Moran, S.; Colvin, V. L.; Hughes, J. B.; Kim, J.-H., Reaction of Water-Stable C_{60} Aggregates with Ozone. *Environmental Science & Technology* **2007,** *41*, (21), 7497-7502.
149. Hou, W.-C.; Kong, L.; Wepasnick, K. A.; Zepp, R. G.; Fairbrother, D. H.; Jafvert, C. T., Photochemistry of Aqueous C_{60} Clusters: Wavelength Dependency and Product Characterization. *Environ. Sci. Technol.* **2010,** *44*, (21), 8121-8127.
150. Kim, J.; Yamada, Y.; Suzuki, Y.; Ciston, J.; Sato, S., Pyrolysis of Epoxidized Fullerenes Analyzed by Spectroscopies. *J. Phys. Chem. C* **2014,** *118*, (13), 7076-7084.
151. Kumar, A.; Singh, F.; Govind; Shivaprasad, S. M.; Avasthi, D. K.; Pivin, J. C., X-ray photoelectron and X-ray Auger electron spectroscopy studies of heavy ion irradiated C60 films. *Appl. Surf. Sci.* **2008,** *254*, (22), 7280-7284.
152. Lee, J.; Cho, M.; Fortner, J. D.; Hughes, J. B.; Kim, J.-H., Transformation of Aggregated C_{60} in the Aqueous Phase by UV Irradiation. *Environ. Sci. Technol.* **2009,** *43*, (13), 4878-4883.
153. Lee, J.; Song, W.; Jang, S. S.; Fortner, J. D.; Alvarez, P. J. J.; Cooper, W. J.; Kim, J.-H., Stability of Water-Stable C_{60} Clusters to OH Radical Oxidation and Hydrated Electron Reduction. *Environ. Sci. Technol.* **2010,** *44*, (10), 3786-3792.
154. Song, P. a.; Liu, H.; Shen, Y.; Du, B.; Fang, Z.; Wu, Y., Fabrication of dendrimer-like fullerene (C_{60})-decorated oligomeric intumescent flame retardant for reducing the thermal oxidation and flammability of polypropylene nanocomposites. *J. Mater. Chem.* **2009,** *19*, (9), 1305-1313.
155. Zhu, Y.; Yi, T.; Zheng, B.; Cao, L., The interaction of C_{60} fullerene and carbon nanotube with Ar ion beam. *Appl. Surf. Sci.* **1999,** *137*, (1-4), 83-90.
156. Cataldo, F.; Iglesias-Groth, S., On the action of UV photons on hydrogenated fulleranes $C_{60}H_{36}$ and $C_{60}D_{36}$. *Mon. Not. Roy. Astron. Soc.* **2009,** *400*, (1), 291-298.
157. Markovic, Z.; Trajkovic, V., Biomedical potential of the reactive oxygen species generation and quenching by fullerenes (C_{60}). *Biomaterials* **2008,** *29*, (26), 3561-3573.
158. Yamakoshi, Y.; Sueyoshi, S.; Fukuhara, K.; Miyata, N., OH and $O_2^{\cdot-}$ generation in aqueous C60 and C70 solutions by photoirradiation: An EPR study. *J. Am. Chem. Soc.* **1998,** *120*, (47), 12363-12364.
159. Chao, T. C.; Song, G. X.; Hansmeier, N.; Westerhoff, P.; Herckes, P.; Halden, R. U., Characterization and Liquid Chromatography-MS/MS Based Quantification of Hydroxylated Fullerenes. *Anal. Chem.* **2011,** *83*, (5), 1777-1783.

160. Cataldo, F., Polymeric fullerene oxide (fullerene ozopolymers) produced by prolonged ozonation of C_{60} and C_{70} fullerenes. *Carbon* **2002,** *40*, (9), 1457-1467.
161. Wu, J.; Alemany, L. B.; Li, W.; Petrie, L.; Welker, C.; Fortner, J. D., Reduction of Hydroxylated Fullerene (Fullerol) in Water by Zinc: Reaction and Hemiketal Product Characterization. *Environ. Sci. Technol.* **2014,** *48*, (13), 7384-7392.
162. Brant, J. A.; Labille, J.; Robichaud, C. O.; Wiesner, M., Fullerol cluster formation in aqueous solutions: Implications for environmental release. *J. Colloid Interface Sci.* **2007,** *314*, (1), 281-288.
163. Wang, J.; Chen, Z.; Chen, B., Adsorption of Polycyclic Aromatic Hydrocarbons by Graphene and Graphene Oxide Nanosheets. *Environ. Sci. Technol.* **2014,** *48*, (9), 4817-4825.
164. Cataldo, F., Fullerane, the hydrogenated C_{60} fullerene: Properties and astrochemical considerations. *Fuller. Nanotub. Carbon Nanostruct.* **2003,** *11*, (4), 295-316.
165. Chen, K. L.; Elimelech, M., Relating Colloidal Stability of Fullerene (C_{60}) Nanoparticles to Nanoparticle Charge and Electrokinetic Properties. *Environ. Sci. Technol.* **2009,** *43*, (19), 7270-7276.
166. Qu, X.; Hwang, Y. S.; Alvarez, P. J. J.; Bouchard, D.; Li, Q., UV Irradiation and Humic Acid Mediate Aggregation of Aqueous Fullerene (nC_{60}) Nanoparticles. *Environ. Sci. Technol.* **2010,** *44*, (20), 7821-7826.
167. Tremblay, J.-F., Mitsubishi Chemical Aims at Breakthrough. *Chem. Eng. News* **2002,** *80*, (49), 16-17.
168. Fortner, J. D.; Lyon, D. Y.; Sayes, C. M.; Boyd, A. M.; Falkner, J. C.; Hotze, E. M.; Alemany, L. B.; Tao, Y. J.; Guo, W.; Ausman, K. D.; Colvin, V. L.; Hughes, J. B., C_{60} in Water: Nanocrystal Formation and Microbial Response. *Environ. Sci. Technol.* **2005,** *39*, (11), 4307-4316.
169. Jafvert, C. T.; Kulkarni, P. P., Buckminsterfullerene's (C_{60}) Octanol−Water Partition Coefficient (Kow) and Aqueous Solubility. *Environ. Sci. Technol.* **2008,** *42*, (16), 5945-5950.
170. Heymann, D., Solubility of C_{60} in Alcohols and Alkanes. *Carbon* **1996,** *34*, (5), 627-631.
171. Sayes, C. M.; Fortner, J. D.; Guo, W.; Lyon, D.; Boyd, A. M.; Ausman, K. D.; Tao, Y. J.; Sitharaman, B.; Wilson, L. J.; Hughes, J. B.; West, J. L.; Colvin, V. L., The Differential Cytotoxicity of Water-Soluble Fullerenes. *Nano Lett.* **2004,** *4*, (10), 1881-1887.
172. Sayes, C. M.; Gobin, A. M.; Ausman, K. D.; Mendez, J.; West, J. L.; Colvin, V. L., Nano-C_{60} cytotoxicity is due to lipid peroxidation. *Biomaterials* **2005,** *26*, (36), 7587-7595.
173. Oberdörster, E., Manufactured Nanomaterials (Fullerenes, C_{60}) Induce Oxidative Stress in the Brain of Juvenile Largemouth Bass. *Environ. Health Perspect.* **2004,** *112*, (10), 1058-1062.
174. Ringwood, A. H.; Levi-Polyachenko, N.; Carroll, D. L., Fullerene Exposures with Oysters: Embryonic, Adult, and Cellular Responses. *Environ. Sci. Technol.* **2009,** *43*, (18), 7136-7141.
175. Shinohara, N.; Matsumoto, T.; Gamo, M.; Miyauchi, A.; Endo, S.; Yonezawa, Y.; Nakanishi, J., Is Lipid Peroxidation Induced by the Aqueous Suspension of Fullerene C_{60} Nanoparticles in the Brains of Cyprinus carpio? *Environ. Sci. Technol.* **2008,** *43*, (3), 948-953.
176. Han, B.; Karim, M. N., Cytotoxicity of Aggregated Fullerene C_{60} Particles on CHO and MDCK Cells. *Scanning* **2008,** *30*, (2), 213-220.
177. Andreja, T.; Biljana, T.-M.; Duska, K.; Maja, M.; Kristina, J.; Ljubica, V.; Aleksandar, P.; Svetlana, J.; Miroslav, D.; Zoran, M.; Vladimir, T., Oxidative stress-mediated hemolytic

activity of solvent exchange-prepared fullerene (C_{60}) nanoparticles. *Nanotechnol.* **2010,** *21*, (37), 375102.
178. Matsuda, S.; Matsui, S.; Shimizu, Y.; Matsuda, T., Genotoxicity of Colloidal Fullerene C_{60}. *Environ. Sci. Technol.* **2011,** *45*, (9), 4133-4138.
179. Dhawan, A.; Taurozzi, J. S.; Pandey, A. K.; Shan, W.; Miller, S. M.; Hashsham, S. A.; Tarabara, V. V., Stable Colloidal Dispersions of C_{60} Fullerenes in Water: Evidence for Genotoxicity. *Environ. Sci. Technol.* **2006,** *40*, (23), 7394-7401.
180. Xu, A.; Chai, Y.; Nohmi, T.; Hei, T., Genotoxic responses to titanium dioxide nanoparticles and fullerene in gpt delta transgenic MEF cells. *Part. Fibre Toxicol.* **2009,** *6*, (1), 1-13.
181. Alargova, R. G.; Deguchi, S.; Tsujii, K., Stable Colloidal Dispersions of Fullerenes in Polar Organic Solvents. *J.Am.Chem.Soc.* **2001,** *123*, (43), 10460-10467.
182. Cheng, X.; Kan, A. T.; Tomson, M. B., Naphthalene Adsorption and Desorption from Aqueous C_{60} Fullerene. *J. Chem. Eng. Data* **2004,** *49*, (3), 675-683.
183. Deguchi, S.; Mukai, S.-a.; Yamazaki, T.; Tsudome, M.; Horikoshi, K., Nanoparticles of Fullerene C_{60} from Engineering of Antiquity. *J. Phys. Chem. C* **2009,** *114*, (2), 849-856.
184. Murdianti, B. S.; Damron, J. T.; Hilburn, M. E.; Maples, R. D.; Hikkaduwa Koralege, R. S.; Kuriyavar, S. I.; Ausman, K. D., C_{60} Oxide as a Key Component of Aqueous C_{60} Colloidal Suspensions. *Environ. Sci. Technol.* **2012,** *46*, (14), 7446-7453.
185. Duncan, L. K.; Jinschek, J. R.; Vikesland, P. J., C_{60} Colloid Formation in Aqueous Systems: Effects of Preparation Method on Size, Structure, and Surface Charge. *Environ. Sci. Technol.* **2007,** *42*, (1), 173-178.
186. Hou, W.-C.; Jafvert, C. T., Photochemical Transformation of Aqueous C_{60} Clusters in Sunlight. *Environ. Sci. Technol.* **2008,** *43*, (2), 362-367.
187. Lee, J.; Cho, M.; Fortner, J. D.; Hughes, J. B.; Kim, J. H., Transformation of Aggregate C_{60} in the Aqueous Phase by UV Irradiation. *Environ. Sci. Technol.* **2009,** *43*, (13), 4878-4883.
188. Hwang, Y. S.; Li, Q. L., Characterizing Photochemical Transformation of Aqueous nC_{60} under Environmentally Relevant Conditions. *Environ. Sci. Technol.* **2010,** *44*, (8), 3008-3013.
189. Fortner, J. D.; Kim, D. I.; Boyd, A. M.; Falkner, J. C.; Moran, S.; Colvin, V. L.; Hughes, J. B.; Kim, J. H., Reaction of Water-Stable C_{60} Aggregates with Ozone. *Environ. Sci. Technol.* **2007,** *41*, (21), 7497-7502.
190. Hou, W.-C.; Jafvert, C. T., Photochemistry of Aqueous C_{60} Clusters: Evidence of $^1O_2$ Formation and its Role in Mediating C_{60} Phototransformation. *Environ. Sci. Technol.* **2009,** *43*, (14), 5257-5262.
191. Lee, J.; Fortner, J. D.; Hughes, J. B.; Kim, J.-H., Photochemical Production of Reactive Oxygen Species by C_{60} in the Aqueous Phase During UV Irradiation. *Environ. Sci. Technol.* **2007,** *41*, (7), 2529-2535.
192. Xie, Q.; Perez-Cordero, E.; Echegoyen, L., Electrochemical detection of C_{60}^{6-} and C_{70}^{6-}: Enhanced stability of fullerides in solution. *J.Am.Chem.Soc.* **1992,** *114*, (10), 3978-3980.
193. Anachkov, M. P.; Cataldo, F.; Rakovsky, S. K., Ozone Reaction with C_{70} and C_{60} Fullerenes: The effect of temperature on the reaction kinetics. *Fullerenes, Nanotubes, Carbon Nanostruct.* **2004,** *12*, (4), 745-752.
194. Heymann, D.; Bachilo, S. M.; Weisman, R. B.; Cataldo, F.; Fokkens, R. H.; Nibbering, N. M. M.; Vis, R. D.; Chibante, L. P. F., $C_{60}O_3$, a Fullerene Ozonide: Synthesis and Dissociation to $C_{60}O$ and O_2. *J.Am.Chem.Soc.* **2000,** *122*, (46), 11473-11479.

195. Kniaz, K.; Fischer, J. E.; Selig, H.; Vaughan, G. B. M.; Romanow, W. J.; Cox, D. M.; Chowdhury, S. K.; McCauley, J. P.; Strongin, R. M.; Smith, A. B., Fluorinated fullerenes: synthesis, structure, and properties. *J.Am.Chem.Soc.* **1993,** *115*, (14), 6060-6064.
196. Hawkins, J. M.; Lewis, T. A.; Loren, S. D.; Meyer, A.; Heath, J. R.; Shibato, Y.; Saykally, R. J., Organic chemistry of C_{60} (buckminsterfullerene): chromatography and osmylation. *J. Org. Chem.* **1990,** *55*, (26), 6250-6252.
197. Bruno, C.; Doubitski, I.; Marcaccio, M.; Paolucci, F.; Paolucci, D.; Zaopo, A., Electrochemical Generation of C_{60}^{2+} and C_{60}^{3+}. *J.Am.Chem.Soc.* **2003,** *125*, (51), 15738-15739.
198. Tajima, Y.; Takeuchi, K., Discovery of $C_{60}O_3$ Isomer Having C3v Symmetry. *J. Org. Chem.* **2002,** *67*, (5), 1696-1698.
199. Cox, D. M.; Cameron, S. D.; Tuinman, A.; Gakh, A.; Adcock, J. L.; Compton, R. N.; Hagaman, E. W.; Kniaz, K.; Fischer, J. E., X-ray Photoelectron and NMR Studies of Polyfluorinated C_{60}: Evidence that C-C Bonds Are Broken. *J.Am.Chem.Soc.* **1994,** *116*, (3), 1115-1120.
200. Khakina, E. A.; Yurkova, A. A.; Peregudov, A. S.; Troyanov, S. I.; Trush, V. V.; Vovk, A. I.; Mumyatov, A. V.; Martynenko, V. M.; Balzarini, J.; Troshin, P. A., Highly selective reactions of $C_{60}Cl_6$ with thiols for the synthesis of functionalized [60]fullerene derivatives. *Chem. Commun.* **2012,** *48*, (57), 7158-7160.
201. Olah, G. A.; Bucsi, I.; Lambert, C.; Aniszfeld, R.; Trivedi, N. J.; Sensharma, D. K.; Prakash, G. K. S., Polyarenefullerenes, $C_{60}(H\text{-}Ar)_n$, obtained by acid-catalyzed fullerenation of aromatics. *J.Am.Chem.Soc.* **1991,** *113*, (24), 9387-9388.
202. Tebbe, F. N.; Becker, J. Y.; Chase, D. B.; Firment, L. E.; Holler, E. R.; Malone, B. S.; Krusic, P. J.; Wasserman, E., Multiple, reversible chlorination of C_{60}. *J.Am.Chem.Soc.* **1991,** *113*, (26), 9900-9901.
203. Troshin, P. A.; Łapiński, A.; Bogucki, A.; Połomska, M.; Lyubovskaya, R. N., Preparation and spectroscopic properties of chlorofullerenes $C_{60}Cl_{24}$, $C_{60}Cl_{28}$, and $C_{60}Cl_{30}$. *Carbon* **2006,** *44*, (13), 2770-2777.
204. Shustova, N. B.; Popov, A. A.; Sidorov, L. N.; Turnbull, A. P.; Kemnitz, E.; Troyanov, S. I., Preparation and crystallographic characterization of $C_{60}Cl_{24}$. *Chem. Commun.* **2005**, (11), 1411-1413.
205. Troshin, P. A.; Popkov, O.; Lyubovskaya, R. N., Some New Aspects of Chlorination of Fullerenes. *Fullerenes, Nanotubes, Carbon Nanostruct.* **2003,** *11*, (2), 165-185.
206. Cataldo, F., New Developments on the Photochlorination of C_{60} and C_{70} Fullerene and Preparation of Fullerene Derivatives: Polyfluorofullerenes and Polyfullerols. *Fullerene Sci. Tech.* **1996,** *4*, (5), 1041-1059.
207. Crittenden, J. C. M. W. H., *Water treatment principles and design*. J. Wiley: Hoboken, N.J., 2005.
208. Deborde, M.; von Gunten, U., Reactions of chlorine with inorganic and organic compounds during water treatment—Kinetics and mechanisms: A critical review. *Water Research* **2008,** *42*, (1–2), 13-51.
209. Tchobanoglous, G.; Burton, F. L.; Stensel, H. D.; Metcalf; Eddy, *Wastewater Engineering: Treatment and Reuse*. McGraw-Hill: 2003.
210. Clesceri, L. S.; Greenberg, A. E.; Eaton, A. D., *Standard Methods for the Examination of Water and Wastewater, 20th Edition*. APHA American Public Health Association: 1998.
211. Rook, J. J., *Formation of haloforms during chlorination of natural waters*. 1974.

212. Bellar, T. A.; Lichtenberg, J. J.; Kroner, R. C., The occurrence of organohalides in chlorinated drinking waters. *J Am Water Works Assoc* **1974,** *66*, (12), 703-706.
213. Krasner, S. W.; Weinberg, H. S.; Richardson, S. D.; Pastor, S. J.; Chinn, R.; Sclimenti, M. J.; Onstad, G. D.; Thruston, A. D., Occurrence of a New Generation of Disinfection Byproducts. *Environ. Sci. Technol.* **2006,** *40*, (23), 7175-7185.
214. Hrudey, S. E., Chlorination disinfection by-products, public health risk tradeoffs and me. *Water Research* **2009,** *43*, (8), 2057-2092.
215. Cotton, F. A., *Advanced Inorganic Chemistry*. Wiley: 1999.
216. Wang, C.; Shang, C.; Ni, M.; Dai, J.; Jiang, F., (Photo)chlorination-Induced Physicochemical Transformation of Aqueous Fullerene nC_{60}. *Environ. Sci. Technol.* **2012,** *46*, (17), 9398-9405.
217. Alpatova, A. L.; Baumann, M. J.; Davies, S. H.; Masten, S. J., Evidence for covalently bonded chlorine-fullerene formed by ozonation and chlorination at room temperature. *Environ. Chem. Lett.* **2013,** *11*, (3), 309-313.
218. Eaton, A. D.; Franson, M. A. H.; Association, A. P. H.; Association, A. W. W.; Federation, W. E., *Standard Methods for the Examination of Water & Wastewater*. American Public Health Association: 2005.
219. Chang, R., *General chemistry*. Random House: 1986.
220. Xiao, Y.; Wiesner, M. R., Characterization of surface hydrophobicity of engineered nanoparticles. *J. Hazard. Mater.* **2012,** *215–216*, (0), 146-151.
221. Wu, J.; Alemany, L. B.; Li, W.; Petrie, L.; Welker, C.; Fortner, J. D., Reduction of Hydroxylated Fullerene (Fullerol) in Water by Zinc: Reaction and Hemiketal Product Characterization. *Environ. Sci. Technol.* **2014**.
222. Hou, W.-C.; Moghadam, B. Y.; Westerhoff, P.; Posner, J. D., Distribution of Fullerene Nanomaterials between Water and Model Biological Membranes. *Langmuir* **2011,** *27*, (19), 11899-11905.
223. Chen, K. L.; Elimelech, M., Aggregation and Deposition Kinetics of Fullerene (C_{60}) Nanoparticles. *Langmuir* **2006,** *22*, (26), 10994-11001.
224. Qu, X.; Hwang, Y. S.; Alvarez, P. J. J.; Bouchard, D.; Li, Q., UV Irradiation and Humic Acid Mediate Aggregation of Aqueous Fullerene (nC_{60}) Nanoparticles. *Environ. Sci. Technol.* **2010,** *44*, (20), 7821-7826.
225. Li, W.; Liu, D.; Wu, J.; Kim, C.; Fortner, J. D., Aqueous Aggregation and Surface Deposition Processes of Engineered Superparamagnetic Iron Oxide Nanoparticles for Environmental Applications. *Environ. Sci. Technol.* **2014**.
226. Chen, K. L.; Elimelech, M., Relating Colloidal Stability of Fullerene (C_{60}) Nanoparticles to Nanoparticle Charge and Electrokinetic Properties. *Environ. Sci. Technol.* **2009,** *43*, (19), 7270-7276.
227. Huynh, K. A.; Chen, K. L., Aggregation Kinetics of Citrate and Polyvinylpyrrolidone Coated Silver Nanoparticles in Monovalent and Divalent Electrolyte Solutions. *Environ. Sci. Technol.* **2011,** *45*, (13), 5564-5571.
228. Chowdhury, I.; Duch, M. C.; Mansukhani, N. D.; Hersam, M. C.; Bouchard, D., Colloidal Properties and Stability of Graphene Oxide Nanomaterials in the Aquatic Environment. *Environ. Sci. Technol.* **2013,** *47*, (12), 6288-6296.
229. Petosa, A. R.; Jaisi, D. P.; Quevedo, I. R.; Elimelech, M.; Tufenkji, N., Aggregation and Deposition of Engineered Nanomaterials in Aquatic Environments: Role of Physicochemical Interactions. *Environ. Sci. Technol.* **2010,** *44*, (17), 6532-6549.

230. Bouchard, D.; Ma, X.; Isaacson, C., Colloidal Properties of Aqueous Fullerenes: Isoelectric Points and Aggregation Kinetics of C60 and C60 Derivatives. *Environ. Sci. Technol.* **2009,** *43*, (17), 6597-6603.
231. Chen, K. L.; Elimelech, M., Influence of humic acid on the aggregation kinetics of fullerene (C_{60}) nanoparticles in monovalent and divalent electrolyte solutions. *J. Colloid Interface Sci.* **2007,** *309*, (1), 126-134.
232. Chen, K. L.; Mylon, S. E.; Elimelech, M., Aggregation Kinetics of Alginate-Coated Hematite Nanoparticles in Monovalent and Divalent Electrolytes. *Environ. Sci. Technol.* **2006,** *40*, (5), 1516-1523.
233. Saleh, N. B.; Pfefferle, L. D.; Elimelech, M., Aggregation Kinetics of Multiwalled Carbon Nanotubes in Aquatic Systems: Measurements and Environmental Implications. *Environ. Sci. Technol.* **2008,** *42*, (21), 7963-7969.
234. Zhang, S.; Jiang, Y.; Chen, C.-S.; Spurgin, J.; Schwehr, K. A.; Quigg, A.; Chin, W.-C.; Santschi, P. H., Aggregation, Dissolution, and Stability of Quantum Dots in Marine Environments: Importance of Extracellular Polymeric Substances. *Environ. Sci. Technol.* **2012,** *46*, (16), 8764-8772.
235. Trinh, L. T.; Kjøniksen, A.-L.; Zhu, K.; Knudsen, K.; Volden, S.; Glomm, W.; Nyström, B., Slow salt-induced aggregation of citrate-covered silver particles in aqueous solutions of cellulose derivatives. *Colloid Polym. Sci.* **2009,** *287*, (12), 1391-1404.
236. French, R. A.; Jacobson, A. R.; Kim, B.; Isley, S. L.; Penn, R. L.; Baveye, P. C., Influence of Ionic Strength, pH, and Cation Valence on Aggregation Kinetics of Titanium Dioxide Nanoparticles. *Environ. Sci. Technol.* **2009,** *43*, (5), 1354-1359.
237. Anderson, R.; Barron, A. R., Reaction of Hydroxyfullerene with Metal Salts: A Route to Remediation and Immobilization. *J.Am.Chem.Soc.* **2005,** *127*, (30), 10458-10459.
238. Li, W.; Hinton, C. H.; Lee, S. S.; Wu, J.; Fortner, J. D., Surface engineering superparamagnetic nanoparticles for aqueous applications: design and characterization of tailored organic bilayers. *Environ. Sci. Nano* **2015**.
239. Lin, Y.-P.; Valentine, R. L., Reductive Dissolution of Lead Dioxide (PbO2) in Acidic Bromide Solution. *Environ. Sci. Technol.* **2010,** *44*, (10), 3895-3900.
240. Hill, C. G., *An introduction to chemical engineering kinetics & reactor design*. Wiley: 1977.
241. Davis, M. E.; Davis, R. J., *Fundamentals of Chemical Reaction Engineering*. McGraw-Hill: 2003.
242. Wang, T. X.; Margerum, D. W., Kinetics of Reversible Chlorine Hydrolysis: Temperature Dependence and General-Acid/Base-Assisted Mechanisms. *Inorg. Chem.* **1994,** *33*, (6), 1050-1055.
243. Morris, J. C., The Acid Ionization Constant of HOCl from 5 to 35 °. *J. Phys. Chem.* **1966,** *70*, (12), 3798-3805.
244. Sivey, J. D.; McCullough, C. E.; Roberts, A. L., Chlorine Monoxide (Cl_2O) and Molecular Chlorine (Cl_2) as Active Chlorinating Agents in Reaction of Dimethenamid with Aqueous Free Chlorine. *Environ. Sci. Technol.* **2010,** *44*, (9), 3357-3362.
245. Cherney, D. P.; Duirk, S. E.; Tarr, J. C.; Collette, T. W., Monitoring the Speciation of Aqueous Free Chlorine from pH 1 to 12 with Raman Spectroscopy to Determine the Identity of the Potent Low-pH Oxidant. *Appl. Spectrosc.* **2006,** *60*, (7), 764-772.
246. Sivey, J. D.; Roberts, A. L., Assessing the Reactivity of Free Chlorine Constituents Cl_2, Cl_2O, and HOCl Toward Aromatic Ethers. *Environ. Sci. Technol.* **2012,** *46*, (4), 2141-2147.

247. Harrison, R. M.; Perry, R.; Wellings, R. A., Chemical kinetics of chlorination of some polynuclear aromatic hydrocarbons under conditions of water treatment processes. *Environ. Sci. Technol.* **1976,** *10*, (12), 1156-1160.
248. Oyler, A. R.; Liukkonen, R. J.; Lukasewycz, M. T.; Heikkila, K. E.; Cox, D. A.; Carlson, R. M., Chlorine disinfection chemistry of aromatic compounds. Polynuclear aromatic hydrocarbons: rates, products, and mechanisms. *Environ. Sci. Technol.* **1983,** *17*, (6), 334-342.
249. Hu, J.; Jin, X.; Kunikane, S.; Terao, Y.; Aizawa, T., Transformation of pyrene in aqueous chlorination in the presence and absence of bromide ion: Kinetics, products, and their aryl hydrocarbon receptor-mediated activities. *Environ. Sci. Technol.* **2006,** *40*, (2), 487-493.
250. Hotze, E. M.; Labille, J.; Alvarez, P.; Wiesner, M. R., Mechanisms of photochemistry and reactive oxygen production by fullerene suspensions in water. *Environ. Sci. Technol.* **2008,** *42*, (11), 4175-4180.
251. Brant, J. A.; Labille, J.; Robichaud, C. O.; Wiesner, M., Fullerol cluster formation in aqueous solutions: Implications for environmental release. *J. Colloid Interface Sci.* **2007,** *314*, (1), 281-288.
252. Puri, B. R.; Gandhi, D. L.; Mahajan, O. P., Adsorption of bromine by carbons from solution in carbon tetrachloride. *Carbon* **1977,** *15*, (3), 173-176.
253. Silverstein, R. M.; Bassler, G. C.; Morrill, T. C., *Spectrometric Identification of Organic Compounds*. Wiley: 1991.
254. Wade, J. L. G., *Organic Chemistry*. Pearson Education: 2008.
255. Wu, J.; Goodwin, D. G.; Peter, K.; Benoit, D.; Li, W.; Fairbrother, D. H.; Fortner, J. D., Photo-Oxidation of Hydrogenated Fullerene (Fullerane) in Water. *Environ. Sci. Technol. Lett.* **2014,** *1*, (12), 490-494.
256. Papirer, E.; Lacroix, R.; Donnet, J.-B.; Nansé, G.; Fioux, P., XPS study of the halogenation of carbon black—Part 2. Chlorination. *Carbon* **1995,** *33*, (1), 63-72.
257. Wren, A. G.; Phillips, R. W.; Tolentino, L. U., Surface reactions of chlorine molecules and atoms with water and sulfuric acid at low temperatures. *J. Colloid Interface Sci.* **1979,** *70*, (3), 544-557.
258. Li, G.; Han, Z.; Piao, G.; Zhao, J.; Li, S.; Liu, G., To distinguish fullerene C_{60} nanotubes and C_{60} nanowhiskers using Raman spectroscopy. *Mater. Sci. Eng. B* **2009,** *163*, (3), 161-164.
259. Bethune, D. S.; Meijer, G.; Tang, W. C.; Rosen, H. J.; Golden, W. G.; Seki, H.; Brown, C. A.; de Vries, M. S., Vibrational Raman and infrared spectra of chromatographically separated C_{60} and C_{70} fullerene clusters. *Chem. Phys. Lett.* **1991,** *179*, (1–2), 181-186.
260. Li, B.; Zhou, L.; Wu, D.; Peng, H.; Yan, K.; Zhou, Y.; Liu, Z., Photochemical Chlorination of Graphene. *ACS Nano* **2011,** *5*, (7), 5957-5961.
261. Ferrari, A. C.; Meyer, J. C.; Scardaci, V.; Casiraghi, C.; Lazzeri, M.; Mauri, F.; Piscanec, S.; Jiang, D.; Novoselov, K. S.; Roth, S.; Geim, A. K., Raman Spectrum of Graphene and Graphene Layers. *Phys. Rev. Lett.* **2006,** *97*, (18), 187401.
262. Brant, J.; Lecoanet, H.; Hotze, M.; Wiesner, M., Comparison of Electrokinetic Properties of Colloidal Fullerenes (nC_{60}) Formed Using Two Procedures. *Environ. Sci. Technol.* **2005,** *39*, (17), 6343-6351.
263. Song, M.; Liu, S.; Yin, J.; Wang, H., Interaction of Human Serum Album and C60 Aggregates in Solution. *Int. J. Mol. Sci.* **2011**.
264. Hardy, W. B., A Preliminary Investigation of the Conditions which Determine the Stability of Irreversible Hydrosols. *J. Phys. Chem. B* **1899,** *4*, (4), 235-253.

265. Chen, K. L.; Elimelech, M., Interaction of Fullerene (C_{60}) Nanoparticles with Humic Acid and Alginate Coated Silica Surfaces: Measurements, Mechanisms, and Environmental Implications. *Environ. Sci. Technol.* **2008,** *42*, (20), 7607-7614.
266. Bazin, H.; Descotes, G.; Bouchu, A.; Petit-Ramel, M., Comparison of calcium complexation of some carboxylic acids derived from Dglucose and D-fructose. *Can. J. Chem.* **1995,** *73*, (8), 1338-1347.
267. Pfeiffer, D. R.; Reed, P. W.; Lardy, H. A., Ultraviolet and fluorescent spectral properties of the divalent cation ionophore A23187 and its metal ion complexes. *Biochemistry* **1974,** *13*, (19), 4007-4014.
268. Verrall, K. E.; Warwick, P.; Fairhurst, A. J., Application of the Schulze–Hardy rule to haematite and haematite/humate colloid stability. *Colloids Surf A Physicochem Eng Asp.* **1999,** *150*, (1–3), 261-273.
269. Martell, A. E. S., R.M.; Motekaitis, R.J., NIST Critically Selected Stability Constants of Metal Complexes Database. *National Institute of Science and Technology:Gaitherburg, MD* **2004**.
270. Deguchi, S.; Alargova, R. G.; Tsujii, K., Stable Dispersions of Fullerenes, C60 and C70, in Water. Preperation and Characterization. *Langmuir* **2001,** *17*, 6013-6017.
271. Lee, J.; Cho, M.; Fortner, J. D.; Hughes, J. B.; Kim, J.-H., Transformation of Aggregated C60 in the Aqueous Phase by UV Irradiation. *Environ. Sci. Technol.* **2009,** *43*, (13), 4878-4883.
272. Dai, L. M.; Mau, A. W. H.; Zhang, X. Q., Synthesis of fullerene- and fullerol-containing polymers. *Journal of Materials Chemistry* **1998,** *8*, (2), 325-330.
273. Zhou, A. H.; Zhang, J. D.; Xie, Q. J.; Yao, S. Z., Application of double-impedance system and cyclic voltammetry to study the adsorption of fullerols ($C_{60}(OH)_n$) on biological peptide-adsorbed gold electrode. *Biomaterials* **2001,** *22*, (18), 2515-2524.
274. Vileno, B.; Marcoux, P. R.; Lekka, M.; Sienkiewicz, A.; Feher, T.; Forro, L., Spectroscopic and photophysical properties of a highly derivatized C_{60} fullerol. *Adv. Funct. Mater.* **2006,** *16*, (1), 120-128.
275. Badamshina, E.; Gafurova, M., Hydroxylated fullerenes and fullerene-containing poly(urethanes). *Polymer Science Series B* **2007,** *49*, (7), 182-190.
276. Husebo, L. O.; Sitharaman, B.; Furukawa, K.; Kato, T.; Wilson, L. J., Fullerenols Revisited as Stable Radical Anions. *J. Am. Chem. Soc.* **2004,** *126*, (38), 12055-12064.
277. Chiang, L. Y.; Upasani, R. B.; Swirczewski, J. W.; Soled, S., Evidence of hemiketals incorporated in the structure of fullerols derived from aqueous acid chemistry. *J. Am. Chem. Soc.* **1993,** *115*, (13), 5453-5457.
278. Xiao, Y.; Wiesner, M. R., Transport and Retention of Selected Engineered Nanoparticles by Porous Media in the Presence of a Biofilm. *Environ. Sci. Technol.* **2013,** *47*, (5), 2246-2253.
279. Britto, R. S.; Garcia, M. L.; Martins da Rocha, A.; Flores, J. A.; Pinheiro, M. V. B.; Monserrat, J. M.; Ferreira, J. L. R., Effects of carbon nanomaterials fullerene C_{60} and fullerol $C_{60}(OH)_{18–22}$ on gills of fish Cyprinus carpio (Cyprinidae) exposed to ultraviolet radiation. *Aquatic Toxicology* **2012,** *114–115*, (0), 80-87.
280. Mohan, H.; Chiang, L. Y.; Mittal, J. P., Radiation chemical investigations on aqueous solutions of C60(OH)18. *Res. Chem. Intermed.* **1997,** *23*, (5), 403-414.
281. Lu, C.-Y.; Yao, S.-D.; Lin, W.-Z.; Wang, W.-F.; Nian-Yun, L.; Tong, Y.-P.; Rong, T.-W., Studies on the fullerol of C60 in aqueous solution with laser photolysis and pulse radiolysis. *Radiat. Phys. Chem.* **1998,** *53*, (2), 137-143.

282. Mirkov, S. M.; Djordjevic, A. N.; Andric, N. L.; Andric, S. A.; Kostic, T. S.; Bogdanovic, G. M.; Vojinovic-Miloradov, M. B.; Kovacevic, R. Z., Nitric oxide-scavenging activity of polyhydroxylated fullerenol, C60(OH)24. *Nitric Oxide* **2004,** *11*, (2), 201-207.
283. Wang, W.-J.; Chiu, H. S.; Chang, C. S.; Chiang, L. Y., Electrochemistry of nitrated fullerene derivatives. *Diamond and Related Materials* **2009,** *18*, (2–3), 469-471.
284. Olah, G. A.; Bucsi, I.; Lambert, C.; Aniszfeld, R.; Trivedi, N. J.; Sensharma, D. K.; Prakash, G. K. S., Polyarenefullerenes, C_{60}(H-Ar)$_n$, obtained by acid-catalyzed fullerenation of aromatics. *J. Am. Chem. Soc.* **1991,** *113*, (24), 9387-9388.
285. Shustova, N. B.; Popov, A. A.; Sidorov, L. N.; Turnbull, A. P.; Kemnitz, E.; Troyanov, S. I., Preparation and crystallographic characterization of $C_{60}Cl_{24}$. *Chem. Commun.* **2005**, (11), 1411-1413.
286. Wang, C.; Shang, C.; Ni, M.; Dai, J.; Jiang, F., (Photo)chlorination-Induced Physicochemical Transformation of Aqueous Fullerene nC_{60}. *Environ. Sci. Technol.* **2012,** *46*, (17), 9398-9405.
287. Reimhult, K.; Petersson, K.; Krozer, A., QCM-D Analysis of the Performance of Blocking Agents on Gold and Polystyrene Surfaces. *Langmuir* **2008,** *24*, (16), 8695-8700.
288. Li, W.; Liu, D.; Wu, J.; Kim, C.; Fortner, J. D., Aqueous Aggregation and Surface Deposition Processes of Engineered Superparamagnetic Iron Oxide Nanoparticles for Environmental Applications. *Environ. Sci. Technol.* **2014**.
289. Penfold, J.; Staples, E.; Tucker, I.; Thomas, R. K., Adsorption of Mixed Anionic and Nonionic Surfactants at the Hydrophilic Silicon Surface. *Langmuir* **2002,** *18*, (15), 5755-5760.
290. Naderi, A.; Claesson, P. M., Adsorption Properties of Polyelectrolyte−Surfactant Complexes on Hydrophobic Surfaces Studied by QCM-D. *Langmuir* **2006,** *22*, (18), 7639-7645.
291. Sauerbrey, G., Verwendung von Schwingquarzen zur Wägung dünner Schichten und zur Mikrowägung. *Zeitschrift für Physik* **1959,** *155*, (2), 206-222.
292. Chen, K. L.; Elimelech, M., Interaction of Fullerene (C_{60}) Nanoparticles with Humic Acid and Alginate Coated Silica Surfaces: Measurements, Mechanisms, and Environmental Implications. *Environ. Sci. Technol.* **2008,** *42*, (20), 7607-7614.
293. Oyler, A. R.; Liukkonen, R. J.; Lukasewycz, M. T.; Heikkila, K. E.; Cox, D. A.; Carlson, R. M., Chlorine disinfection chemistry of aromatic compounds. Polynuclear aromatic hydrocarbons: rates, products, and mechanisms. *Environ. Sci. Technol.* **1983,** *17*, (6), 334-342.
294. Nowell, L. H.; Hoigné, J., Photolysis of aqueous chlorine at sunlight and ultraviolet wavelengths—II. Hydroxyl radical production. *Water Research* **1992,** *26*, (5), 599-605.
295. Buxton, G. V.; Subhani, M. S., Radiation chemistry and photochemistry of oxychlorine ions. Part 1.-Radiolysis of aqueous solutions of hypochlorite and chlorite ions. *Journal of the Chemical Society, Faraday Transactions 1: Physical Chemistry in Condensed Phases* **1972,** *68*, (0), 947-957.
296. Gallard, H.; von Gunten, U., Chlorination of Phenols: Kinetics and Formation of Chloroform. *Environ. Sci. Technol.* **2002,** *36*, (5), 884-890.
297. Barton, S. S.; Evans, M. J. B.; Koresh, J. E.; Tobias, H., The effect of chlorination on the adsorptive properties of water on carbon cloth. *Carbon* **1987,** *25*, (5), 663-667.
298. Reyerson, L. H.; Wishart, A. W., The sorption of chlorine by activated charcoal. *J. Phys. Chem.* **1938,** *42*, (5), 679-685.
299. Chiang, L. Y.; Upasani, R. B.; Swirezewski, J. W.; Soled, S., Evidence of Hemiketals Incorporated in the Structure of Fullerols Derived from Aqueous Acid Chemistry. *J. Am. Chem. Soc.* **1993,** *115*, 5453-5457.

300. Fulmer, G. R.; Miller, A. J. M.; Sherden, N. H.; Gottlieb, H. E.; Nudelman, A.; Stoltz, B. M.; Bercaw, J. E.; Goldberg, K. I., NMR Chemical Shifts of Trace Impurities: Common Laboratory Solvents, Organics, and Gases in Deuterated Solvents Relevant to the Organometallic Chemist. *Organometallics* **2010,** *29*, (9), 2176-2179.
301. Ballutaud, D.; Simon, N.; Girard, H.; Rzepka, E.; Bouchet-Fabre, B., Photoelectron spectroscopy of hydrogen at the polycrystalline diamond surface. *Diamond and Related Materials* **2006,** *15*, (4–8), 716-719.
302. Morgan, W. E.; Van Wazer, J. R.; Stec, W. J., Inner-orbital photoelectron spectroscopy of the alkali metal halides, perchlorates, phosphates, and pyrophosphates. *J. Am. Chem. Soc.* **1973,** *95*, (3), 751-755.
303. Thorn, R. J.; Carlson, K. D.; Crabtree, G. W.; Wang, H. H., States determined by photoelectron spectroscopy in the perchlorate and perrhenate of TMTSF. *Journal of Physics C: Solid State Physics* **1985,** *18*, (28), 5501.
304. Chi, Z.; Zhugan, L.; Fengcai, L., Conducting polyphenylquinoxaline. *Polymer* **1991,** *32*, (17), 3075-3079.
305. Pérez-Cadenas, A.; amp; x; n, F.; Maldonado-Hódar, F. J.; Moreno-Castilla, C., On the nature of surface acid sites of chlorinated activated carbons. *Carbon* **2003,** *41*, (3), 473-478.
306. Song, J. E.; Phenrat, T.; Marinakos, S.; Xiao, Y.; Liu, J.; Wiesner, M. R.; Tilton, R. D.; Lowry, G. V., Hydrophobic Interactions Increase Attachment of Gum Arabic- and PVP-Coated Ag Nanoparticles to Hydrophobic Surfaces. *Environ. Sci. Technol.* **2011,** *45*, (14), 5988-5995.
307. Chang, X.; Bouchard, D. C., Multiwalled Carbon Nanotube Deposition on Model Environmental Surfaces. *Environ. Sci. Technol.* **2013,** *47*, (18), 10372-10380.
308. Li, W.; Liu, D.; Wu, J.; Kim, C.; Fortner, J. D., Aqueous Aggregation and Surface Deposition Processes of Engineered Superparamagnetic Iron Oxide Nanoparticles for Environmental Applications. *Environ. Sci. Technol.* **2014,** *48*, (20), 11892-11900.
309. Meyer, E. E.; Rosenberg, K. J.; Israelachvili, J., Recent progress in understanding hydrophobic interactions. *Proceedings of the National Academy of Sciences* **2006,** *103*, (43), 15739-15746.
310. Chin, K. K.; Chuang, S.-C.; Hernandez, B.; Campos, L. M.; Selke, M.; Foote, C. S.; Garcia-Garibay, M. A., Photophysical properties of non-homoconjugated 1,2-dihydro, 1,2,3,4-tetrahydro and 1,2,3,4,5,6-hexahydro-C_{60} derivatives. *Photochemical & Photobiological Sciences* **2008,** *7*, (1), 49-55.
311. Bogdanović, G.; Kojić, V.; Đorđević, A.; Čanadanović-Brunet, J.; Vojinović-Miloradov, M.; Baltić, V. V., Modulating activity of fullerol $C_{60}(OH)_{22}$ on doxorubicin-induced cytotoxicity. *Toxicology in Vitro* **2004,** *18*, (5), 629-637.
312. Xia, T.; Kovochich, M.; Brant, J.; Hotze, M.; Sempf, J.; Oberley, T.; Sioutas, C.; Yeh, J. I.; Wiesner, M. R.; Nel, A. E., Comparison of the Abilities of Ambient and Manufactured Nanoparticles To Induce Cellular Toxicity According to an Oxidative Stress Paradigm. *Nano Letters* **2006,** *6*, (8), 1794-1807.
313. Zhu, X. S.; Zhu, L.; Li, Y.; Duan, Z. H.; Chen, W.; Alvarez, P. J. J., Developmental toxicity in zebrafish (Danio rerio) embryos after exposure to manufactured nanomaterials: Buckminsterfullerene aggregates (nC_{60}) and fullerol. *Environ. Toxicol. Chem.* **2007,** *26*, (5), 976-979.
314. Bergosh, R. G.; Meier, M. S.; Laske Cooke, J. A.; Spielmann, H. P.; Weedon, B. R., Dissolving Metal Reductions of Fullerenes. *The Journal of Organic Chemistry* **1997,** *62*, (22), 7667-7672.

315. Jehoulet, C.; Bard, A. J.; Wudl, F., Electrochemical reduction and oxidation of C_{60} films. *J. Am. Chem. Soc.* **1991,** *113*, (14), 5456-5457.
316. Heymann, D.; Bachilo, S. M.; Weisman, R. B.; Cataldo, F.; Fokkens, R. H.; Nibbering, N. M. M.; Vis, R. D.; Chibante, L. P. F., $C_{60}O_3$, a Fullerene Ozonide: Synthesis and Dissociation to $C_{60}O$ and O_2. *J. Am. Chem. Soc.* **2000,** *122*, (46), 11473-11479.
317. Olah, G. A.; Bucsi, I.; Aniszfeld, R.; Surya Prakash, G. K., Chemical reactivity and functionalization of C_{60} and C_{70} fullerenes. *Carbon* **1992,** *30*, (8), 1203-1211.
318. Bausch, J. W.; Prakash, G. K. S.; Olah, G. A.; Tse, D. S.; Lorents, D. C.; Bae, Y. K.; Malhotra, R., Considered novel aromatic systems. 11. Diamagnetic polyanions of the C_{60} and C_{70} fullerenes: preparation, ^{13}C and ^{7}Li NMR spectroscopic observation, and alkylation with methyl iodide to polymethylated fullerenes. *J. Am. Chem. Soc.* **1991,** *113*, (8), 3205-3206.
319. Yanilkin, V. V.; Gubskaya, V. P.; Morozov, V. I.; Nastapova, N. V.; Zverev, V. V.; Berdnikov, E. A.; Nuretdinov, I. A., Electrochemistry of Fullerenes and Their Derivatives. *Russian Journal of Electrochemistry* **2003,** *39*, (11), 1147-1165.
320. Stinchcombe, J.; Penicaud, A.; Bhyrappa, P.; Boyd, P. D. W.; Reed, C. A., Buckminsterfulleride(1-) salts: synthesis, EPR, and the Jahn-Teller distortion of C_{60}^-. *J. Am. Chem. Soc.* **1993,** *115*, (12), 5212-5217.
321. Arnold, W. A.; Roberts, A. L., Pathways of chlorinated ethylene and chlorinated acetylene reaction with Zn(0). *Environ. Sci. Technol.* **1998,** *32*, (19), 3017-3025.
322. Hernandez, R.; Zappi, M.; Kuo, C.-H., Chloride Effect on TNT Degradation by Zerovalent Iron or Zinc during Water Treatment. *Environ. Sci. Technol.* **2004,** *38*, (19), 5157-5163.
323. Yan, W.; Herzing, A. A.; Kiely, C. J.; Zhang, W.-X., Nanoscale zero-valent iron (nZVI): Aspects of the core-shell structure and reactions with inorganic species in water. *Journal of Contaminant Hydrology* **2010,** *118*, (3-4), 96-104.
324. Song, H.; Carraway, E. R.; Kim, Y. H.; Batchelor, B.; Jeon, B.-H.; Kim, J.-g., Amendment of hydroxyapatite in reduction of tetrachloroethylene by zero-valent zinc: Its rate enhancing effect and removal of Zn(II). *Chemosphere* **2008,** *73*, (9), 1420-1427.
325. Limousy, L.; Dutournie, P.; Hadjiev, D., Kinetics of Nitrite Reduction by Zinc Metal: Influence of Metal Shape on the Determination of Kinetic Parameters. *Water Environment Research* **2010,** *82*, (7), 648-656.
326. Hayashi, S.; Hayamizu, K., Chemical shift standards in high-resolution solid-state NMR (1) ^{13}C, ^{29}Si and ^{1}H Nuclei. *Bulletin of the Chemical Society of Japan* **1991,** *64*, 685-687.
327. Chiou, C. T.; Freed, V. H.; Schmedding, D. W.; Kohnert, R. L., Partition coefficient and bioaccumulation of selected organic chemicals. *Environ. Sci. Technol.* **1977,** *11*, (5), 475-478.
328. Stumm, W.; Morgan, J. J., *Aquatic chemistry: chemical equilibria and rates in natural waters*. Wiley: 1996.
329. Georgakilas, V.; Pellarini, F.; Prato, M.; Guldi, D. M.; Melle-Franco, M.; Zerbetto, F., Supramolecular self-assembled fullerene nanostructures. *Proceedings of the National Academy of Sciences* **2002,** *99*, (8), 5075-5080.
330. Yannoni, C. S.; Johnson, R. D.; Meijer, G.; Bethune, D. S.; Salem, J. R., ^{13}C NMR study of the C_{60} cluster in the solid state: Molecular motion and carbon chemical shift anisotropy. *J. Phys. Chem.* **1991,** *95*, (1), 9-10.
331. Cataldo, F.; Heymann, D., A study of polymeric products formed by C_{60} and C_{70} fullerene ozonation. *Polymer Degradation and Stability* **2000,** *70*, (2), 237-243.